Exploitation of Diazonium Chemistry: Synthesis, Characterization and Applications of Metal Nanoparticle-Linked Organic Frameworks and Nanographitic Materials

Thesis Submitted to AcSIR for the Award of the Degree of
DOCTOR OF PHILOSOPHY
in Chemical Sciences

By

PRAKASH S. P.

Registration No: 10CC11A39007

Under the guidance of

Dr. K. R. Gopidas

CSIR-NATIONAL INSTITUTE FOR INTERDISCIPLINARY
SCIENCE AND TECHNOLOGY (CSIR-NIIST)
THIRUVANANTHAPURAM-695 019, KERALA, INDIA

May, 2017

DECLARATION

I hereby declare that the matter embodied in the Ph. D. thesis entitled: **"Exploitation of Diazonium Chemistry: Synthesis, Characterization and Applications of Metal Nanoparticle-Linked Organic Frameworks and Nanographitic Materials"** is the result of an independent work carried out by me at the Photosciences and Photonics, Chemical Sciences and Technology Division of the CSIR-National Institute for Interdisciplinary Science and Technology (CSIR-NIIST), Thiruvananthapuram, under the supervision of Dr. K. R. Gopidas and the same has not been submitted elsewhere for other degree or diploma.

In keeping with the general practice of reporting scientific observations, research material obtained from other investigations has been duly cited and acknowledged in the thesis.

Prakash S. P.

Thiruvananthapuram

May 2017

सीएसआईआर- राष्ट्रीय अंतर्विषयी विज्ञान तथा प्रौद्योगिकी संस्थान
CSIR-NATIONAL INSTITUTE FOR INTERDISCIPLINARY SCIENCE & TECHNOLOGY
इंडस्ट्रियल इस्टेट पी.ओ., तिरुवनंतपुरम - 695 019, केरल, भारत
Industrial Estate P.O., Thiruvananthapuram - 695 019, Kerala, INDIA.

डॉ. के.आर. गोपिदास, एफ.ए.एससी
Dr. K. R. Gopidas F.A.Sc.
मुख्य वैज्ञानिक
Chief Scientist
रसायन विज्ञान तथा प्रौद्योगिकी प्रभाग
Chemical Sciences and Technology Division

May 10, 2017

<u>CERTIFICATE</u>

This is to certify that the work incorporated in this Ph.D. thesis entitled *"Exploitation of Diazonium Chemistry: Synthesis, Characterization and Applications of Metal Nanoparticle-Linked Organic Frameworks and Nanographitic Materials"* submitted by Mr. *Prakash S. P.* to Academy of Scientific and Innovative Research (AcSIR) in fulfillment of the requirements for the award of the Degree of *Doctor Of Philosophy in Chemical Sciences*, embodies original research work under my supervision/guidance. I further certify that this work has not been submitted to any other University or Institution in part or full for the award of any degree or diploma. Research material obtained from other sources has been duly acknowledged in the thesis. Any text, illustration, table etc., used in the thesis from other sources, have been duly cited and acknowledged.

Prakash S. P.   Dr. K. R. Gopidas

                                                                    (Thesis Supervisor)

टेलीफोन /Telephone: 91-471-2515390(O), 9446520537(M)
फैक्स /Fax : +91-471-2491712, ई-मेल /E-mail: gopidaskr@niist.res.in, gopidaskr@gmail.com

CONTENTS

CHAPTER 1: **Diazonium Chemistry, Supported Metal nanoparticles and Graphene: An Overview**

CHAPTER 2: **Palladium-Nanoparticle-Linked Organic Frameworks: Heterogeneous Recyclable Catalysts in Aqueous Medium**

CHAPTER 3: **Highly Stable Copper Nanoparticles Linked to Organic Frameworks as Recyclable Catalyst for Three-Component Click Cycloaddition in Water**

CHAPTER 4: **Synthesis, Functionalization, Characterization and Energy Applications of Nanographite Materials**

LIST OF FIGURES

LIST OF SCHEMES

LIST OF TABLES

LIST OF ABBREVIATIONS

1.   4-AP-   4-nitrophenol
2.   4-NP-   4-aminophenol
3.   Å-   Angstrom
4.   α-   Specific catalytic activity
5.   AFM-   Atomic force microscopy
6.   BE-   Binding Energy
7.   BPBDT-   4,4'-Biphenylene-bis-diazonium tetrafluoroborate
8.   C-   Cell capacitance
9.   CAP-   Cross linked aromatic polymer
10.   CNOF-   Copper- nanoparticle linked organic frameworks
11.   CNT-   Carbon nano tubes
12.   CG-   Commercial graphene
13. C_{sp}-   Specific capacitance
14.   CV-   Cyclic Voltammetry
15.   CVD-   Chemical Vapour Deposition
16.   D-   Diameter
17. $D°$-   Bond-dissociation energy
18.   DMF-   N,N-dimethylformamide
19.   DTA-   Differential thermal analysis
20.   EC-   Electrochemical capacitor
21.   EDLC-   Electric double layer capacitors
22.   EIS-   Electrochemical impedance spectroscopy
23.   ES-   Energy storage
24. f-   Scan rate
25.   F-   Frequency
26.   Fcc-   Face centered cubic
27.   FTIR-   Fourier transform infrared spectroscopy
28.   G1-   First generation dendrimer
29. G_{ads}-   Free energy change for adsorption
30.   GC-MS-   Gas chromatography–mass spectrometry
31.   GNRs-   Graphene nano ribbons
32.   GO-   Graphite oxide
33.   HBC-   Hexa-peri-hexabenzocoronene
34.   HG-   Hydrated graphene
35.   HOPG-   Highly oriented pyrolytic graphite
36.   HRTEM-   High resolution transmission electron microscope
37.   ICP-AES-   Inductively coupled plasma atomic emission spectroscopy

38.	*La*-	Crystallite size in graphene
39.	mM-	Millimolar
40.	MNOF-	Metal-Nanoparticle-linked Organic Frameworks
41.	MWCNTs-	Multi walled carbon nano tubes
42.	NCD-	Nanoparticle cored dendrimers
43.	NMP-	N-methylpyrrolidone
44.	NMR-	Nuclear magnetic resonance spectroscopy
45.	NSG-	Sodium salt of sulfonated graphene
46.	PAH-	Polycyclic aromatic hydrocarbon
47.	PMMA-	Poly(methyl methacrylate)
48.	PNIPAM-	Poly(N-isopropylacrylamide)
49.	PNOF-	Palladium- nanoparticle linked organic frameworks
50.	ppm-	Parts per million
51.	PPS-	Poly(styrenesulfonate)
52.	PTFE -	Polytetrafluoroethylene
53.	PXRD-	Powder
54.	RT-	Room temperature
55.	SAED-	Selected area electron diffraction
56.	SAMS-	Self-assembled monolayers
57.	SC-	Sodium cholate
58.	SDBS-	Sodium dodecylbenzenesulfonate
59.	SEM-	Scanning
60.	SG-	Sulfonated graphene
61.	SSA-	Specific surface area
62.	SWNT-	Single walled nano tubes
63.	TBA-	tetrabutylammonium hydroxide
64.	TGA-	Thermogravimetric analysis
65.	TOF-	Turnover frequency
66.	TON-	Turnover number
67.	UHV-	Ultra high vaccum
68.	V-	Voltage
69.	Vis-	Visible
70.	UV-	Ultraviolet
71.	WHO-	World Health Organisation
72.	XPS-	X-ray photoelectron spectroscopy
73.	XRD-	X-ray Powder Diffraction

PREFACE

This thesis focuses on the exploitation of diazonium chemistry for the preparation of supported metal nanoparticles and graphitic materials. Reduction of diazonium salts in the presence of solid supports has recently evolved as a technique to graft organic residues onto solid surfaces. If a diazonium salt is reduced electrochemically in an aprotic solvent, aryl radicals are formed, which exhibit a tendency to get covalently attached to the cathode surface. If the reduction is performed chemically, the aryl radicals get attached to available solid surfaces or organic moieties. This technique has been exploited for the modification of solid surfaces with mono- or multilayers of organic materials. Herein, we have explored the possibility of exploiting the reaction further to prepare porous metal nanoparticle-linked organic frameworks (MNOF) and nano graphitic materials. We have also checked the potential of MNOFs as catalysts for selected organic reactions and graphitic materials for energy storage applications.

Metal nanoparticles captured in porous materials as well as graphitic materials with the high surface area have wide applications in gas storage, gas generation, gas sensing, and in recyclable catalytic applications. For practical applications, it is preferable to have nano materials with high stability. On the other hand, production of such materials like supported nanoparticles and graphene-based materials in stable form with good quality often results in poor yields. High yield production of such materials is often associated with high cost and requires highly sophisticated techniques. Hence high yield production of those materials still remains an important topic of research. Herein we tried to explore the ability of diazonium salts to produce highly reactive radicals to prepare these graphitic materials as well as supported nanoparticles in high yield.

The thesis is divided into four chapters. The **first chapter** is a review of the literature on diazonium salts and their potential applications. The catalytic applications of palladium nanoparticles captured in various solid supports are also discussed. A brief introduction to the classification and various methods available for the preparation of graphene were also discussed.

In the **second** chapter of the thesis palladium nanoparticle linked organic frameworks are described. 4,4'-Biphenylene-bis diazonium tetrafluoroborate and a palladium salt were reduced simultaneously to result in the formation of palladium atoms and 4,4'-biphenylene biradicals. The palladium atoms underwent clustering forming palladium nanoparticles, whereas the 4,4'-biphenylene biradicals underwent rapid addition reactions to other radicals and also to nanoparticle surfaces. The resulting product was palladium nanoparticles covalently linked to an organic framework (PNOF). The effects of different reaction conditions upon metal content as well as on the morphology of the PNOF were studied. The PNOF structure was probed by different experimental techniques. The PNOFs were evaluated as heterogeneous recyclable catalyst in aqueous medium for reduction of 4-nitrophenol and Suzuki coupling reactions. The catalyst exhibited high reactivity even in Suzuki couplings of aryl chlorides.

In the **third** chapter, synthesis, characterization and catalytic applications of highly stable copper nanoparticles linked to aromatic frameworks are reported. Synthesis of these nanoparticles was achieved in a one-pot reaction which involved the simultaneous reduction of $CuCl_2.2H_2O$ and 4,4'-biphenylene-bis-diazonium tetrafluoroborate using sodium borohydride. Copper atoms formed upon reduction of Cu ions undergo clustering, leading to the formation of copper nanoparticles. At the same time, 4,4'-biphenylene-bis-diazonium tetrafluoroborate was converted to biphenylene biradicals, which undergoes rapid addition reactions with each other and also onto the nanoparticle surfaces resulting in the formation of aromatic framework linked Cu nanoparticles. Four different types of nanoparticles were prepared by varying the concentration of the metal salts and the ligands. The structure and morphology of these materials were studied using XRD, XPS, SEM and HRTEM analysis. The materials were found to be very good catalysts for click reactions between azides and alkynes and exhibited TOF values as high as 305,400 h^{-1}. They also efficiently catalyzed the one-pot click reactions involving azide precursors, sodium azide, and alkyne. TOF up to 99,000 h^{-1} were observed for these reactions.

In the **fourth** chapter, a new procedure for the synthesis of graphene from diazonium salts in high yield is discussed. The graphene analogue obtained was further

modified by sulfonation reaction. The sulfonated material, as well as the graphene analogue obtained, was characterized by different techniques including IR, TG, NMR, UV-Visible absorption and XRD analysis. The morphological characterizations were done using SEM, AFM and HRTEM analysis. Both the materials were checked for their potential in energy storage applications. The capacitance value of 45.5 F g^{-1} was obtained for the sodium salt of sulfonated graphene in 3 electrode configuration.

__Note:__ The abbreviations of various compounds given here correspond to those given under the respective Chapters.

Diazonium Chemistry, Supported Metal nanoparticles and Graphene: An Overview

1.1 Introduction

Diazonium salts are reactive intermediates formed from primary aromatic amines upon reaction with nitrous acid in the presence of a mineral acid (generally hydrochloric acid) at low temperature (-5 °C to 5 °C) (Mo 2013). The reaction proceeds as shown in equation 1.1. Under the same reaction conditions aliphatic primary amines will give the corresponding alcohol. The alcohol formation occurs due to the decomposition of the diazonium salts derived from the aliphatic amines with the evolution of nitrogen (Kirmse 1976).

$$Ar-NH_2 \ + \ NaNO_2 \ + \ 2HCl \ \longrightarrow \ Ar-\overset{\oplus}{N}\equiv N\}\overset{\ominus}{Cl} \ + \ NaCl \ + \ H_2O \qquad (1.1)$$

1.2 Mechanism

The different steps involved in the reaction are shown in equation 1.2. The acidic nitrite solution is a source of electrophilic nitrosonium ion **1**. One of the hydrogen atoms of the primary amino group will be replaced by the nitrosonium group to form the N-nitroso derivative **2**, which is in equilibrium with its hydroxydiazo tautomer **3**. Tautomer **3** under acidic conditions will give the diazonium ion **4**.

$$Ar-\overset{..}{N}H_2 \qquad \overset{\oplus}{N}=O \quad \xrightarrow{-H^{\oplus}} \quad Ar-\underset{H}{N}-N=O \quad \rightleftharpoons \quad Ar-\overset{..}{N}=N-OH \quad \xrightarrow{H^{\oplus}} \quad Ar-\overset{\oplus}{N}\equiv N \ + \ H_2O \quad (1.2)$$

$$\qquad \textbf{1} \qquad\qquad\qquad \textbf{2} \qquad\qquad\qquad \textbf{3} \qquad\qquad\qquad \textbf{4}$$
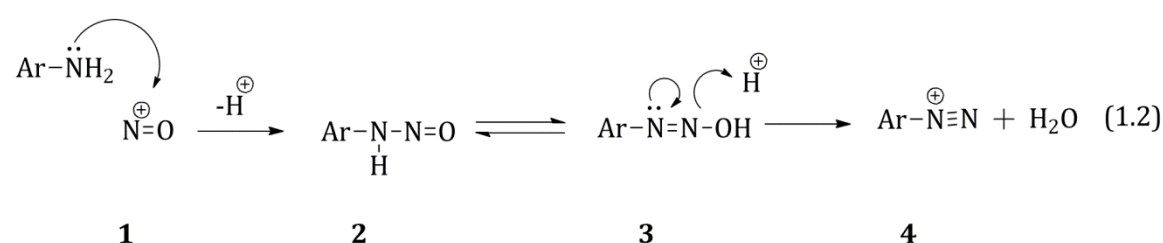
1.3 Synthesis

The process of synthesizing diazonium compounds is called "diazotation", "diazoniation", or "diazotisation". The reaction was first reported by Peter Griess in

1858; afterward she discovered several reactions of this new class of compounds (Griess 1858; 1864; 1866). The main method for the synthesis of diazonium salts is treatment of aromatic amines such as aniline with nitrous acid (Mo 2013).

The general procedure for the synthesis of diazonium salts involves the following steps. In the first step amine is dissolved in minimum amount of water containing 2.5 - 3 equivalents of a mineral acid (most cases hydrochloric acid). If necessary, heat can be applied to dissolve the amine completely to get a clear solution. Before the next diazotisation step, the solution should be cooled in ice till the temperature is reached and maintained at 0 - 5 °C. During this cooling slight precipitation of the amine hydrochloride (or sulfate) can occur. The next step is the small-portion wise addition of aqueous sodium nitrite solution. The precipitate of amine salt, if any, will dissolve during this step to give a clear solution. The completion of the reaction can be monitored by testing the presence of excess nitrous acid in the solution using an external indicator (moist potassium iodide-starch paper). The diazonium salt formed will be stable and their secondary reactions will be prevented in the presence of more than 0.5 - 1 equivalents of excess acid. In order to prevent the partial conversion to the corresponding alcohol by hydrolysis, it is necessary to keep the reaction mixture in very cold condition. The following are the salient features observed during the synthesis of various diazonium salts (Patai 1978).

➢ The reaction can be conducted more rapidly at room temperature for some anilines (ex:-nitronanilines), which react very slowly at low temperature, and the diazonium compounds formed are somewhat more stable.

➢ For amines which are sparingly soluble in water, finely suspended amines in the acidic condition can be used for the reactions; the fine suspension can be generally obtained by cooling a hot solution with vigorous stirring. In such cases it is observed that the amines will go into solution as reaction proceeds since the product formed is water soluble.

In the case of weak basic amines such as 2,4-dinitroaniline or picramide (the corresponding trinitro compound), a solution of sodium nitrite in concentrated sulfuric acid can be used, since the generated reagent, nitrosonium hydrogen sulfate, is a very effective diazotising medium.

$$HNO_2 + H_2SO_4 \rightleftharpoons [H_2NO_2]^{\oplus}[HSO_4]^{\ominus} \xrightarrow{H_2SO_4} [\overset{\oplus}{N}O][H\overset{\ominus}{S}O_4] + H_3\overset{\oplus}{O} + HS\overset{\ominus}{O}_4 \quad (1.3)$$
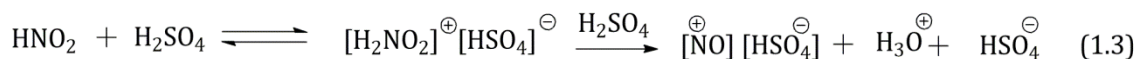
➢ The best diazotising reagent for the bis-diazotisation reaction (for example, *m*-phenylenediamine) is a mixture of HNO_2 and H_2SO_4. This is due to the fact that unless all the amino groups are extensively protonated, side reactions such as self-coupling will occur.

➢ Same reagent should be used if the molecule contains functional groups which can undergo self-coupling reactions (for example, 4-amino-3,5-diiodobenzoic acid).

➢ The self-coupling reactions are used to prepare azo dyes (for example, Bismarck Brown) under normal diazotisation conditions. See equation 1.4
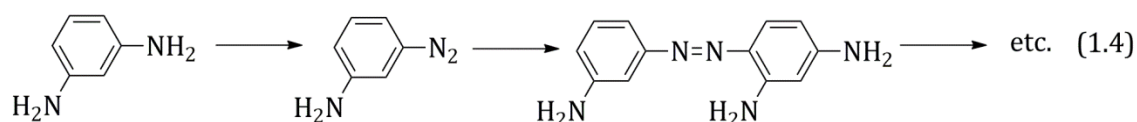
➢ It may be possible in some cases to isolate solid diazonium salts if the reaction is conducted in very small amount of water.

➢ If solid diazonium salts are desired, instead of $NaNO_2/HCl$, a solution of organic nitrite (such as pentyl (Pn) nitrite) in ethanol containing HCl gas can be used as diazotising agent. The solid product will precipitate as a crystalline solid.

$$Ph-\overset{\oplus}{N}H_3 + Pn-O-NO \xrightarrow{HCl} Ph-\overset{\oplus}{N}{\equiv}N\}\overset{\ominus}{Cl} + PnCl + 2H_2O \quad (1.5)$$
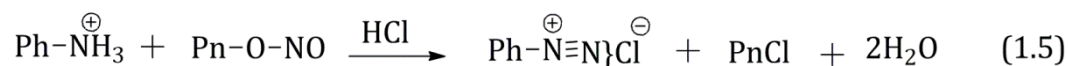
1.4 Applications

In the solid form diazonium salts are likely to be dangerously explosive as they are very sensitive to any shock or stimulus. The stimulus of heat, friction or even dryness can lead to explosion. Because of the explosive nature isolation of diazonium salts were seldom attempted earlier. Only in-situ generated diazonium salts were used for chemical reactions, for which the readily-accessible aqueous

solutions were sufficient. Scientists have now realized that the highly reactive species generated from diazonium salts using various stimuli can be cleverly used in various fields of research, especially in material synthesis (Pinson 2005). In the following section general uses of diazonium salts are summarized, which include the earlier chemical synthesis and modern applications involving isolated diazonium salts.

1.4.1 Reactions Involving Replacement of the Diazo-Group

Under appropriate conditions the diazo group can be replaced by atoms or groups. The atoms or groups include H, I, Br, Cl, F, OH, CN, NO_2, SO_2H and phenyl ring. The reaction follows S_N1 mechanism and involves elimination of the diazo group as molecular nitrogen as shown in equation 1.6. A nucleophile then adds to the aryl cation formed to give the product.

$$Ar-\overset{\oplus}{N}\equiv N \quad \xrightarrow{-N_2} \quad (\overset{\oplus}{Ar}) \quad \underset{-\overset{\oplus}{H}}{\xrightarrow{+H_2O}} \quad ArOH \qquad (1.6)$$
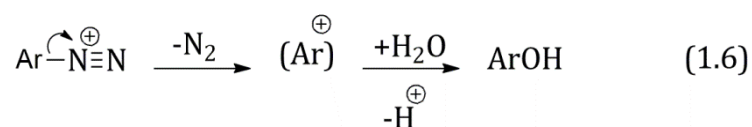
1.4.2 Reactions Involving Coupling Reactions

Diazonium salts undergo coupling reactions under basic conditions. Azo compounds are readily prepared by this method. The method involves treating diazonium salts with phenol in the presence of sodium hydroxide or amine in the presence of sodium acetate as shown in the following equations.

$$Ar-\overset{\oplus}{N}\equiv N \quad \langle\text{---}\rangle-O^{\ominus} \longrightarrow Ar-N=N-\langle\text{---}\rangle=O \xrightarrow[+\overset{\oplus}{H}]{-\overset{\oplus}{H}} Ar-N=N-\langle\text{---}\rangle-OH \qquad (1.7)$$

$$Ar-\overset{\oplus}{N}\equiv N \quad \langle\text{---}\rangle-\ddot{N}HR_2 \longrightarrow Ar-N=N-\langle\text{---}\rangle=\overset{\oplus}{N}R_2 \xrightarrow{-\overset{\oplus}{H}} Ar-N=N-\langle\text{---}\rangle-NHR_2 \qquad (1.8)$$
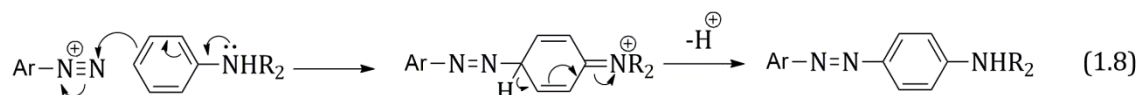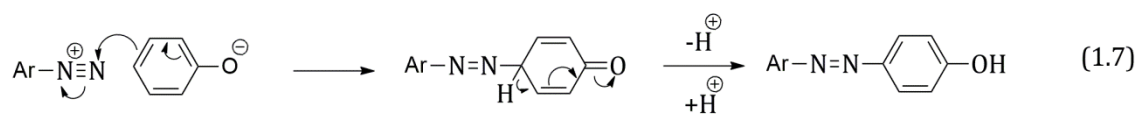
1.4.3 Grafting the organic moiety to a surface

Grafting of an organic moiety to an available solid surface is one of the major steps involved in the preparation of several functional materials. Diazonium salts are increasingly being used for this purpose. Grafting using diazonium salt is quite

simple in that the reaction can be controlled by applying certain stimuli like electricity, light, heat or solution reduction. Occasionally the grafting occurs spontaneously in which case the driving force may be the heat or light available at ambient conditions. Grafting using light, heat or electricity requires special instruments but in these cases good control over the amount grafted is usually possible. Solution reduction method does not need any special apparatus but achieving control over the amount grafted is difficult in this case. Grafting of an organic group onto a semiconductor/conductor surface by the solution reduction method is illustrated in Scheme 1.1. Upon receiving an electron from the reducing agent the diazonium salt eliminates dinitrogen to form an aryl radical. The aryl radical is highly reactive and get attached to the surface as shown in Scheme 1.1.
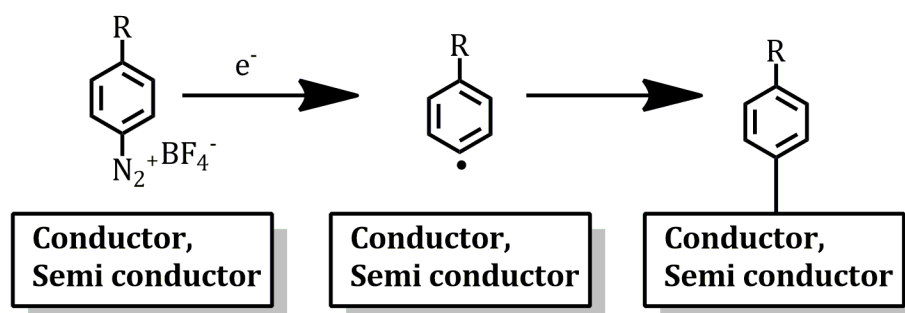
Scheme 1.1 Mechanism of attachment of organic layer to a surface.

1.5 Attachment of organic layers to conductive or semi conductive surfaces

Metal objects are usually covered with polymers to prevent corrosion and enhance aesthetics. Home appliances made of steel covered with polymer layers are the best examples of such objects. These objects are mainly made by the deposition of a suitable polymer on the metal surface. Mainly three methods are used for such deposition. These include (i) roll-coating from a liquid or solution, (ii) roll-bonded cladding from a solid polymer and (iii) cataphoresis, which is a very advanced electrophoretic method for metal surface treatment. The bond formed between the polymers and the metal surfaces are generally weak in all these cases. Hence these methods are insufficient in applications where materials having very strong bond between organic layer and the surface are necessary. Such application areas include biomedical field (prostheses, stents etc.), sensors, corrosion protection etc. Only few

methods are available for the formation of such strong bonds especially with metal surfaces. In the following section we will briefly discuss about the methods which allow covalent modification of surfaces such as carbon (Downard 2000; Maeda 2011) silicon, semiconductors (Wayner 2002) and metals (Palacin 2004) by organic materials.

The formation of covalent bonds between a solid surface and an organic molecule through carbon would seem quite easy to achieve in accordance with the general organic chemistry concepts. In actual practice, however, there are only few methods that can be used for such covalent bond formation. These methods include: (1) electrochemical oxidation of amines, alcohols or carboxylates (Hernández 2014), (2) oxidative electrolysis of hydrazides (Pinson 2005), (3) gas phase hydrogen radical reactions (Kuo 1999), (4) thermal reactions under ultrahigh vacuum conditions (Nakamura 2004) and (5) photochemical irradiation (Nakamura 2004). For example, electrochemical oxidation of amines (RNH_2) in the presence of carbon leads to modification of the above surfaces by NHR group (Hernández 2014). Similarly Carbon-OR modified surfaces can be prepared by oxidation of alcohols (ROH) in the presence of carbon surfaces (Maeda 2011) and Carbon–R surfaces can be prepared by the oxidation of carboxylates ($RCOO^-$) if the surface is glassy carbon (GC) or highly oriented pyrolitic graphite (HOPG)(Maeda 2011).

Hydrogenated silicon surfaces are easier to derivatize compared to carbon surfaces. This is due to the fact that the Si-H bond ($D° \sim$ 330-380 kJ mol^{-1}) is weak compared with the aromatic C-H bond ($D°$ = 460 kJ mol^{-1}) ($D°$ is bond-dissociation energy). As with carbon surfaces, several chemical, electrochemical, thermal and photochemical methods are available for the modification of porous silicon surfaces (Wayner 2002). Si-R (R is an alkyl chain with functional groups) modified surfaces will form during these reactions.

Covalent modifications of metal surfaces are more difficult compared to that of silicon and carbon. This often leads to the formation of weak organic-metal surface bonds as in the case of self-assembled monolayers (SAMS) formed on gold or copper with thiols (ΔG_{ads} = -21 kJ mol^{-1}) (Finklea 1996) (ΔG_{ads} is free energy change). Hence the above mentioned methods have little practical uses for metals. Therefore methods which give strong bonds are necessary in the cases of metals. Two methods are available for the formation of such strong bonds which are: (1)

Electrochemical reduction of vinylic compounds $H_2C=CHR$, in aprotic medium and (2) reduction of diazonium salts. Reduction of vinylic compounds usually gives comparatively strong metal-carbon bonds (Palacin 2004). Using this method several metals (nickel, iron, etc.) can be covalently bonded to thin polymeric layers. The second method, which is reduction of diazonium salts, is the subject matter of this thesis and hence is discussed in detail below.

1.5.1 Attachment of organic layers on solid surfaces using diazonium salts

Pinson and co-workers have recently reviewed the grafting of aryl groups onto electrode surfaces through the electrochemical reduction of aryl diazonium salts (Pinson 2005). Aryl diazonium salts can be easily reduced because of their electron deficient nature. The diazonium salt decomposes almost spontaneously upon receiving an electron to give aryl radicals and dinitrogen as shown in equation 1.9.

$$Ar-\overset{\oplus}{N}\equiv N \; + \; e^{\ominus} \longrightarrow \; (\overset{\bullet}{Ar}) \; + \; N_2 \qquad (1.9)$$

Aryl radicals thus produced are very reactive and undergo the usual radical reactions. If the reduction reaction is performed electrochemically, the local concentration of aryl radicals will be very high at the electrode surface and this results in the grafting of these radicals on to the electrode surface. This method has been exploited for the modification of solid surfaces such as carbon [carbon fibers (Delamar 1997), carbon black (Allongue 1997), carbon nanotubes (Dyke 2003), HOPG (Liu 1995; Kariuki 2001), diamond (Wang 2004)], semiconductors [Si (de Villeneuve 1997; Allongue 2003), GaAs (Stewart 2004)] and metals [Au (Paulik 2007; Liu 2007), Pt (Bernard 2003), Fe (Shimura 2006), Zn (Bernard 2003), Cu (Hurley 2004), Pd (Stewart 2004) etc.].

The nature of bonding between the solid (metal, electrode or semiconductor) substrate and organic residues was studied by several groups. Pinson *et al*. (Pinson 2005) showed that the organic-coated metal surfaces can withstand ultrasonic treatment, which was taken as evidence for the presence of strong covalent bonds between the substrate and organic residues. It was observed that the grafted organic layer resists ultrasonic cleaning in a variety of solvents such as acetonitrile, dimethyl

formamide, dimethyl sulfoxide, benzene, benzonitrile, acetone, methanol, ethanol, dichloromethane and chloroform for 15 minutes and it was stable for one month under ambient conditions (de Villeneuve 1997). 4-Bromophenyl layers on Si surface could resist HF (40%) for two minutes and NH_4F (10 M) for one minute (Kariuki 2001; Stewart 2004; Hurley 2004; Combellas 2005). 4-Nitrophenyl modified carbon surfaces could produce Auger signals for the aromatic layer even at 700 K under ultra-high vacuum (Combellas 2008). The possibility of any weak interaction (such as *van der* Waals or hydrogen bonding) being responsible for stabilizing the organic layer on the solid surfaces was excluded based on the observation that the organic layer can be removed only by mechanical polishing or by scratching with an AFM tip.

Reaction of *in situ* generated aryl radicals with surfaces can lead to formation of multiple layers as shown in Scheme 1.2, which results in increasing layer thickness with time. Electron transfer followed by dinitrogen elimination results in the formation of the aryl radical, which can get grafted onto the electrode surface (Scheme 1.2). When a second aryl radical is generated it can attack either the electrode surface or the already attached aryl ring. The latter reaction results in the formation of a cyclohexadienyl radical which upon elimination of a proton and an electron can get aromatized. These reactions can be accomplished either through an electron transfer to the electrode or the diazonium salt followed by the loss of a
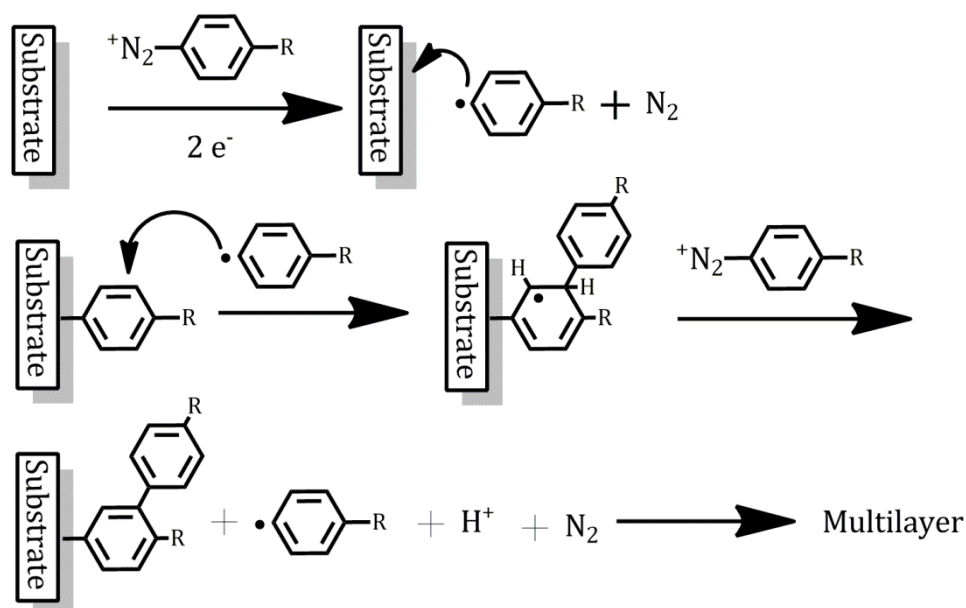
Scheme 1.2 Mechanism of multilayer formation.

proton. If excess diazonium salt is present, the sequence of reactions ultimately lead to formation of thick polyphenylene coating on the surface (Pinson 2005).

Detailed studies on multiple layering during diazonium reduction process were performed by Podvorica and co-workers (Combellas 2005). They observed that substituent position in the aryl ring exerts a remarkable influence in the multi layering process (Scheme 1.3). Grafting of the aryl group will not occur if the 2- and 6- positions of the diazophenyl group are occupied by methyl groups. This is most probably due to the steric protection afforded by the 2- and 6-methyl groups. If the *meta* and *para* positions of the grafted ring are unsubstituted formation of multiple layers can occur. If the *para* position is substituted, the incoming aryl radicals can target the free *meta* position, resulting in multilayer formation. If both the *meta* positions are blocked with bulky substituents such as tert-butyl groups, multiple
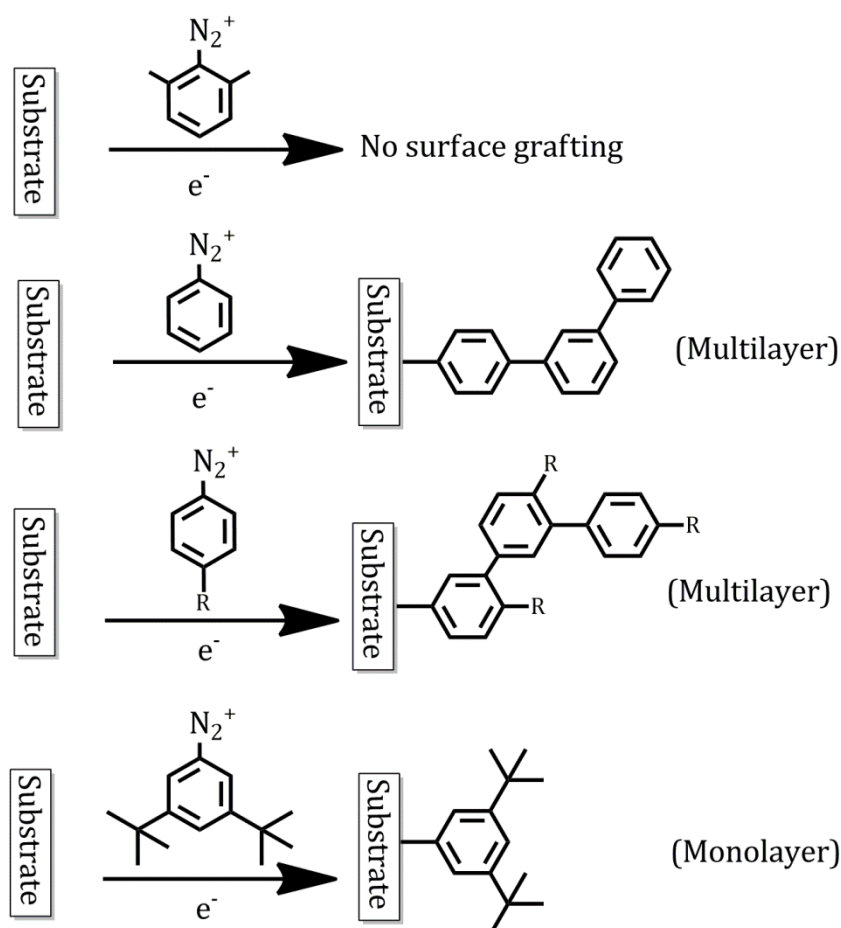
Scheme 1.3 Effect of substituent position on the surface grafting of diazonium salts

layering will not occur. In this case, even though the para position of the initially attached phenyl ring is free, the steric crowding provided by the two bulky meta substituents prevents the attack of aryl radical at the para position.

A comparative study for assessing the stabilities of diazonium and thiol modified gold surfaces was carried out by McDermott and co-workers (Shewchuk 2009). Gold surfaces were treated with 4-nitrobenzenethiol and 4-nitrobenzene diazonium salt to get the thiol and diazonium stabilized surfaces. The surfaces were subjected to various treatments like vigorous sonication, refluxing in different solvents and chemical displacement reaction with octanethiol. Partial ligand desorption were observed from both surfaces under sonication and refluxing conditions. Complete ligand displacement was observed for the thiol modified surface in presence of octanethiol. The extent of ligand displacement was much less for the diazo derived surface, which suggests that the diazonium derived films have better stability over the thiol monolayer analogues.

1.5.2 Some applications of electro grafting of diazonium salts

Covalently bonded organic layers formed by electro grafting of diazonium salts have a number of applications. Some possible uses are given in this section. Molecular junctions, made by connecting molecules on both sides to a conductor, are part of different possible molecular electronic devices. McCreery constructed electronic circuits having molecular junctions using the diazonium salts (Solak 2002). He constructed such device by sandwiching nitroazobenzene between carbon surface and a mercury contact as shown in Scheme 1.4. The carbon surface used is pyrolized photoresist deposited on Si. The organic group used was nitrobiphenyl. He bonded nitrobiphenyl to the carbon surfaces by reduction of the corresponding diazonium salt. It is also possible to attach phenyl, fluorenyl, anthracenyl or biphenyl by the same method. The remaining contact is made by a mercury drop. Better contact can also be made by a deposited layer of titanium protected by a second layer of gold. They studied the behavior of the devices in the absence of solvent or supporting electrolyte in the junction. It is found that, a conductance switching is observed if the potential between the two conductors is varied. Covalently bonded aryl layers have high stability and low energy barrier for the injection of electrons between the metal and organic molecule. Hence such devices will open up interesting properties in the molecular electronic devices.
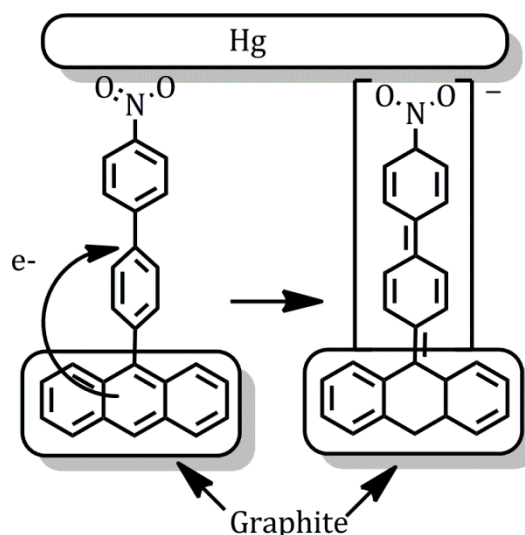
Scheme 1.4 Molecular junction formed by sandwiching nitrobiphenyl between carbon surface and a mercury drop.

Nanotubes are interesting class of materials currently investigated for their possible use in molecular electronics as well as for the formation of composite materials. A major problem associated with these materials is their low solubility which makes their processing very difficult. One of the possible solutions to overcome this problem is sidewall derivatization. Tour and co-workers were able to use diazonium chemistry to derivatize single walled nano tubes (SWNT) (Bahr 2001; Dyke 2003). Through XPS analysis they had shown that polyaryl chains can be grown on the walls of the nanotube. Through Raman analysis they found that multilayer functionalization is also possible. The best soluble carbon nanotubes were obtained by grafting 4-*tert*-butylphenyl groups from the corresponding diazonium salt. Study of viscoelastic properties of dispersions of the material obtained from SWNTs modified with $-C_6H_4COOC_{10}H_{20}OH$ in a polystyrene matrix showed that these are behaving like true composites (Mitchell 2002). This composite behaviour confirms the formation of a percolated SWNT network structure. This network formation is an interesting result since the underivatized SWNTs behaves like unfilled polymer.

It is also observed that further chemical modification of surfaces, which were initially modified through the diazonium route, is very easy. One of the best examples of such modification is shown in Scheme 1.5 (Coulon, 2002). In earlier

studies functionalized styrene-divinyl benzene beads were used as the surfaces to conduct majority of combinatorial chemistry. During the process these beads will be subjected to numerous consecutive chemical reactions and finally the desired molecule will be cleaved from the bead. It has been found that carbon felt modified by chloromethylphenyl group through the electrochemical reduction of the corresponding diazonium salt can be used for such combinatorial reactions. As shown in Scheme 1.5 initial grafting of diazonium salt will give **5**. The chlorine atom on the grafted organic moiety can undergo nucleophilic substitution with bromobenzenethiolate to form the modified surface **6**. Under Suzuki reaction conditions **6** leads to the formation of **7**. Electrochemical reduction of the C–S bond will result in the cleavage of the product biphenyl derivative **8**. Since the surface used is a conductive carbon material it is very easy to perform the final electrochemical cleavage.
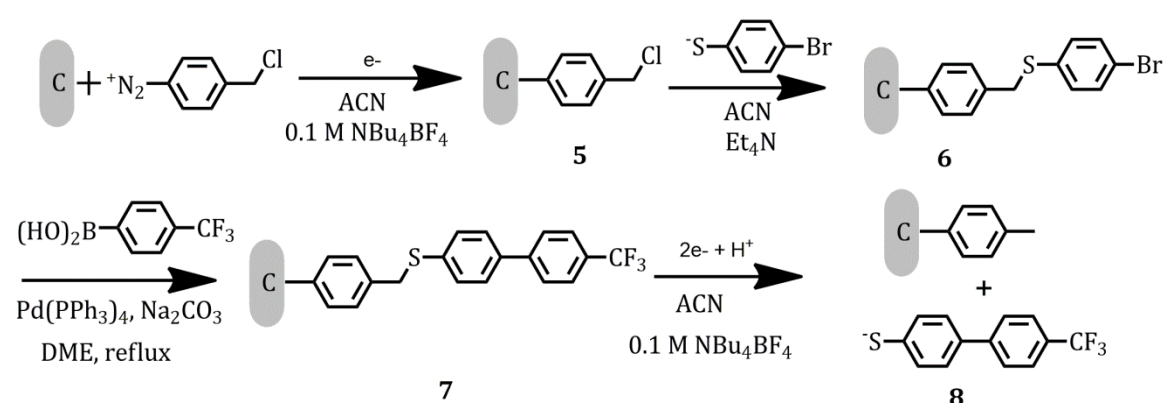
Scheme 1.5 Carbon felt modification by chloromethylphenyl group through reduction of diazonium salt and further using it for combinatorial reactions.

Corrosion resistance of iron surfaces can also be improved by the post-functionalization of modified surfaces (Chaussé 2002). This can be achieved by binding polymers to the organic molecules initially grafted onto the iron surface by diazonium salts (Adenier 2002). Another interesting application of surfaces electro grafted with diazonium salts is that they can be used for the preparation of derivatized electrodes. These electrodes will be able to respond specifically to a given substance. Nanomolar level detection of dopamine is the best example of such use. Detection and measurement of nano molar levels of dopamine in extracellular

fluids of the central nervous system, especially in the presence of higher concentrations of ascorbic acid (200–500 mM), is highly challenging because both these compounds are oxidized at nearly the same potential. With carbon electrodes modified using *p*-phenylacetate groups it was possible to detect dopamine (20 mM) in the presence of ascorbic acid (2 mM) at pH 7.4 (Downard 1995). This modification can be easily achieved through electro grafting of the corresponding diazonium salt. The electrodes grafted with cathechol by post-functionalization of 4-carboxy or 4-amino phenyl groups also showed similar selectivity (Bath 2001). This selectivity is due to the difference in electrostatic interaction between the anionic surfaces of the electrode with dopamine and ascorbic acid. At this pH dopamine is mono-cationic while ascorbic acid is anionic.

1.6 Origin of the work

Our group has exploited the potential of diazonium salts to form covalent bond to metal surfaces to synthesize Au and Pd nanoparticle-cored dendrimers (NCD) in which Au and Pd-NCDs are stabilized with metal–carbon covalent bonds (Kumar 2010; 2011; 2012). The Pd–NCDs were found to be excellent catalysts for hydrogenation as well as C-C bond forming reactions (Kumar 2011; 2012). Our group also used the AuG1 NCD, in which the Fréchet-type dendrons assembled on the surface of the gold nanoparticle in close proximity to each other, for the preparation of stable covalently cross-linked organic nanoparticles (Krishnakumar 2014). These covalently cross-linked organic nanoparticles were prepared through a sacrificial template assisted synthesis method. AuG1 NCD is found to be excellent material for the preparation of organic nanoparticles in this way. In this method diazonium chemistry was initially used for the preparation of AuG1 NCDs. In the second step, the gold core was removed within a short time to generate large number of dendron radicals in a small volume to form covalently cross-linked organic nanoparticles. This material exhibited stimuli responsive morphological transformations for encapsulation and controlled release of the guest molecules.

We have attached ruthenium complexes onto the surface of organic nanoparticles again by using the diazonium grafting methodology. Diazonium group-substituted *tris*-bipyridylruthenium(II) complex was reduced with sodium borohydride in the presence of the organic nanoparticles. The tris-

bipyridylruthenium complex radical generated get attached to the organic nanoparticles.

In the above mentioned cases we have exploited either the ability of diazonium salts to form covalent bonds with surfaces as in the case of NCDs or the ability for the self-coupling of the radicals generated as in the case of covalently cross-linked organic nanoparticles. In the present thesis, we have explored the possibility of exploiting the reaction further by using bis-diazonium salts. The diazonium salt used in this work is 4,4'-biphenylene-bis-diazonium tetrafluoroborate (BPBDT). We reduced the bis-diazonium salt in the presence of metal salts. Reduction of the metal salt resulted in the formation of metal nanoparticles and reduction of the bis-diazo salt led to formation of bis-biphenylene radicals as shown in Scheme 1.6. The bis-biphenylene radical is highly reactive and undergoes rapid radical–radical coupling or addition to the *ortho* or *meta* positions of phenyl rings to create a complex organic polymeric framework. These radicals can add to the metal nanoparticles also through metal-C covalent bonds, which would lead to entrapment of the nanoparticles in the organic framework. We have designated these structures as Metal-Nanoparticle-linked Organic Frameworks (MNOF). The microporous organic framework formation as well as nanoparticle insertion into the framework could be accomplished in a single reduction step as shown in Scheme 1.6. It may be noted that the actual MNOF structure is uncertain and the structure shown is only one of the several possibilities.
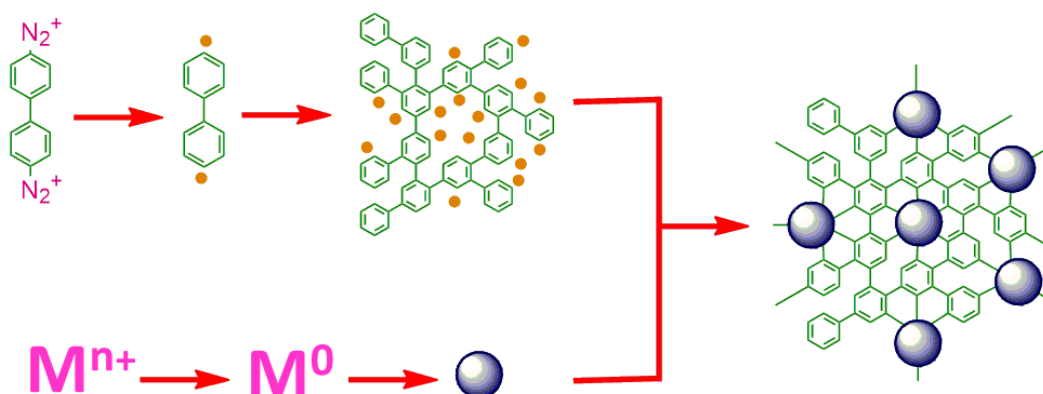
Scheme 1.6 Possible mechanism for the formation of MNOF.

In Chapter 2 of the thesis we describe the synthesis, characterization and catalytic applications of Pd-nanoparticle linked organic frameworks (PNOF). PNOF were found to be good catalysts for reduction reactions and Suzuki reactions. These reactions are also studied in Chapter 2. In Chapter 3 of the thesis we report the synthesis and characterization of copper nanoparticle-linked organic frameworks (CNOF). The CNOF were found to be good catalysts for click reactions. Use of CNOF in various click reactions is studied in detail in Chapter 3. The MNOFs reported here can be considered as examples of supported metal nanoparticles. Usually supported metal nanoparticle preparations are tedious and involve several steps. A brief discussion about supported nanoparticles is given in Section 1.7 in order to compare the catalytic activities of these materials with the MNOF reported in this work.

If reduction of the bis-diazonium salt is performed in the absence of any metal salts, we expect random radical addition and substitution reactions of the biphenylene diradical to give an organic framework as shown in Scheme 1.7. Since the radical addition or substitution can occur only in the plane of the aromatic ring, the resulting structure would be a two dimensional material. If these two dimensional framework is subjected to Scholl oxidation reaction intramolecular C-C bond formation will take place leading to formation of a planar, fully aromatic framework as shown in Scheme 1.7. The material formed in this way will be similar to graphene analogs. In Chapter 4 of the thesis we describe our attempts to prepare graphene analogs in this way. The graphene analogs thus prepared were sulfonated to get water soluble materials. The graphene analog and the sulfonated derivative were characterized and their applications were studied. In order to place our work in the proper context a brief discussion of graphene and related materials is given in Section 1.8.
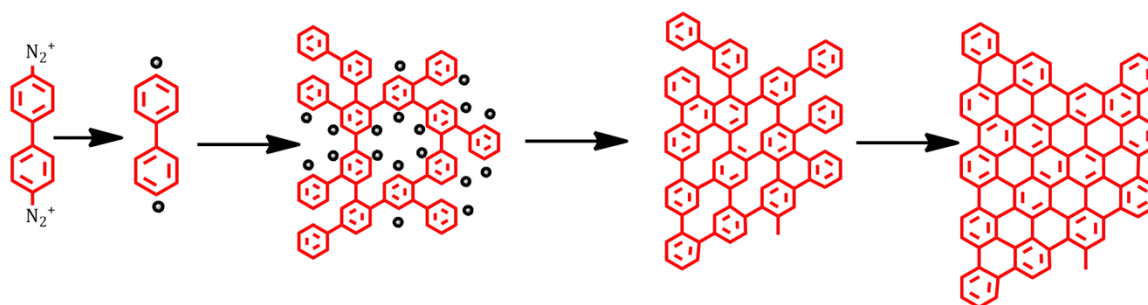
Scheme 1.7 Different reaction steps and possible mechanism for the formation graphitic materials.

1.7 Supported metal nanoparticles

Supported metal nanoparticles are of immense importance in the field of heterogeneous catalysis (Lee 2006; Akagi 2007; Chen 2008; Risse 2008). Nanoparticles of palladium, gold and bimetallic nanoparticles of palladium and gold on various supports have been synthesized and their catalytic applications were studied. Until 1980s gold was considered to be an inactive metal for catalysis. One of the most exciting recent developments in the field of catalysis is the recognition that gold is an extremely good catalytic metal when prepared as supported nanoparticles. At present intense efforts are made to prepare supported metal nanoparticles with specific morphologies that can function as effective, robust and reusable catalysts.

Metal nanoparticles captured in porous materials, such as organic frameworks (Hermes 2005), covalent organic frameworks (Kalidindi 2012), zeolites (Riahi 2002), carbon nanotubes (Meng 2001), polymers (Ogasawara 2010; Price 2005), silica (Parlett 2013), organically modified silicates (Pagliaro 2011) and glass (Schmçger 2008) have wide applications in gas storage (Kalidindi 2012), gas generation (Zhou 2010), gas sensing (Mubeen 2007), and in recyclable catalytic applications (Campelo 2009). For practical applications it is preferable to have small nanoparticles on solid supports. The interactions between nanoparticles and the solid surface are often very weak and, hence, the nanoparticle will leach out irreversibly from these supports limiting their applications as long-lived recyclable systems (Molnr 2011). Moreover, preparations of such materials often require harsh reaction conditions. Hence, for recyclable applications it is necessary to prepare highly stable nanoparticle support under mild reaction conditions.

1.7.1 Advantages of Supported Metal Nanoparticles as Catalyst

Due to the high surface to volume ratio, metal nanoparticles are considered as promising catalysts in chemical synthesis (Roucoux 2002; Min 2007; Arcadi 2008). However, high tendency towards agglomeration and difficulty in separation often create difficulties in catalysis, especially for the ultra-small size particles. The metal nanoparticles that are deposited or synthesized on a support greatly address these problems (Lee 2006; Akagi 2007; Chen 2008; Risse 2008). These supporting materials play a significant role in catalyst performance. Besides its ability to prevent agglomeration of the particles, they also influence the size and shape of the

nanoparticles during synthesis. Finally, the nature as well as the chemical structure of the support itself, along with the interaction between the support and the metal nanoparticles, may also affect the catalysis by metal nanoparticles. For example PNIPAM-grafted Au nanoparticles have an advantage to be dispersed both in aqueous phase and organic phase ($CHCl_3$) depending on the hydrophilicity or hydrophobicity of the polymer brushes (Wei 2007). Another example is the hybrid polymer-grafted metal nanoparticles made by different thiol-terminated polymers which exhibit selective solubility in solvents (Shan 2005). Hence supported nanoparticles open up broader advantages over unsupported ones such as recyclability, easy separation and using of wide range of solvents in reactions. It also contributes towards selectivity over nanoparticles but not upto the extent possible for the specially designed metal complexes.

1.7.2 Factors Affecting the Catalytic Properties of Supported Metal Nanoparticles

The main factors which affect the specific catalytic activity are size of the nanoparticle, number of reaction cycles, and the rate of the catalytic reaction (Ponec 1983; Sachtler 1976; Guczi 1994). Another factor is the support that can change the properties of supported nanoparticles by affecting their electronic and crystal structure. The electronic properties of a metal nanoparticle depend on the number of atoms constituting it. Nanoparticles of 20-25 atoms have increased ionization energies reaching 1-1.5 eV, and this increase in ionization energy will decrease the electron affinity by 2–3 eV (Stakheev 1999). Hence the adsorption energies of nucleophilic molecules such as alkenes or alkynes on the catalyst surface can vary considerably. This can affect the activation of the substrate towards reactions. Sometimes the strong adsorption can lead to blocking of the particle surface and thus decrease the catalytic activity of the substrates.

Changing particle size changes the coordination numbers of surface atoms. The surface of large sized particles most probably contains crystallographic planes having atoms with high coordination numbers. On the other hand, in small particles surface atoms will reside on the edges of the crystallographic planes or on edge junctions. As a result, reactions involving surface metal atoms strongly depend on the size of catalyst particles. This dependence is related to the geometric effect.

Furthermore, the absorption energy on low coordinated atoms is much higher compared with that on a plane surface.

The electronic and crystal structure of metal nanoparticles is affected by the support surface (Homeyer 1990). In addition, increasing metal-support interaction energy can affect the shape of metal nanoparticles. When the interaction energy is low, the particle shape is determined by the most favourable crystallographic configuration. For example palladium with an edge-centred lattice prefers a cube-octahedron shape. As the interaction energy increases, preference is given to a planar shape allowing a larger nanoparticle-support surface contact. Thus, the particle–support interaction affects the surface area and relative shares of different crystallographic edges available for reaction.

1.7.3 Catalytic Activity of Palladium nanoparticles

Catalytic activity of metal nanoparticles supported on the acid form of zeolite was first reported in late 1960s for the hydrogenolysis of neopentane (Sinfelt 1960; Gray 1967; Mojet 1996). Homeyer *et al.* showed that the catalytic activity of palladium nanoparticles supported by the acid form of zeolite Y in the hydrogenolysis of ethane is 5-10 times higher compared with the Pd/NaY system and two orders of magnitude higher than with the Pd/SiO_2 system (Homeyer 1989; Stakheev 1991). On the other hand it was found that the number of cycles of the neopentane hydrogenolysis reaction on metal nanoparticles supported on an alkaline support like zeolite KL decreases, as the alkalinity of the support is increased (Sachtler 1992; Moretti 1992). These results clearly indicate that, the support affects the catalytic activity of Pd nanoparticles. They become electron-deficient on acidic supports and electron-excess on alkaline supports.

Quantitative differentiation between effects associated with nanoparticle size and effects associated with metal–support interaction were studied by monitoring the catalytic activity of palladium nanoparticles of the same size and shape but with widely varied electronic properties for the neopentane hydrogenolysis reaction (Figure 1.1.) (Alexeev 1998; Lin 1993). X-Ray photoelectron spectroscopy was used to establish that the higher the local concentration of Brønsted acidic centers, the higher the positive charge on palladium nanoparticles. The specific catalytic activities of encapsulated nanoparticles in the neopentane hydrogenolysis reaction are compared in Figure 1.1. The neopentane hydrogenolysis rate increases two

orders of magnitude in going from Pd/NaY to Pd/NaHY and Pd/HY. Therewith, the reaction temperature shifts by 50–60 °C to the low-temperature range.
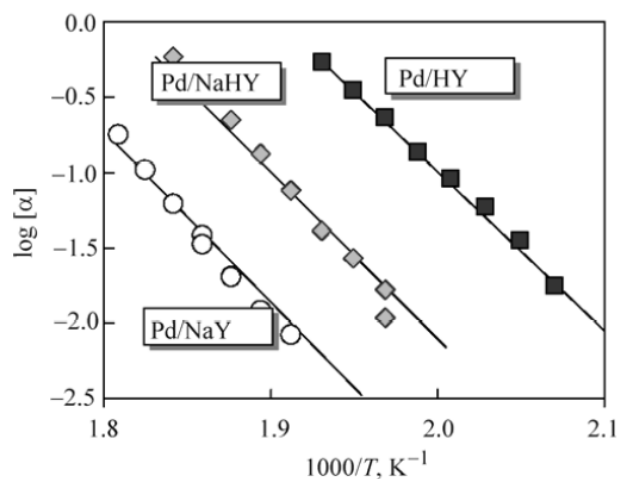
Figure 1.1 Effect of electron deficiency of supported palladium nanoparticles on specific catalytic activity (α) in neopentane hydrogenolysis (Reprinted with permission from the ref. Stakheev 2010).

In the hydrogenation of aromatic hydrocarbons, however, geometric factors affect the specific catalytic activity of metal nanoparticles only slightly, except for ultrafine (3–6 atoms) nanoparticles which are virtually inactive in such reactions (Ryndin 1988). Substituted aromatic compounds such as toluene are more nucleophilic than benzene and as a consequence more sensitive to the electronic structure of metal particles. Thus, the rate of benzene hydrogenation catalysed by supported metal nanoparticles, increases 2–3 times in going from the acidic aluminium silicate to SiO_2 support and the rate of toluene hydrogenation increases 5-6 times (Sárkány 1986; Silvestre-Alberto 2005). Corma and co-workers studied the catalytic activity of palladium on a mesoporous MSM-41 silica and Y zeolite in naphthalene hydrogenation to show that Pd/HY exhibits a higher specific activity due to the interaction of Pd nanoparticles localized in large zeolite cavities with strong Brønsted acidic centres (Corma 2004; 2005). The high activity of electron-deficient nanoparticles in aromatic hydrogenation is associated with a change in the nature of hydrogen adsorption (Corma 1997; Han 2007).

The rate of palladium-catalysed alkene and alkyne hydrogenation is affected much even if palladium nanoparticles are supported on an inert support, i.e., in the absence of a strong electronic palladium- support interaction. The specific activity drastically decreases, when the size of nanoparticle gets below a certain limit. This phenomenon is especially pronounced with 3 - 5 nm range (dispersity 0.2 – 0.4) (Papp 2005; Ma 2008; Yang 2009; Feng 2010; Wang 2010). Larger nanoparticles are more active, even though the number of metal atoms available for reaction decreases. The Pd/Al_2O_3 catalyst with a medium dispersity of metal particles showed the highest activity in alkyne hydrogenation reactions (Ungureanu 2008). In the hydrogenation of olefins with a longer hydrocarbon chain (C > 4), a slightly stronger dependence of the specific catalytic activity of nanoparticles on their size is observed. Model Pd/Al_2O_3 systems were used to show that the specific catalytic activity in *n*-pentene hydrogenation increases 4 - 5 times as the nanoparticle size increases from 1 to 5 nm (Liu 2008).

Semi hydrogenation of 1,3- butadiene is a typical example of the effect of size of supported Pd nanoparticles on selectivity (Sarkany 1995; Cervantes 2003). Semi hydrogenation of 1,3- butadiene employing Pd catalyst can take place by either 1,2 or 1,4 addition to produce 1-butene or 2-butene, respectively. The proposed reaction intermediates and the reaction routes suggested by *Wells et al.* (Phillipson 1969; Bates 1970) are shown in Scheme 1.8a. Boitiaux *et al.* (Boitiaux 1987) have proposed another interpretation as shown in Scheme 1.8b.

It is found that, as the size increase from 2 to 8 nm, selectivity toward 1-butene increases which indicates the effect of size on selectivity. 1,2-hydrogen addition favors over 1,4-addition on increasing the size. Structure of the nanoparticle also affects the hydrogenation of 1,3-butadiene. This sensitivity arises due to the face of nanoparticle available for the reaction. It is found that the activity increases in the order Pd(111) < Pd(100) < Pd(110) (Alberto 2005; Katano 2003).

Supported palladium nanoparticles are known to catalyse important carbon-carbon cross coupling reactions such as Heck reactions, Suzuki-Miyura coupling and Stille coupling reactions. For the Heck coupling reactions, the alkenylation of aromatic compounds through the reaction of substituted aromatics and alkenes, (Scheme 1.9) Pd nanoparticles supported on silica (Aksin 2006; Niembro 2008; Papp 2005; Ungureanu 2008) are found to be good catalysts. Both amorphous
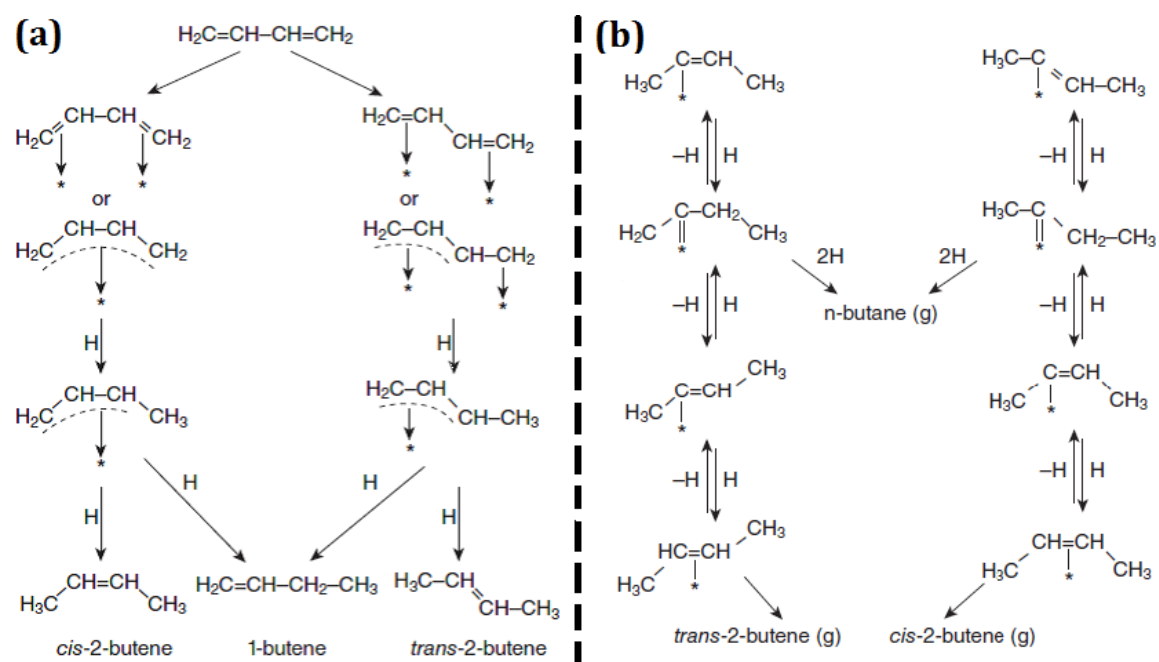
Scheme 1.8 Possible mechanism of hydrogenation of 1,3- butadiene proposed by (a) Wells and (b) Boitiaux (reproduced with permission from the ref. Zhang 2011).

(Aksin 2006; Niembro 2008) and ordered (Papp 2005; Ungureanu 2008) silica materials were found to be useful supports for palladium nanoparticles. For better activity the silica supports required modifications such as a long-chain alkyl groups to make the matrix hydrophobic. Catalytic efficiency of the materials, having palladium nanoparticles on various other inorganic supports such as carbon and metal oxides were also investigated (Martínez 2005; Kantam 2006; Monopoli 2010). Catalytic efficiency of various polymer supported nanoparticles was also studied (Cui 2005; Alacid 2006). Polymeric materials can be equally useful as shown by the performance of polystyrene-based catalysts with palladacycle (Herrmann 1999) and anchored N-heterocyclic carbene (NHC)-Pd complexes (Broggi 2008).
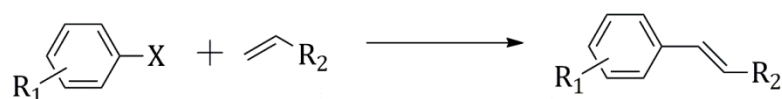
Scheme 1.9 Heck Coupling.

The Suzuki- Miyaura, the cross-coupling reactions between aromatic or vinyl halides and boranes, boronic acids, or esters to form biaryls, were also studied extensively using supported palladium nanoparticles as catalysts (Scheme 1.10). The major supports are silica (Yang 2006; MacQuarrie 2010), polymer (Ohtaka 2009; Cho 2006) and various inorganic materials (Maegawa 2007; Amoroso 2010). Among these Pd nanoparticles on silica (0.48 % Pd- SiO_2), on polystyrene (26.6 % Pd- PS), on polystyrene-co-polyvinylpyridine core-shell structure (Pd-PS-co-PVPy) and on organostannoxane-based materials (Pd-Sn-dendr1 and Pd-Sn-dendr2) were found to be very good catalysts for Suzuki reactions.
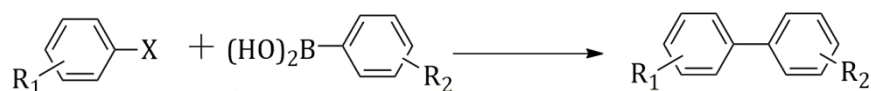
Scheme 1.10 Suzuki Coupling.

Stille coupling, the palladium-catalysed coupling of organo-stannanes with organic halides (Scheme 1.11) has been studied less frequently and applied less widely when compared to the Heck and Suzuki reactions. The results of recycling studies with silica supported Pd particles for Stille reactions were very promising. 0.48 % Pd- SiO_2 which was found to be very good catalyst for Suzuki reactions was also found to be very suitable to perform the Stille reactions (Tsvelikhovsky 2008; Badetti 2008).
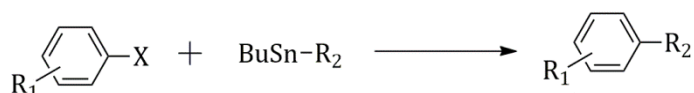
Scheme 1.11 Stille Coupling.

In recent years metal organic frameworks (MOFs) and covalent organic frameworks (COFs) are used as support for the palladium nanoparticles (Opelt 2008; Gao 2010; Zhang 2012; Huang 2001; Yuan 2010). In this regard, MOFs offer several advantages derived from their three dimensional structures and organic linkers that stabilize palladium nanoparticles in addition to their robust nature and

moderate thermal stability. Although, more information is needed to assess the robust nature of MOFs as host materials to embed palladium nanoparticles, MOFs containing palladium nanoparticles have shown excellent activity for many organic reactions. Supported palladium nanoparticles are found to be efficient heterogenous catalysts for the several hydrogenation and carbon-carbon bond forming reactions. Even though the rates of these reactions are somewhat low compared to homogenous catalysts, the recyclability and purification of catalyst are found to be highly efficient.

1.8 Graphene

Graphene (2D graphite) is one of the materials that was "rediscovered" several times similar to carbon nanotubes. Single layer graphene was reported for the first time in 1968 (Morgan 1968), but in 1960s itself Boehm reported single and few layers of graphene oxide. Theoretically, graphene has been studied and used for describing properties of various carbon-based materials for sixty years (Wallace 1947; McClure 1956; Slonczewski 1958). Forty years later it is realized that graphene provides an excellent condensed-matter analogue of (2+1)-dimensional quantum electrodynamics (Semenoff 1984; Fradkin 1986; Haldane 1988) and since then it became a thriving theoretical toy model. Even then it was presumed not to exist in the free-state and considered only as an integral part of 3D materials like fullerenes and nanotubes (Fradkin 1986). These general beliefs were suddenly changed and the free standing layer of graphene turned into reality by the outstanding work of Novoselov and co-workers (Novoselov 2004; 2005). The confirmation of its charge carriers as massless Dirac fermions (Novoselov 2005[b]; Zhang 2005) was an outstanding achievement and since then the graphene 'gold rush' has begun. In 2010, Geim and Novoselov received the Nobel Prize in Physics, for the "groundbreaking experiments regarding the two dimensional material, graphene" (http://www.nobelprize.org/nobel_prizes/ physics/laureates/2010). It is for their study published in 2004 and not for "discovery" of graphene as often misunderstood (Novoselov 2004). An intriguing and detailed history of graphene can be obtained from the review articles published by Dreyer *et al.* (2010) and Boehm *et al.* (2010).

The term "Graphene" is given to a flat monolayer of carbon atoms closely packed into a two-dimensional (2D) honeycomb lattice. It is a basic building block

for all other-dimensional graphitic materials (Figure 1.2; Geim 2007). The International Union for Pure and Applied Chemistry (IUPAC) defines graphene as "a single carbon layer of graphite structure, describing its nature by analogy to a polycyclic aromatic hydrocarbon of quasi-infinite size" (Fitzer 1995). In the current literature the word "graphene" is hardly adhered to this definition and used to label a wide variety of carbon materials. These materials deviate in various ways from the IUPAC definition. The main four deviations are: (i) the number of layers of graphene is often more than one ("single layer" parameter is violated), (ii) a large sheet of "graphene" build up from the fragments of small single or few layer graphene "stitched" together at grain boundaries ("quasi-infinite size" parameter is violated), (iii) chemically modified graphene materials of various thickness or with a large amount of heteroatoms, mostly oxygen-containing groups and (iv) damaged graphene sheets with nanometer crystallite size or contain a large amount of defects such as sp^3- hybridized carbon atoms and physical holes with close resemblance to amorphous carbon.
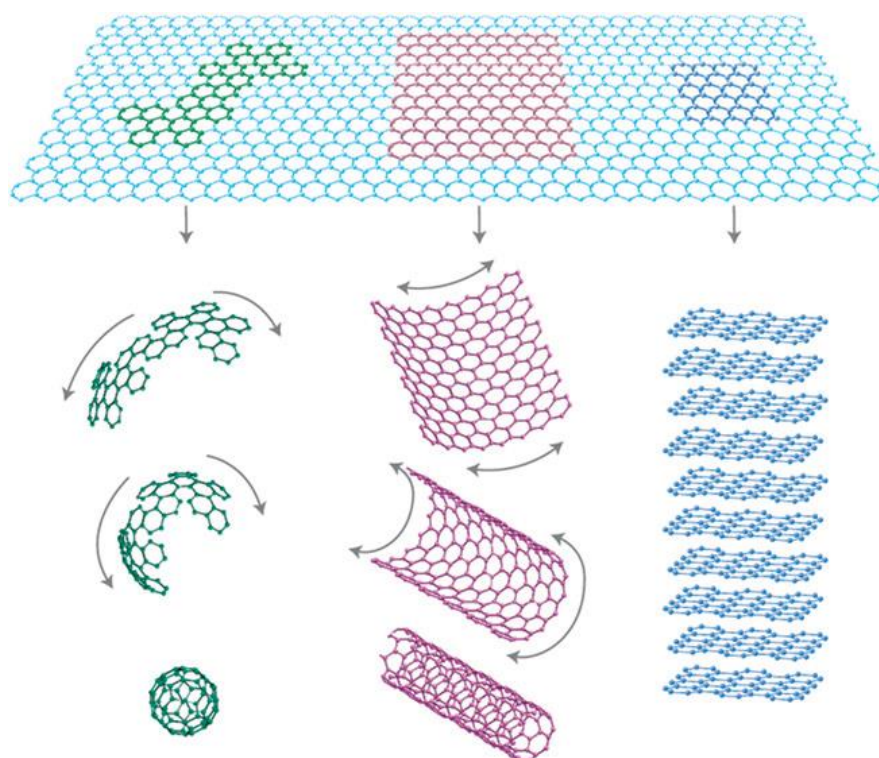
Figure 1.2 Graphene: mother of all graphitic forms. (Reproduced with permission from the ref. Geim 2007).

1.8.1 Classification

Graphene based materials can be broadly classified into four categories namely 0D (fullerenes), 1D (nanotubes), 2D (Graphene) and 3D (Graphite). The basic building block, 2D graphene, of all these materials is the most unstable among all the four. Free standing 2D Graphene will not exist and transform into any one of the other three forms. 2D graphene can be further classified into three according to the number of layers. They are (1) single layer, (2) few layers (no. of layers between 2 and 9) and (3) multilayer (≥10 layers). The IUPAC definition of graphite (Fitzer 1995) requires long range staking of graphene layers along the z-axis in ABA or ABC order. This condition is in some cases quite often not fulfilled as in the case of multilayer graphene and such material can be called as ultrathin graphite (Tiberj 2001; Lenski 2011). The properties of graphene will depend on the change in dimensionality as well as with the number of layers.

1.8.2 Properties

Long-range π-conjugation in graphene provides extraordinary thermal, mechanical, and electrical properties. These have been the interest of many theoretical studies for quite a long time and became an exciting area for experimentalists recently. People even used the graphene based materials as catalyst for several reactions like esterification (Navalon 2014). Even though graphene is considered as a good alternative for materials in various fields, due to the high cost of production of good quality graphene scientific community is now focusing mainly on the research for the production of good quality graphene and their electrochemical applications.

1.8.3 Preparation of Graphene

A number of synthetic methods have been developed for the production of graphene. Each of these methods produce graphene with different characteristics and possessing different scalability. This difference in characteristics influences its properties. Hence the properties of the graphene depend somewhat on its origin. The preparation methods of graphene can be broadly classified into (i) top-down and (ii) bottom-up methods which are summarized in scheme 1.12. The top-down methods generally include the exfoliation of graphite aiming at weakening of the *van der* Waals forces between the graphene layers. The exfoliation of graphite can be made possible through several methods. This includes mechanical (e.g., Scotch tape),

chemical (e.g., solution-based exfoliation, graphite oxide exfoliation/reduction), and electrochemical (oxidation/reduction and exfoliation) processes. Nowadays the fabrication of graphene nano ribbons achieved by opening of CNTs became a special category of process under the top-down approach. This unzipping of CNTs can be achieved through chemical or thermal routes. In the bottom-up approaches single or few layer graphene structures were generated through assembling the small molecular building blocks by means of catalytic (e.g., CVD), thermal (e.g., SiC decomposition), or chemical (organic synthesis) processes.
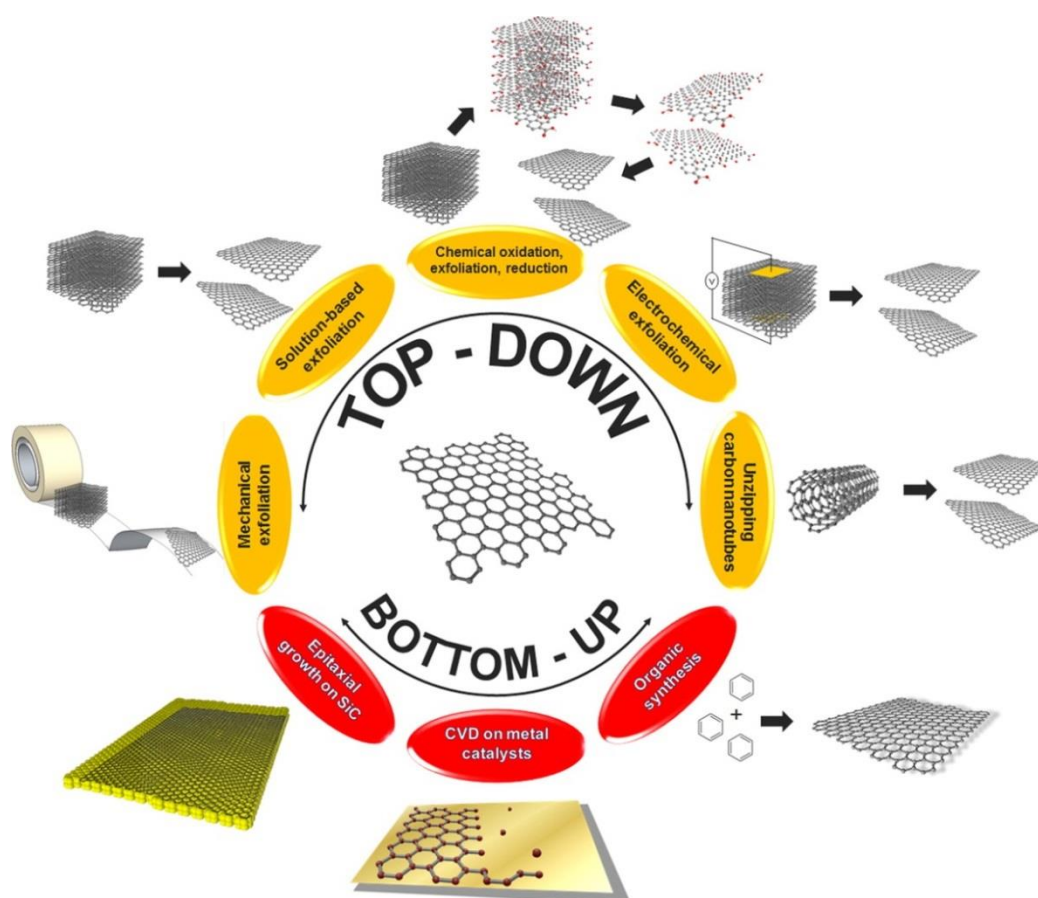
Scheme 1.12 Illustration of the current preparation methods for graphene and graphene- related materials (Reproduced with permission from the ref. Ambrosi 2014).

1.8.3.1 Top-down Methods

Graphite is highly anisotropic in nature. In a single graphene sheet carbon atoms are linked through sp^2 bonds in a honeycomb lattice network with interatomic distance of 1.42 Å. When it comes to graphite crystal along the z-axis the

graphene sheets are held by weak van der Waals forces with 3.35 Å interlayer distances. Hence it is very much possible to exfoliate graphite into smaller units through either mechanical or chemical means. Prolonged exfoliation will ultimately result in single graphene layers. In the following subsections, the most common top-down methods for the preparation of graphene are described.

1.8.3.1.1 Mechanical Exfoliation of Graphite

Micromechanical cleavage of highly oriented pyrolytic graphite (HOPG) is the first method described to isolate single layer graphene (Novoselov 2004). In this method layer of graphene was repeatedly peeled off from HOPG by means of an adhesive tape to get single graphene layer. The monolayer obtained was successively transferred onto SiO_2 wafer surface through a wet or dry transfer technique. This method is commonly known as the "Scotch-tape method". Primary experimental studies on this graphene showed extraordinary electronic (Novoselov 2004; Novoselov 2005; Wu 2007; Guinea 2009), mechanical (Lee 2008) and thermal conductive (Balandin 2008) properties. This simple Scotch-tape method enabled the isolation of single layer graphene with size up to 1 mm with minimal alteration to the graphene sheet (Geim 2009). Since the highest quality achieved so far is through this method, the graphene obtained by this method is considered as pristine. This method for production of graphene opens up wide applications in several branches of science (Geim 2007). However, due to the low reproducibility and lack of potential for large-scale implementation, it can only be used for fundamental studies and basic research. Bulk quantities of materials are required for electrode fabrications for use in electrochemical applications. In addition it is documented that the electron transfer occurs about 10^6 times faster at defects or edge-like portions of carbon materials compared to defect-free planes (Banks 2005; Kampouris 2010). The extremely low density of defects present on pristine graphene will be a significant drawback for the electron transfer applications. Due to these reasons the mechanical exfoliation method is inappropriate for the production of graphene for electrochemical purposes. Hence for practical applications especially for electrochemical applications other production methods should be considered.

1.8.3.1.2 Solution-Based Exfoliation of Graphite

Solution-based exfoliation of HOPG can be achieved by minimizing the energy loss during exfoliation using organic solvents with surface tensions of ~ 40 mJm^{-2}

(Hernandez 2008). Generally adopted treatment to drive the exfoliation is the concurrent ultra-sonication. Coleman and co-workers obtained good quality graphene sheets in N-methylpyrrolidone (NMP) solvent (Hernandez 2008). On the other hand Novoselov and co-workers used N,N-dimethylformamide (DMF) as solvent to obtain a graphene suspension (Blake 2008). Several other polar and non-polar organic solvents have also been investigated (Hernandez 2010). Even though this method can be scaled-up for larger volumes, the maximum achievable yield is generally quite low at the moment. Dai and co-workers achieved about 90% of single layer graphene in DMF by ultra-sonication of tetrabutylammonium hydroxide (TBA) and oleum intercalated graphite (Li 2008). The exfoliation in aqueous medium were also achieved in presence of surfactants such as sodium dodecylbenzenesulfonate (SDBS), sodium cholate (SC) (Lotya 2009; 2010), and 1-pyrenecarboxylic acid (Englert 2009). The major drawback of this method is the breaking of the graphene sheet produced into very small and inhomogeneous flakes due to ultra-sonication. To avoid this spontaneous exfoliation in NMP on graphite preliminarily intercalated with potassium was also studied (Valles 2008). Also spontaneous exfoliation of HOPG in chlorosulfonic acid produced high concentration of single layer graphene up to 2 mg mL^{-1} (Behabtu 2010).

Considering the quality and the ease for large-scale production, solution-based exfoliation of graphite is definitely an appealing approach. However it will produce a large variety of flakes consisting of different number of layers, which will be very difficult for further separation (Green 2006). Also prolonged ultra-sonication will produce small-sized graphene flakes and nanometric graphitic impurities. These impurities can alter the density of edge-like planes which dramatically affects the electrochemical properties (Wang 2013). Surfactants such as sodium cholate used as exfoliating agents remain embedded on the graphene sheets and these can also alter the properties (Brownson 2011; 2011a; Bonanni 2010).

1.8.3.1.3 Electrochemical Exfoliation of Graphite

The electrochemical methods for exfoliation of graphite were known since the 1980s. In those studies aqueous and organic solutions of intercalated graphite were produced by intercalating ions and compounds such as sulfuric acid (Jnioui 1982), Li$^+$ (Takada 1985), F$^-$ (Noel 1994; Takenaka 1987) and Ni^{2+} (Inagaki, 1988).

In the electrochemical exfoliation cathodic (reduction) or anodic (oxidation) potentials or currents were applied in aqueous or organic electrolytes to a graphite-based (usually HOPG) working electrode in the presence of reference (SCE, Ag/AgCl, etc.) and auxiliary (usually Pt) electrodes. Intercalation of negatively charged ions to the oxidized graphite electrode takes place, when a positive potential is applied. Subsequently exfoliation process will take place while applying negative potential. Widely studied electrolytes are sulfuric acid (Su 2011) and poly(styrenesulfonate) (PSS) (Wang 2009). Recently, SDS surfactant in aqueous solution was also studied and produced graphene flakes with 500 nm size and one and two layer thickness (Alanyalioglu 2012). In these studies intercalations were done at +2 V and exfoliation achieved at a potential of -1 V. High anodic potential will produce graphene oxide having large numbers of oxygen functional groups. Number of functional group can be reduced by reversing the applied potential. But that process cannot create defect-less graphene structures (Su 2011). To avoid this limitation cathodic reduction/intercalation method to generate non-oxidized graphene sheets were attempted. In this method initial intercalation of positive ions were achieved without formation of oxygen functionalities by applying a negative potential. Morales *et al*. obtained remarkable results by the intercalation of H_3O^+ ion at negative potentials and perchlorate anion at positive potential using perchloric acid as electrolyte. Stable graphene flake dispersions in NMP were obtained by thermally expanding these intercalated graphites under microwave treatment (Morales 2011). A high negative potential (-15 V) and Li^+ ions in propylene carbonate electrolyte improved the yield to 70% graphene flakes with a thickness of less than five layers (Wang 2011). Further improvement was achieved using a two-stage expansion process. This process involves the initial expansion of graphite in a Li^+ containing electrolyte followed by another expansion in a tetra-n-butylammonium electrolyte by applying -5 V in both stages. In this processes extreme potentials as well as ultra-sonication were not required. Besides this a direct electrochemical functionalization with aryl diazonium salt can also be done on the expanded graphite to provide functionalized graphene sheets (Zhong 2012).

Compared to other methods electrochemical exfoliation has the advantage that this method is more environment friendly, need only ambient conditions, can be controlled by varying the applied potential/current, and generally very fast. One of

the major disadvantages is the introduction of oxygen functional groups which have profound influence on the electrochemical properties of the graphene produced. Similar changes in electrochemical properties also occur by the irreversible "functionalization caused by the use of surfactants (Brownson 2011; 2011a; Bonanni 2012). Moreover, it is very difficult to get graphene with homogeneous size and layer distribution through this method.

1.8.3.1.4 Chemical Oxidation of Graphite, Exfoliation and Reduction

Chemical route involves the intercalation of chemical species within the graphitic layers followed by a subsequent expansion/decomposition process that forces the layers apart. Well-known chemical approach is the expansion of graphitic layers through oxidative intercalation using strong oxidizing agents in the presence of concentrated sulfuric and nitric acids. In 1859, Brodie, used potassium chlorate as an oxidant to produce graphite containing several oxygen functional groups all over the graphitic sp^2 carbon network structure by introducing several sp^3 carbon atoms (Brodie 1859). This method was improved by Staudenmaier in1898 (Staudenmaier 1898), followed by Hofmann and König in 1937 (Hofmann 1937), Hummers and Offeman in 1958 (Hummers 1958), and lately Tour and co-workers in 2010 (Marcano 2010), to obtain the material known nowadays as graphite oxide (GO) (Dreyer 2010). Staudenmaier, Hofmann and König used potassium chlorate as an oxidizing agent while potassium permanganate was used by Hummers and Offeman, and Tour and co-workers. The second method is more advantageous over the first one since it avoids the formation of dangerous and explosive ClO_2 gas. The oxygen functional group will increase interlayer distance from 3.35 Å in graphite to over 6 Å in GO. Hence a simple ultra-sonication is enough to separate the layers (Dreyer 2010). Isolated sheets of GO is called graphene oxide and the method offers a large-scale production of graphene oxide (Zhu 2010). Graphene oxide exhibits high electrical resistivity and photoluminescence due to the disrupted sp^2-hybridized carbon and band gap opening due to quantum confinement effect from small sp^2 domains. The oxygen functionalities can be exploited to produce novel supporting materials for composites or sensors by chemical modifications.

In order to use graphene oxide as a graphene precursor it is necessary to eliminate oxygen functional groups as far as possible to re-establish the planar sp^2-network. Three main approaches were developed to achieve this which includes

thermal, electrochemical and chemical methods. In the thermal reduction method, GO is thermally shocked at about 1000 °C to generate gaseous species such as CO_2, CO, and H_2O within the interlayers to increase the internal pressure that leads to the exfoliation of GO with the elimination of oxygen functional groups (Schniepp 2006; McAllister 2007). Recent studies suggested that more complex organic molecules are also generated during the above process (Sofer 2013). This simple and easily scalable method gives thermally reduced graphene having better conductivity but with structural damages and defects. The electrochemical reduction of GO can be easily controlled and performed under ambient conditions. This method does not involve toxic chemical agents and requires only simple instrumentation. The third and widely used approach involves elimination of oxygen functional groups using chemical reaction/reduction performed on aqueous dispersion of GO. The widely used reducing agent is hydrazine (Hofmann 1937). By using hydrazine reduced graphene with a C/O ratio of over 10 were obtained recently (Stankovich 2007). Subsequently, several reducing agents including sodium borohydride (Gao 2009), lithium aluminum hydride (Ambrosi 2012), hydroquinone (Wang 2008), hydroxylamine (Zhou 2011), and more eco-friendly L-ascorbic acid (Gao 2010), saccharides (Zhu 2010), tea extract (Thakur 2012), wild carrot root (Kuila 2012), and even bacteria (Akhavan 2012) were studied Although the chemically reduced graphene materials exhibit better properties compares to GO they are much inferior to pristine graphene since complete removal of oxygen is not possible. Even then chemical reduction becomes an attractive route due to high scalability.

1.8.3.1.5 Opening/Unzipping Carbon Nanotubes: Graphene Nano ribbons

In this method carbon nanotubes (CNTs) are used as the starting material to produce the so-called graphene nano ribbons (GNRs). GNRs differ from graphene due to its higher aspect ratio (at least 10) with a typical width of < 50 nm (Chen 2012). Band gap of GNRs vary with their width. Hence large-scale fabrication of GNRs with controlled width and length will open up new applications in electronic devices (Wu 2007). For this purposes the longitudinal opening of CNTs is an interesting approach. A variety of methods have been proposed to unzip/open the CNTs. Dai and co-workers used multi walled CNTs (MWCNTs) on a layer of poly(methyl methacrylate)(PMMA) to produce embedded GNRs by an argon plasma treatment (Jiao 2009). A more scalable method was proposed by Tour and co-

workers, who treated MWCNTs with concentrated sulfuric acid and potassium permanganate (Kosynkin 2009) to unzip the nanotubes longitudinally while, at the same time, introducing oxygen functionalities. Improvement has been achieved by introducing H_3PO_4 in the oxidation process to reduce the formation of vacancies (Higginbotham 2010). The structural damages occurring during the initial oxidative longitudinal unzipping cannot be repaired and hence the electronic properties of the nano ribbons are often compromised. To reduce the damages a reductive process which involve heating MWCNTs in the presence of potassium in a glass tube at 250 °C was used. The GNR produced through this approach had fewer defects and exhibited electrical and electronic properties comparable to pristine graphene (Kosynkin 2011).

The intercalations of Li– NH_3 into MWCNTs followed by thermal exfoliation (Cano-Márquez 2009) as well as the use of metal nanoparticles for catalytic unzipping (Elías 2009) were also studied recently. Control over the unzipping process along the folded edges was achieved by the acidic oxidation treatment on double-walled CNTs (Kang 2012). The oxidative treatment on MWCNTs resulted in large graphene sheets in some cases through the "unscrolling" of the nanotubes (Wong 2013). In addition to the previously mentioned parameters as in the case of graphene, the electronic properties of GNRs prepared by the unzipping of CNTs are strongly influenced by the density of defects, structural vacancies, and aspect ratios. Since CNTs is the starting material, the presence of metallic or carbonaceous impurities has an intense influence on the electrochemical properties of the GNRs.

1.8.3.2 Bottom-up Methods

In the bottom-up approaches graphene sheets were build up by combining small organic molecules through catalytic processes. Carbon-containing molecules combine to form sp^2-hybridized carbon network under special conditions. Few nanometer sized graphene molecules could also be prepared from small molecules through solution based catalytic reactions. High-temperature chemical vapor deposition (CVD) will also facilitate the deposition of carbon atoms into planar structures onto solid metal surfaces such as Pt, Cu, and Ni. Under higher temperature graphene can be produced from silicon carbide (SiC) wafers. Initially sublimate Si atoms will form, with consequent rearrangement of the remaining carbon atoms into graphitic layers. The three main bottom-up methods used to

synthesize graphene are chemical synthesis, epitaxial growth on SiC, and chemical vapor deposition.

1.8.3.2.1 Chemical Vapor Deposition

Recently large area, high-quality single or few layer graphene has been prepared by chemical vapor deposition (CVD) methods. This method has become one of the most promising techniques for the production of graphene in industrial-scale (Novoselov 2012). Despite its poorer electronic properties compared to the mechanically exfoliated graphene, graphene produced by CVD have shown excellent performances as electronic transistors (Farmer 2009), transparent conductive electrodes (Li 2009), electrochemical devices (Ambrosi 2013) and corrosion inhibiting coatings (Prasai 2012; Rafiee 2012). The CVD procedure involves decomposition of a carbon source in the presence of a transition-metal catalyst at high-temperature. During this process decomposed carbon atoms will rearrange into sp^2-hybridized carbon networks. Generally CNTs will form during the CVD process if metal nanoparticle were used as catalysts (Yudasaka 1995). CVD in the presence of metal surfaces such as ruthenium (Sutter 2008), platinum (Roumen 2010), iridium (Coraux 2010), nickel (Reina 2009), or copper (Li 2009) two-dimensional graphene will be produced. Nickel and Copper are the most widely used surfaces (Reina 2009; Li 2009; Kim 2009; Sun 2010). Carbon feed stock usually used are gases such as methane, ethane, or propane (Wassei 2012). In some cases solid source were also used (Sun 2010). Usually Ni surfaces will produce graphene with high polycrystalline nature consisting of areas with different layers. While Cu generally produces mono crystalline, mostly single layer graphene. This can be attributed to the higher solubility of carbon in Ni compared to Cu. Hence in Ni substrate crystallization of carbon atoms in uncontrolled orientation will occur during the cooling. On the other hand, only single or double layer graphene is created over Cu during cooling. The production technique to grow millimeter sized single layer and crystalline graphene were achieved by precise tuning of the deposition temperature, pressure, cooling time, and quality of metal substrates (Li 2011; Hao 2013; Tao 2012; Gong 2012). Despite these improvements single crystalline graphene has not yet been produced.

Transfer of graphene from the substrate to another arbitrary surface is also an integral part of the preparation steps for CVD graphene. Since the graphene film

has limited or no use if it is not transferred or if the metal catalyst substrate is not removed. Usually polymer-supported metal etching/transfer or mechanical exfoliations with special functionalized polymers are used for the transfer of CVD graphene onto arbitrary substrates (Kang 2012). During transfer significant degradation in the quality of graphene can occur due to the formation of wrinkles or structural damages from tearing and ripping (Hong 2012). Hence developing better transfer processes became more important than developing better CVD growth techniques (Kang 2012). Etching of metal substrate while the graphene is supported by an inert polymer such as PMMA or PDMS is the most commonly used techniques for transfer (Li 2009; Kim 2009). Several other substrates such as PTFE, PVC, PC, CN/CA, PET, paper, and cotton cloth have been investigated and applied via hot/cold lamination process (Martins 2013). This type of procedure generally causes mechanical stress, structural damages, alterations and contamination by metallic impurities. This will dramatically alter the electronic (Hu 2011) and electrochemical properties (Ambrosi 2014) of graphene. For example the etching agents such as $FeCl_3$, $Fe(NO_3)_3$ etc. will contaminate the transferred graphene with Fe impurities (Ambrosi 2014). In addition, incomplete etching will leave behind Ni or Cu metal as contaminates (Chng 2011; Ambrosi 2014).

Rummeli and co-workers were able to separate PMMA–graphene from the growth substrates by generating O_2 bubbles from a mixture of NH_4OH, H_2O_2, and H_2O (Gorantla 2014). Loh and coworkers demonstrated a face-to-face transfer of wafer-scale graphene films in which CVD graphene is adopted as an electrode material without any transfer process (Gao 2014). But in this method any fractures or holes, even at the sub-micrometer level on the graphene film will leave the redox active metal catalyst exposed to interact with external agents (Ambrosi 2013; Brownson 2012). Also small graphitic islands will dominate its electrochemistry toward biologically active molecules (Brownson 2011; Brownson 2011[b]).

1.8.3.2.2 Epitaxial Growth on SiC

On SiC substrates at high temperatures under ultrahigh vacuum (UHV) conditions graphene growth can be achieved (Berger 2004). Under these conditions Si atoms sublime away to leave an exposed layer of carbon atoms leads to the formation of graphitic layers. Very thin graphitic layers or single sheets can be achieved through the precise control of the sublimation temperature (Berger 2006).

Due to the presence of substrate-induced corrugations and irregular orientations graphene layers grown on SiC show different electronic properties compared to that of mechanically exfoliated graphene (Berger 2004; de Heer 2007). Since graphene on SiC wafers can be easily integrated into current industrial procedure they have very promising potential in the electronics industry. The high cost of single-crystal SiC wafers is the main limiting factor. According to Loh and co-workers epitaxial graphene obtained in SiC wafer possessed poor electrocatalytic properties like slow electron transfer rates. But its electrochemical performance can be enhanced by applying an anodizing potential to increase the density of defects and to introduce oxygen functionalities (Lim 2010).

1.8.3.2.3 Chemical Synthesis

The synthesis of small "graphene molecules" is a very interesting topic. It provides good control over the preparation of graphene with well-defined shape and edges. Since graphene is a polycyclic aromatic hydrocarbon (PAH) of infinite size, it makes sense to create graphene by combining small PAH molecules. But PAH that are larger than a few nanometers become highly insoluble in most organic solvents. This drawback impedes further synthetic growth and facilitates uncontrolled side reactions. Müllen and co-workers, the main contributors in this area, synthesized graphene nano-ribbons of 30 nm length (Yang 2008) and the largest graphene molecule synthesized consisted of 222 carbons with a size of 3.2 nm (Cai 2010; Chen 2012). Even though the size limitation of graphene is a major obstacle in the chemical synthesis, it opens up a promising route for clean and scalable fabrication method for graphene.

1.8.3.3 3D Graphene

The problem of restacking of individual isolated graphene sheets deposited on conducting surfaces for electrochemical purposes, which downplays the advantage of high surface area and decreases the availability of electro-active sites, can be avoided by the construction of well-defined porous 3D graphene structures. For this purpose two synthetic approaches have been developed. In one method graphene layers were deposited on Ni 3D foam through the CVD route (Chen 2011; Brownson 2013). In another attempt well-defined 3D pyrolyzed porous photoresist films fabricated by lithography were converted to 3D graphene with a pore size of ~500 nm (about two orders of magnitude lower than that of the first one) (Xiao

2012). 3D graphene shows faster heterogeneous electron transfer than 3D porous carbon and enhanced oxygen reduction activity (Xiao 2012; Brownson 2013). 3D graphene can act as a standalone sensing platform (Dong 2012). It can serve as 3D conducting support for catalytic particles (Pt or Pd nanoparticles or Ni/Co hydrogel) for enhanced oxygen reduction (Sattayasamitsathit 2013; Chen 2013). It can also act as support for transition metal dichalcogenides in electrochemical hydrogen evolution reaction (Chang 2013). The underlying Ni layer also provides electrocatalytic sites for enzyme-less glucose oxidation (Xiao 2012).

1.9 Outline of the thesis

Work described in the present thesis involves the synthesis and characterization of metal nanoparticle-linked organic frameworks and their catalytic applications. The thesis also describes a new protocol for the preparation of nano graphitic materials and their applications. In Chapter 2 of the thesis, synthesis and detailed characterization of palladium nanoparticle-linked organic frameworks (PNOF) are described. The effects of different reaction conditions upon metal content as well as the morphology of the PNOF were studied. The PNOF structure was probed by different experimental techniques. The PNOFs were evaluated as heterogeneous recyclable catalyst in aqueous medium for reduction of 4-nitrophenol and Suzuki coupling reactions. The catalyst exhibited high reactivity even in Suzuki couplings of aryl chlorides.

Chapter 3 of the thesis deals with the synthesis and characterization of Copper nanoparticle-linked organic frameworks (CNOF). Four different types of CNOFs were prepared by varying the concentration of the metal salts and the ligands. The structure and morphology of these materials were studied using XRD, XPS, SEM and HRTEM analysis. The materials were found to be very good catalysts for click reactions between azides and alkynes and exhibited TOF as high as 305400 h^{-1}. They also efficiently catalyzed the one-pot click reactions involving azide precursors, sodium azide and alkyne. TOF up to 99000 h^{-1} were observed for these reactions.

The fourth chapter of the thesis deals with preparation and characterization studies of nano graphitic materials. The nano graphitic materials obtained were sulfonated to get water-soluble derivatives. The sulfonated material was characterized using various methods and these studies are reported in Chapter 4.

This chapter also briefly describes some applications of the nano graphitic materials and sulfonated derivatives.

1.10 References

Adenier, A.; Cabet-Deliry, E.; Lalot, T.; Pinson J.; Podvorica, F. *Chem. Mater*. **2002**, *14*, 4576-4585.

Akagi, T.; Baba, M.; Akashi, M. *Polymer* **2007**, *48*, 6729-6747.

Akhavan, O.; Ghaderi, E. *Carbon* **2012**, *50*, 1853-1860.

Aksin, Ö.; Türkmen, H.; Artok, L.; Çetinkaya, B.; Ni, C.; Büyükgüngör, O.; Özkal, E. *J. Organomet. Chem.* **2006***, 691,* 3027-3036.

Alexeev, O.; Panjabi, G.; Gates, B. C. *J. Catal*. **1998**, *173*, 196-209.

Alanyalioglu, M.; Jose Segura, J.; Oro-Sole, J.; Casan-Pastor, N. *Carbon* **2012**, *50*, 142-152.

Alacid, E.; Nájera, C. *Synlett* **2006**, 2959-2964.

Allongue, P.; Delamar, M.; Desbat, B.; Fagebaume, O.; Hitmi, R.; Pinson, J.; Saveant, J.-M. *J. Am. Chem. Soc.* **1997**, *119,* 201-207.

Allongue, P.; de Villeneuve, C. H.; Cherouvrier, G.; Cortes, R.; Bernard, M. C. *J. Electroanal. Chem*. **2003**, *550*, 161-174.

Ambrosi, A.; Chua, C. K.; Bonanni, A.; Pumera, M. *Chem. Mater*. **2012**, *24*, 2292-2298.

Ambrosi, A.; Pumera, M. *J. Phys. Chem. C* **2013**, *117*, 2053-2058.

Ambrosi, A.; Bonanni, A.; Sofer, Z.; Pumera, M. *Nanoscale* **2013**, *5*, 2379-2387.

Ambrosi, A.; Pumera, M. *Nanoscale* **2014**, *6*, 472-476.

Ambrosi, A.; Chua, C. K.; Bonanni, A.; Pumera, M. *Chem. Rev.* **2014**, *114*, 7150-7188.

Amoroso, F.; Colussi, S.; Zotto, A. D.; Llorca, J.; Trovarelli, A. *J. Mol. Catal. A: Chem.* **2010***, 315*, 197-204.

Arcadi, A. *Chem. Rev.* **2008**, *108***,** 3266-3325.

Badetti, E.; Caminade, A.-M.; Majoral, J.-P.; Moreno-Mañas, M.; Sebastián, R. M. *Langmuir* **2008***, 24,* 2090-2101.

Bahr, J. L.; Yang, J.; Kosynkin, D. V.; Bronikowski, M. J.; Smalley R. E.; Tour, J. M. *J. Am. Chem. Soc.* **2001**, *123*, 6536-6542.

Balandin, A. A.; Ghosh, S.; Bao, W. Z.; Calizo, I.; Teweldebrhan, D.; Miao, F.; Lau, C. N. *Nano Lett*. **2008**, *8*, 902-907.

Banks, C.; Davies, T.; Wildgoose, G.; Compton, R. *Chem. Commun*. **2005**, 829-841.

Bates, A. J.; Leszczynski, Z. K.; Phillipson, J. J.; Wells, P. B.; Wilson, G. R. *J. Chem. Soc. A* **1970**, 2435-2441.

Bath, B. D.; Martin, H. B.; Wightman R. M.; Anderson, M. R. *Langmuir*, **2001**, *17*, 7032-7039.

Behabtu, N.; Lomeda, J.; Green, M.; Higginbotham, A.; Sinitskii, A.; Kosynkin, D.; Tsentalovich, D.; Parra-Vasquez, A.; Schmidt, J.; Kesselman, E.; Cohen, Y.; Talmon, Y.; Tour, J.; Pasquali, M. *Nat. Nanotechnol.* **2010**, *5*, 406-411.

Bernard, M.-C.; Chaussé, A.; Cabet-Deliry, E.; Chehimi, M. M.; Pinson, J.; Podvorica, F.; Vautrin-Ul, C. *Chem. Mater.* **2003**, *15,* 3450-3462.

Berger, C.; Song, Z. M.; Li, T. B.; Li, X. B.; Ogbazghi, A. Y.; Feng, R.; Dai, Z. T.; Marchenkov, A. N.; Conrad, E. H.; First, P. N.; de Heer, W. A. *J. Phys. Chem. B* **2004**, *108*, 19912-19916.

Berger, C.; Song, Z.; Li, X.; Wu, X.; Brown, N.; Naud, C.; Mayou, D.; Li, T.; Hass, J.; Marchenkov, A. N.; Conrad, E. H.; First, P. N.; de Heer, W. A. *Science* **2006**, *312*, 1191-1196.

Blake, P.; Brimicombe, P. D.; Nair, R. R.; Booth, T. J.; Jiang, D.; Schedin, F.; Ponomarenko, L. A.; Morozov, S. V.; Gleeson, H. F.; Hill, E. W.; Geim, A. K.; Novoselov, K. S. *Nano Lett.* **2008**, *8*, 1704-1708.

Boehm, H.-P. *Angew. Chem. Int. Ed.* **2010**, *49*, 9332-9335.

Boitiaux , J. P.; Cosyns , J.; Robert, E. *Appl. Catal.* **1987**, *32*, 145-168.

Bonanni, A.; Pumera, M. *Electrochem. Commun.* **2012**, *16*, 19-21.

Brodie, B. C. *Philos. Trans. R. Soc. Lon.* **1859**, *149*, 249-259.

Broggi, J.; Clavier, H.; Nolan, S. P. *Organomet.* **2008**, *27*, 5525-5531.

Brownson, D. A. C.; Banks, C. E. *Electrochem. Commun.* **2011**, *13*, 111-113.

Brownson, D. A. C.; Metters, J. P.; Kampouris, D. K.; Banks, C. E. *Electroanalysis* **2011**, *23*, 894-899.

Brownson, D. A. C.; Banks, C. E. *RSC Adv.* **2012**, *2*, 5385-5389.

Brownson, D. A. C.; Banks, C. E. *Phys. Chem. Chem. Phys.* **2011**, *13*, 15825-15828.

Brownson, D. A. C.; Gomez-Mingot, M.; Banks, C. E. *Phys. Chem. Chem. Phys.* **2011**, *13*, 20284-20288.

Brownson, D. A. C.; Figueiredo-Filho, L. C. S.; Ji, X.; Gomez-Mingot, M.; Iniesta, J.; Fatibello-Filho, O.; Kampouris, D. K.; Banks, C. E. *J. Mater. Chem. A* **2013**, *1*, 5962-5972.

Cai, J. M.; Ruffieux, P.; Jaafar, R.; Bieri, M.; Braun, T.; Blankenburg, S.; Muoth, M.; Seitsonen, A. P.; Saleh, M.; Feng, X. L.; Müllen, K.; Fasel, R. *Nature* **2010**, *466*, 470-473.

Campelo, J. M.; Luna, D.; Luque, R.; Marinas, J. M.; Romero, A. A.; *ChemSusChem* **2009**, *2*, 18-45.

Cano-Márquez, A.; Rodríguez-Macías, F.; Campos-Delgado, J.; Espinosa-González, C.; Tristán-López, F.; Ramírez-González, D.; Cullen, D.; Smith, D.; Terrones, M.; Vega-Cantú, Y. *Nano Lett.* **2009**, *9*, 1527-1533.

Cervantes, G. G.; Aires, F. J. C. S.; Bertolini, J. C. *J. Catal.* **2003**, *214*, 26-32.

Chang, Y.-H.; Lin, C.-T.; Chen, T.-Y.; Hsu, C.-L.; Lee, Y.-H.; Zhang, W.; Wei, K.-H.; Li, L.-J. *Adv. Mater*. **2013**, *25*, 756-760.

Chaussé, A.; Chehimi, M. M.; Karsi, N.; Pinson, J.; Podvorica F.; Vautrin-Ul, C. *Chem. Mater*. **2002**, *14*, 392-400.

Chen, M. S.; Goodman, D. W. *Chem. Soc. Rev.* **2008**, *37*, 1860-1870.

Chen, L.; Hernandez, Y.; Feng, X.; Müllen, K. *Angew. Chem. Int. Ed*. **2012**, *51*, 7640-7654.

Chen, Z. P.; Ren, W. C.; Gao, L. B.; Liu, B. L.; Pei, S. F.; Cheng, H. M. *Nat. Mater*. **2011**, *10*, 424-428.

Chen, S.; Duan, J. J.; Jaroniec, M.; Qiao, S. Z. *Angew. Chem. Int. Ed*. **2013**, *52*, 13567-13570.

Chng, E. L. K.; Pumera, M. *Chem. Asian J.* **2011**, *6*, 2304-2307.

Cho, J. K.; Najman, R.; Dean, T. W.; Ichihara, O.; Muller, C.; Bradley, M. *J. Am. Chem. Soc.* **2006,** *128*, 6276-6277.

Chua, C. K.; Sofer, Z.; Pumera, M. *Chem. Asian J.* **2012**, *7*, 2367-2372.

Combellas, C.; Kanoufi, F.; Pinson, J.; Podvorica, F. I. *Langmuir*, **2005,** *21*, 280-286.

Combellas, C.; Kanoufi, F.; Pinson, J.; Podvorica, F. I. *J. Am. Chem. Soc*. **2008**, *130,* 8576–8577.

Coraux, J.; ǸDiaye, A. T.; Busse, C.; Michely, T. *Nano Lett*. **2008**, *8*, 565-570.

Corma, A.; Martinez, A.; Martinez-Soria, V. *J. Catal*. **1997**, *169*, 480-489.

Coulon, E.; Pinson, J.; Bourzat, J.-D.; Commerçon, A.; Pulicani, J.-P. *J. Org. Chem*. **2002**, *67*, 8513-8518.

Cui, Y.; Zhang, L. *J. Mol. Catal. A: Chem.* **2005***, 237*, 120-125.

de Heer, W. A.; Berger, C.; Wu, X. S.; First, P. N.; Conrad, E. H.; Li, X.; Li, T.; Sprinkle, M.; Hass, J.; Sadowski, M. L.; Potemski, M.; Martinez, G. *Solid State Commun*. **2007**, *143*, 92-100*.*

de Villeneuve, C. H.; Pinson, J.; Bernard, M. C.; Allongue, P. *J. Phys. Chem. B,* **1997**, *101*, 2415-2420.

Delamar, M.; Desarmot, G.; Fagebaume, O.; Hitmi, R.; Pinson, J.; Saveant, J.-M. *Carbon* **1997***, 35,* 801-807.

Dong, X.; Wang, X.; Wang, L.; Song, H.; Zhang, H.; Huang, W.; Chen, P. *ACS Appl. Mater. Interfaces* **2012***, 4*, 3129-3133.

Downard, A. J.; Roddick, A. D.; Bond, A. M. *Anal. Chim. Acta* **1995***, 317*, 303-310.

Downard, A. J. *Electroanalysis,* **2000***, 12*, 1085-1096.

Dreyer, D. R.; Ruoff, R. S.; Bielawski, C. W. *Angew. Chem. Int. Ed.* **2010***, 49*, 9336-9344.

Dreyer, D. R.; Park, S.; Bielawski, C. W.; Ruoff, R. S. *Chem. Soc. Rev.* **2010***, 39*, 228-240

Dyke, C. A.; Tour, J. M. *Nano Lett*. **2003**, *3*, 1215-1218.

Elías, A. L.; Botello-Méndez, A. R.; Meneses-Rodríguez, D.; González, V. J.; Ramírez-González, D.; Ci, L.; Muñoz-Sandoval, E.; Ajayan, P. M.; Terrones, H.; Terrones, M. *Nano Lett.* **2009**, *10*, 366-372.

Englert, J. M.; Rohrl, J.; Schmidt, C. D.; Graupner, R.; Hundhausen, M.; Hauke, F.; Hirsch, A. *Adv. Mater.* **2009**, *21*, 4265-4269.

Farmer, D.; Chiu, H.-Y.; Lin, Y.-M.; Jenkins, K.; Xia, F.; Avouris, P. *Nano Lett.* **2009**, *9*, 4474-4478.

Feng, Y.; Li, L.; Li, Y.; Zhao, W.; Gu, J.; Shi, J. *J. Mol. Catal. A: Chem.* **2010**, *322*, 50-54.

Finklea, H. O. in Electroanalytical Chemistry; Bard, A. J., Rubinstein, I., Eds.; Marcel Dekker: New York, **1996**, *19*, 109-335.

Fitzer, E.; Kochling, K. H.; Boehm, H. P.; Marsh, H. *Pure Appl. Chem.* **1995**, *67*, 473-506.

Fradkin, E. *Phys. Rev. B* **1986**, *33*, 3263-3268.

Gao, W.; Alemany, L. B.; Ci, L. J.; Ajayan, P. M. *Nat. Chem.* **2009**, *1*, 403-408.

Gao, J.; Liu, F.; Liu, Y.; Ma, N.; Wang, Z.; Zhang, X. *Chem. Mater.* **2010**, *22*, 2213-2218.

Gao, L.; Ni, G.-X.; Liu, Y.; Liu, B.; Neto, A. H. C.; Loh, K. P. *Nature* **2014**, *505*, 190-194.

Geim, A.; Novoselov, K. *Nat. Mater.* **2007**, *6*, 183-191.

Geim, A. K. *Science* **2009**, *324,* 1530-1534.

Gong, Y.; Zhang, X.; Liu, G.; Wu, L.; Geng, X.; Long, M.; Cao, X.; Guo, Y.; Li, W.; Xu, J.; Sun, M.; Lu, L.; Liu, L. *Adv. Funct. Mater.* **2012**, *22*, 3153-3159.

Gorantla, S.; Bachmatiuk, A.; Hwang, J.; Alsalman, H. A.; Kwak, J. Y.; Seyller, T.; Eckert, J.; Spencer, M. G.; Rummeli, M. H. *Nanoscale* **2014**, *6*, 889-896.

Green, A.; Hersam, M. *Nano Lett.* **2009**, *9*, 4031-4036.

Griess, J. P. *Ann. Chem. Justus Liebigs* **1858**, *106*, 123-125.

Griess, J. P. *Philos. Trans. R. Soc. London*, **1864**, *154*, 667-731.

Griess, J. P. *Ann. Chem. Justus Liebigs* **1866**, 137, 39-91.

Guczi, L.; Sárkány, A.; Spivey, J. J.; Agarwal, S. K. *Catalysis Volume 11* Royal Society of Chemistry, **1994**, *11*, 318-378.

Guinea, F.; Katsnelson, M. I.; Geim, A. K. *Nat. Phys.* **2009**, *6*, 30-33.

Haldane, F. D. M. *Phys. Rev. Lett.* **1988**, *61*, 2015-2018.

Han, P.; Wang, X.; Qiu, X.; Ji, X.; Gao, L. *J. Mol. Catal. A: Chem*. **2007**, *272*, 136-141.

Hao, Y.; Bharathi, M. S.; Wang, L.; Liu, Y.; Chen, H.; Nie, S.; Wang, X.; Chou, H.; Tan, C.; Fallahazad, B.; Ramanarayan, H.; Magnuson, C. W.; Tutuc, E.; Yakobson, B. I.; McCarty, K. F.; Zhang, Y.-W.; Kim, P.; Hone, J.; Colombo, L.; Ruoff, R. S. *Science* **2013**, *342*, 720-723.

Hermes, S.; Schroter, M. K.; Schmid, R.; Khodeir, L.; Muhler, V.; Tissler, A.; Fischer, R. W. R.; Fischer, A. *Angew. Chem. Int. Ed.* **2005**, *44*, 6237-6241.

Hernandez, Y.; Nicolosi, V.; Lotya, M.; Blighe, F. M.; Sun, Z. Y.; De, S.; McGovern, I. T.; Holland, B.; Byrne, M.; Gun'ko, Y. K.; Boland, J. J.; Niraj, P.; Duesberg, G.;

Krishnamurthy, S.; Goodhue, R.; Hutchison, J.; Scardaci, V.; Ferrari, A. C.; Coleman, J. N. *Nat. Nanotechnol.* **2008**, *3*, 563-568.

Hernandez, Y.; Lotya, M.; Rickard, D.; Bergin, S. D.; Coleman, J. N. *Langmuir* **2010**, *26*, 3208-3213.

Hernández, D. M.; González, M. A.; Astudillo, P. D.; Hernández, L. S.; González, F. J. *Procedia Chem.* **2014**, *12*, 3-8.

Herrmann, W. A.; Bohm, V. P. M.; Reisinger, C. P. *J. Organomet. Chem.* **1999**, *576*, 23-41.

Higginbotham, A.; Kosynkin, D.; Sinitskii, A.; Sun, Z.; Tour, J. *ACS Nano* **2010**, *4*, 2059-2069.

Hofmann, U.; König, E. Z. *Anorg. Allg. Chem.* **1937**, *234*, 311-336.

Homeyer, S. T.; Karpinski, Z.; Sachtler, W. M. H. *J. Catal.,* **1990**, *123*, 60-73.

Hong, S. K.; Song, S. M.; Sul, O.; Cho, B. J. *J. Electrochem. Soc.* **2012**, *159*, K107-K109.

Hu, F. M.; Ma, T. X.; Lin, H. Q.; Gubernatis, J. E. *Phys. Rev. B* **2011**, *84*, 075414 (6 pages).

Huang, Y.; Zheng, Z.; Liu, T.; Lu, J.; Lin, Z.; Li, H.; Cao, R. *Catal. Commun*, **2011**, *14*, 27-31.

Hummers, W. S.; Offeman, R. E. *J. Am. Chem. Soc.* **1958**, *80*, 1339-1339.

Hurley, B. L.; McCreery, R. L. *J. Electrochem. Soc.* **2004**, *151*, B252-B259.

Inagaki, M.; Iwashita, N.; Wang, Z. D.; Maeda, Y. *Synth. Met.* **1988**, *26*, 41-47.

Jiao, L.; Zhang, L.; Wang, X.; Diankov, G.; Dai, H. *Nature* **2009**, *458*, 877-880.

Jnioui, A.; Metrot, A.; Storck, A. *Electrochim. Acta* **1982**, *27*, 1247-1252.

Kalidindi, S. B.; Oh, H.; Hirscher, M.; Esken, D.; Wiktor, I.; Turner, S.; Tendeloo, G. V.; Fischer, R. A. *Chem. Eur. J.* **2012**, *18*, 10848-10856.

Kampouris, D. K.; Banks, C. E. *Chem. Commun.* **2010**, *46*, 8986-8988.

Kang, J.; Shin, D.; Bae, S.; Hong, B. *Nanoscale* **2012**, *4*, 5527-5537.

Kang, Y. R.; Li, Y. L.; Deng, M. Y. *J. Mater. Chem.* **2012**, *22*, 16283-16287.

Kantam, M. L.; Roy, S.; Roy, M.; Subhas, M. S.; Likhar, P. R.; Sreedhar, B. *Synlett* **2006**, 2747-2750.

Kariuki, J. K.; McDermott, M. T. *Langmuir* **2001**, *17,* 5947-5951.

Katano, S.; Kato, H. S.; Kawai, M.; Domen, K. *J. Phys. Chem. B* **2003**, *107*, 3671-3674.

Kim, K. S.; Zhao, Y.; Jang, H.; Lee, S. Y.; Kim, J. M.; Kim, K. S.; Ahn, J.-H.; Kim, P.; Choi, J.-Y.; Hong, B. H. *Nature* **2009**, *457*, 706-710.

Kirmse, W. *Angew. Chem. Int. Ed.* **1976**, *15,* 251-320.

Kosynkin, D. V.; Higginbotham, A. L.; Sinitskii, A.; Lomeda, J. R.; Dimiev, A.; Price, B. K.; Tour, J. M. *Nature* **2009**, *458*, 872-876.

Kosynkin, D. V.; Lu, W.; Sinitskii, A.; Pera, G.; Sun, Z. Z.; Tour, J. M. *ACS Nano* **2011**, *5*, 968-974.

Krishnakumar, S.; Gopidas, K. R. *J. Mater. Chem. B* **2014**, *2*, 5576-5584.

Kuila, T.; Bose, S.; Khanra, P.; Mishra, A. K.; Kim, N. H.; Lee, J. H. *Carbon* **2012**, *50*, 914-921

Kumar, V. K. R.; Gopidas, K. R. *Chem. Asian J.* **2010**, *5*, 887-896.

Kumar, V. K. R.; Gopidas, K. R. *Tetrahedron Lett.* **2011**, *52*, 3102-3105.

Kumar, V. K. R.; Krishnakumar, S.; Gopidas, K. R. *Eur. J. Org. Chem.* **2012**, 3447-3458.

Kuo T.-C.; McCreery, R. L. *Anal. Chem.* **1999**, *71*, 1533-1560.

Lee, K.; Zhang, J. J.; Wang, H. J.; Wilkinson, D. P. *J. Appl. Electrochem.* **2006**, *36***, 507-522.

Lee, C.; Wei, X.; Kysar, J. W.; Hone, J. *Science* **2008**, *321*, 385-388.

Lenski, D. R.; Fuhrer, M. S. *J. Appl. Phys.* **2011**, *110*, doi: 10.1063/1.3605545.

Li, X.; Cai, W.; An, J.; Kim, S.; Nah, J.; Yang, D.; Piner, R.; Velamakanni, A.; Jung, I.; Tutuc, E.; Banerjee, S. K.; Colombo, L.; Ruoff, R. S. *Science* **2009**, *324*, 1312-1314.

Li, X.; Zhang, G.; Bai, X.; Sun, X.; Wang, X.; Wang, E.; Dai, H. *Nat. Nanotechnol.* **2008**, *3*, 538-542.

Li, X.; Zhu, Y.; Cai, W.; Borysiak, M.; Han, B.; Chen, D.; Piner, R.; Colombo, L.; Ruoff, R. *Nano Lett.* **2009**, *9*, 4359-4363.

Li, W.; Tan, C.; Lowe, M.; Abruña, H.; Ralph, D. *ACS Nano* **2011**, *5*, 2264-2270.

Lim, C. X.; Hoh, H. Y.; Ang, P. K.; Loh, K. P. *Anal. Chem.* **2010**, *82*, 7387-7393.

Lin, S. D.; Vannice, M. A. *J. Catal.* **1993**, *143*, 539-553.

Liu, G.; Bocking, T.; Gooding, J. J. *J. Electroanal. Chem.* **2007**, *600*, 335-344.

Liu, Y.-C.; McCreery, R. L. *J. Am. Chem. Soc.*, **1995**, *117*, 11254–11259.

Lotya, M.; Hernandez, Y.; King, P. J.; Smith, R. J.; Nicolosi, V.; Karlsson, L. S.; Blighe, F. M.; De, S.; Wang, Z. M.; McGovern, I. T.; Duesberg, G. S.; Coleman, J. N. *J. Am. Chem. Soc.* **2009**, *131*, 3611-3620.

Lotya, M.; King, P.; Khan, U.; De, S.; Coleman, J. *ACS Nano* **2010**, *4*, 3155-3162.

Low, C. T. J.; Walsh, F. C.; Chakrabarti, M. H.; Hashim, M. A.; Hussain, M. A. *Carbon* **2013**, *54*, 1-21.

Ma, X.; Zhou, Y.; Zhang, J.; Zhu, A.; Jiang, T.; Han, B. *Green Chem.* **2008**, *10*, 59-66.

MacQuarrie, S.; Nohair, B.; Horton, J. H.; Kaliaguine, S.; Crudden, C. M. *J. Phys. Chem. C* **2010**, *114*, 57-64.

Maeda, H.; Yamauchi Y.; Ohmori, H. *Curr. Top. Anal. Chem.,* **2001**, *2*, 121-133.

Maegawa, T.; Kitamura, Y.; Sako, S.; Udzu, T.; Sakurai, A.; Tanaka, A.; Kobayashi, Y.; Endo, K.; Bora, U.; Kurita, T.; Kozaki, A.; Monguchi, Y.; Sajiki, H. *Chem. Eur. J.* **2007**, *13*, 5937-5943.

Marcano, D.; Kosynkin, D.; Berlin, J.; Sinitskii, A.; Sun, Z.; Slesarev, A.; Alemany, L.; Lu, W.; Tour, J. *ACS Nano* **2010**, *4*, 4806-4814.

Martínez, S.; Vallribera, A.; Cotet, C. L.; Popovici, M.; Martín, L.; Roig, A.; Moreno-Manas, M.; Molins, E. *New J. Chem.* **2005**, *29*, 1342-1345.

Martins, L. G. P.; Song, Y.; Zeng, T.; Dresselhaus, M. S.; Kong, J.; Araujo, P. T. *Proc. Natl. Acad. Sci. U. S. A.* **2013***, 110*, 17762-17767.

McAllister, M. J.; Li, J. L.; Adamson, D. H.; Schniepp, H. C.; Abdala, A. A.; Liu, J.; Herrera-Alonso, M.; Milius, D. L.; Car, R.; Prud'homme, R. K.; Aksay, I. A. *Chem. Mater.* **2007***, 19*, 4396-4404.

McClure, J. W. *Phys. Rev.* **1956***, 104,* 666-671.

Meng, Y.; Aldous, L.; Pilgrim, B. S.; Donooe, T. J.; Compton, R. G. *New J. Chem.* **2011***, 35*, 1369-1375.

Min, B. K.; Friend, C. M. *Chem. Rev.* **2007***, 107*, 2709-2724.

Mitchell, C. A.; Bahr, J. F.; Arepalli, S.; Tour J. M.; Krishnamoorti, R. *Macromolecules,* **2002***, 35*, 8825-8830.

Mo, F.; Dong, G.; Zhang, Y.; Wang, J. *Org. Biomol. Chem*. **2013***, 11*, 1582-1593.

Molnár, Á. *Chem. Rev.* **2011***, 111*, 2251-2320.

Monopoli, A.; Nacci, A.; Calò, V.; Ciminale, F.; Cotugno, P.; Mangone, A.; Giannossa, L. C.; Azzone, P.; Cioffi,P. *Molecules* **2010***, 15*, 4511-4525.

Mojet, B. L.; Kappers, M. J.; Miller, J.T.; Koningsberger, D. C. *Stud. Surf. Sci. Catal.* **1996***, 101*, 1165-1174.

Morales, G. M.; Schifani, P.; Ellis, G.; Ballesteros, C.; Martinez, G.; Barbero, C.; Salavagione, H. J. *Carbon* **2011***, 49*, 2809-2816.

Moretti, G.; Stakheev, A. Y.; Sachtler, W. M. H. *J. Electron. Spectrosc. Relat. Phenom.* **1992***, 58*, 1-13.

Morgan, A. E.; Somorjai, G. A. *Surf. Sci.* **1968***, 12*, 405-425.

Mubeen, S.; Zhang, T.; Yoo, B.; Deshusses, M. A.; Myung, N. V. *J. Phys. Chem. C* **2007***, 111*, 6321-6327.

Nakamura, T.; Suzuki, M.; Ishihara, M.; Ohana, T.; Tanaka, A.; Koga, Y. *Langmuir,* **2004***, 20*, 5846-5849.

Navalon, S.; Dhakshinamoorthy, A.; Alvaro, M.; Garcia, H. *Chem. Rev.* **2014***, 114*, 6179-6212.

Niembro, S.; Shafir, A.; Vallribera, A.; Alibés, R. *Org. Lett*. **2008***, 10*, 3215-3218.

Nkosi, B.; Coville, N. J.; Hutchings, G. J. *J. Chem. Soc., Chem. Commun*. **1988**, 71-72.

Noel, M.; Santhanam, R.; Flora, M. F. *J. Appl. Electrochem.* **1994***, 24*, 455-459.

Novoselov, K.; Fal'ko, V.; Colombo, L.; Gellert, P.; Schwab, M.; Kim, K. *Nature* **2012***, 490*, 192-200.

Novoselov, K. S.; Geim, A. K.; Morozov, S. V.; Jiang, D.; Katsnelson, M. I.; Grigorieva, I. V.; Dubonos, S. V.; Firsov, A. A. *Nature* **2005**, *438,* 197-200.

Novoselov, K. S.; Geim, A. K.; Morozov, S. V.; Jiang, D.; Zhang, Y.; Dubonos, S. V.; Grigorieva, I. V.; Firsov, A. A. *Science* **2004***, 306*, 666-669.

Novoselov, K.; Jiang, D.; Schedin, F.; Booth, T.; Khotkevich, V.; Morozov, S.; Geim, A. *Proc. Natl. Acad. Sci. U. S. A.* **2005***, 102*, 10451-10453.

Ohtaka, A.; Teratani, T.; Fujii, R.; Ikeshita, K.; Shimomura, O.; Nomura, R. *Chem. Commun.* **2009**, 7188-7190.

Opelt, S.; Turk, S.; Dietzsch, E.; Henschel, A.; Kaskel, S.; Klemm, E. *Catal. Commun.* **2008**, *9*, 1286-1290.

Palacin, S.; Bureau, C.; Charlier, J.; Deniau, G.; Mouanda B.; Viel, P. *ChemPhysChem* **2004**, *5*, 1468-1481.

Pagliaro, M.; Pandarus, V.; Béland, F.; Ciriminna, R.; Palmisanoa, G.; Carà, P. D. *Catal. Sci. Technol.* **2011**, *1*, 736-739.

Papp, A.; Galbács, G.; Molnár, Á. *Tetrahedron Lett.* **2005**, *46*, 7725-7728.

Parlett, C. M. A.; Bruce, D. W.; Hondow, N. S.; Newton, M. A.; Lee, A. F.; Wilson, K. *ChemCatChem* **2013**, *5*, 939-950.

Patai, S. *Chemistry of the Diazonium and Diazo Groups: Part 1* & Part 2. **1978,** Wiley-Blackwell.

Paulik, M. G.; Brooksby, P. A.; Abell, A. D.; Downard, A. J. *J. Phys. Chem. C* **2007**, *111*, 7808-7815.

Phillipson, J. J.; Wells, P. B.; Wilson, G. R. *J. Chem. Soc. A* **1969**, 1351-1363 .

Pinson, J.; Podvorica, F. *Chem. Soc. Rev.* **2005**, *34*, 429-439.

Ponec, V. *Adv. Catal.* **1983**, *32*, 149-214.

Prasai, D.; Tuberquia, J. C.; Harl, R. R.; Jennings, G. K.; Bolotin, K. I. *ACS Nano* **2012**, *6*, 1102-1108.

Price, K. E.; McQuade, D. T. *Chem. Commun.* **2005**, 1714-1716.

Rafiee, J.; Mi, X.; Gullapalli, H.; Thomas, A. V.; Yavari, F.; Shi, Y.; Ajayan, P. M.; Koratkar, N. A. *Nat. Mater.* **2012**, *11*, 217-222.

Reina, A.; Jia, X.; Ho, J.; Nezich, D.; Son, H.; Bulovic, V.; Dresselhaus, M. S.; Kong, J. *Nano Lett.* **2009**, *9*, 30-35.

Riahi, G.; Guillemot, D.; Polisset-Tfoin, M.; Khodadadi, A. A.; Fraissard, J. *Catal. Today* **2002**, *72*, 115-121.

Risse, T.; Shaikhutdinov, S.; Nilius, N.; Sterrer, M.; Freund, H.-J. *Acc. Chem. Res.* **2008**, *41,* 949-956.

Roucoux , A.; Schulz, J.; Patin, H. *Chem. Rev.* **2002**, *102*, 3757-3778.

Roumen, V.; Alexander, M.; Roumen, H. P.; Raymond, K.; Myrjam, M.; Annick, V.; Chris Van, H. *Nanotechnology* **2010**, *21*, 095602.

Ryndin, Yu. A.; Nosova, L. V.; Boronin, A. I.; Chuvilin, A. L.; *Appl. Catal.* **1988**, *42*, 131-141.

Sachtler, W. M. H.; Stakheev, A. Y. *Catal. Today* **1992**, *12*, 283-295.

Sachtler, W. M. H. *Catal. Rev.-Sci. Eng.* **1976**, *14*, 193-210.

Sárkány, A.; Weiss, A. H.; Guczi, L. *J. Catal.* **1986**, *98,* 550-553.

Sarkany, A.; Zsoldos, Z.; Stefler , G.; Hightower, J. W.; Guzci, L. *J. Catal.* **1995**, *157*, 179-189.

Sattayasamitsathit, S.; Gu, Y. E.; Kaufmann, K.; Jia, W. Z.; Xiao, X. Y.; Rodriguez, M.; Minteer, S.; Cha, J.; Burckel, D. B.; Wang, C. M.; Polsky, R.; Wang, J. *J. Mater. Chem. A* **2013***, 1*, 1639-1645.

Schmçger, C.; Szuppa, T.; Tied, A.; Schneider, F.; Stolle, A.; Ondruschka, B. *ChemSusChem* **2008***, 1*, 339-347.

Schniepp, H. C.; Li, J. L.; McAllister, M. J.; Sai, H.; Herrera- Alonso, M.; Adamson, D. H.; Prud'homme, R. K.; Car, R.; Saville, D. A.; Aksay, I. A. *J. Phys. Chem. B* **2006***, 110*, 8535-8539.

Semenoff, G. W. *Phys. Rev. Lett.* **1984***, 53,* 2449-2452.

Silvestre - Alberto, J.; Rupprechter , G.; Freund , H. - J. *J.* Catal. **2005***, 235*, 52-59.

Shan, J.; Nuopponen, M.; Jiang, H.; Viitala, T.; Kauppinen, E.; Kontturi, K.; Tenhu, H. *Macromolecules* **2005***, 38*, 2918-2926.

Shewchuk, D. M.; McDermott, M. T. *Langmuir* **2009***, 25,* 4556-4563.

Shimura, T.; Aramaki, K. *Corros. Sci*. **2006***, 48,* 3784-3801.

Slonczewski, J. C.; Weiss, P. R. *Phys. Rev.* **1958***, 109,* 272-279.

Sofer, Z.; Simek, P.; Pumera, M. *Phys. Chem. Chem. Phys.* **2013***, 15*, 9257-9264.

Solak, A. O.; Ranganathan, S.; Itoh, T.; McCreery, R. L. *Electrochem. Solid-State Lett.* **2002***, 5*, E43-E46.

Stankovich, S.; Dikin, D. A.; Piner, R. D.; Kohlhaas, K. A.; Kleinhammes, A.; Jia, Y.; Wu, Y.; Nguyen, S. T.; Ruoff, R. S. *Carbon* **2007***, 45*, 1558-1565.

Stakheev, A. Y.; Sachtler, W. M. H. *J. Chem. Soc. Faraday Trans.* **1991***, 87*, 3703-3708.

Staudenmaier, L. *Ber. Dtsch. Chem. Ges.* **1898***, 31*, 1481-1487.

Stakheev, A. Y.; Kustov, L.M. *Appl. Catal.* **1999***, 188*, 3-35.

Stakheev, A. Y.; Mashkovskii, I. S. Baeva, G. N.; Telegina, N. S. *Russ. J. Gen. Chem.* **2010**, *80*, 618-629.

Stewart, M. P.; Maya, F.; Kosynkin, D. V.; Dirk, S. M.; Stapleton, J. J.; McGuiness, C. L.; Allara, D. L.; Tour, J. M. *J. Am. Chem. Soc.* **2004**, *126*, 370-378.

Sun, Z.; Yan, Z.; Yao, J.; Beitler, E.; Zhu, Y.; Tour, J. M. *Nature* **2010***, 468*, 549-552.

Sutter, P. W.; Flege, J.-I.; Sutter, E. A. *Nat. Mater.* **2008***, 7*, 406-411.

Su, C.-Y.; Lu, A.-Y.; Xu, Y.; Chen, F.-R.; Khlobystov, A. N.; Li, L.-J. *ACS Nano* **2011***, 5*, 2332-2339.

Takada, Y.; Fujii, R. *Tanso* **1985**, *122*, 110-113.

Takenaka, H.; Kawaguchi, M.; Lerner, M.; Bartlett, N. *J. Chem. Soc. Chem. Commun*. **1987**, 1431-1432.

Tao, L.; Lee, J.; Chou, H.; Holt, M.; Ruoff, R. S.; Akinwande, D. *ACS Nano* **2012***, 6*, 2319-2325.

Thakur, S.; Karak, N. *Carbon* **2012***, 50*, 5331-5339.

Tiberj, A.; Huntzinger, J.-R.; Camassel, J.; Hiebel, F.; Mahmood, A.; Mallet, P.; Naud, C.; Veuillen, J.-Y. *Nanoscale Res. Lett.* **2011***, 6*, 478.

Tsvelikhovsky, D.; Blum, J. *Eur. J. Org. Chem.* **2008**, 2417-2422.

Ungureanu, S.; Deleuze, H.; Sanchez, C.; Popa, M. I.; Backov, R. *Chem. Mater.* **2008**, *20*, 6494-6500.

Valles, C.; Drummond, C.; Saadaoui, H.; Furtado, C. A.; He, M.; Roubeau, O.; Ortolani, L.; Monthioux, M.; Penicaud, A. *J. Am. Chem. Soc.* **2008**, *130*, 15802-15804.

Wang, J.; Firestone, M. A.; Uciello, O.; Carlisle, J. A. *Langmuir* **2004**, *20*, 11450-11456.

Wang, P.; Lu, Q.; Li, J. *Mater. Res. Bull.* **2010**, *45*, 129-134.

Wang, G. X.; Yang, J.; Park, J.; Gou, X. L.; Wang, B.; Liu, H.; Yao, J. *J. Phys. Chem. C* **2008**, *112*, 8192-8195.

Wang, L.; Ambrosi, A.; Pumera, M. *Chem. Asian J.* **2013**, *8*, 1200-1204.

Wang, G.; Wang, B.; Park, J.; Wang, Y.; Sun, B.; Yao, J. *Carbon* **2009**, *47*, 3242-3246.

Wang, J.; Manga, K. K.; Bao, Q.; Loh, K. P. *J. Am. Chem. Soc.* **2011**, *133*, 8888-8891.

Wang, G. X.; Yang, J.; Park, J.; Gou, X. L.; Wang, B.; Liu, H.; Yao, J. *J. Phys. Chem. C* **2008**, *112*, 8192-8195.

Wallace, P. R. *Phys. Rev.* **1947**, *71,* 622-634.

Wassei, J. K.; Mecklenburg, M.; Torres, J. A.; Fowler, J. D.; Regan, B. C.; Kaner, R. B.; Weiller, B. H. *Small* **2012**, *8*, 1415-1422.

Wayner, D. M.; Wolkow, R. A. *J. Chem. Soc. Perkin Trans.* **2002**, *2,* 23-34.

Wei, G.; Wen, F.; Zhang, X.; Zhang, W.; Jiang, X.; Zheng, P.; Shi, L. *J. Colloid Interface Sci.* **2007**, *316,* 53-58.

Wong, C. H. A.; Pumera, M. *Phys. Chem. Chem. Phys.* **2013**, *15*, 7755-7759.

Wu, J. S.; Pisula, W.; Mullen, K. *Chem. Rev.* **2007**, *107*, 718-747.

Xiao, X. Y.; Michael, J. R.; Beechem, T.; McDonald, A.; Rodriguez, M.; Brtunbach, M. T.; Lambert, T. N.; Washburn, C. M.; Wang, J.; Brozik, S. M.; Wheeler, D. R.; Burckel, D. B.; Polsky, R. *J. Mater. Chem.* **2012**, *22*, 23749-23754.

Xiao, X. Y.; Beechem, T. E.; Brumbach, M. T.; Lambert, T. N.; Davis, D. J.; Michael, J. R.; Washburn, C. M.; Wang, J.; Brozik, S. M.; Wheeler, D. R.; Burckel, D. B.; Polsky, R. *ACS Nano* **2012**, *6*, 3573-3579.

Yang, Q.; Ma, S.; Li, J.; Xiao, F.; Xiong, H. *Chem. Commun.* **2006**, 2495-2497.

Yang, X. Y.; Dou, X.; Rouhanipour, A.; Zhi, L. J.; Rader, H. J.; Müllen, K. *J. Am. Chem. Soc.* **2008**, *130*, 4216-4217.

Yang, H.; Han, X.; Li, G.; Wang, Y. *Green Chem.* **2009**, *11*, 1184-1193.

Yuan, B.; Pan, Y.; Li, Y.; Yin, B.; Jiang, H. *Angew. Chem. Int. Ed.* **2010**, *49*, 4054-4058.

Yudasaka, M.; Kikuchi, R.; Matsui, T.; Ohki, Y.; Yoshimura, S. *Appl. Phys. Lett.* **1995**, *67*, 2477.

Zhang, Y.; Tan, J. W.; Stormer, H. L.; Kim, P. *Nature* **2005**, *438,* 201-204.

Zhang, W.; Wang, D.; Yan, R. Supported Nanoparticles and Selective Catalysis: A Surface Science Approach, In *Selective Nanocatalysts and Nanoscience*, Eds. Wiley-VCH, 2011, Chapter 2, 29-73.

Zhang, M.; Guan, J.; Zhang, B.; Su, D.; Williams, C. T.; Liang, C. *Catal. Lett.* **2012**, *142*, 313-318.

Zhong, Y. L.; Swager, T. M. *J. Am. Chem. Soc.* **2012**, *134*, 17896-17899.

Zhou, X.; Zhang, J.; Wu, H.; Yang, H.; Zhang, J.; Guo, S. *J. Phys. Chem. C* **2011**, *115*, 11957-11961.

Zhou, X.; Huang, Y.; Liu, C.; Liao, J.; Lu, T.; Xing, W. *ChemSusChem* **2010**, *3*, 1379-1382.

Zhu, C.; Guo, S.; Fang, Y.; Dong, S. *ACS Nano* **2010**, *4*, 2429-2437.

Zhu, Y. W.; Murali, S.; Cai, W. W.; Li, X. S.; Suk, J. W.; Potts, J. R.; Ruoff, R. S. *Adv. Mater.* **2010**, *22*, 3906-3924.

Palladium-Nanoparticle-Linked Organic Frameworks: Heterogeneous Recyclable Catalysts in Aqueous Medium

2.1 Abstract

4,4'-Biphenylene-bisdiazonium tetrafluoroborate and a palladium salt were reduced simultaneously to result in the formation of palladium atoms and 4,4'-biphenylene biradicals. The palladium atoms underwent clustering forming palladium nanoparticles, whereas the 4,4'-biphenylene biradicals underwent rapid addition reactions to other radicals and also to nanoparticle surfaces. The resulting product contains palladium nanoparticles covalently linked to an organic framework (PNOF). The effects of different reaction conditions upon metal content as well as on the morphology of the PNOF were studied. The PNOF structure was probed by different experimental techniques. The PNOFs were evaluated as a heterogeneous recyclable catalyst in aqueous medium for reduction of 4-nitrophenol and Suzuki coupling reactions. The catalyst exhibited high reactivity even in Suzuki couplings of aryl chlorides.

2.2 Introduction

Many historians consider, the conclusion "forms a new quantity of water equal to that decomposed" made by Scottish chemist Elizabeth Fulhame in 1794 to explain better burning of substances like coal and charcoal when they are slightly wet, as the first scientific account of a catalyst (Fulhame 1794). In that sense, a catalyst is defined as "a material that speeds reactions by making or breaking chemical bonds, without being consumed". In modern chemistry "Catalyst not only makes transformations accessible but also directs the reaction in new ways." Catalysis is like bulldozing chemical pathways between reactants and products that might otherwise take forever into a shortcut. Thus, a really good catalyst is similar to a multilane superhighway (Figure 2.1).

More than 15 Nobel prizes awarded for work on catalysis shows the importance of this field of research. Thousands of scientists around the globe work
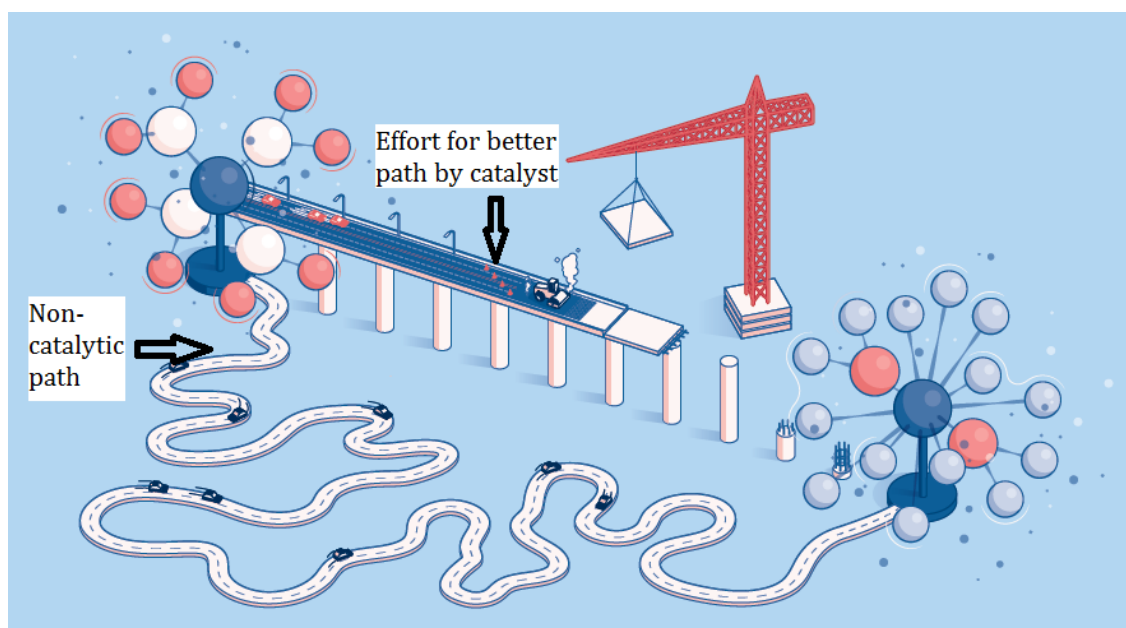
Figure 2.1 Cartoon representation of the purpose of using a catalyst in a chemical reaction (Reproduced with permission from the reference Lim 2016).

in this filed because catalysts are used in almost 90% of processes in the industry. Apart from the sustainability, the objective of catalysis is to direct reactions through precisely defined corridors. They (1) allow to skip reaction steps, (2) reduce waste, (3) minimize energy use and (4) do more with less. Catalysis plays a major role in "green chemistry" by avoiding pollution before it happens (Lim 2016). Catalysts are the key to unlocking energy sources other than coal, oil, and gas, which are difficult to use due to inertness. Catalyst can make the splitting of water in more economically viable means. Catalyst can also provide new ways to utilize the materials like biomass and carbon dioxide. The number of publications in this field is tripling every year for the past decade. Researchers are working towards better catalysts using various approaches. These include: (a) design of new small-molecule complexes, (b) chemical tailoring of biological enzymes, (c) pursuing advances in nanotechnology, (d) design of catalysts that can be activated by light, (e) design of catalysts that can be incorporated into the DNA double helix and (f) catalyst design using modern computational modelling tools.

Industrial catalysts most often consist of a metal ion surrounded by 'ligands'. In the majority of the cases the reaction in question i.e., making or breaking chemical bonds in a specific way, is performed by the metal. The ligands often control the

access of the reactants to the metal ion (Nicewicz 2008). Usually, the ligands used are carbon-based. Most of the studies in this area are focused on tailoring these ligands to produce a catalyst capable of performing the desired reaction in a specific manner. Catalyst design often uses tedious and complex synthetic protocols. Most of the catalysts used at present are based on expensive metals such as platinum, ruthenium iridium etc. The emphasis at present is to construct catalysts using earth-abundant elements such as iron, nickel or copper or by using easy-to-make or cheap ligands.

Another very important aspect is the development of heterogeneous catalysts. Most versatile homogeneous catalysts are unstable to prolonged exposure to heat. Homogeneous catalysts generally offer high performance and selectivity but perform poorly when it comes to separation and reuse. Hence large-scale industry tends to use heterogeneous-catalysts which are easily separable and recyclable (Vieira 2017). Designing solid heterogeneous catalysts with atomic precision was a difficult task previously. But rapid advances in nanotechnology made it possible to prepare robust solid catalysts with performance similar to those of homogeneous catalysts (Bell 2003).

Other than recovery and recyclability, the use of green solvents such as water and ambient temperature conditions also greatly influence catalyst design. Ambient temperature conditions and use of water as a solvent will make the industrial process cheaper and environmentally friendly than processes that require toxic organic solvents and large amounts of heat. Keeping all these aspects in mind we have tried to synthesize heterogeneous catalyst in a single step in which the active metal nanoparticles were stabilized with metal-carbon covalent bonds. Other than the metal only carbon and hydrogen are present in this material. This will open up a new and efficient pathways to prepare catalyst with carbon containing stabilizing agents which otherwise requires sophisticated preparation techniques. The catalyst exhibited very good activity in aqueous medium at ambient conditions.

Recently, our group has exploited the surface grafting potential of the radicals generated from diazonium salts through solution reduction to synthesize Au and Pd nanoparticle-cored dendrimers (NCD) with metal–carbon bonds (Kumar 2010; 2011; 2012). We observed that Pd-NCDs are good catalysts for hydrogenation

and C-C bond forming reactions (Kumar 2011; 2012). Herein, we have explored the possibility of exploiting the reaction further to prepare porous metal nanoparticle-linked organic frameworks (MNOF), in which the metal nanoparticles are captured in the organic framework through several metal–carbon covalent bonds. The microporous organic framework formation as well as nanoparticle insertion into the framework could be accomplished in a single reduction step as shown in Scheme 2.1. Our strategy involved the simultaneous reduction of a bisdiazonium tetrafluoroborate and a metal salt. The bisdiazonium salt, upon reduction, generates an organic biradical of high reactivity. The metal salt, upon reduction, generates metal atoms that can undergo clustering to generate metal nanoparticles. The organic biradicals can undergo coupling reactions to generate a complex organic framework. They can also form covalent bonds with the growing metal nanoparticles. Both reactions will occur leading to the formation of MNOF. Thus our strategy would enable us to synthesize metal nanoparticles trapped in organic frameworks through several metal–carbon covalent bonds in one step.
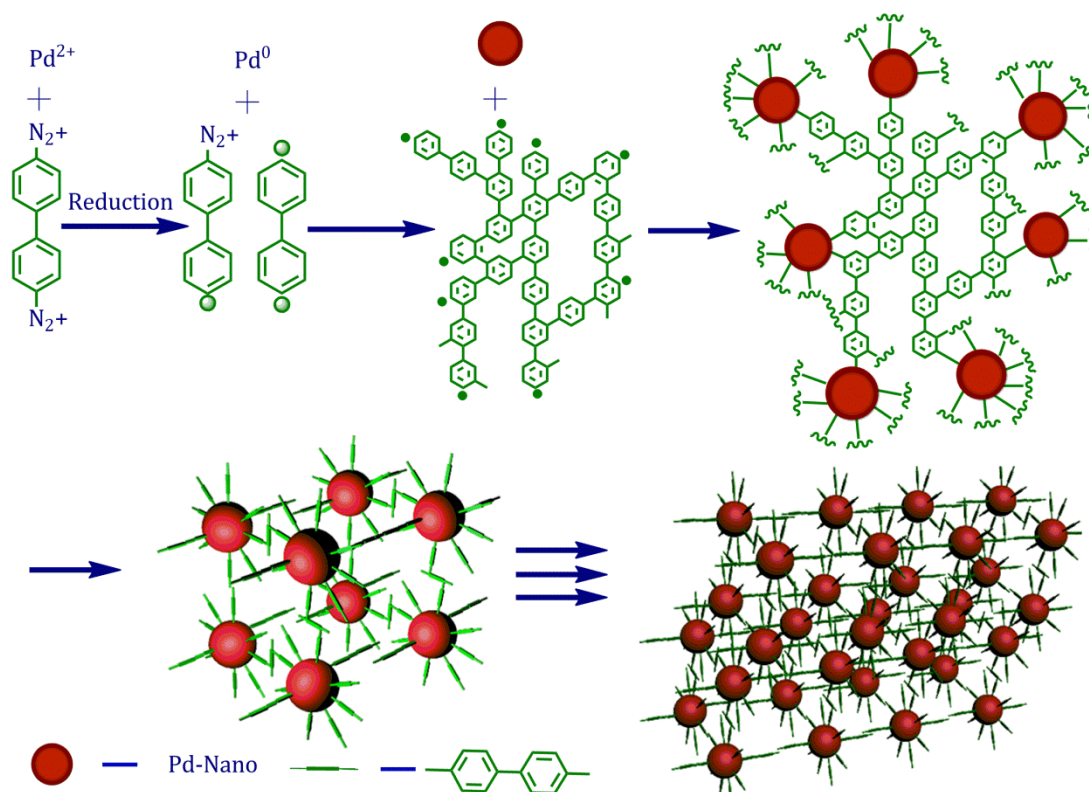
Scheme 2.1 The various stages of MNOF formation.

2.3 Results and Discussion

2.3.1 Synthesis

We employed the palladium salt K_2PdCl_4, which was reduced using sodium borohydride in the presence of 4,4'-biphenylenebisdiazonium tetrafluoroborate (BPBDT). Reduction of the Pd salt resulted in the formation of Pd nanoparticles and reduction of the bisdiazonium salt led to the formation of bisbiphenylene diradical as shown in Scheme 2.1. The bisbiphenylene diradical is highly reactive and undergoes rapid radical–radical coupling or addition to the ortho or meta positions of phenyl rings to create a complex organic polymeric framework. These radicals can add to the Pd nanoparticles also through Pd-C covalent bonds, which would lead to entrapment of the nanoparticle in the organic framework. We have designated these structures as palladium-nanoparticle-linked organic frameworks (PNOF). A schematic representation of the events taking place in the reaction is given in Scheme 2.1. It may be noted that the actual PNOF structure is uncertain and the structure shown is only one of the several possibilities.

By varying the relative concentrations of the Pd salt and bisdiazonium fluoroborate, we were able to prepare three PNOF systems (Table 2.1). A sample without Pd (designated as BLANK) was also prepared. In all cases, yields of the materials were near quantitative. Commercially available reagents were used as received without further purification.

Table 2.1 List of materials under investigation.

Material Code	K_2PdCl_4 (mmol)	BPBDT (mmol)	Surface Area (m^2/g)	Yield (%)
PNOF1	1	0.5	8.54	98
PNOF2	1	1	11.33	95
PNOF3	1	2	14.95	95
BLANK	0	1	-	90

2.3.2 Characterizations

PNOF samples obtained were all black powders insoluble in water and most organic solvents. Suspensions of these materials in water/ethanol (9:1) mixture

settled quickly, but in organic solvents, they disperse very finely and settled only very slowly. The specific surface areas (SSA) of the PNOFs were measured by the nitrogen sorption method and the values obtained are presented in Table 2.1. The specific surface areas obtained were 9 m^2g^{-1} for PNOF1, 11 m^2g^{-1} for PNOF2, and 15 m^2g^{-1} for PNOF3. The results indicate that the surface area increases with decrease in metal content of the PNOF. The low values of SSA suggest that these materials are not very porous.

2.3.2.1 TGA Analysis

To determine the metal content in these samples, they were subjected to thermo gravimetric analysis (TGA) in an argon atmosphere and the results are presented in Figure 2.2. TGA analysis revealed that PNOF1 had the highest metal content of 62% followed by PNOF2 (42%) and PNOF3 (29 %). For the three PNOF materials, decomposition occurred in two stages. The first stage that occurs at approximately 100 °C may be caused by the removal of solvent molecules or small organic fragments. The second decomposition stage occurs above 300 °C and this most probably can be attributed to the breaking of Pd-C bonds. The BLANK material exhibited the typical thermogravimetric behavior of a polyaryl polymer. In this case 100% decomposition of the material was observed at temperatures >500 °C. The higher decomposition temperature for BLANK may be attributed to the high C-C bond energy (463 kJ mol^{-1} for C-C between phenyl rings) relative to the energy for Pd-C single bonds (436 kJ mol^{-1}) (Ghosh 2008 [a,b]; Gutzler 2009).
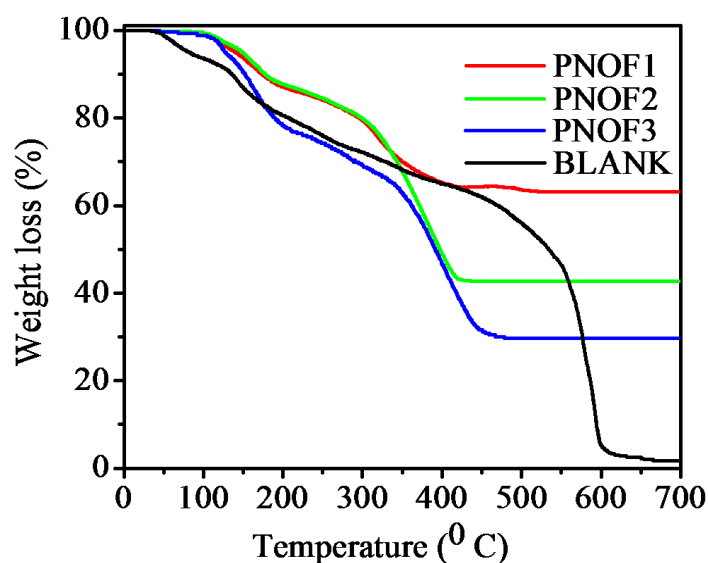
Figure 2.2 Thermo gravimetric analysis of BLANK, PNOF3, PNOF2, and PNOF1.

2.3.2.2 IR studies

The PNOF reported here were prepared by the simultaneous reduction of the bisdiazonium salt and the metal ion. IR spectrum of the bisdiazonium salt BPBDT exhibited a peak at 2274 cm^{-1} attributable to the vibrational stretching of the diazo group as shown in Figure 2.3 (top panel). The IR spectra of the PNOFs or BLANK (Figure 2.3) did not contain the diazo peak at 2274 cm^{-1} indicating that unreacted diazo groups are not present in any of the samples. Only the characteristic stretching vibrations corresponding to the aromatic C-H (3033 cm^{-1}) and C-C vibrations of the polyphenyl skeleton (multiple peaks between 1600 and 1400 cm^{-1}) are present in the IR spectra of PNOF samples. As the organic content in the PNOF samples increases, the intensities of these IR peaks increase as seen from Figure 2.3. The organic content in PNOF1 is minimum and, hence, vibrational peaks attributable to the ligand are very weak in this sample. The intensities of the C-H, C-C, and C=C
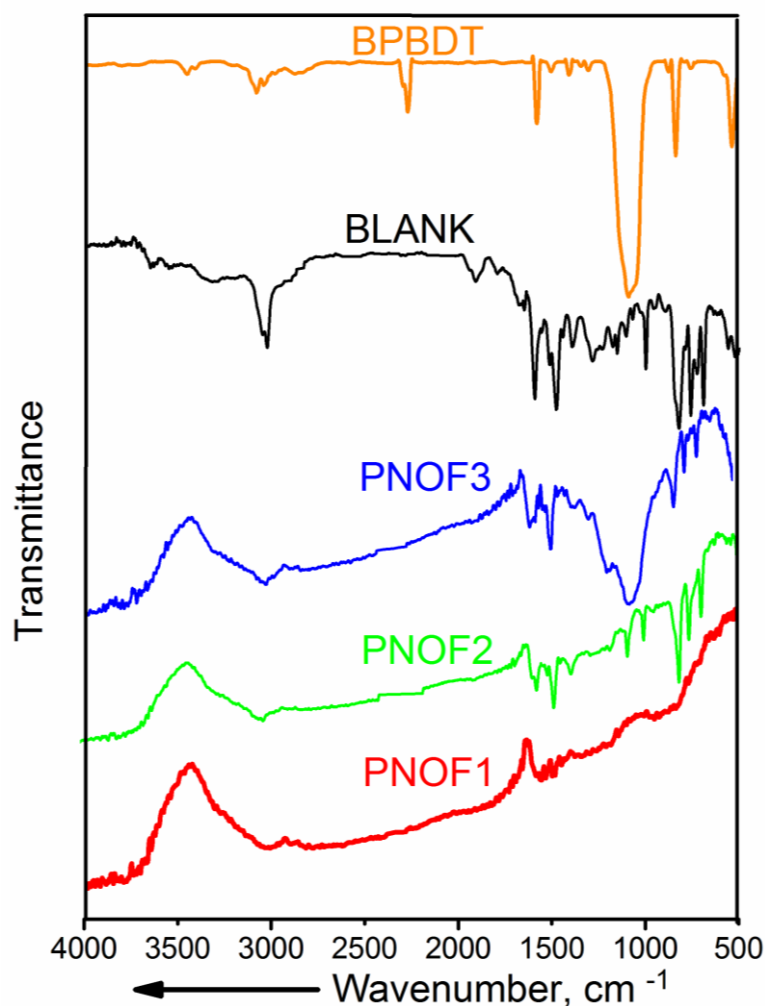
Figure 2.3 IR spectra of BPBDT, BLANK, PNOF3, PNOF2, and PNOF1.

vibrations are maximum in the BLANK sample, because this sample is composed entirely of the organic framework.

2.3.2.3 Absorption studies

Absorption spectra of the PNOFs were taken in toluene. The materials were dispersed in toluene by sonicating for five minutes and then filtered before recording the spectra (Figure 2.4). Pd nanoparticles do not show a plasmon band and the absorption spectrum of Pd nanoparticles consists of a smoothly increasing absorption at increasing energy (Kumar 2010; 2011) . PNOF1 and PNOF2 exhibited absorption spectra that were similar to the reported absorption spectra of Pd nanoparticles. PNOF3 exhibited a shoulder at approximately 390 nm and this absorption is attributable to the organic framework. It is clear from Figure 2.4 that the BLANK exhibited absorption at 390 nm. The absorption spectra thus suggest that PNOF1 and PNOF2 have a higher Pd nanoparticle content and PNOF3 has more contribution from the organic framework.
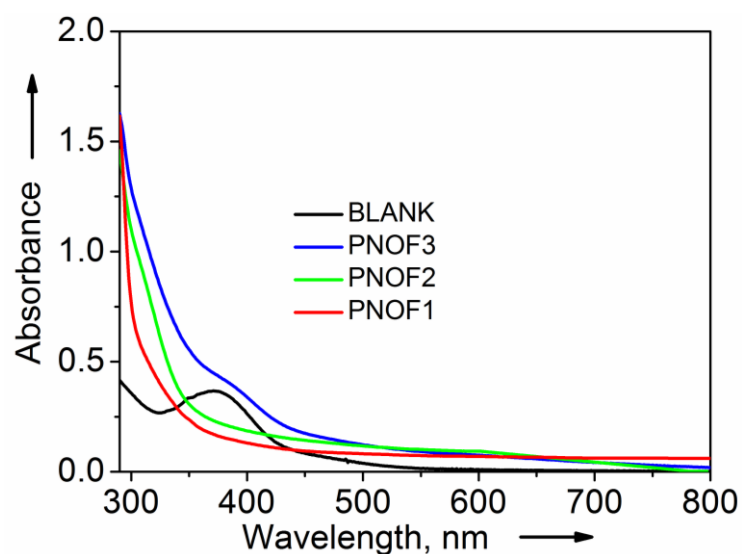
Figure 2.4 Absorption spectra of BLANK, PNOF3, PNOF2, and PNOF1.

2.3.2.4 NMR studies

NMR spectra of the BLANK and PNOF were obtained in $CDCl_3$. As the samples were not very soluble, suspensions in $CDCl_3$ were employed to obtain the spectra. ^1H NMR spectra of the diazonium salt BPBDT, BLANK, and the PNOFs are given in Figure 2.5. The ^1H NMR spectrum of BPBDT taken in D_2O showed two sharp doublets at δ 8.64 and 8.21 ppm, and this pattern is characteristic of 1,4-

disubstituted benzene derivatives. The ^{1}H NMR spectrum of PNOF1 also showed only two broad doublets (δ 7.41 and 7.47 ppm). The ^{1}H NMR spectra of the PNOFs became more and more complex as the organic content in the samples increased, as can be seen from Figure 2.5. The BLANK sample exhibited a very complex NMR pattern in the δ 7 - 8 ppm range. In fact, a very complex pattern is expected based on the framework structure shown in Scheme 2.1.
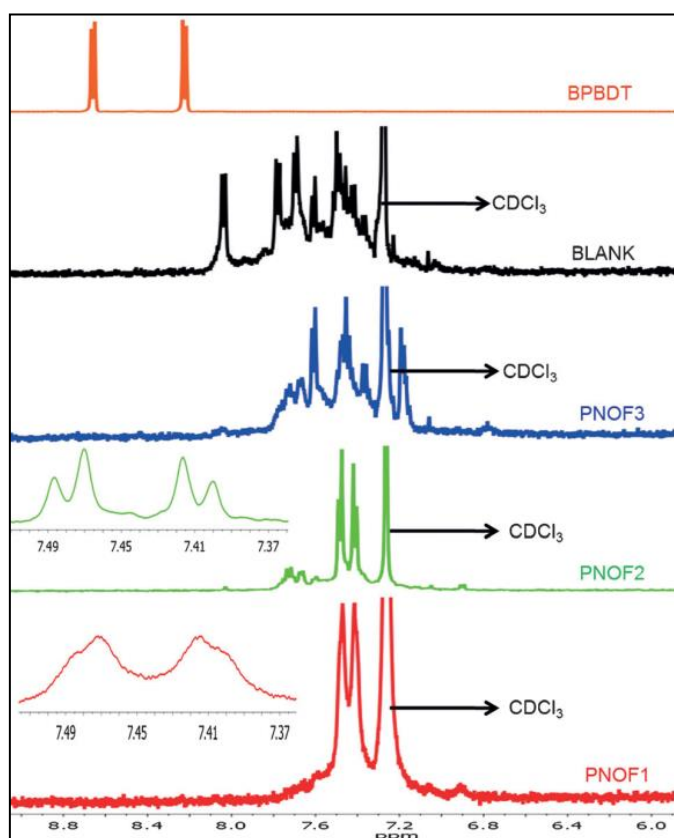
Figure 2.5 ^{1}H NMR spectra of BPBDT, BLANK, PNOF3, PNOF2, and PNOF1. Insets give expanded spectra between δ 7.35 and 7.54 for PNOF1 and PNOF2. The solvent peak is marked by the arrow.

It is widely known that if organic residues are linked to metal nanoparticles, the ^{1}H NMR signals of the metal-attached moiety highly broadened and, hence, may not be observable (Ghosh 2008 [a,b]) . The ^{1}H NMR signals we observed for the PNOF are most probably attributable to organic residues placed somewhat away from the metal particles. In the case of PNOF1, only two signals (δ 7.41 and 7.47 ppm) were observed, as expected for a 4,4'-disubstituted biphenyl residue. The

double doublet nature of the peaks is not predominant probably owing to the presence of metal residues close to the biphenyl moiety, which leads to signal broadening. As the metal content decreases, the average distance between metal nanoparticles increases and more and more NMR signals are observed. In the case of PNOF2, the peaks at δ 7.41 and 7.47 ppm are still prominent but additional signals can also be seen. Some characteristics of these two peaks (double doublet) can be clearly observed in the PNOF2 spectrum. PNOF3 has high organic content and exhibits NMR signals very similar to those of BLANK, as expected.

2.3.2.5 XRD analysis

To confirm the presence of nanoparticles in the PNOFs, powder XRD (PXRD) patterns were obtained and these are shown in Figure 2.6. For the palladium-containing samples, diffraction peaks were obtained at 2θ angles of 40.1°, 46.1°, 67.5° and 81.8°. The d spacings corresponding to these XRD lines are 0.22, 0.19, 0.14, and 0.12 nm. These d spacings correspond to (111), (200), (220), and (311) planes with the lattice constant 3.871 Å. These observations confirm the presence of metallic palladium with face-centered cubic (fcc) crystalline structure in the PNOFs. The PXRD pattern for BLANK reveals broader peaks between 15° and 30°. This indicates that the sample is somewhat amorphous in nature. PXRD of the PNOFs also have broad peaks in these regions and the intensities of these organic peaks decrease with increasing metal content of the PNOF. This indicates that the PNOFs have palladium nanoparticles and organic frameworks present in them.
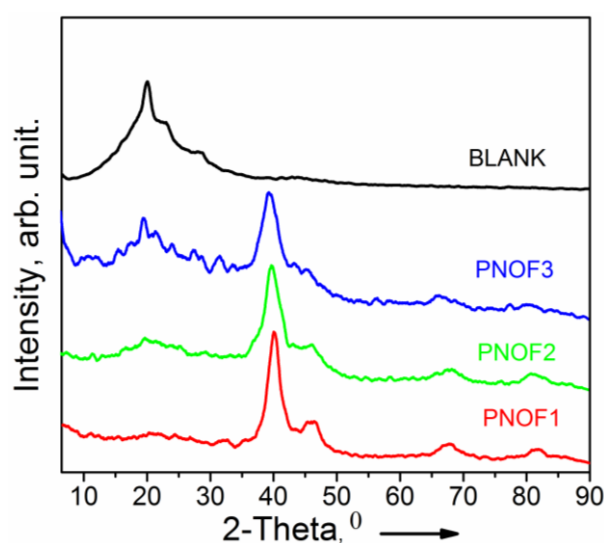
Figure 2.6 XRD patterns of BLANK, PNOF3, PNOF2, and PNOF1.

2.3.2.6 XPS studies

To obtain further information about the nature of bonding between Pd nanoparticles and organic residues and also the oxidation state of Pd in the PNOFs, X-ray photoelectron spectroscopy (XPS) analyses were performed. XPS survey spectra for the PNOFs are shown in Figure 2.7. For all PNOFs, Pd 3d and C 1s peaks are clearly observed along with a small O 1s peak. The O 1s peak may be attributed to the solvent entrapped in the materials during the sample preparation.
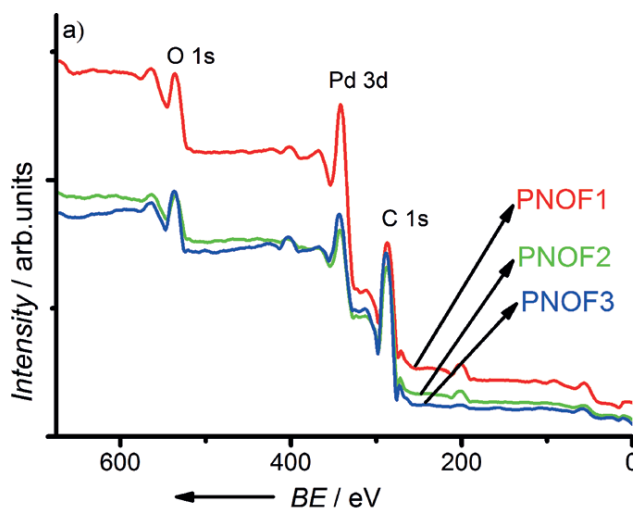
Figure 2.7 XPS survey spectra of PNOF materials. BE = Binding energy.

A close inspection of the C 1s peaks of the PNOFs reveals that these can be deconvoluted into three components using the curve-fitting program (Figure 2.8). For all three PNOFs, the major peak at 285 eV can be resolved into C-C (284.5 eV) and C-H (285.3 eV) contributions. Carbon bonded to Pd is known to give a signal at a lower energy of 282.3 eV because of the screening of the core hole by Pd valence electrons (Franzén 2005; Molnàr 2011; Choi 2012; Pagliaro 2012; Pascanu 2013). In the case of PNOF1, the Pd-C signal is very prominent at 282.3 eV. This signal is less prominent in the case of PNOF2. In the case of PNOF3, the Pd content is much less and, hence, the peak is hardly noticeable, but can still be resolved by the curve fitting program as seen in Figure 2.8. The XPS data thus clearly establish that in these PNOFs, the Pd clusters are covalently linked to carbon atoms and not merely trapped in an organic framework.

One can also notice in Figure 2.8 that the intensity of the C-C signal increases relative to that of the C-H signal as we go from PNOF1 to PNOF3. This indicates that

the degree of crosslinking of the aryl groups is more in PNOF3 and cross-linking is occurring by replacement of C-H bonds. This can be taken as an indirect evidence for formation of the organic network structure by coupling of aryl radicals to the ortho and/or meta positions of the phenyl rings as suggested in Scheme 2.1.
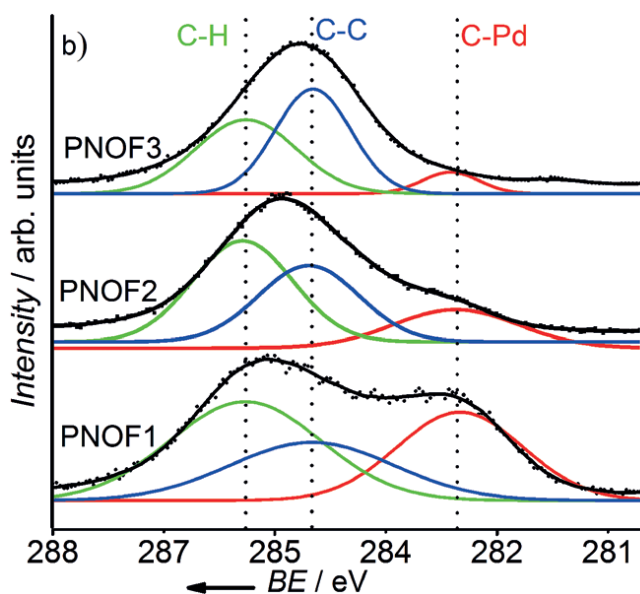
Figure 2.8 X-ray photoemission spectra of the C1s. BE = Binding energy.

The XPS data for Pd 3d for all the three PNOFs are shown in Figure 2.9. The Pd 3d contains two spin-orbit components namely $3d_{5/2}$ and $3d_{3/2}$ (Yang 2009). All the three PNOFs contain the signal from both Pd^0 and Pd^{II}. Overall four peaks are present, which are identified as Pd^0 $3d_{5/2}$ (335.4 eV), Pd^0 $3d_{3/2}$ (340.5 eV), Pd^{2+} $3d_{5/2}$ (337.4 eV), and Pd^{2+} $3d_{3/2}$ (342.6 eV), and clearly marked in Figure 5 c. The binding energies corresponding to the Pd^{2+} $3d_{5/2}$ and Pd^{2+} $3d_{3/2}$ remains the same for all the three PNOFs.

In the PNOFs, Pd^{2+} signals could arise in two ways. One possibility is that the surface of Pd nanoparticles contain Pd in the +2 oxidation state (Cheon 2008; Zhou 2010; Johnston 2012; Friederici 2012), and these are involved in covalent bonding to the organic framework through Pd^{II}-C bonds. The second possibility is the presence of Ar-Pd^{II}-Ar moieties, with Ar referring to small organic residues. If the Pd^{2+} signals actually arise from Ar-Pd^{II}-Ar residues, we would expect that the contributions from such structures would be more in PNOFs with larger organic

content. The XPS data actually shows the reverse trend. Intensities of the Pd^{2+} bands are in the order PNOF1>PNOF2>PNOF3. The number of nanoparticles in a given area in the TEM image also follows the same order. Hence, we propose that the Pd^{2+} signals arise from Pd^{II}-C bonds involving the Pd^{2+} present on the surface of the nanoparticles.
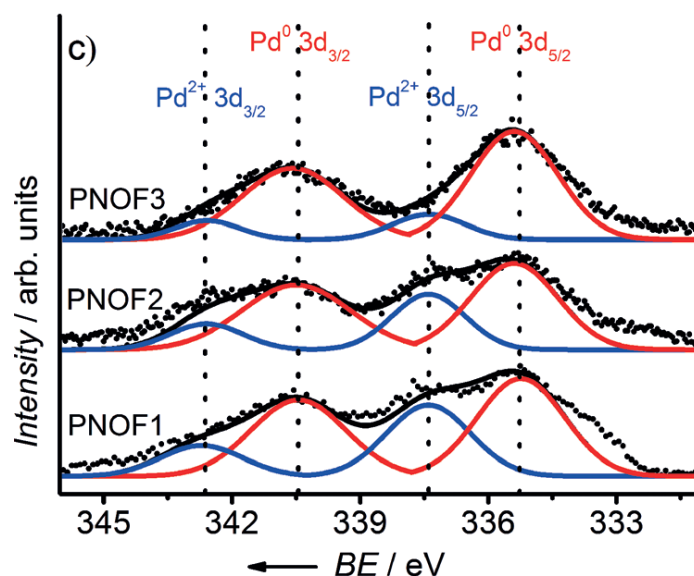
Figure 2.9 X-ray photoemission spectra of the Pd 3d. BE = Binding energy.

2.3.2.7 SEM analysis

SEM images of the PNOFs and BLANK are presented in Figure 2.10. A close examination of the SEM image of the BLANK (Figure 2.10 a) revealed that the structure consisted of irregularly stacked small planar flakes. The irregular packing leads to the formation of crevices and fissures on the surface. The small flakes most probably are the organic frameworks. In the case of PNOFs (Figure 2.10 b–d), two types of structures could be identified in the SEM image. A relatively large (>1 μm) crystalline structure with smooth hard-ice-like surface constitutes the major fraction. Clusters of small planar flakes were seen adhered at several locations on the surfaces of the large structures. Domains containing such clusters are less in PNOF1, which has the highest metal content.

The bisphenylene radicals generated in the reduction of the diazonium salts undergo random addition reactions leading to the formation of planar organic networks as shown in Scheme 2.1. The flakes that we observe in the SEM image of

BLANK most probably are large planar network structures. These undergo stacking owing to π-π interactions. If metal nanoparticles are present, the growing organic framework can attach itself to metal nanoparticles. As the metal nanoparticle is three-dimensional, attachment of small aromatic frameworks leads to the formation of three-dimensional structures. Small organic frameworks containing only a few or no nanoparticles can also be present in the reaction medium and these may get attached to the larger particles, giving rise to the observed morphology.
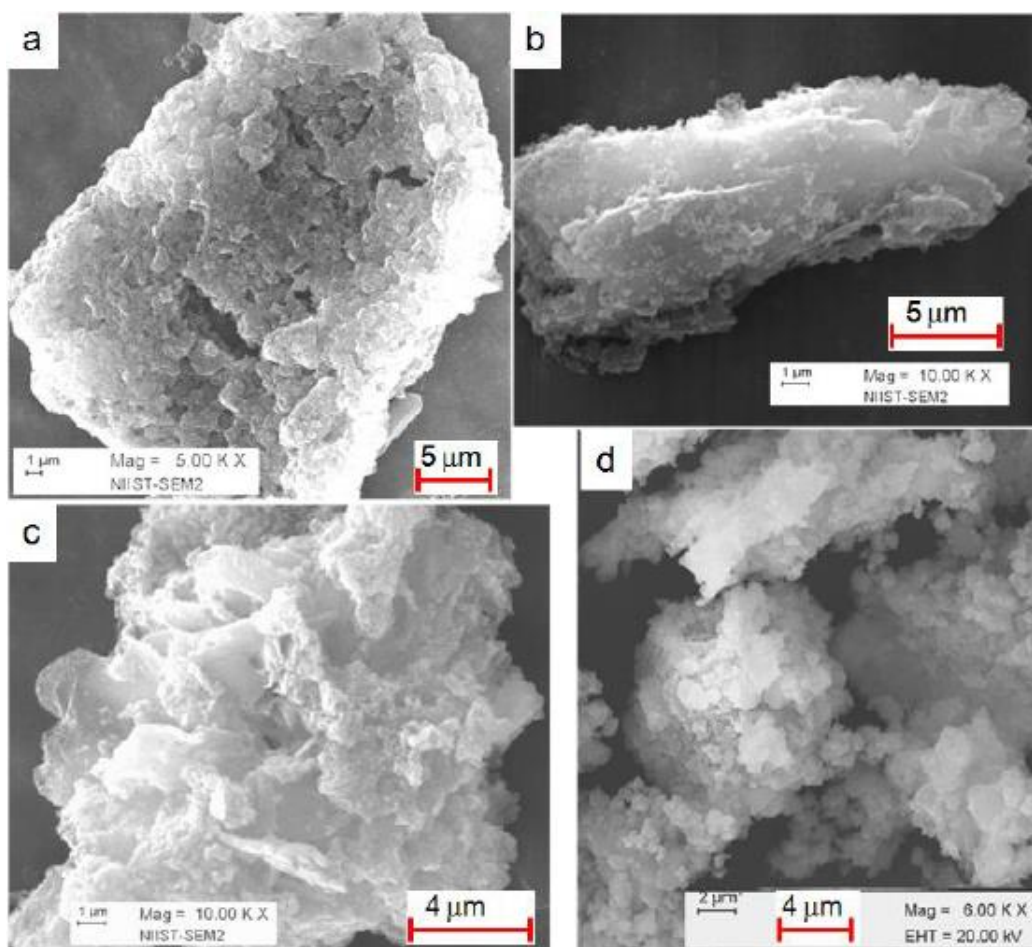
Figure 2.10 SEM images (a) BLANK (b) PNOF3, (c) PNOF2 and (d) PNOF1.

2.3.2.8 HRTEM analysis

TEM images of BLANK and PNOFs are given in Figure 2.11. In the case of BLANK the TEM image reveals the presence of cavities and crevices. The TEM image confirms the conclusion obtained from the SEM analysis that the BLANK is formed by the aggregation of large numbers of smaller flaky substances. TEM images of

PNOF1–PNOF3 exhibit contours of a soft substance within which are embedded the metal nanoparticles. In all the three PNOFs, the majority of the metal nanoparticles are 5-8 nm in size as revealed by the core-size histogram (Figure 2.12). No metal
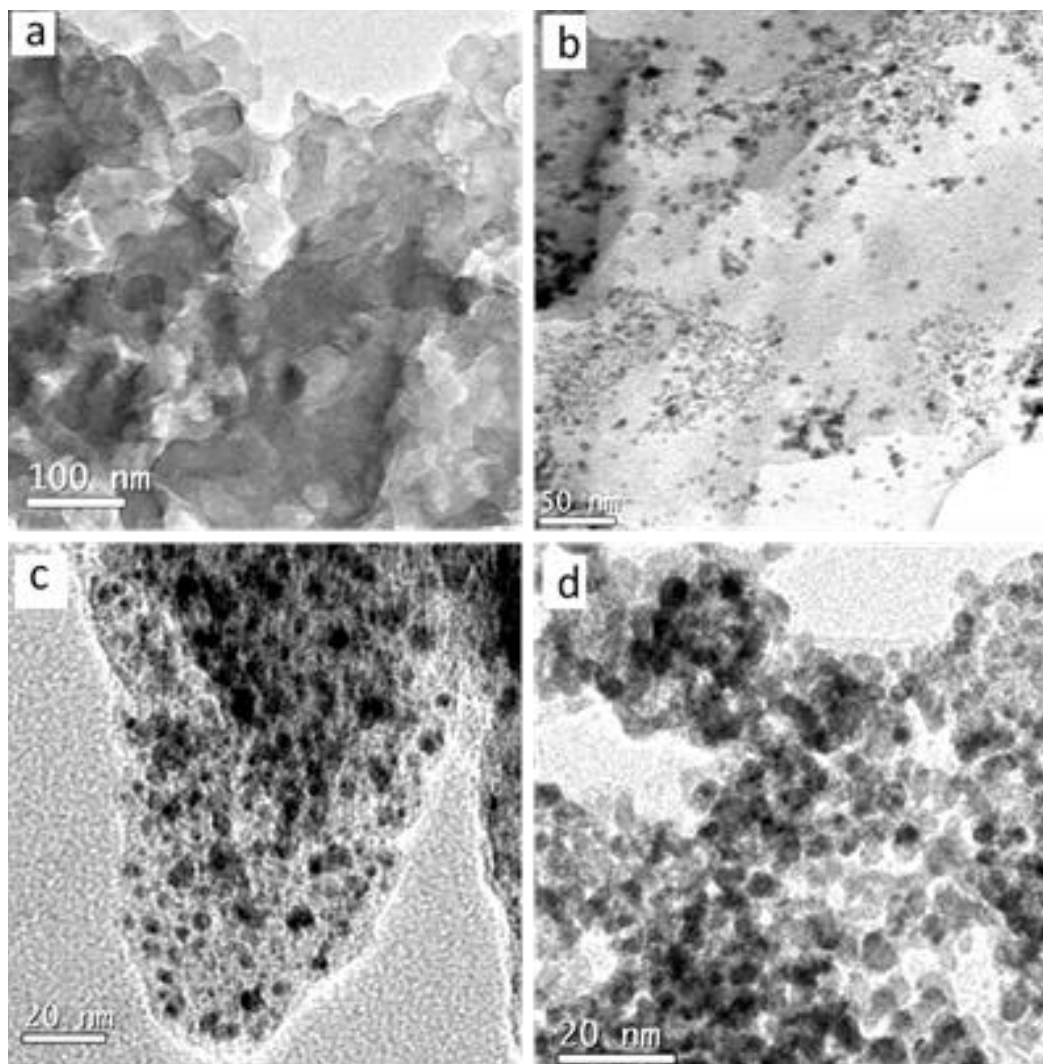
Figure 2.11 TEM images (a) BLANK (b) PNOF3, (c) PNOF2 and (d) PNOF1.
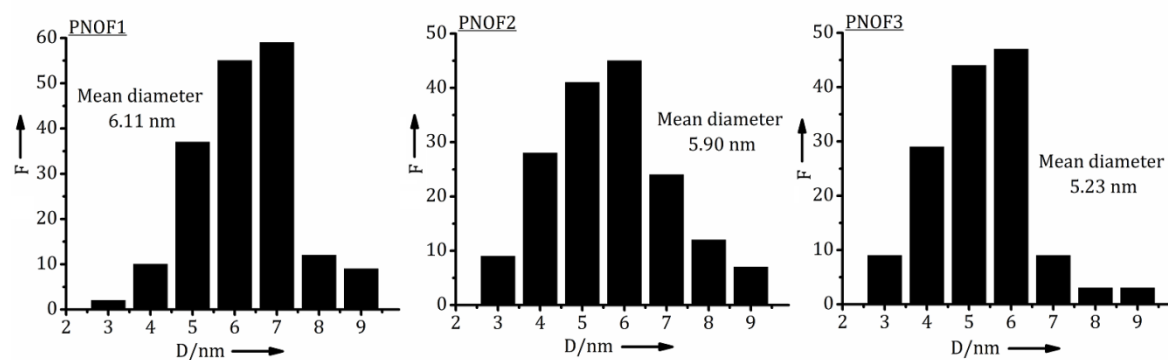
Figure 2.12 Core-size histograms for PNOFs; (F=frequency).

particles are seen outside the contours of the organic framework in Figures 2.11b-d. This confirms that the metal nanoparticles are covalently attached to the network. If the nanoparticles were entrapped in the network by noncovalent interactions, small numbers of these particles could have been found outside the contours. We did not observe such nanoparticles outside the organic framework.

2.3.3 Estimation of number of surface atoms in PNOF

It was possible to estimate the total number of atoms and number of atoms on the surface of nanoparticles from TEM experiments (Gopidas 2003 [a,b]; Lewis 2006). It can be assumed for large "spherical" metal nanoparticles that:

$$V_{cluster} = N V_{atom} \qquad (2.1)$$

$$4/3\ \pi\ (R_{cluster})^3 = N\ 4/3\ \pi\ (R_{atom})^3 \qquad (2.2)$$

Where N, $V_{cluster}$, and $R_{cluster}$ are the total number of atoms, volume, and radius of a single cluster, respectively. V_{atom} and R_{atom} are the volume and radius of single atom, respectively. By rearranging 2.2 will change to

$$R_{cluster} = N^{1/3}\ R_{atom} \qquad (2.3)$$

Or

$$N = (R_{cluster}/\ R_{atom})^3 \qquad (2.4)$$

If we assume that the cluster is spherical, its suraface area ($S_{cluster}$) can be calculated using the relation

$$S_{cluster} = 4\ \pi\ (R_{cluster})^2 \qquad (2.5)$$

Similarly the number of surface atoms (N_S) can be calculated by the relation

$$N_S = (4\ \pi\ (R_{cluster})^2)\ /\ (\pi\ (R_{atom})^2) \qquad (2.6)\ (Lewis\ 2006)$$

By applying equation 2.3 in 2.5 we will get the relation

$$N_S = 4\ N^{2/3} \qquad (2.7)$$

N_S for all the PNOFs were calculated as above from values of $R_{cluster}$ obtained from TEM and known value of R_{atom} for Pd. The percentage of surface Pd atoms in the PNOFs and their weight percentages were calculated as given in Tables 2.2- Table 2.4.

Table 2.2 Physical data for Pd-nanoparticles in PNOF1.

Average Pd-nanoparticle diameter   = 6.11 nm

Average Pd-nanoparticle radius	= 3.56 nm
Average radius of Pd atom	= 0.137 nm
Total no. of Pd atoms per nanoparticles N	= $(R_{cluster}/ R_{atom})^3$
	= $((3.56 \times 10^{-9})/(0.137 \times 10^{-9}))^3$
	= 17546
No. of surface Pd atoms per nanoparticles Ns	= $4 \times (17546)^{2/3}$
	= 2701
Percentage of surface atom	= 15. 39 %
Weight percentage of Pd in PNOF1	= 62%

Weight percentage of Pd in the surface of nanoparticles in PNOF1 = 62% × 0.1539

= 9.54%

Table 2.3 Physical data for Pd-nanoparticles in PNOF2.

Average Pd-nanoparticle diameter	= 5.90 nm
Average Pd-nanoparticle radius	= 2.95 nm
Average radius of Pd atom	= 0.137 nm
Total no. of Pd atoms per nanoparticles N	= $(R_{cluster}/ R_{atom})^3$
	= $((2.95 \times 10^{-9})/(0.137 \times 10^{-9}))^3$
	= 9984
No. of surface Pd atoms per nanoparticles Ns	= $4 \times (9984)^{2/3}$
	= 1855
Percentage of surface atom	= 18. 58 %
Weight percentage of Pd in PNOF2	= 42%

Weight percentage of Pd in the surface of nanoparticles in PNOF2 = 42% × 0.1858

= 7.80 %

Table 2.4 Physical data for Pd-nanoparticles in PNOF3.

Average Pd-nanoparticle diameter	= 5.23 nm
Average Pd-nanoparticle radius	= 2.62 nm
Average radius of Pd atom	= 0.137 nm
Total no. of Pd atoms per nanoparticles N	= $(R_{cluster}/ R_{atom})^3$

$$= ((2.62 \times 10^{-9})/(0.137 \times 10^{-9}))^3$$

$$= 6995$$

No. of surface Pd atoms per nanoparticles Ns $\quad = 4 \times (6995)^{2/3}$

$$= 1463$$

Percentage of surface atom $\quad\quad\quad\quad\quad\quad = 20.91\%$

Weight percentage of Pd in PNOF3 $\quad\quad\quad = 29\%$

Weight percentage of Pd in the surface of nanoparticles in PNOF3 $= 29\% \times 0.2091$

$$= 6.06\%$$

The PNOFs were employed as catalysts in Suzuki reactions. In order to compare the catalytic efficiencies of PNOFs to previously reported catalysts, turnover frequencies (TOF) need to be determined. In order to calculate TOF values, it was necessary to find out the total number of reaction sites present in the catalysts. In the case of metal nanoparticles, the number of active sites can be taken as equal to the total number of atoms or the number of surface atoms present in the cluster (Umpierre 2011). We have calculated TOF in both ways. We employed 5 mg or 1 mg of PNOFs as a catalyst. Total number of Pd atoms as well as surface Pd atoms present in 5 mg and 1 mg of PNOFs were calculated and given in Table 2.5.

Table 2.5 Amount Pd (mmol) in PNOFs.

Amount of PNOF	5 mg PNOF1	5 mg PNOF2	1 mg PNOF1	1 mg PNOF2	5 mg PNOF3
Total Pd (mmol)[a]	29.14×10^{-3}	19.74×10^{-3}	5.83×10^{-3}	3.95×10^{-3}	2.73×10^{-3}
Surface Pd (mmol)[a]	4.48×10^{-3}	3.67×10^{-3}	0.9×10^{-3}	0.73×10^{-3}	0.57×10^{-3}

[a] atomic mass of Pd = 106.4

2.3.4 Catalytic Applications

The PNOFs were found to be good catalysts for selected organic reactions. In this study we report the catalytic activity of the synthesized PNOFs in the following two reactions: 1) reduction of 4-nitrophenol (4-NP) in water, and 2) Suzuki coupling reaction between aromatic halides and phenylboronic acid in water.

2.3.4.1 Reduction of 4-nitrophenol

The reduction of 4-NP to 4-aminophenol (4-AP) is a very important reaction industrially as 4-AP is the key intermediate in the synthesis of antipyretic and analgesic drugs. 4-AP is also used as a photographic developer, dyeing agent, and anticorrosion lubricant (Saha 2010). In the laboratory, this reaction is accomplished by using sodium borohydride in the presence of a catalyst as shown in Scheme 2.2.
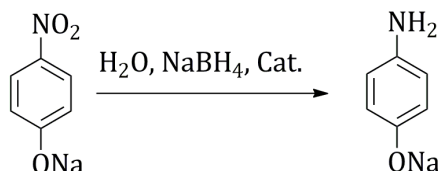
Scheme 2.2 Catalytic reduction of 4-NP.

The reaction is also used as a model reaction to examine the performance of metal nanoparticle catalysts and several such reports are available in the recent literature (Wu 2011; Hu 2011; Lin 2012; Yang 2013; Huang 2012; Lu 2014). The reaction can be followed by UV/Vis-spectroscopy. 4-NP exhibits very strong absorption at 317 nm. In the presence of sodium borohydride, this absorption shifts to 400 nm because of the formation of 4-nitrophenolate. Upon reduction, the 4-nitrophenolate will be converted into 4-aminophenolate, which absorbs at 310 nm. The reduction reaction can thus be monitored by observing the decrease of absorption at 400 nm. The rate of the reaction can be calculated from the rate of disappearance of the 400 nm absorption.

In Figure 2.13, the absorption spectra taken at different time intervals for the 4-NP/sodium borohydride/PNOF1 system are shown (data for the PNOF2 and PNOF3 are shown in Figures 2.14 and 2.15). To make a direct comparison of rates, the catalyst amounts were varied such that the Pd content remained the same in all three cases. Two isosbestic points were observed at 278 and 315 nm, suggesting that the reduction proceeded without producing byproducts.

In Figure 2.16, plots of absorbance versus time are shown for these reactions. In the presence of PNOF1, the reaction was completed in 4.5 min. When PNOF2 was employed as the catalyst, the reaction was completed in 6 min, whereas the PNOF3-catalyzed reaction took 15 min for completion.
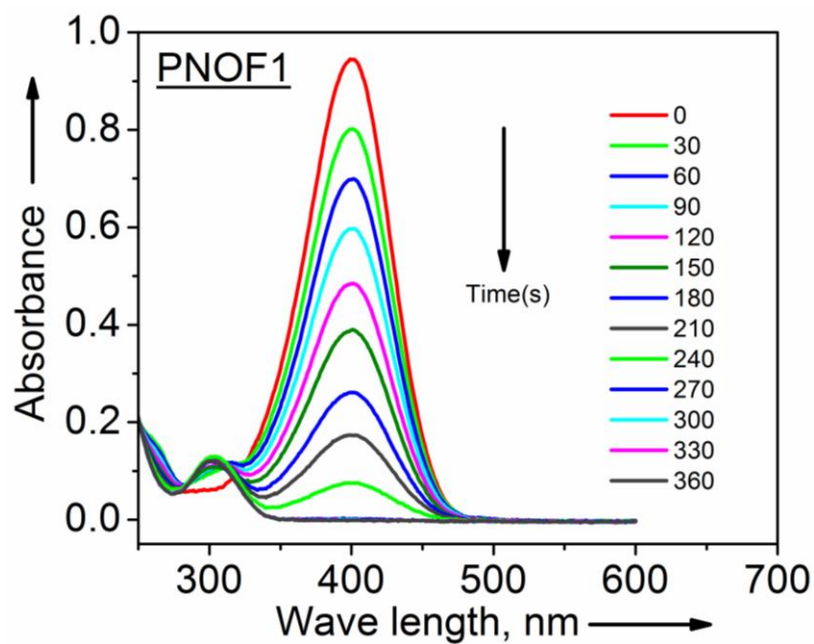
Figure 2.13 UV-visible absorption spectra of the catalytic reduction process of 4-nitrophenol to 4-aminophenol by PNOF1.
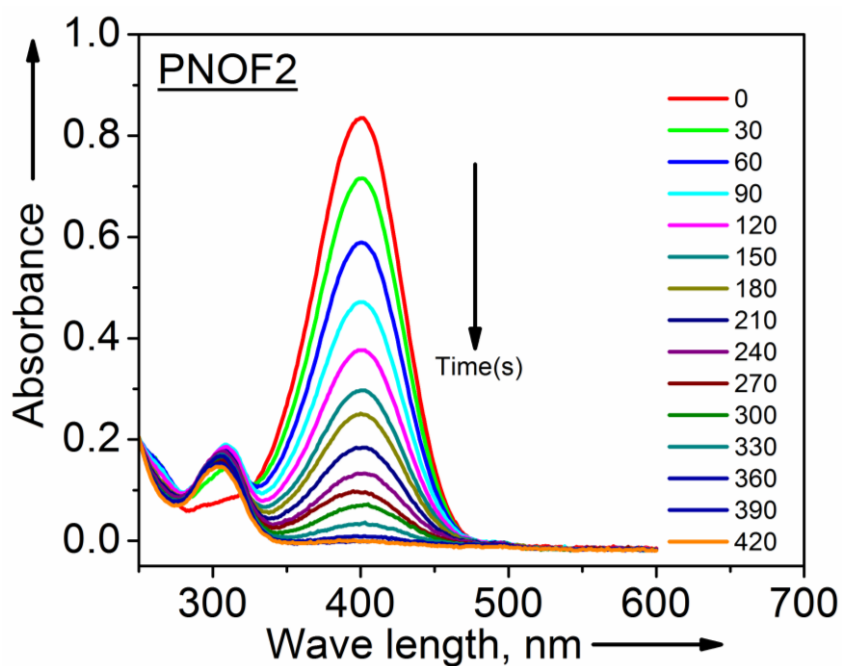
Figure 2.14 UV-visible absorption spectra of the catalytic reduction process of 4-nitrophenol to 4-aminophenol by PNOF2.
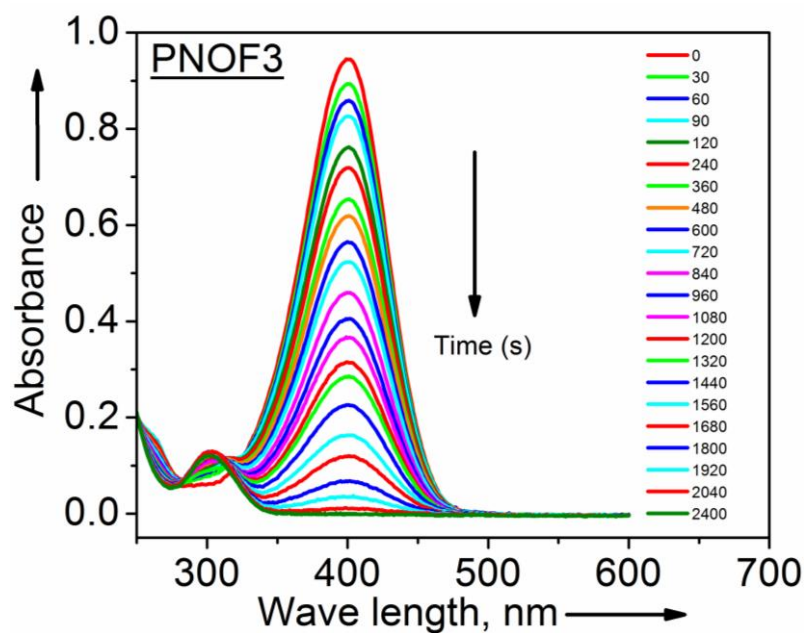
Figure 2.15 UV-visible absorption spectra of the catalytic reduction process of 4-nitrophenol to 4-aminophenol by PNOF3.
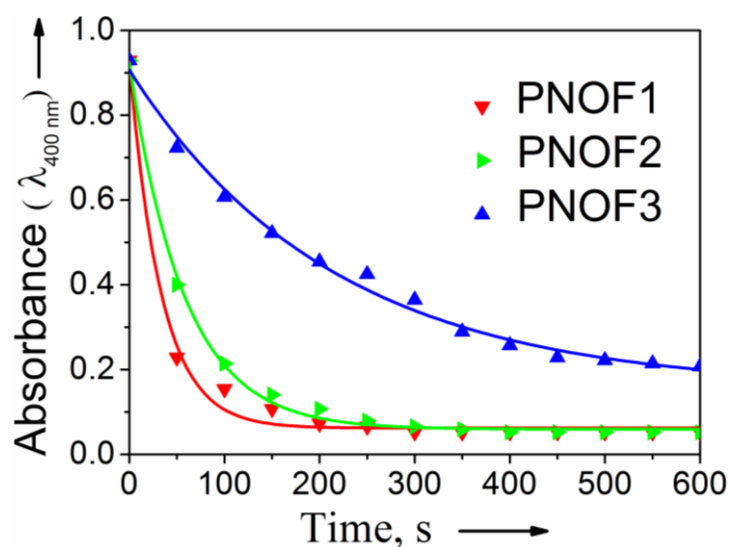
Figure 2.16 Plot of absorbance at 400 nm vs. time for the the catalytic reduction process of 4-nitrophenol to 4-aminophenol, by PNOFs.

The reduction reaction was performed under pseudo-first order conditions employing a large excess of sodium borohydride. Under these conditions, the apparent rate constant of the reaction can be obtained from the slopes of $\ln(C_t/C_0)$ versus time plots, for which C_t is the concentration of 4-NP at time t and C_0 is the

initial concentration. As the absorbance is proportional to concentrations, the absorbance values at zero time (A_0) and at time t (A_t) can be used instead of C_0 and C_t. In Figure 2.17, plots of $\ln(A_t/A_0)$ versus time for the 4-NP reduction reactions catalyzed by the three PNOFs are shown. The rate constants obtained from the plots are k_{PNOF1} = 12.44 × 10^{-3} s^{-1}, k_{PNOF2} = 11.56 × 10^{-3} s^{-1} and k_{PNOF3} = 5.88 × 10^{-3} s^{-1}. Rate constants obtained for PNOF1- and PNOF2-catalyzed reactions are comparable to or higher than those previously reported by others (Wu 2011; Hu 2011; Huang 2012; Lin 2012; Yang 2013; Lu 2014) (13.1 × 10^{-3} s^{-1}, 11.6 × 10^{-3} s^{-1}, and 1.75 × 10^{-3} s^{-1}, Lin 2012) suggesting that the PNOFs have good potential for use in industry for this reaction.
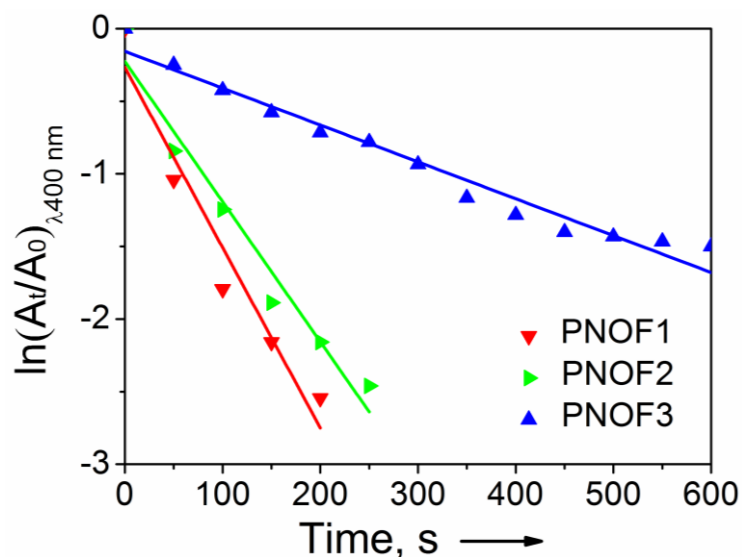
Figure 2.17 Plot of $\ln(A_t/A_0)$ at 400 nm vs. time for the catalytic reduction process of 4-nitrophenol to 4-aminophenol, by PNOFs.

2.3.4.2 Suzuki coupling reactions

Suzuki reaction involves the coupling of an aryl boronic acid with an aryl halide in the presence of a palladium catalyst and an added base to give aryl-aryl coupled products. These cross-coupling reactions can be catalyzed by several forms of Pd catalysts including Pd on carbon. It is generally believed that active zero-valent palladium is responsible for Suzuki coupling reactions (Stille 1977; Matos 1998; Muñoz 2001). In earlier reports, phosphine ligands were used to stabilize the zero-valent Pd. Ligand-free coupling in water–ethanol/water–acetone solvents are reported using Pd salts as catalysts.

The major drawback of these methods is the lack of recyclability of the catalysts employed in these studies (Franzén 2005; Liu 2006). At present, investigations in this area are directed towards the development of supported metal nanoparticles for easy recovery and catalyst reusability (Han 2008; Wu 2008; Zhu 2010; Molnàr 2011; Amatore 2012; Dhakshinamoorthy 2012; Niu 2012; Ganapathy 2013; Friederici 2013; Szulmanowicz 2013). The performances of most of the new catalysts developed have been evaluated by using cross-coupling reactions of phenylboronic acid and halobenzenes.

As the reaction involves the use of a base, we made an attempt to find out the most suitable base for PNOF-catalyzed Suzuki reactions. For this purpose, we performed the reaction between phenylboronic acid and 4-bromoacetophenone (Scheme 2.3) using PNOF2 and different bases in an aqueous medium under conditions shown in Table 2.6. The yields shown in the table are values obtained by using GC– MS using 1,2,3- trimethoxybenzene as an internal standard. It is clear from Table 2.6 that hydroxides, carbonates, and KF are the best bases for the Suzuki reactions if PNOF is used as the catalyst.
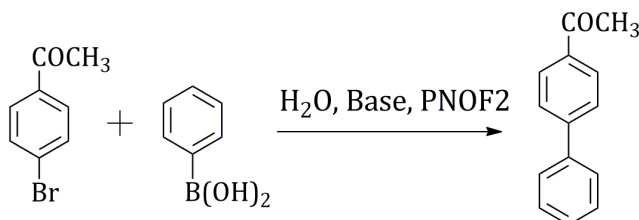
Scheme 2.3 Suzuki coupling reaction.

We studied Suzuki reactions between several aryl halides and phenyl boronic acid using PNOFs as catalysts (Scheme 2.4). For most of these reactions, K_2CO_3 was used as the base. The reaction conditions and yields for PNOF1-catalyzed Suzuki reactions are shown in Table 2.7. Similar data for PNOF2- and PNOF3-catalyzed reactions are given in Table 2.8 and Table 2.9. The results in Table 2.7 reveal that PNOF1 catalyzes Suzuki reactions of aryl chlorides, bromides, and iodides in aqueous solution. For the reactions of aryl chlorides, higher catalyst loadings and the presence of a phase transfer agent such as tetrabutylammonium bromide was required to obtain the yield reported in Table 2.7. If activated chlorides are employed, very good yields were obtained at 90 °C within 6 h. For unactivated aryl

Table 2.6 Suzuki coupling reactions catalyzed by PNOF2 using different bases.

Entry[a]	Base	Temperature (^{0}C)	Time (h)	Yield (%)
1	Cs_2CO_3	55	2	>99
2	Na_2CO_3	55	2	>99
3	NaOH	55	2	>99
4	$NaHCO_3$	55	2	92
5	CH_3COONa	55	2	17
6	NaOMe	55	2	27
7	K_2CO_3	55	2	>99
8	$KHCO_3$	55	2	89
9	KOH	55	2	>99
10	KF	55	2	>99
11	K_3PO_4	55	2	83
12	Et_3N	55	2	48
13	K_2CO_3	RT	12	>99
14	K_2CO_3	40	6	>99
15	K_2CO_3	75	0.5	96

[a] Conditions: aryl halide (1 mmol), phenylboronic acid (1.2 mmol), base (2 mmol), and PNOF2 (1 mg) were stirred in water
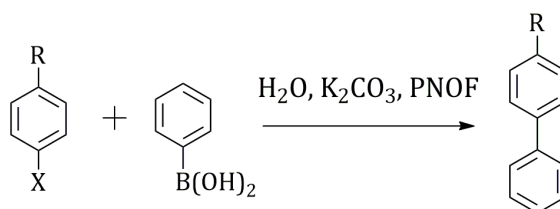
Scheme 2.4 Suzuki coupling reaction of aryl halides with phenyl boronic acid in presence of PNOF.

Table 2.7 Suzuki coupling reactions of various aryl halides catalyzed by PNOF1.

Entry[a]	Halide	Temperature (^0C)	Time (h)	Yield (%)
1	4-Chloroactophenone	90	6	94[b]
2	4-Chlorobenzonitrile	90	6	91[b][c]
3	4-Chloronitrobenzne	90	6	96[b]
4	4-Chlorotoluene	90	12	24[b]
5	4-Chloroanisole	90	12	11[b]
6	4-Chlorotoluene	104	12	78[b]
7	4-Chloroanisole	104	12	62[b]
8	4-Bromoacetophenone	55	2	>99
9	4-Bromotoluene	75	2	>99
10	4-Bromoanisole	75	2	>99
11	4-Iodooacetophenone	RT	2	>99
12	4-Iodotoluene	RT	6	>99
13	4-Iodoanisole	RT	6	>99

[a] Unless otherwise stated aryl halide (1 mmol), phenylboronic acid (1.2 mmol), K_2CO_3 (2 mmol), and PNOF1 (1 mg) were suspended in water (5 mL) and stirred for indicated time interval at definite temperatures. [b] phenylboronic acid was added in four portions to minimize the self-coupling of boronic acid. [c] base used was KF (2 mmol).

chlorides such as 4-chlorotoluene or 4-chloroanisole, yields were poor at 90 °C. Yields could be improved by heating the solution to reflux and increasing the reaction time. For the activated bromo derivative 4-bromoacetophenone, near quantitative yield was obtained within 2 h at 55 °C. For unactivated bromo derivatives, slightly higher temperatures were required for the completion of the reaction. For the iodo derivatives, reactions could be performed at room temperature as shown in Table 2.7. Similar results were obtained for PNOF2 (Table 2.8) and PNOF3 (Table 2.9).

Table 2.8 Suzuki coupling reactions of various aryl halides catalyzed by PNOF2.

Entry[a]	Halide	Temperature (^{0}C)	Time (h)	Yield (%)
1	4-Chloroanisole	104	12	22[b]
2	4-Bromoacetophenone	55	2	>99
3	4-Bromotoluene	75	2	>99
4	4-Bromoanisole	75	2	>99
5	4-Iodooacetophenone	RT	2	>99
6	4-Iodotoluene	RT	6	>99
7	4-Iodoanisole	RT	6	>99

[a] Unless otherwise stated aryl halide (1 mmol), phenylboronic acid (1.2 mmol), K_2CO_3 (2 mmol), and PNOF2 (1 mg) were suspended in water (5 mL) and stirred for indicated time interval at definite temperatures. [b] phenylboronic acid was added in four portions to minimize the self-coupling of boronic acid.

Table 2.9 Suzuki coupling reactions of various aryl halides catalyzed by PNOF3.

Entry[a]	Halide	Temperature (^{0}C)	Time (h)	Yield (%)
1	4-Bromoacetophenone	55	2	>99
2	4-Bromotoluene	75	2.5	>99
3	4-Bromoanisole	75	3	>99
4	4-Iodooacetophenone	RT	3.5	>99
5	4-Iodotoluene	RT	3.5	>99
6	4-Iodoanisole	RT	10	>99

[a] Unless otherwise stated aryl halide (1 mmol), phenylboronic acid (1.2 mmol), K_2CO_3 (2 mmol), and PNOF3 (1 mg) were suspended in water (5 mL) and stirred for indicated time interval at definite temperatures.

2.3.4.2.1 Recovery of the catalysts

All the three PNOF catalysts were found to exhibit good recyclability in Suzuki reactions. The reaction between 4-bromoacetophenone and phenylboronic acid was selected for the recyclability study. The catalyst and reagents were

suspended in water and heated for the required time (2 h for PNOF1 and PNOF2, and 3.5 h for PNOF3). At completion, the mixture was cooled when some of the product precipitated out as shown in Figure 2.18a. The mixture was extracted with ethyl acetate. The PNOFs exhibit a tendency to be present in the organic layer even though their density is higher than that of water. This is demonstrated by the photograph in Figure 2.18b, in which almost all the PNOF catalyst is present at the interface of the two solvents or sticking to the walls of the test tube in the ethyl acetate layer. The ethyl acetate is then removed by using a dropping pipette leaving the catalyst floating on the water surface. When a few drops of ethanol were added to the aqueous layer, the PNOFs started settling down as shown in Figure 2.18c. Within 4–5 min the catalyst would settle completely and this can be recovered by centrifugation. The reaction can be repeated with the recovered catalyst. We observed that the activity remains the same even after four cycles. The isolated yields in all these reactions were between 96 and 98 %. We also checked the recyclability of the catalyst without isolating it from the reaction medium. In this case, the organic layer was carefully separated from the aqueous layer shown in Figure 2.18b and the aqueous layer containing the catalyst was again used for the reaction. The reaction yields were the same even in the 10th cycle (see Figure 2.19) in this case.
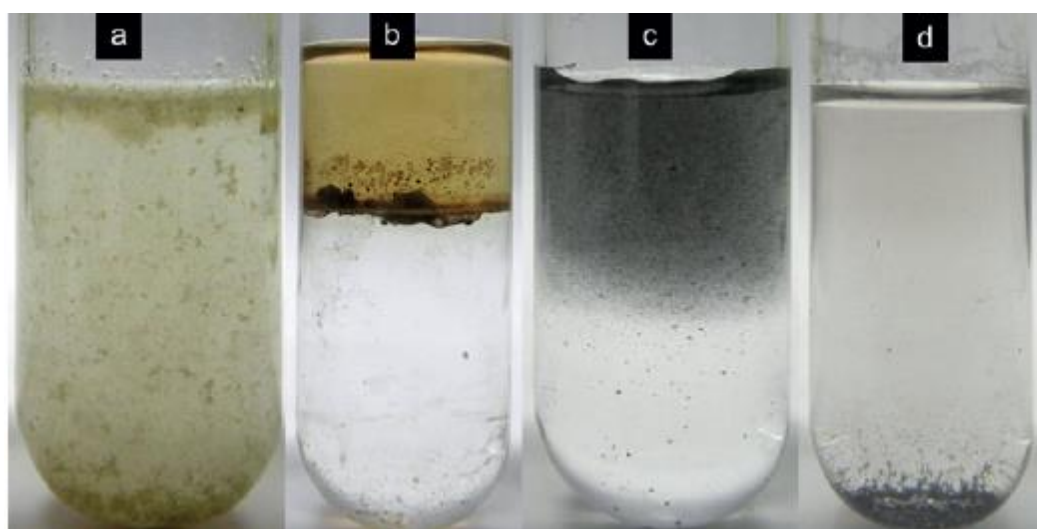
Figure 2.18 Various stages of the reaction and recovery of PNOF. (a) reaction mixture, (b) extraction with ethyl acetate, (c) settling of PNOF after addition of ethanol and (d) settled PNOF 2 min after addition of ethanol.
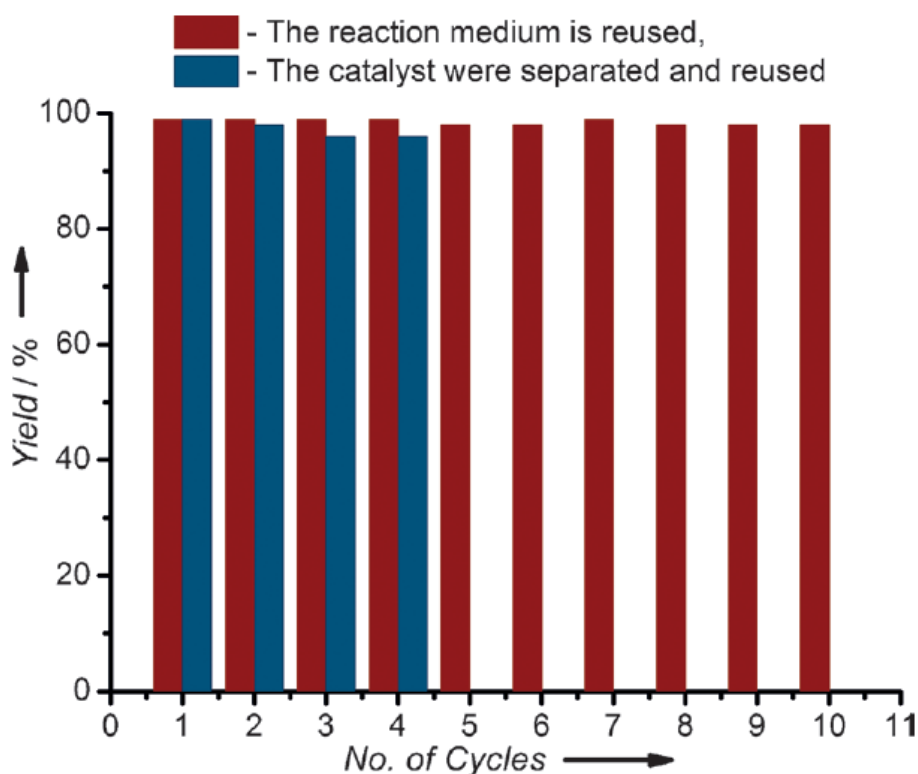
Figure 2.19 Recyclability of PNOF1 for the Suzuki coupling reaction between phenylboronic acid and 4-bromoacetophenone.

2.3.4.2.2 Stability of the catalysts

      Two sets of high-resolution (HR) TEM experiments were performed to check the stability of the PNOFs. In the first experiment, PNOF1 and PNOF2 employed in the Suzuki coupling reaction of 4-chloroanisole (see Table 2.7, entry 7 for PNOF1 and Table 2.8 entry 1 for PNOF2) at reflux temperature for 12 h, were recovered as described above and subjected to HRTEM analysis. In the second set of experiments, the PNOFs (1 mg each) were kept at reflux with stirring in toluene (5 mL) for a week. At the end of this time, the PNOFs were collected and subjected to HRTEM analysis. In both sets of experiments, we did not observe leaching out of Pd black or formation of Pd nanoparticles outside of the organic network. The crystallinity and crystal lattice of the nanoparticles are still maintained as is clear from Figure 2.20, Figure 2.21 and Figure 2.22. We also recorded the powder XRD for the recovered catalyst and we did not find any changes in the XRD pattern.
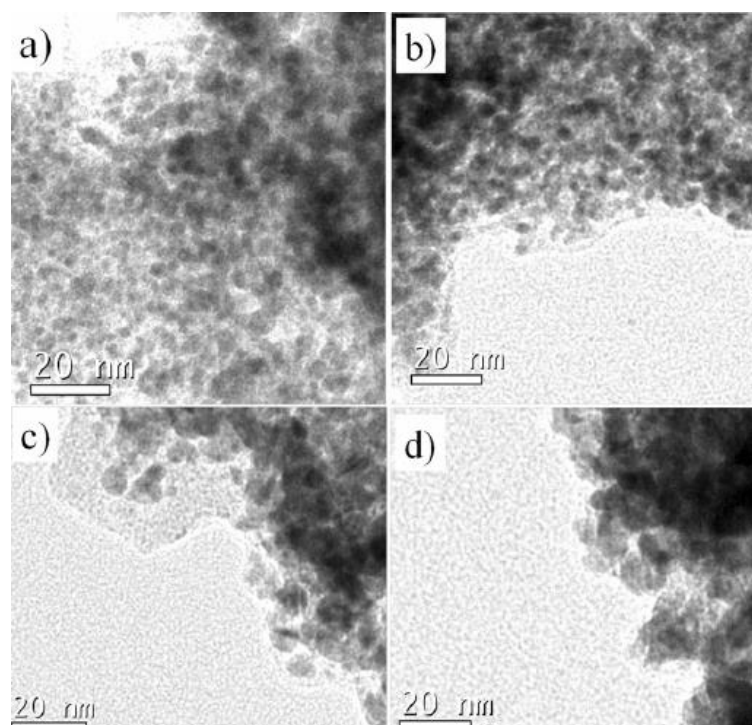
Figure 2.20 TEM images of (a) PNOF2 after heating at reflux, (b) PNOF1 after heating at reflux, (c) PNOF2 after catalysis reaction and (d) PNOF1 after catalysis reaction.
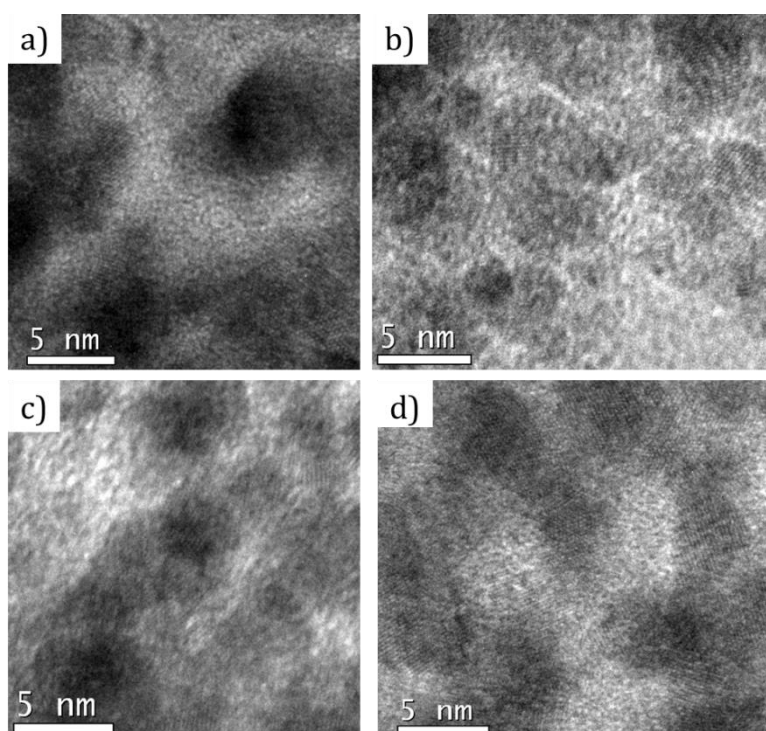
Figure 2.21 Magnified TEM images of (a) PNOF2 after heating at reflux, (b) PNOF1 after heating at reflux, (c) PNOF2 after catalysis reaction and (d) PNOF1 after catalysis reaction.
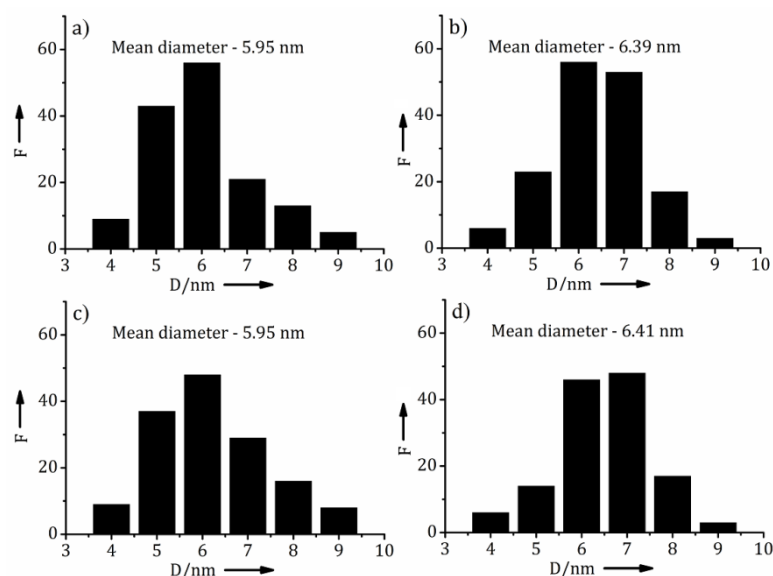
Figure 2.22 Size distribution of (a) PNOF2 after heating at reflux, (b) PNOF1 after heating at reflux, (c) PNOF2 after catalysis reaction and (d) PNOF1 after catalysis reaction; (F=frequency).

2.3.4.2.3 Leaching tests of the catalysts

A major factor that decreases the catalytic activity of supported Pd catalysts is the leaching of palladium from the nanoparticles into solution. To see if any leached out Pd is present in the aqueous solution, the solution was filtered after ten minutes of the Suzuki reaction of 4-bromoacetophenone at 90 °C (60% conversion) and the same reaction was performed by using the aqueous layer without adding PNOF. Even after heating and stirring for 24 h, we did not observe the formation of any products. We also subjected the aqueous layer to inductively coupled plasma atomic emission spectrometric (ICP–AES) analysis. The presence of Pd was not detected (detection limit 0.05 ppm), which suggests that leaching of palladium is not a significant problem in the case of PNOFs, most probably because of the covalent bonding between the Pd cluster and the organic framework.

To estimate the amount of Pd leached into the product, Suzuki reaction of 4-bromoacetophenone was performed at 90 °C and the product obtained was subjected to ICP–AES analysis. Pd contamination of the product was found to be less than 2 ppm, indicating that leaching of Pd into the product is not a major problem in

these reactions. Thus, ICP–AES analysis of both filtrate and product suggested that in aqueous medium catalysis occurs in a heterogeneous manner.

To compare the catalytic efficiencies of PNOFs with those of previously reported Pd catalysts in the Suzuki reactions, we determined the turnover numbers (TON = number of moles of product/number of moles of Pd in the catalyst) and turnover frequencies (TOF = TON/reaction time) of these catalysts. In the case of recyclable catalysts, it was proposed that TOF values are better determined from the slopes of TON versus reaction time plots (Umpierre 2011). In the case of nanoparticle catalysis, it is generally assumed that metal atoms on the surface of the nanoparticle only are involved in catalysis (Lewis 2006; Bandari 2010; Bandari 2011). Thus, one can calculate two sets of TON and TOF values. In the first set, the total amount of Pd in the catalyst is used in the calculation, and in the second set, the number of surface Pd atoms only are used in the calculation. We calculated TONs by both methods. TOF values were calculated from the slope of TON-versus-time plots. TOF values thus obtained are summarized in the Tables 2.10, 2.11 and 2.12.

TOFs obtained in this study for the reaction between activated aryl chlorides and phenylboronic acid was in the range 8-10 h^{-1}, if the total palladium is used in the calculation. If only the surface atoms are considered, these values increase up to 55 h^{-1}. For deactivated aryl chlorides, values as high as 40 h^{-1} are obtained at higher temperatures. These values are comparable to those reported recently by others (Rosario-Amorin 2009; Karimi 2010; Pascanu 2013). We have obtained TOF values up to 600 h^{-1} for bromides and 3500 h^{-1} for iodides. The values could be further increased for iodides and bromides by increasing the reaction temperature.

PNOF1 and PNOF2 exhibit better catalytic activity in Suzuki reactions than Pd nanoparticle catalysts previously reported. For example, the reaction of 4-bromoacetophenone with phenylboronic acid in water catalyzed by previously reported Pd nanoparticles captured in silica required 10 h at 90 °C for 95% conversion (Parlett 2013). With PNOF1 and PNOF2 the reaction could be completed in 2 h time. Reactions of aryl iodides with phenylboronic acid using Pd nanoparticles stabilized on poly(N-vinyl-2-pyrrolidone) required refluxing conditions in the water-ethanol mixture (Li 2000). These reactions could be performed in 100% yield

at room temperature by using PNOF1 or PNOF2. In addition, the PNOFs were very stable and could be recovered and reused several times without loss of activity.

Table 2.10 TOF calculated for Suzuki coupling in the presence of PNOF1.

Entry	Halide	Temperature (^{0}C)	Amount of PNOF1 (mg)	TOF (h^{-1}) A	TOF (h^{-1}) B
1	4-Chloroactophenone	90	5	10.4	67.3
2	4-Chlorobenzonitrile	90	5	8.6	55.3
3	4-Chloronitrobenzne	90	5	10.5	67.6
4	4-Chlorotoluene	90	5	2.4	15.3
5	4-Chloroanisole	90	5	1.0	6.7
6	4-Chlorotoluene	104	5	6.3	40.6
7	4-Chloroanisole	104	5	4.5	29.4
8	4-Bromoacetophenone	55	1	276.8	1796.3
9	4-Bromotoluene	75	1	290.0	1876.7
10	4-Bromoanisole	75	1	241.8	1040.4
11	4-Iodooacetophenone	RT	1	588.4	3496.0
12	4-Iodotoluene	RT	1	427.3	2723.6
13	4-Iodoanisole	RT	1	398.2	2538.1

A- Calculated based on total Pd

B- Calculated based on Surface

Table 2.11 TOF calculated for Suzuki coupling in the presence of PNOF2.

Entry	Halide	Temperature (^{0}C)	Amount of PNOF2 (mg)	TOF (h^{-1})	
				A	B
1	4-Chloroanisole	104	5	1.5	8.20
2	4-Bromoacetophenone	55	1	38.4	2057.4
3	4-Bromotoluene	75	1	398.6	2155.5
4	4-Bromoanisole	75	1	332.4	1797.4
5	4-Iodooacetophenone	RT	1	808.6	4373.0
6	4-Iodotoluene	RT	1	587.3	3176.3
7	4-Iodoanisole	RT	1	547.3	2959.8

A- Calculated based on total Pd
B- Calculated based on Surface

Table 2.12 TOF calculated for Suzuki coupling in the presence of PNOF3.

Entry	Halide	Temperature (^{0}C)	Amount of PNOF3 (mg)	TOF (h^{-1})	
				A	B
1	4-Bromoacetophenone	55	1	105.3	5010.5
2	4-Bromotoluene	75	1	110.3	525.4
3	4-Bromoanisole	75	1	92.0	438.1
4	4-Iodooacetophenone	RT	1	223.7	1066.0
5	4-Iodotoluene	RT	1	162.5	774.3
6	4-Iodoanisole	RT	1	151.4	721.5

A- Calculated based on total Pd
B- Calculated based on Surface

2. 4 Conclusions

We have synthesized palladium-nanoparticle-linked organic frameworks by the simultaneous reduction of a bisdiazonium fluoroborate and a palladium salt by

using sodium borohydride. By varying the molar ratio of the Pd and diazonium salts we prepared three PNOFs. These materials were characterized by various spectroscopic and microscopic techniques. The catalytic efficiencies of these PNOFs were evaluated in the reduction of 4-nitrophenol to 4-aminophenol and the rates of the PNOF-catalyzed reactions were found to be similar to or better than the rates of other catalysts reported recently. These materials also catalyzed C-C bond-forming reactions such as Suzuki reactions between aromatic halides (including chlorides) and phenylboronic acids. Performances of PNOFs as catalysts in Suzuki reactions were equal to or better than those of other catalysts reported recently. Most of the catalysts reported for Suzuki coupling reactions of aromatic chlorides are either nonreusable homogeneous catalyst or heterogeneous catalysts made through difficult procedures. In many of these cases, the Suzuki reactions required inert reaction conditions. On the other hand, the PNOFs are synthesized in one step in nearly quantitative yield. They are highly stable towards air and moisture and no special care is required to perform Suzuki reactions with these catalysts. We observed that the PNOF catalysts could be recovered and reused several times without any loss of activity. Moreover, the procedure we employed here for the preparation of PNOFs could easily be adapted for the preparation of other metal-nanoparticle organic frameworks. Other bis- or polydiazonium salts could also be employed, in which case organic frameworks with different structures and morphologies may be obtained.

2.5 Experimental Section

2.5.1 Materials and methods

Commercially available reagents were used as received without further purification. BPBDT was prepared by using a reported procedure (Schiemann 1943). Thermogravimetric analysis in a nitrogen atmosphere at a heating rate of 10 °C min^{-1} was performed by using a Shimadzu DTG-60 equipment. Shimadzu IR Prestige 21 spectrometer was used to record the FTIR spectra. UV/Vis absorption spectra of the materials were recorded on Shimadzu UV-2600 UV-Vis spectrophotometer. The same spectrophotometer was used for monitoring the catalytic reduction of 4-nitrophenol into 4-aminophenol. ^{1}H NMR spectra were recorded by using a 500 MHz Bruker Avance DPX Spectrometer. The X-ray diffractograms of the samples were

recorded on a Phillips diffractometer using Ni-filtered CuKα radiation. XPS measurements were performed by using a commercially available X-ray photoemission spectrometer (Omicron Nanotechnology, Germany) using AlKα (1486.7 eV) as X-ray source operating at 100 W. General scans and core-level spectra were acquired with 1 eV and 50 eV pass energy, respectively. Spectral background (Shirely) deconvolution was performed by using Fityk software. BET surface areas were obtained by using Micrometritics tristar 3000 model surface area analyzer. Samples were heated to 150 °C for 2 h under N_2 atmosphere prior to the measurement. SEM analyses were performed on a Zeiss–EVO' 18cryo SEM special Edition with variable pressure detector working at 20–30 kV. Samples for SEM analysis were prepared in toluene by sonicating them for 30 min. The resulting solution was drop-casted on aluminum stud covered with aluminum foil. Samples on the stud were sputtered with gold of 30 nm thickness before the SEM measurements. Same stock solution drop-casted on a 400 mesh carbon-coated copper grid were used for HRTEM analysis on a FEI–TECNAI30 G2 S-Twin 300 kV microscope. Yields of the Suzuki coupling reactions were obtained using Shimadzu QP2010 Gas chromatograph mass spectrometer. ICP–AES experiments were performed using Thermo Electron IRIS INTREPID II XSP DUO, Flexible axial and radial view instrument, with high concentration capabilities.

2.5.2 Preparation of PNOFs

PNOF1 was prepared by using BPBDT (190 mg, 0.5 mmol) and K_2PdCl_4 (326 mg, 1.0 mmol). The salts were stirred in a mixture of deionized water (50 mL) and toluene (75 mL). A solution of $NaBH_4$ (0.1 m) in methanol (75 mL) was added and stirring was continued for 2 h. The toluene layer was separated and washed with water several times. Methanol (50 mL) was added and the mixture was kept undisturbed for 2 h. PNOF1 settled at the bottom as a fine powder. It was filtered and washed several times with methanol. The yield was 170 mg.

PNOF2 was synthesized by the procedure for PNOF1 but using K_2PdCl_4 (326 mg, 1.0 mmol) and BPBDT (381 mg, 1.0 mmol). The yield was 250 mg.

PNOF3 was also synthesized by the same procedure but using K_2PdCl_4 (326 mg, 1.0 mmol) and BPBDT (762 mg, 2.0 mmol). The yield was 360 mg.

BLANK: K_2PdCl_4 was not used in this preparation. Quantities of other chemicals were the same as for PNOF2 synthesis. The yield was 150 mg.

2.5.3 General procedure for catalytic reactions

2.5.3.1 Reduction of 4-nitrophenol

Aqueous solutions of 4-nitrophenol (0.1 mm, 2.0 mL) and sodium borohydride (0.1m, 1.0 mL) were mixed in a standard cuvette. To this was added a sonicated dispersion of PNOF in water (100 mL from a dispersion of PNOF1, 0.25 mg; PNOF2, 0.37 mg; or PNOF3, 0.55 mg; in water, 1.0 mL; 0.146 mmol Pd for all PNOFs). The mixture was stirred and absorption spectra were recorded at intervals of 30 s.

2.5.3.2 Selection of base: A mixture of PNOF2 (1.0 mg), base (2 mmol), 4-bromoacetophenone (199 mg, 1 mmol), and phenylboronic acid (183 mg, 1.5 mmol) in water (6 mL) was stirred for 2 h at 55 °C. The mixture was extracted with ethyl acetate (3×10 mL). Ethyl acetate layer was dried and the solvent evaporated to get the product.

2.5.3.3 Suzuki coupling reactions of aryl chlorides

A mixture of PNOF (5.0 mg), potassium carbonate (276 mg, 2 mmol), aryl chloride (1 mmol), phenylboronic acid (45 mg, 0.37 mmol), and tetrabutylammonium bromide (225 mg, 0.7 mmol) in water (8 mL) was stirred with heating at the indicated temperature. Phenylboronic acid (135 mg, 1.11 mmol) was added in three equal portions to the reaction mixture at 90 min intervals. Heating was continued till the indicated time. The mixture was extracted with ethyl acetate (3 × 10 mL). Ethyl acetate layer was dried and the solvent evaporated to get the coupling product.

2.5.3.4 Suzuki coupling reactions of aryl bromides

A mixture of PNOF (1.0 mg), potassium carbonate (276 mg, 2 mmol), aryl bromide (1 mmol), and phenylboronic acid (183 mg, 1.5 mmol) in water (6 mL) was stirred for 2 h at the temperature specified. The mixture was extracted with ethyl acetate (3 × 10 mL). Ethyl acetate layer was dried and the solvent evaporated to get the coupling product.

2.5.3.5 Suzuki coupling reactions of aryl iodides

A mixture of PNOF (1.0 mg), potassium carbonate (276 mg, 2 mmol), aryl iodides (1.0 mmol), and phenylboronic acid (183 mg, 1.5 mmol) in water (6 mL) was stirred at RT for the specified time. The mixture was extracted with ethyl acetate (3 × 10 mL). Ethyl acetate layer was dried and the solvent evaporated to get the coupling product.

2.5.4 Recyclability of PNOF

1) For the catalyst recyclability study, the same amounts of materials as mentioned above were used. At the end of the reaction time, ethyl acetate (10 mL) was added and stirred for 5 min. The ethyl acetate layer was carefully separated and the product isolated. Reactants were added to the water layer and reaction repeated for the same time interval. This cycle was repeated ten times and the organic layers obtained each time were separately analyzed.

2) In another set of experiments, ethyl acetate was added to the mixture after completion. The organic layer containing the product was carefully separated. A few drops of ethanol were added to the aqueous layer and the catalyst was allowed to settle. Settled PNOFs was collected by centrifugation and washed with ethanol and water. The recovered catalyst was then used for subsequent cycles. The reaction was repeated for four times.

2.5.5 Test for Pd leaching during the reaction

After carrying out the reaction with 4-bromoactophenone (199 mg, 1 mmol) and phenylboronic acid (183 mg, 1.5 mmol) in water (6 mL) in the presence of potassium carbonate (276 mg, 2 mmol) and PNOF (1 mg) at 90 °C for 10 min (60% conversion), the mixture was filtered. The filtrate was then used for the same reaction in the absence of PNOF1 for 24 h. The reaction mixture was extracted with ethyl acetate (3 × 10 mL) and the organic layer was analyzed by GC–MS. The same experiment was repeated for PNOF2 and PNOF3. Product formation was not observed in any of these cases.

2.5.6 Contamination of Pd in the product

ICP–AES was used to determine the palladium contamination in the product of the Suzuki coupling reactions. Calibration against palladium standard and blank was linear, using 2% nitric acid solutions containing palladium amounts of 0, 1, 5,

and 10 ppm made from 1000 ppm stock solution. The product (1 g) of the Suzuki coupling reaction of 4-bromoacetophenone and boronic acid was digested with a mixture of concentrated nitric acid (4 mL) and concentrated perchloric acid (0.4 mL). The solution was filled up to 25 mL using distilled water and subjected to ICP–AES analysis. Two sets of experiments were conducted with digestion over three days and five days followed by heating at 150 °C for 2 h. Both samples gave the same results indicating that all the palladium was digested.

2.5.7 Calculation of TON and TOF

For the calculation of TONs, the Suzuki coupling reactions were monitored by the GC–MS analysis in the low-conversion range (less than 50%). Aliquots were withdrawn from the reaction mixture at definite intervals (10 min for aryl bromides and iodides and 30 min for aryl chlorides) and subjected to GC–MS analysis. TON values were calculated from the GC–MS yields. TON-versus-time plots were made and straight lines were obtained in all cases. Slopes of these plots gave the TOF values.

2.6 References

Bandari, R.; Hçche, T.; Prager, A.; Dirnberger, K.; Buchmeiser, M. R. *Chem. Eur. J.* **2010**, *16*, 4650-4658.

Bandari, R.; Prager, A.; Höche, T.; Buchmeiser, M. R. *ARKIVOC* **2011**, 54-70.

Bell, A. T. *Science* **2003**, *299*, 1688-1691.

Cheon, Y. E.; Suh, M. P.; *Chem. Eur. J.* **2008**, *14*, 3961-3967.

Choi, H. R.; Woo, H.; Jang, S.; Cheon, J. Y.; Kim, C.; Park, J.; Park, K. H.; Joo, S. H. *ChemCatChem* **2012**, *4*, 1587-1594.

Franzén, R.; Xu, Y. *Can. J. Chem.* **2005**, *83*, 266-272.

Friederici, M.; Angurell, I.; Rossell, O.; Seco, M.; Divins, N.; Llorca, *J. Organometallics* **2012**, *31*, 722-728.

Fulhame, Mrs.; Humphreys, J. "An essay on combustion" **1794**, 1748-1810.

Ghosh, D.; Chen, S. *J. Mater. Chem.* **2008**, *18*, 755-762.

Ghosh, D.; Pradhan, S.; Chen, W.; Chen, S. *Chem. Mater.* **2008**, *20*, 1248-1250.

Gopidas, K. R.; Whitesell, J. K.; Fox, M. A. *Nano Lett.* **2003**, *3*, 1757-1760.

Gopidas, K. R.; Whitesell, J. K.; Fox, M. A. *J. Am. Chem. Soc.* **2003**, *125*, 6491-6502.

Gutzler, R.; Walch, H.; Eder, G.; Kloft, S.; Heckl, W. M.; Lackinger, M. *Chem. Commun.* **2009**, 4456-4458.

Han, W.; Liu, C.; Jina, Z. *Adv. Synth. Catal.* **2008**, *350*, 501-508.

Hu, N.; Yin, J.-Y.; Tang, Q.; Chen, Y.; *J. Polym. Sci. Part A: Polym. Chem*. **2011**, *49*, 3826-3834.

Huang, X.; Li, Y.; Zhou, H.; Zhong, X.; Duan, X.; Huang, Y.; *Chem. Eur. J.* **2012**, *18*, 9505-9510.

Johnston, E. V.; Verho, O.; Kärkäs, M. D.; Shakeri, M.; Tai, C.-W.; Palmgren, P.; Eriksson, K.; Oscarsson, S.; Bäckvall, J.-E.; *Chem. Eur. J.* **2012**, *18*, 12202-12206.

Karimi, B.; Elhamifar, D.; Clark, J. H.; Hunt, A. J. *Chem. Eur. J.* **2010**, 16, 8047-8053.

Kumar, V. K. R.; Gopidas, K. R. *Chem. Asian J.* **2010**, *5*, 887-896.

Kumar, V. K. R.; Gopidas, K. R. *Tetrahedron Lett.* **2011**, *52*, 3102-3105.

Kumar, V. K. R.; Krishnakumar, S.; Gopidas, K. R. *Eur. J. Org. Chem.* **2012**, 3447-3458.

Lewis, D. J.; Day, T. M.; MacPherson, J. V.; Pikramenou, Z. *Chem. Commun.* **2006**, 1433-1435.

Li, Y.; Hong, X. M.; Collard, D. M. El-Sayed, M. A. *Org. Lett.* **2000**, *2*, 2385-2388.

Lim, X. *Nature* **2016**, *537*, 156-158.

Lin, Y.; Qiao, Y.; Wang, Y.; Yan, Y.; Huang, J. *J. Mater. Chem.* **2012**, *22*, 18314-18320.

Liu, L.; Zhang, Y.; Xin, B. *J. Org. Chem.* **2006**, *71*, 3994 –3997.

Lu, X.; Yang, L.; Bian, X.; Chao, D.; Wang, C. *Part. Part. Syst. Charact.* **2014**, *31*, 245-251.

Matos, K.; Soderquist, J. A.; *J. Org. Chem.* **1998**, *63*, 461-470.

Muñoz, M. P.; Martín-Matute, B.; Fernândez-Rivas, C.; Cârdenas, D. J.; Echavarren, A. M. *Adv. Synth. Catal.* **2001**, *343*, 338-342.

Molnàr, À. *Chem. Rev.* **2011**, *111*, 2251-2320.

Nicewicz, D. A.; MacMillan, D. W. C. *Science* **2008**, *322*, 77-80.

Pagliaro, M.; Pandarus, V.; Ciriminna, R.; Béland, F.; Car, P. D. *ChemCatChem* **2012**, *4*, 432-445.

Parlett, C. M. A.; Bruce, D. W.; Hondow, N. S.; Newton, M. A.; Lee, A. F.; Wilson, K. *ChemCatChem* **2013**, *5*, 939-950.

Pascanu, V.; Yao, Q.; Gómez, A. B.; Gustafsson, M.; Yun, Y.; Wan, W.; Samain, L.; Zou, X.; Martín-Matute, B. *Chem. Eur. J.* **2013**, *19*, 17483-17493.

Rosario-Amorin, D.; Wang, X.; Gaboyard, M.; Clérac, R.; Nlate, S.; Heuzé, K. *Chem. Eur. J.* **2009**, *15*, 12636-12643.

Saha, S.; Pal, A.; Kundu, S.; Basu, S.; Pal, T. *Langmuir* **2010**, *26*, 2885-2893.

Schiemann, G.; Winkelmüller, W. *Organic Syntheses, Coll. Vol. 2* (Eds.: Hartman, W. W.; Byers, J. R.; Dickey J. B.) **1943**, pp. 188.

Stille, J. K.; Lau, K. S. Y. *Acc. Chem. Res.* **1977**, *10*, 434-442.

Szulmanowicz, M. S.; Gniewek, A.; Gil, W.; Trzeciak, A. M. *ChemCatChem* **2013**, *5*, 1152-1160.

Umpierre, A. P.; de Jesffls, E.; Dupont, J. *ChemCatChem* **2011**, *3*, 1413-1418.

Vieira, E. G.; Silva, R. O.; Junior, E. F.; Filho, N. L. D. *Appl. Organometal. Chem.* **2017**; *doi.org/10.1002/aoc.3722.*

Wu, L.; Li, Z.-W.; Zhang, F. ;He, Y.-M.; Fana, Q.-H. *Adv. Synth. Catal*. **2008**, *350*, 846-862.

Wu, S.; Tseng, C.; Lin, Y.; Lin, C. H.; Hung, Y.; Mou, C. Y. *J. Mater. Chem*. **2011**, *21*, 789-794.

Yang, H.; Han, X.; Li, G.; Wang, Y. *Green Chem*. **2009**, *11*, 1184-1193.

Yang, H.; Cui, X.; Deng, Y.; Shi, F. *ChemCatChem* **2013**, *5*, 1739-1743.

Zhou, X.; Huang, Y.; Liu, C. Liao, J.; Lu, T.; Xing, W. *ChemSusChem* **2010**, *3*, 1379-1382.

Zhu, Y.; Stubbs, L. P.; Ho, F.; Liu, R.; Ship, C. P.; Maguire, J. A.; Hosmane, N. S. *ChemCatChem* **2010**, *2*, 365-374.

Highly Stable Copper Nanoparticles Linked to Organic Frameworks as Recyclable Catalyst for Three-Component Click Cycloaddition in Water

3.1 Abstract

Synthesis, characterization and catalytic applications of highly stable copper-nanoparticles linked to aromatic frameworks are reported. Synthesis of these nanoparticles was achieved in a one-pot reaction which involved the simultaneous reduction of $CuCl_2.2H_2O$ and 4,4'-biphenylene-bis-diazonium tetrafluoroborate using sodium borohydride. Copper atoms formed upon reduction of Cu ions undergo clustering, leading to the formation of copper nanoparticles. At the same time, 4,4'-biphenylene-bis-diazonium tetrafluoroborate is converted to biphenylene biradical, which undergoes rapid addition reactions with each other and also on to the nanoparticle surfaces resulting in the formation of aromatic framework linked Cu nanoparticles. Four different types of nanoparticles were prepared by varying the concentration of the metal salts and the ligands. The structure and morphology of these materials were studied using XRD, XPS, SEM and HRTEM analysis. The materials were found to be very good catalysts for click reactions between azides and alkynes and exhibited TOF values as high as 305400 h^{-1}. They also efficiently catalyzed the one-pot click reactions involving azide precursors, sodium azide and alkyne. TOF upto 99000 h^{-1} were observed for these reactions.

3.2 Introduction

1,3-Dipolar cycloaddition reactions involving alkynes and azides catalysed by copper is the most common and widely studied example in click chemistry (Huisgen 1965; Moses 2007; Kolb 2011; Abdulkin 2013; Alonso 2015). The product of these reactions are 1,2,3-triazoles which are very resistant to moisture, oxygen and light. Click reactions have wide range of applications in various areas such as synthetic (Johnson 2008), supramolecular (Hua 2010) and combinatorial chemistry (Salisbury 2007) as well as in material (Iha 2009; Kempe 2012), biological (Alonso 2012) and pharmaceutical (Hein 2008) sciences. For example, 1,2,3-triazole-containing

compounds show a wide range of biological activities including fungicidal (Chaudhary 2009), antiallergic (Buckle 1986), antiviral (Xia 2006), antibacterial (Reck 2005), anticancer (Soltis 1996) and anti-HIV (Alvarez 1994) properties.

Only a few azides are available commercially and hence, multi-step reactions are required for the preparation of complex triazoles. Therefore researchers are looking for multi-component one-pot synthesis in which in situ generated azides from diazonium salts, amines, epoxides or even alkenes could be used (Sharghi 2009; Alonso 2011[a,b]; 2013). Toxic side products generated during multi-step reactions and reaction times can be considerably minimized in the one-pot multi-component strategy. Cu(I) complexes are used as catalyst for the click reaction (Pérez 2016). However, some of the Cu(I) complexes are reported to be cytotoxic (Sanghamitra 2005). Cu, Cu_2O or CuO nanoparticles on various support materials can also be used as catalysts but synthesis of such materials often requires harsh reaction conditions (Vukojević 2005; Choi 2012; Pagliaro 2012; Pascanu 2013; Upare 2015; Gawande 2016). In the case of Cu catalysts an important disadvantage is easy deactivation of the catalyst through oxidation. Hence preparation of stable Cu nanoparticles for catalytic applications in water is very challenging (Kaur 2014; Nia 2015; Aslan 2015).

Various support materials such as silica, alumina, graphene, etc. have been used extensively for the preparation of supported Cu and copper oxide nanoparticles. In most of the reported cases synthesis of the stabilizing ligands involved multistep procedures and the catalysts generally have low metal contents (Sreedhar 2008; Dell'Amico 2009; Subramanian 2012; O'Neill 2013; Guo 2014). Herein, we report novel Cu nanoparticle catalysts designated as copper nanoparticle-linked organic frameworks (CNOFs), where the metal nanoparticles are covalently linked to an aromatic frame work support. The capability of copper to attain various oxidation states makes it a suitable candidate for the preparation of nanoparticles with varying composition and morphologies (Yinghuai 2007; Campelo 2009; Lamblin 2010; Molnàr 2011; Allen 2013; Wojcieszak 2013; Popova 2014). The chemical reduction of diazonium salts to aryl radicals which are capable of covalent bond formation with almost any type of solid surfaces is employed herein to construct the organic framework and to link it covalently to the Cu nanoparticle.

This method has been employed to graft organic moieties on to a large number of surfaces (Canning 2002; Hurley 2004; Pinson 2005; Jiang 2006; Mirkhalaf 2006; Shimura 2006; Liu 2007; Chen 2011; Wang 2015; Guerrero 2015; Qiu 2015). Our group has also exploited this methodology to synthesize gold and palladium nanoparticle-cored dendrimers (Kumar 2012; 2012; 2011) and palladium nanoparticle-linked organic frameworks where the organic residues are linked to the nanoparticles by carbon-metal covalent bonds (Chapter 2). In this chapter we extend this strategy to synthesize CNOF, in which the copper nanoparticles are captured in the organic framework through several metal-carbon covalent bonds.

Our strategy involved the simultaneous reduction of a copper salt and a bisdiazonium tetrafluoroborate. The formation of microporous organic framework and insertion of nanoparticles into this framework could be accomplished in a one-pot reaction using $NaBH_4$ as reducing agent. The Cu^{2+} is reduced to Cu atoms that generate copper nanoparticles through clustering of atoms. The bisdiazonium salt upon reduction eliminates two nitrogen molecules and form highly reactive biradicals that undergo random coupling or radical-radical addition reactions leading to the formation of a complex organic framework with large numbers of reactive radical centers capable of covalent bond formation with the growing copper nanoparticles. These two simultaneous reactions will lead to the formation of CNOF as shown in Scheme 3.1. Thus, our approach would permit us to synthesize CNOF in high yields in a single step. It may be noted that all the starting materials and reagents used for the preparation of CNOFs were water soluble, while the product CNOFs were completely insoluble. Hence the separation and purification of the materials were very easy.
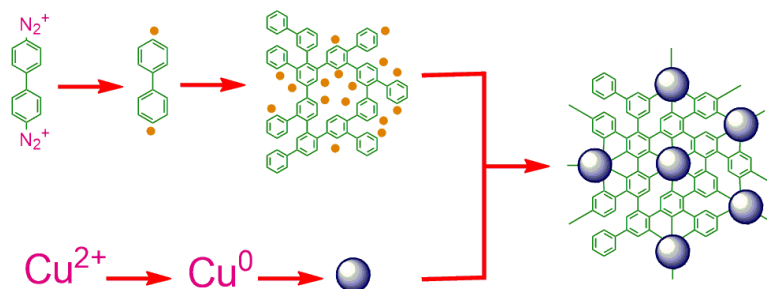
Scheme 3.1 The various stages of CNOF formation.

3.3 Results and Discussion

3.3.1 Synthesis

Synthesis of CNOFs involved the simultaneous reduction of 1,4- biphenylene-bis-diazonium fluoroborate (BPBDT) (Schiemann 1943) and $CuCl_2.2H_2O$ dissolved in toluene:water (2:1) mixture by $NaBH_4$ in methanol. The CNOFs were obtained as black powders insoluble in almost all solvents. The samples were purified by repeated washing with water and organic solvents such as acetone, THF and CH_2Cl_2 followed by drying in vacuum. Dispersions of CNOFs in water settled within 15 minutes, whereas their dispersions in organic solvents took nearly an hour to settle. Irrespective of the density of the solvents and solubility of CNOFs in them, CNOFs always preferred the organic phase in a water-organic biphasic system. By changing the relative concentrations of the bisdiazonium fluoroborate and Cu salt, we were able to synthesize four CNOF systems (Table 3.1).

Table 3.1 List of materials under investigation.

Sl. No.	$CuCl_2.2H_2O$ (mmol)	BPBDT (mmol)	Material Code
1	4	1	CNOF1
2	3	1	CNOF2
3	2	1	CNOF3
4	1	1	CNOF4

3.3.2 Characterizations

3.3.2.1 TGA Analysis

Thermogravimetric analyses (TGA) and differential thermal analysis (DTA) of CNOFs were carried out at a heating rate of 10 °C per minute. The results obtained are presented in Figure 3.1. To get the complete decomposition of the organic framework (into CO_2 and H_2O) TGA were done in the presence of atmospheric oxygen. The thermogram of CNOF4 showed only a small weight loss of less than 0.8% upto 100 °C. This can be attributed to the evaporation of solvents adsorbed to the materials. DTA analysis showed that major exothermic reactions occur at 180 °C and 315 °C. The first peak is due to the oxidation of copper i. e. $Cu_{(s)} \rightarrow Cu_2O_{(s)}$ and

the second peak is due to the oxidation of cuprous oxide $Cu_2O_{(s)} \rightarrow CuO_{(s)}$ (Wang 2012). The DTA also showed peaks at 520 °C and 790 °C. The former peak can be attributed to the combustion of organic frameworks (Wang 2012; Tamaekong) and the latter may be due to possible phase change occurring to CuO. This phase change arises due to melting which starts around 790 °C (Prakash 2011; Luna 2015). The thermogram shows a total weight loss of 21%. Assuming complete decomposition of the organics and oxidation of Cu to CuO, we can assign the remaining 79% to CuO which would correspond to 63% Cu originally present in the CNOF4 and the remaining 37% weight was taken as due to the organic framework. CNOF3 exhibited similar behavior and analysis of TGA and DTA gave Cu wt% of 74. Thermograms of CNOF2 and CNOF1 exhibited total weight gains of 1.8% and 10.6%, respectively. A net weight gain is observed because the weight gain due to oxidation to CuO is more than the weight loss due to decomposition of the organic framework. Analysis of the results gave total metal contents of 81% and 88% for CNOF2 and CNOF1, respectively.
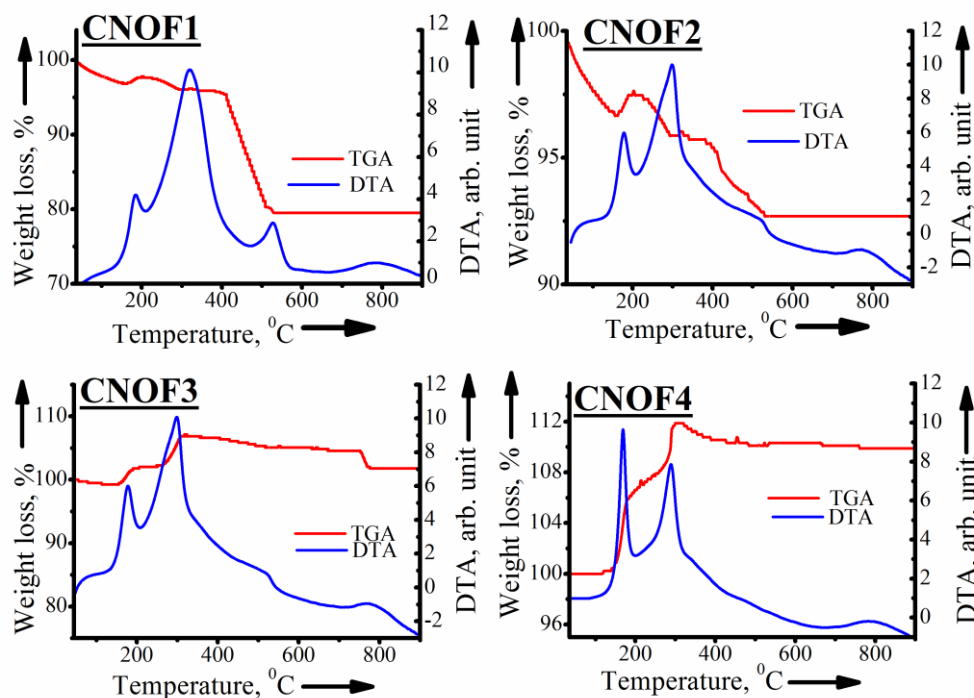
Figure 3.1 TGA (red) and DTA (blue) analysis of CNOFs.

3.3.2.2 IR studies

FTIR spectra for the CNOFs and the ligand BPBDT are shown in Figure 3.2. The IR spectrum of BPBDT (top panel in Figure 3.2) exhibited a band at 2274 cm^{-1} which is characteristic of the diazo group. This band was absent in the IR spectra of all the four CNOFs, indicating the complete removal of diazonium groups. All other IR absorptions corresponding to the C-H (3033 cm^{-1}) and C-C (peaks between 1600 and 1400 cm^{-1}) vibrations present in the ligand were also present in the CNOFs. The intensities of these bands were observed to decrease with increase in the metal content. CNOF1 has the lowest peak intensity (lower panel in Figure 3.2) due to its low organic content.
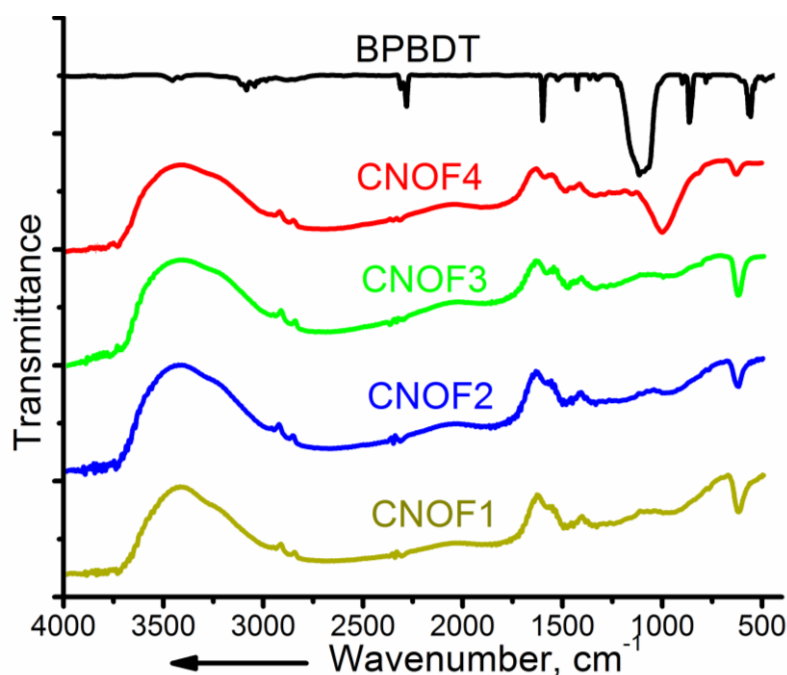
Figure 3.2 IR spectra of BPBDT, CNOF1, CNOF2, CNOF3, and CNOF4.

3.3.2.3 NMR studies

Due to the lack of solubility in organic solvents we employed sonicated suspensions of the CNOFs in CDCl$_3$ for obtaining ^{1}H NMR spectra. In Figure 3.3 we have compared the ^{1}H NMR of CNOFs with that of BPBDT in D$_2$O. ^{1}H NMR of BPBDT showed two sharp doublets at δ 8.64 and 8.21 ppm, as expected for 1,4-disubstituted benzene derivatives. The high δ value is due to the presence of the

diazonium group. In the case of CNOFs these two sharp doublets were absent but a broad and complex band structure in the range 6.7-7.7 ppm could be seen. This indicates complete removal of the diazonium group and formation of a complex structure. In the case of CNOF4, which is having the highest organic content, the multiplet pattern in the aromatic region exhibited sharp peaks. As we go from CNOF4 to CNOF1 the metal content increased and the NMR signals became very broad. Broadening of NMR signals were observed in the case of nanoparticle cored dendrimers (Kumar 2010; 2011) and palladium nanoparticle-linked organic frameworks (Chapter 2). The NMR line broadening arises due to the fast spin-spin relaxation of atoms close to a metal (Mirkhalaf 2006; Ghosh 2008). In the case of CNOF4, the metal content is less and the observed sharp peaks correspond to organic frameworks placed away from the metal. As the metal content increases the average distance between nanoparticles decreases and most of the framework comes under the influence of metal particles leading to a broadening of NMR signals as observed for CNOF1.
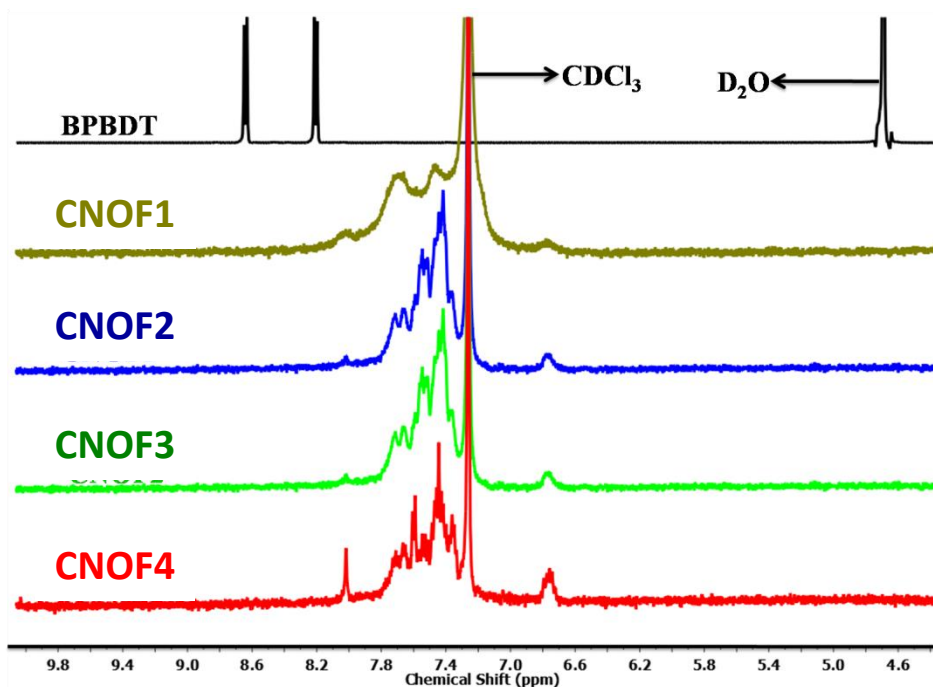
Figure 3.3 NMR spectra of BPBDT, CNOF1, CNOF2, CNOF3, and CNOF4.

3.3.2.4 Absorption studies

Dispersions of CNOF in toluene were sonicated for five minutes and filtered through a 0.45 μm filter pad and the resulting clear solutions were subjected to UV-Visible spectroscopy. The spectra obtained are shown in Figure 3.4. It can be seen from Figure 3.4 that none of the CNOFs exhibited the characteristic plasmon band of Cu nanoparticles at 560–590 nm. The absence of plasmon absorption is attributed to the small size of the nanoparticles (vide infra). It has been reported that plasmon absorption due to Cu nanoparticles can be seen only if the sizes of the particles are larger than 12 nm (Chen 2001; Samim 2007). The CNOF absorption spectra obtained showed increasing absorption in the region below 500 nm.
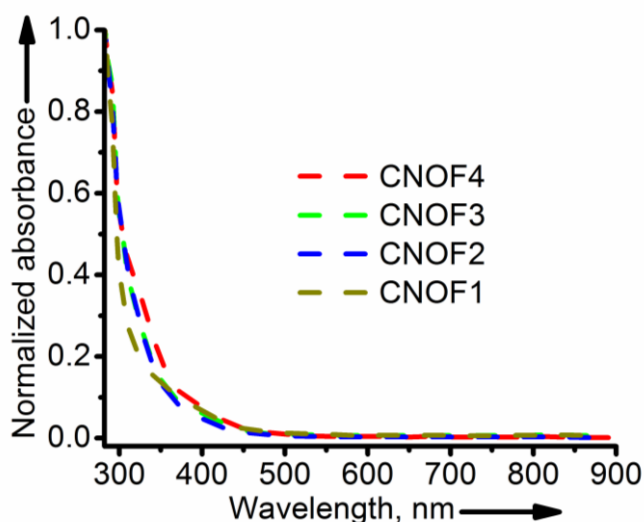
Figure 3.4 Absorption spectra of CNOFs in toluene.

3.3.2.5 XRD analysis

Powder X-ray diffraction (PXRD) analysis was carried out to confirm the presence and crystalline nature of Cu nanoparticles in the CNOFs. The results obtained are presented in Figure 3.5. All the four CNOFs gave intense and broad XRD peaks. Intense peak indicates that the metal clusters are highly crystalline. The broadness of the peaks indicates the nanosize of the particles. The Cu-containing samples exhibited diffraction peaks at 2θ angles of 43.2°, 50.4° and 74.0° with the d-spacing of 0.21 nm, 0.18 nm and 0.13 nm, which correspond to crystal facets of

(111), (200) and (220), respectively (JCPDS no. 00–004-0836) of face-centered cubic (fcc) structure. The crystallite sizes were calculated by using Sherrer's equation from the width of the peak at 2θ angle of 43.2°. The average crystallite sizes are found to be 3.2 nm for CNOF4, 3.4 nm for CNOF3, 3.7 nm for CNOF2 and 4.4 for CNOF1. The PXRD contains impurity peaks arising from Cu_2O at 2θ angles of 36.5° and 61.5° (JCPDS no. 03–065-3288). No peaks were present from CuO impurities. The intensities of peaks from Cu_2O impurities remain unchanged even after one month. This indicates that no further oxidations were taking place and the CNOFs were highly stable. The intensity of the Cu_2O peak at 36.5° increases as we go from CNOF4 to CNOF1. This can be due to decrease in the percentage of organic frameworks. This will lead to the increase in number of surface Cu atoms that can be oxidized to Cu_2O (Fahrenbach 2011).
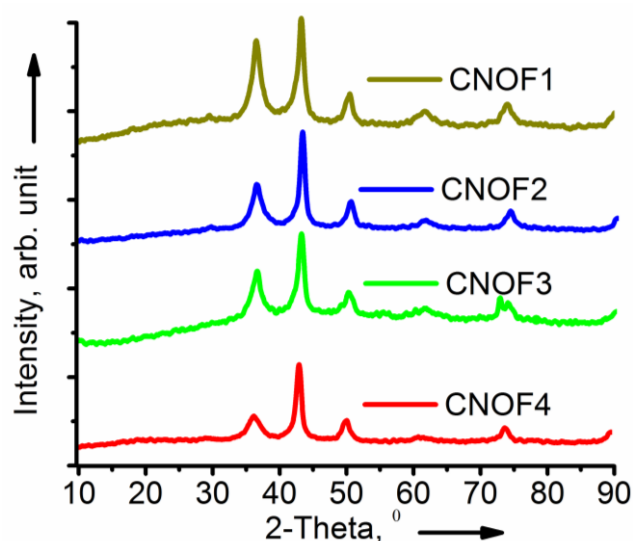
Figure 3.5 XRD patterns for the CNOFs.

3.3.2.6 XPS studies

Information about the oxidation state of Cu and the nature of bonding between the framework and Cu nanoparticle in CNOF were obtained from XPS analysis. XPS survey spectra for the four CNOFs are shown in Figure 3.6. All the CNOFs contain the signals for Copper (75 eV for Cu 3p, 122 eV for Cu 3s, 935 eV for

Cu 2p$_{3/2}$, 955 eV for Cu 2p$_{1/2}$, and 571 eV for Cu LMM-2), carbon (284 eV for C 1s) and oxygen (25 eV for O 2s, 532 eV for O 1s and 980 eV for O KLL). No other characteristic signals corresponding to other atoms were present in the survey spectra. This indicates that no other hetero atoms were present in the CNOFS.
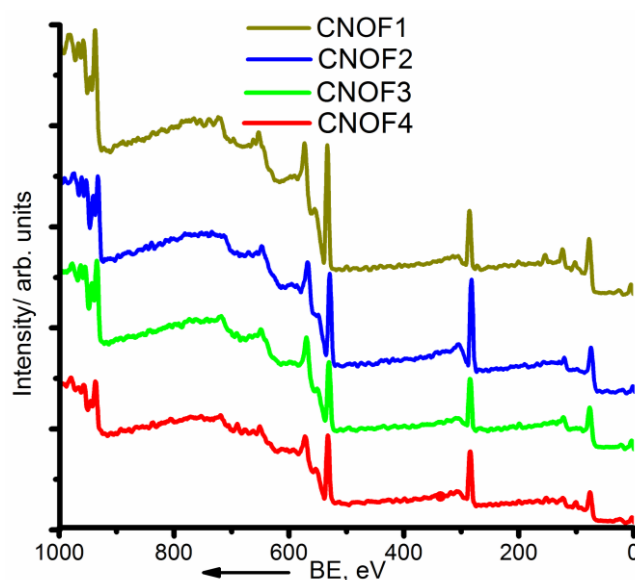
Figure 3.6 XPS survey spectra of CNOF materials. BE= Binding energy.

A curve fitting program was used to deconvolute the C 1s (figure 3.7), O 1s (Figure 3.8) and Cu 2p (Figure 3.9) peaks of CNOF. The C 1s peak observed in the 281–288 eV range could be deconvoluted adequately into C-Cu (283.5 eV) (Yang 2002), C-C (284.5 eV) (PNOF), C-H (285.3 eV) and C-O-Cu (286.3 eV) (Hurley 2004; Dubale 2014) contributions. As we go from CNOF4 to CNOF1 intensity of the C-O-Cu increases relative to the C-Cu peak suggesting that CNOF having higher metal content have more oxide content. Analysis of the C 1s peak thus revealed that the organic framework is linked to Cu through C-Cu or C-O-Cu bonds.

The O 1s XPS peak can be deconvoluted into two as shown in Figure 3.8. The first peak observed at 530.28 eV can be assigned to the oxygen in the Cu$_2$O and the second peak at 533.0 eV can be assigned to the oxygen in the Cu-O-C bonds (Hurley 2004; Chamoulaud 2007; Dubale 2014). As the metal content increases the intensity of Cu$_2$O peak increases due to more surface Cu atoms that can get oxidized. On the

other hand, the intensity of the Cu-O-C peak decreases in intensity with increase in metal content. This may be due to the decrease in the organic content which reduced the number of bonds to the framework. No peaks corresponding to CuO (529.6 eV) were observed in the O 1s XPS of any of the CNOFs (Chamoulaud 2007; Zhang 2009; Dubale 2014). Thus analysis of C 1s and O 1s XPS clearly indicated that the CNOF surface contains only Cu and Cu_2O.
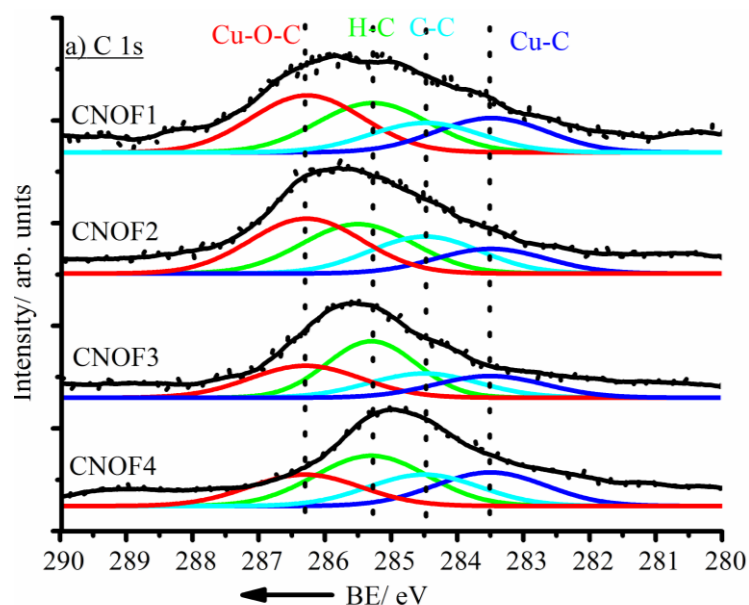
Figure 3.7 X-ray photoemission spectra of C1 s of the CNOF materials. BE= Binding energy.
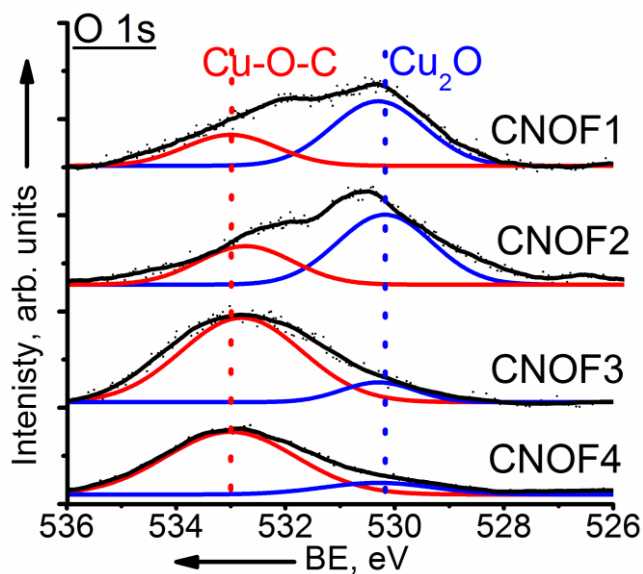
Figure 3.8 X-ray photoemission spectra of O1 s of the CNOF materials. BE= Binding energy.

To find the oxidation state of Cu present on the nanoparticle surfaces, XPS analysis of Cu 2p were carried out and the results are shown in Figure 3.9. All the CNOFs have peaks corresponding to Cu $2p_{3/2}$ and Cu $2p_{1/2}$ spin-orbit components. The Cu $2p_{3/2}$ peak was observed between 934-936 eV and the corresponding shake-up satellite peak was seen between 944-946 eV. The Cu $2p_{1/2}$ peak was seen between 954-956 eV and the corresponding shake-up satellite peak was observed between 964-966 eV. Previous studies have shown that metal nanoparticles stabilized by metal carbon covalent bonds will show M^{2+} peak in the XPS (chapter 2). Similar results are obtained for CNOFs also. Both the Cu $2p_{3/2}$ and Cu $2p_{1/2}$ peaks can be deconvoluted into two peaks each.
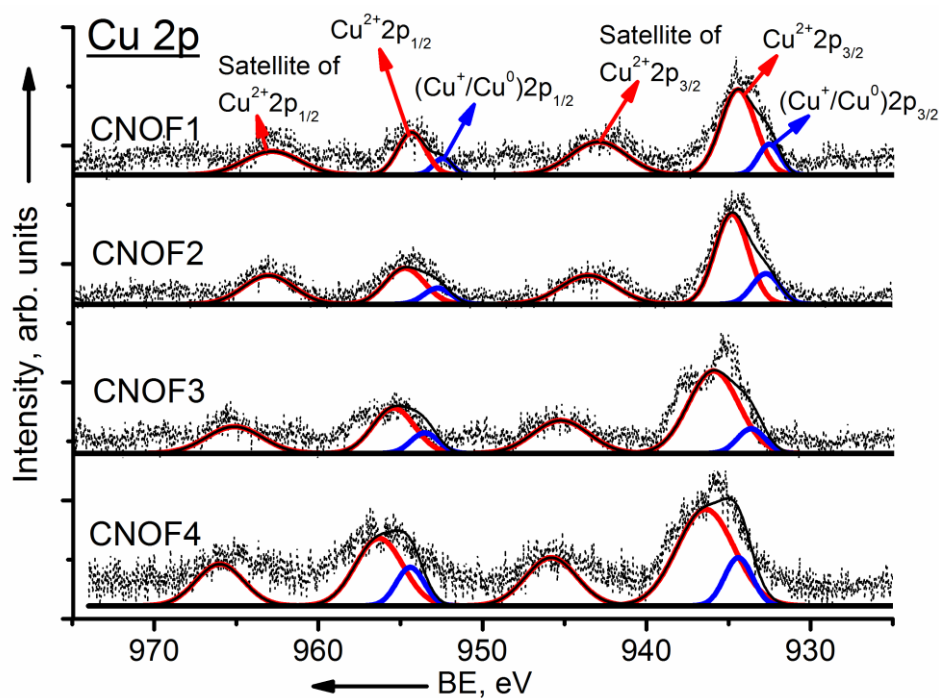
Figure 3.9 X-ray photoemission spectra of Cu 2p of the CNOF materials. BE= Binding energy.

The major peak (934-936 eV) can be assigned to Cu^{2+} and the minor lower energy peak (932-934 eV) can be due to either Cu^+ or Cu^0. It is very difficult to distinguish between Cu^+ and Cu^0 due to the very small energy difference between them. All the peaks obtained for CNOFs were at higher energy compared to those reported for unsupported Cu nanoparticles (Alonso 2010; Chen 2012). It is well

established that binding energy will be higher for supported Cu nanoparticles, especially if the bonding between the nanoparticles and support are stronger (Shargi 2009; Alonso 2010; Lin 2012). Thus the XPS data show that Cu nanoparticles are well bonded to the organic frameworks and not trapped in the organic frameworks.

3.3.2.7 SEM analysis

To study the morphology of the CNOFs we have carried out SEM and HRTEM analysis. The SEM images of CNOFs show large porous structures (Figure 3.10). The organic frameworks generated by the random additions of bisphenylene biradicals are expected to be planar but they get attached to spherical nanoparticles from all directions leading to three-dimensional structures. Since these are not soluble they aggregate and precipitate out during the reaction. The images we see in the SEM are large aggregates of CNOFs.
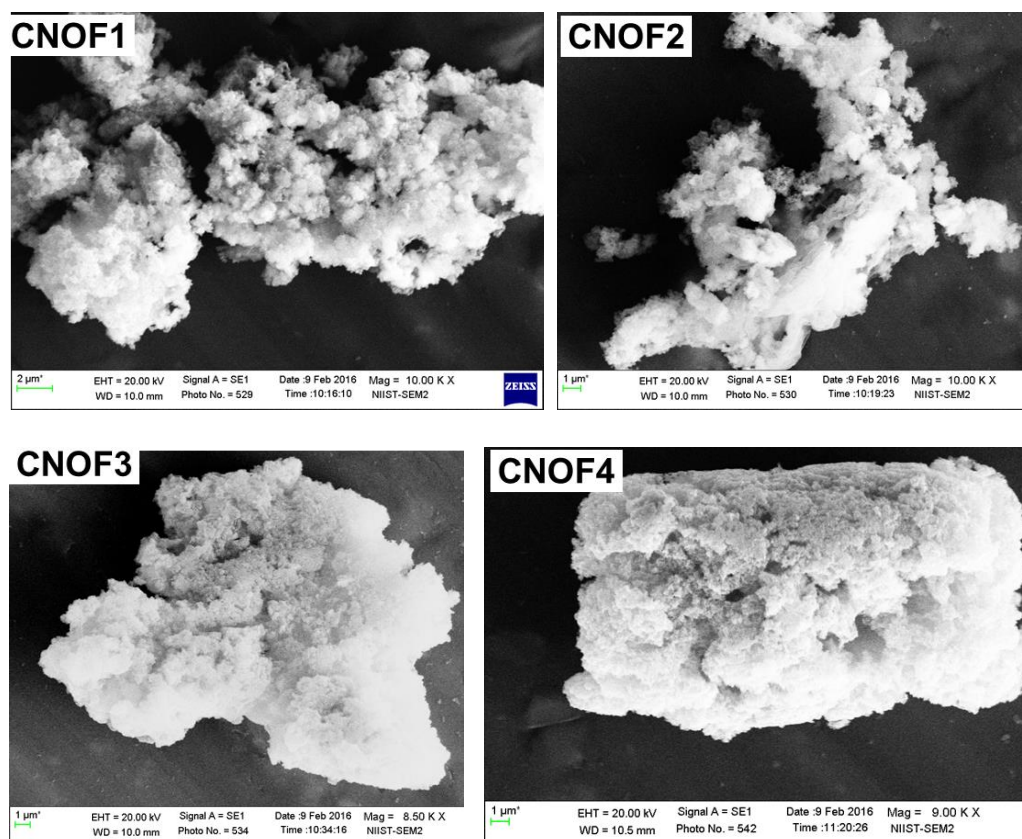
Figure 3.10 SEM image of CNOFs.

3.3.2.8 HRTEM analysis

TEM images of CNOFs (Figures 3.11-3.14) show large numbers of nanoparticles of size ≤ 8 nm embedded within a soft material. Contours of the soft framework can be seen in all TEM images. The average particle size obtained for CNOF1 is 5.7 nm, for CNOF2 4.9 nm, for CNOF3 4.3 nm and for CNOF4 4.2 nm (Figure 3.15). The values obtained were comparable with those calculated from the XRD analysis. Using this data we have calculated the number of surface Cu atoms in the CNOFs and the details are presented in Section 3.3.3. No metal particles were observed outside the contours of the organic framework. Nanoparticles can be found outside the frameworks only if they are entrapped in the frameworks through non-covalent interactions. Absence of particles outside the contours confirms that the metal nanoparticles are covalently attached to the network.
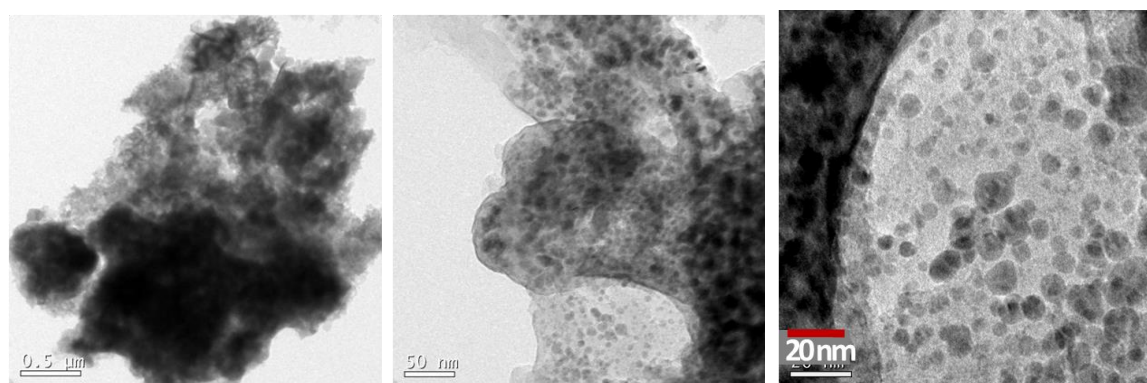
Figure 3.11 HRTEM images of CNOF1.
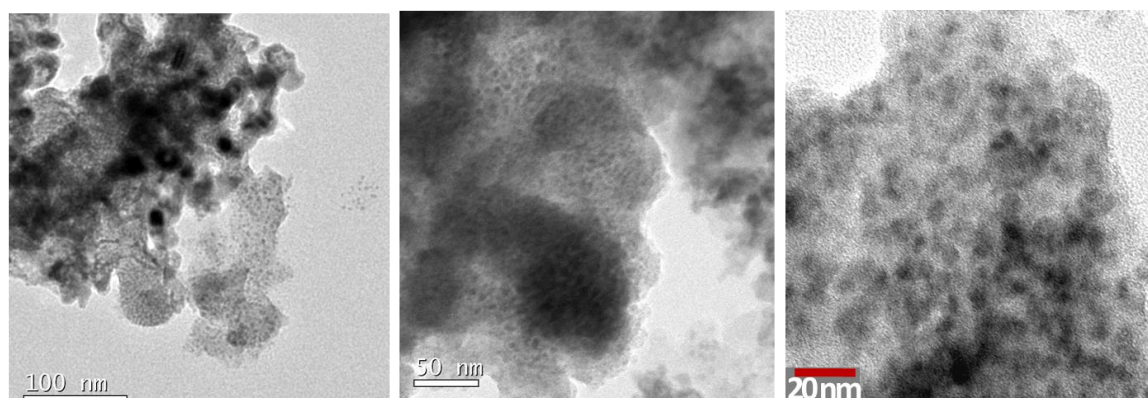
Figure 3.12 HRTEM images of CNOF2.
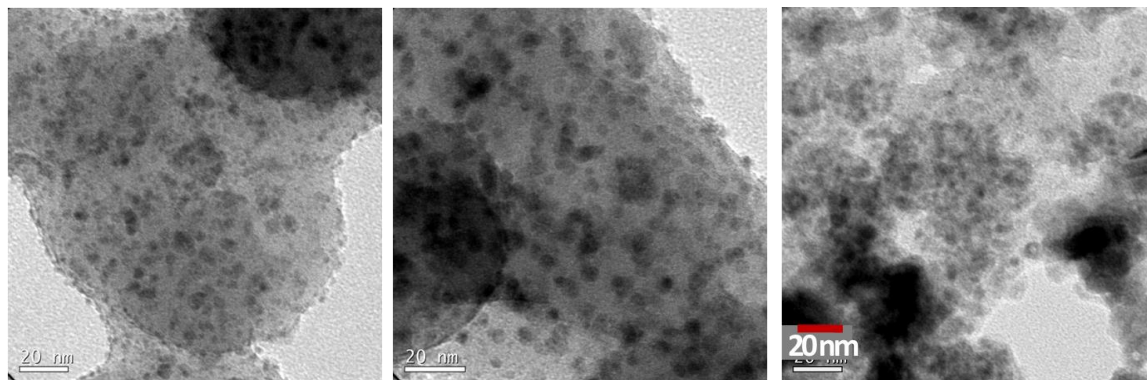
Figure 3.13 HRTEM images of CNOF3
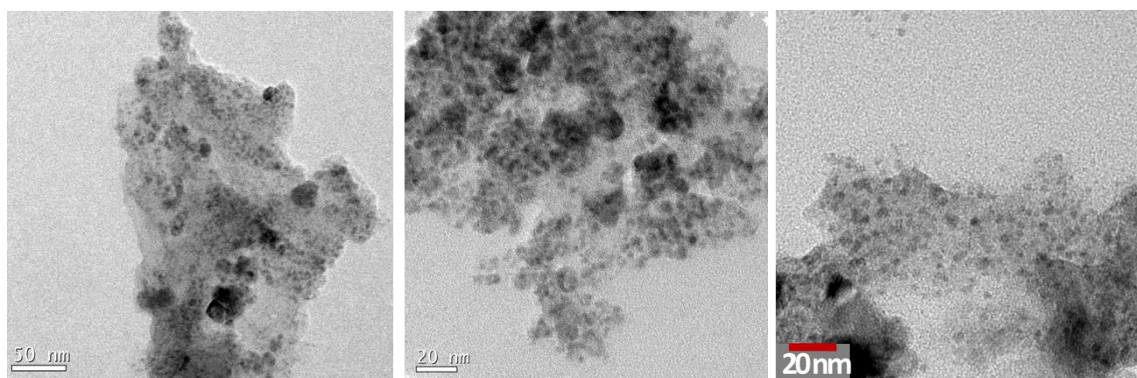
Figure 3.14 HRTEM images of CNOF4
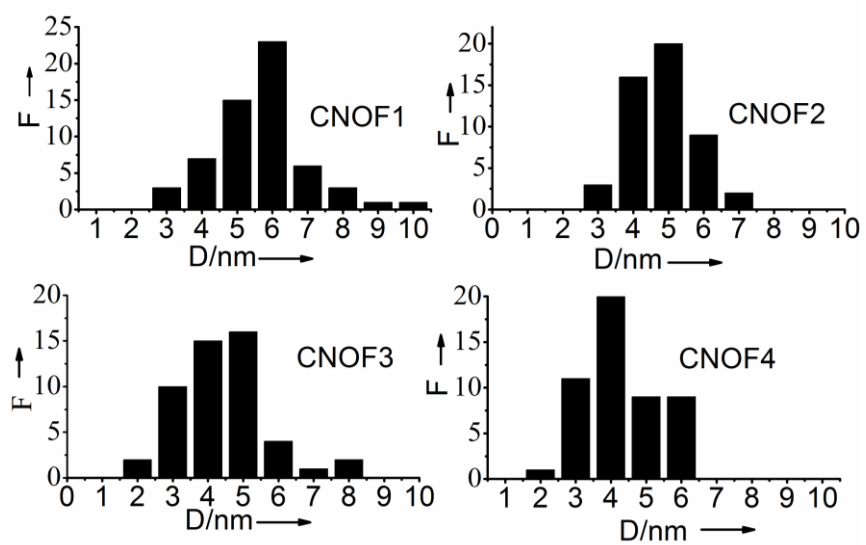
Figure 3.15 Core-size histograms for CNOFs (F=frequency).

To confirm the presence, composition, and packing of the copper nanoparticles, we have done selected area electron-diffraction (SAED) analysis. The results obtained are presented in the Figure 3.16. SAED pattern obtained are in agreement with the presence of copper nanoparticles. SAED pattern also showed the peak due to the presence of Cu_2O impurities. The intensities of such peaks are very low in the case of CNOF3 and CNOF4. In the other two cases, intensities of Cu_2O peaks are somewhat better. As explained in the case of XRD peaks, this can be due to increased amounts of Cu_2O on the surfaces of CNOF1 and CNOF2 nanoparticles.
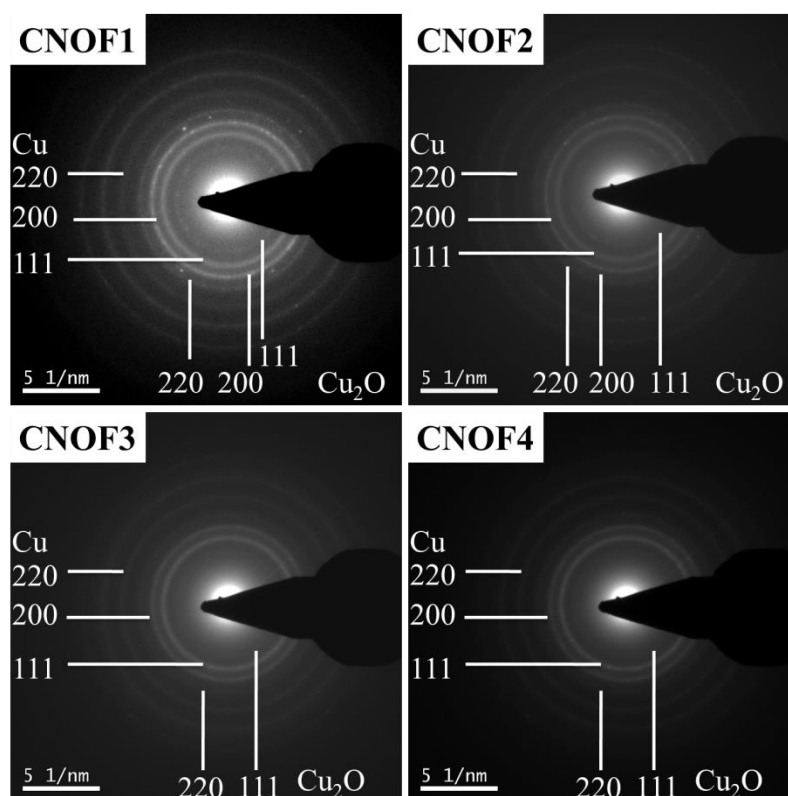
Figure 3.16 SAED pattern obtained for the CNOFs

3.3.3 Physical data of nanoparticles

Physical data for the nanoparticles in CNOFs were calculated as explained in Chapter 2 by assuming that the amounts of oxides are negligible.

Table 3.2 Physical data for Cu-nanoparticles in CNOF1.

Average Cu -nanoparticle diameter   = 5.7 nm

Average Cu -nanoparticle radius   = 2.85 nm

Average radius of Cu atom	= 0.128 nm
Total no. of Cu atoms per nanoparticles (N)	= $(R_{cluster}/R_{atom})^3$
	= $((2.85 \times 10^{-9})/(0.128 \times 10^{-9}))^3$
	= 11038
No. of surface Cu atoms per nanoparticles (Ns)	= $4 \times (11038)^{2/3}$
	= 1983
Percentage of surface atom	= 17.97 %
Weight percentage of Cu in CNOF1	= 88 %
Weight percentage of Cu in the surface of nanoparticles in CNOF1	= 88 × 0.1797
	= 15.81 %

Table 3.3 Physical data for Cu -nanoparticles in CNOF2.

Average Cu -nanoparticle diameter	= 4.9 nm
Average Cu -nanoparticle radius	= 2.45 nm
Average radius of Cu atom	= 0.128 nm
Total no. of Cu atoms per nanoparticles (N)	= $(R_{cluster}/R_{atom})^3$
	= $((2.45 \times 10^{-9})/(0.128 \times 10^{-9}))^3$
	= 7012
No. of surface Cu atoms per nanoparticles (Ns)	= $4 \times (7012)^{2/3}$
	= 1465
Percentage of surface atom	= 20.89 %
Weight percentage of Cu in CNOF2	= 81%
Weight percentage of Cu in the surface of nanoparticles in CNOF2 = 81 × 0.2089	
	= 16.92%

Table 3.4 Physical data for Cu -nanoparticles in CNOF3.

Average Cu -nanoparticle diameter	= 4.3 nm
Average Cu -nanoparticle radius	= 2.15 nm
Average radius of Cu atom	= 0.128 nm
Total no. of Cu atoms per nanoparticles (N)	= $(R_{cluster}/ R_{atom})^3$
	= $((2.15 \times 10^{-9})/(0.128 \times 10^{-9}))^3$
	= 4739
No. of surface Cu atoms per nanoparticles (Ns)	= $4 \times (4739)^{2/3}$
	= 1129
Percentage of surface atom	= 23.82 %
Weight percentage of Cu in CNOF3	= 74%

Weight percentage of Cu in the surface of nanoparticles in CNOF3 = 74 × 0.2382

$$= 17.63\%$$

Table 3.5 Physical data for Cu -nanoparticles in CNOF4.

Average Cu -nanoparticle diameter	= 4.2 nm
Average Cu -nanoparticle radius	= 2.1 nm
Average radius of Cu atom	= 0.128 nm
Total no. of Cu atoms per nanoparticles (N)	= $(R_{cluster}/ R_{atom})^3$
	= $((2.1 \times 10^{-9})/(0.128 \times 10^{-9}))^3$
	= 4416
No. of surface Cu atoms per nanoparticles (N_s)	= $4 \times (4416)^{2/3}$
	= 1077
Percentage of surface atom	= 24.38 %
Weight percentage of Cu in CNOF4	= 63%

Weight percentage of Cu in the surface of nanoparticles in CNOF4   = 62 × 0.2438

= 15.36 %

Table 3.6 Amount Cu (mmol) in CNOFs

CNOF	1	2	3	4
Amount of CNOF (mg)	5	5	5	5
Amount of Cu (mg)	4.40	4.05	3.75	3.15
Amount of Total Cu (mol)[a]	69.24×10^{-6}	63.73×10^{-6}	59.01×10^{-6}	49.57×10^{-6}
Amount of surface Cu (mol)	12.44×10^{-6}	13.32×10^{-6}	13.88×10^{-6}	12.45×10^{-6}

[a] Atomic mass of Cu = 63.55

3.3.4 Catalytic activity of CNOFs for the click reactions

Although it is generally believed that Cu^1 is the key catalyst involved in the click reaction (Rodionov 2005) Cu with all the possible oxidation states are found to catalyze this reaction (Meldal 2008; Jin 2012; Chahdoura 2014). For example, different kinds of copper nano structures including copper, copper oxides (both Cu_2O and CuO nanoparticles) and PVP-stabilized Cu_2O nanoparticles, were recently found to catalyze these reactions. It is generally believed that either binuclear or mononuclear copper species is involved as the key intermediate in the Cu(I) catalyzed reactions. Lack of reactivity of disubstituted alkynes in Cu(I) catalyzed reactions indicates that the deprotonation of the terminal alkyne plays a major role in the generation of Cu(alkynyl) intermediate (Wang 2016).

We found that CNOF1-CNOF4 can catalyze click reactions shown in Scheme 3.2. The results obtained are summarized in Table 3.7. Table 3.7 shows that TON and TOF are very high for benzyl azide but somewhat low for 4-nitrophenylazide. Click reactions between alkynes and aryl azides are generally slow (Chanda 2013), which explains the low TOF value.

Although all the CNOFs are good catalysts for the click reaction between azides and alkynes, we did not explore these reactions any further because only few azides are commercially available. There are reports in the literature where click reactions are performed using in situ generated azides (Sharghi 2009; Alonso 2011). Alkyl and benzyl azides can be prepared from the corresponding halides and sodium azide (NaN_3). The generation of azide and its subsequent reaction with
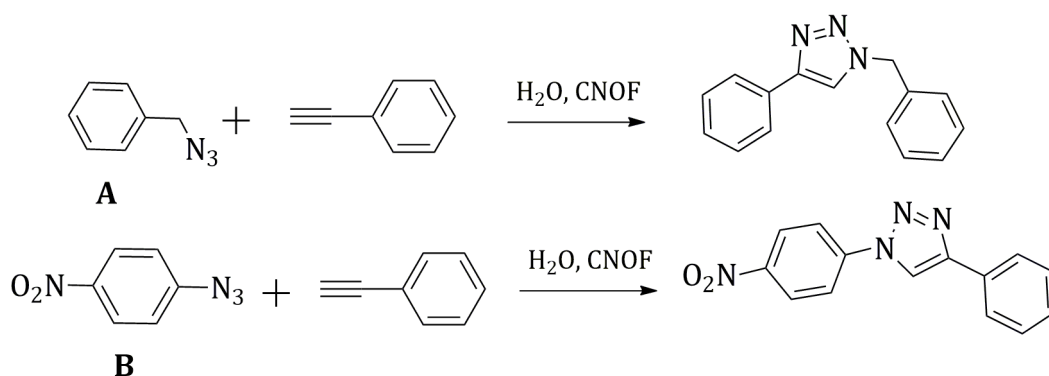
Scheme 3.2 CNOF catalyzed 1,3-dipolar cycloaddition between phenylacetylene with (A) benzyl and (B) 4-nitrophenyl azide.

alkynes can be thus accomplished in a one-pot reaction using azide precursor, sodium azide, alkyne and the click catalyst. Copper oxide nanoparticles and copper nanoparticles supported on carbon were reported as catalysts in these three-component click reactions (Lipshutz 2006; Li 2008; Sharghi 2009; Alonso 2010). We observed that the CNOFs are better catalysts for the one-pot reactions and this aspect was studied in detail using CNOF2 as catalyst.

Table 3.7 CNOF catalyzed 1,3-dipolar cycloaddition of phenylacetylene with benzyl or 4-nitrophenyl azide.

Entry[a]	Azide	CNOF (mol%)	Yield(%)/Time(h)[b]	TON	TOF (h[-1])
1	**A**	1/6.9	95/0.25	76300	305400
2	**A**	2/6.4	97/0.25	72800	291300
3	**A**	3/5.9	95/0.35	68400	207400
4	**A**	4/5.0	95/0.40	76300	181600
5	**B**	1/6.9	93/10	74700	7470
6	**B**	2/6.4	97/10	72800	7280
7	**B**	3/5.9	91/10	65500	6550
8	**B**	4/5.0	83/10	66600	6660

[a]Conditions: Azide (1 mmol), Alkyne (1.1 mmol), CNOF (5 mg) and water (4 mL) were stirred in aerobic conditions at 40 °C for **A** and at 70 °C for **B**. [b] Calculated through GC-MS analysis. TON = (Yield) / (100 × number of moles of surface Cu atoms in the CNOF). TOF = TON/ Time.

In order to select one catalyst for this study, we performed a control experiment employing benzyl bromide, sodium azide, and phenyl acetylene in water at 70 °C, with CNOFs as catalyst as shown in Scheme 3.3. The results are presented in Table 3.8 which showed that CNOF2 gave the best yield. In order to optimize the reaction conditions with CNOF2, the one-pot reaction (Scheme 3.4) was performed under the various reaction conditions mentioned in Table 3.9. It can be seen from Table 3.9 that the reaction did not occur below 60 °C. At 70 °C the reaction was completed in 40 min whereas at 100 °C reaction was completed within 20 min. Further experiments have shown that higher temperatures are required only for the azide formation step. Once the azide is formed the CNOF2 is capable of catalyzing the click reaction at room temperature. Thus the reaction conditions could be modified as in entry 9 and 10 of Table 3.9. In these cases benzyl bromide/sodium
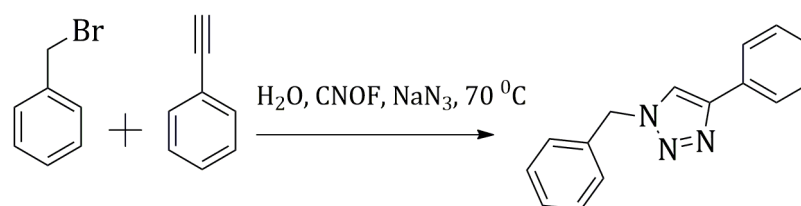
Scheme 3.3 Three-component 1,3-dipolar cycloaddition of benzyl bromide and phenylacetylene catalyzed by CNOFs.

Table 3.8 Click reaction of benzyl bromide and phenylacetylene catalyzed by CNOFs.

Entry[a]	Catalyst	Cu (mol %)	Yield (%)	TON[b]
1	CNOF1	6.9	80	64300
2	CNOF2	6.4	85	63800
3	CNOF3	5.9	84	60500
4	CNOF4	5.0	76	61000
5	No Catalyst	0	-	-

[a] Benzyl halide (1 mmol), phenylacetylene (1.1 mmol), NaN_3(1.1 mmol), and CNOF (5 mg) were suspended in water (4 mL) and stirred for 30 minutes at 70 °C. [b] TON = (Yield in %) / (100 × number of moles of surface Cu atoms in the catalyst).

azide mixture was heated to 60 (or 70) °C, cooled to room temperature followed by addition of the alkyne and CNOF2. Stirring at RT for 30 min. gave near quantitative yields in both cases. This method is very much suited when the alkynes employed are very volatile. Heating at higher temperatures in these cases led to low yields due to loss of the alkyne by evaporation.
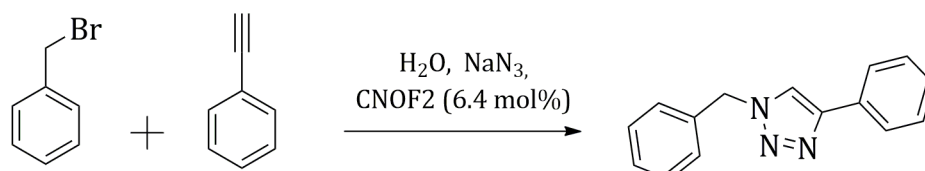
Scheme 3.4 Three-component 1,3-dipolar cycloaddition catalyzed by CNOF3 using benzyl bromides.

Table 3.9 Temperature dependent three-component 1,3-dipolar benzyl azide-phenylacetylene cycloaddition catalyzed by CNOF3.

Entry[a]	T[°C]	Time[min]	Yield[%][b]	TON	TOF
1	RT	30	-		
2	50	30	-		
3	60	30	57	42700	85500
4	60	60	99	74300	74300
5	70	30	85	63800	127600
6	70	40	99	74300	110900
7	100	20	93	69800	211500
8	100	30	99	74300	148600
9	RT[c]	30[e]	99	74300	148600
10	RT[d]	30[e]	99	74300	148600

[a] Conditions: Benzyl bromide (1 mmol), NaN$_3$ (1.1 mmol), phenylacetylene (1.1. mmol), CNOF2 (5 mg) and water (4 mL) were stirred in aerobic conditions at the indicated temperature. [b] Yields were calculated through GC-MS analysis. Before the addition of phenylacetylene and CNOF2 the reaction mixture were stirred at [c] 60 °C and [d] 70 °C for 1 h respectively. [e] The time indicated was measured after the addition of catalyst and phenylacetylene.

We have carried out several one-pot click reactions (Scheme 3.5) using CNOF2 as catalyst. The reaction conditions and yields are shown in Table 3.10. An examination of Table 3.10 shows that the one-pot click reactions using CNOF2 as catalyst gave excellent yields in all cases studied. For most of the reactions in Table 3.10 yields are > 95%. With highly volatile alkynes (entries 17–19) reactions were carried out by heating the halide and NaN$_3$ at 70 °C, cooling to room temperature and then adding the alkyne and CNOF2 followed by stirring at RT. For these cases, the time indicated in Table 3.10 corresponds to stirring at RT.

$$R_1-X \ + \ R_2-\!\!\!\equiv \quad \xrightarrow[\text{CNOF2 (6.4 mol\%)}]{\text{H}_2\text{O, NaN}_3, \ 70\,^0\text{C}} \quad R_1-\overset{\displaystyle N=N}{\underset{\displaystyle N}{\diagup}}\!\!\diagdown R_2$$
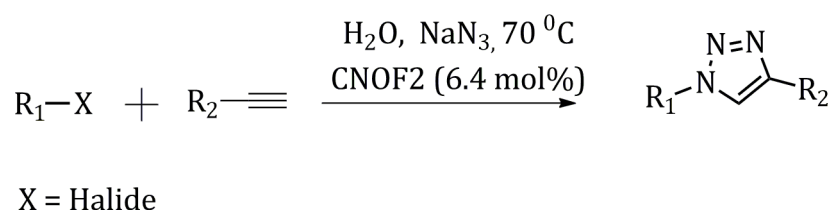
X = Halide

Scheme 3.5 Three-component 1,3-dipolar cycloaddition catalyzed by CNOF2 using halides.

Table 3.10 Three-component 1,3-dipolar cycloadditions catalysed by CNOF2

Entry[a]	Halide	Alkyne	Time (%)[b]	Yield (h)[c]	TON	TOF (h⁻¹)
1	1a	2a	0.75	99	74300	99000
2	1a	2b	4	98	73500	18300
3	1a	2c	3	98	73500	24500
4	1a	2d	1	98	73500	73500
5[d]	1a	2e	2	92	69000	34500
6	1b	2a	4	97	72800	18200
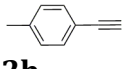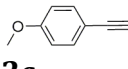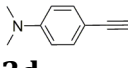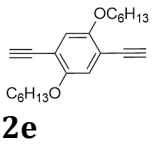
Table 3.10 Three-component 1,3-dipolar cycloadditions catalysed by CNOF2 (continued from previous page)

Entry[a]	Halide	Alkyne	Time (%)[b]	Yield (h)[c]	TON	TOF (h^{-1})
7	1c (Br, 4-methylbenzyl bromide)	2a	4	97	72800	18200
8	1d (Cl, benzyl chloride)	2a	8	87	65300	8160
9	1b	2b	4	98	73500	18300
10	1b	2c	4	99	74300	18500
11	1b	2d	1	99	74300	74300
12[d]	1b	2e	2	90	67500	33700
13	1c	2b	4	98	73500	18300
14	1c	2c	4	97	72800	18200
15	1c	2d	1	98	73500	73500
16	1c	2b	2	93	69800	34900
17[e]	1a	2f (trimethylsilylacetylene)	12	99	74300	6190
18	1b	2f	12	96	72000	6000
19	1c	2f	12	93	69800	5810
20	1e (ethyl bromoacetate)	2a	1	98	73500	73500
21[d]	1a	2g (1-octyne)	12	83	62300	5190
22[d]	1a	2h (O$_2$N-phenylacetylene)	4	88	66000	16500
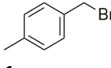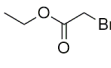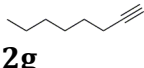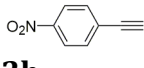
[a] Conditions: A mixture of alkyne (1.1 mmol), halide (1.0 mmol), NaN$_3$ (1.1 mmol) and CNOF2 (5 mg) were stirred in water (4 mL) under aerobic conditions at 70 ºC. [b] Monitored through TLC. [c] Calculated using GC-MS analysis. [d] 0.5mmol alkyne was used and isolated yield were given. [e] Before the addition of alkyne and catalyst the reaction mixture were stirred for one hour at 70 °C further cooled to RT and after that, the addition reaction continued at RT. TON = (Yield) / (100 × number of moles of surface Cu atoms in the CNOF). TOF = TON/ Time.

In all the reactions reported in Table 3.10, benzyl or alkyl halides are converted in situ to azides. With aryl halides, this reaction is not possible. Instead one can use diazonium salts as precursors of azides for the preparation of aryl-substituted triazoles. We have studied one-pot reactions using aryl diazonium salts, as shown in Scheme 3.6. The reactions studied are listed in Table 3.11. We have employed three different diazonium salts and three different alkynes and for all

N_2^+ + R_2 ≡ $\xrightarrow[\text{CNOF2 (6.4 mol\%)}]{\text{H}_2\text{O, NaN}_3,\ 12\ \text{h, 70 }^0\text{C}}$

3a = -NO$_2$; 3b = -CH$_3$; 3c = -Br
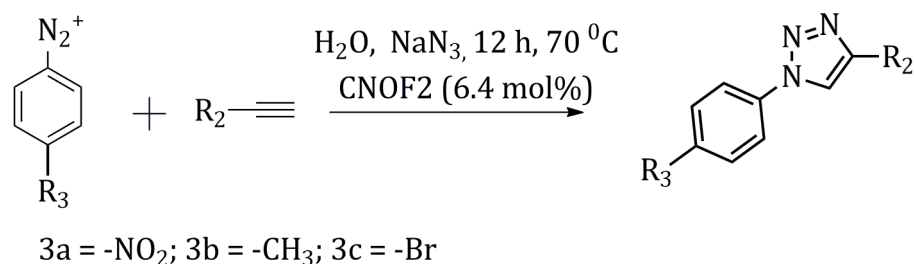
Scheme 3.6 Three-component 1,3-dipolar cycloaddition catalyzed by CNOF2 using aromatic diazonium compounds.

Table 3.11 Three-component 1,3-dipolar cycloadditions catalyzed by CNOF2 using aromatic diazonium compounds.

Entry[a]	Diazonium salt	Alkyne	Yield (%)[b]
1	3a	2a	92
2	3a	2b	87
3	3a	2c	86
4	3b	2a	89
5	3b	2b	85
6	3b	2c	79
7	3c	2a	91
8	3c	2b	86
9	3c	2c	82
10	3a	2f[c]	-

[a] Conditions: Diazonium salt (1 mmol), NaN$_3$ (1.1 mmol), Alkyne (1.1. mmol), CNOF2 (5 mg) and water (4 mL) were stirred in aerobic conditions at 70 °C. [b] Isolated yield. [c] Reaction at 45 °C.

these reactions yields were above 80% as shown in Table 3.11. These studies established that CNOF2 is a very good catalyst for one-pot click reactions.

3.3.4.1 Catalyst recovery studies

We observed that the CNOF catalysts could be recovered and reused several times in the one-pot click reactions. The reaction between benzyl bromide and phenylacetylene in the presence of NaN_3 was selected for the recyclability study. After heating the reaction mixture at 70 °C for one hour (1.5 h for CNOF2), the mixture was cooled to RT and extracted with ethyl acetate in a dropping funnel. The mixture is allowed to stand undisturbed for a few min. The CNOF catalyst, which is insoluble in water and ethyl acetate, settles at the interface of the two liquids. Careful removal of the water layer will leave the catalyst in a very small volume of ethyl acetate (less than 0.5 mL) at the bottom. This layer is also taken into the water layer and reactions were repeated with the aqueous layer containing the catalyst. We have checked the recyclability of the catalyst in this way for ten cycles. Time taken to complete the reaction increased from 45 minutes to more than 3 h for the 10th cycle. The catalyst recovered after the 5th cycle was analyzed using HRTEM. The results obtained are shown in Figure 3.17, which shows that the average particle size decreased from 4.9 nm to 1.9 nm. The particle size distribution also got narrowed. This means that some leaching of Cu occurs into the solution during each cycle. Comparing to Figure 3.12, we may suggest that leaching occurred preferentially from bigger particles so that after 5 cycles particles of nearly uniform size were formed.
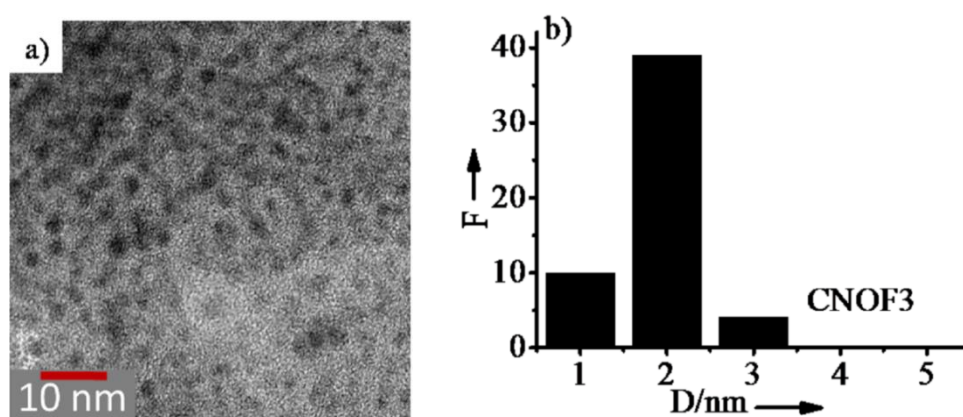
Figure 3.17 (a) HRTEM of recovered CNOF2 and (b) Core-size histograms; (F=frequency).

3.3.4.2 Leaching tests of the catalysts

According to World Health Organization's (WHO) guideline, copper content of 2.0 mg L^{-1} in drinking water is the safe limit (Araya 2004). Increase in copper level in the body can generate more reactive oxygen species. These can badly affect the body and will cause various diseases (Crisponi 2010). Apart from this toxic effect, leaching of Cu from nanoparticles into solution during the reaction is the major factor that has a detrimental effect on the catalytic activity of supported Cu catalysts. To see if any leaching out of Cu is occurring during the reaction inductively coupled plasma atomic emission spectroscopic (ICP-AES) analysis was performed (see the experimental section). We observed 0.25% of Cu leaching in one cycle when 5 mg CNOF2 and 1 mmol of the reactants were used for the reaction. ICP-AES analysis of the product was also carried out (see the experimental section). It was found that the product was not contaminated with Cu (detection limit was 0.01 ppm).

Recently reported catalysts for click reactions with high TOF include, dendrimer nanoreactor for part-per-million Cu^1 catalyst (TON =510000, TOF= 21200 h^{-1}) (Deraedt 2014), amphiphilic Cu^1 catalyst for two component click reaction (TON=86000, TOF 3600 h^{-1}) (Wang 2016) and alumina supported CuI for three component click reactions (TON=495, TOF= 4950 h^{-1}) (Agalave 2015). The TOF and TON values obtained with our catalyst for both two-component (Table 3.7) and three component reactions (Table 3.8, Table 3.9, Table 3.10, and Table 3.11) are comparable and even higher than the recently reported values.

It is a well-accepted principle that nanoparticle catalysts on supports are better than bulk metal catalysts owing to the large surface to volume ratio and the distribution of the particles on the support surface. Synthesis and applications of copper nanoparticle catalysts is reviewed recently (Das 2016). Cu or Cu(I) nanoparticles supported on ionic polymer (Chtchigrovsky 2009), zeolite (Chassaing 2008), Wyoming's montmorillonite clay (Jlalia 2008), silica (Lee 2009), activated carbon (Lipshutz 2006) and charcoal (Alonso 20100) are reported to catalyze click reactions and hence it is very much imperative on our part to compare the CNOFs with these catalysts. In few of the above cases, the catalyst preparation required harsh conditions such as heating at 500-600 °C. Cu supported on ionic polymer and zeolite required azides for the reaction and reactions were carried out in DMF:water

(4:1) or methanol-water mixtures. The mol% of catalyst required was also very high in the former case. In the case of Wyoming's clay, reaction required CH_2Cl_2 solvent. In the case of Cu on silica inert conditions such as nitrogen atmosphere is required for the successful conduct of the reaction. Cu on activated carbon and charcoal worked very well in the one-pot reactions, but the former required THF and triethylamine and the latter used dioxane as solvent. In both cases, catalysts were not stable and could not be reused. Compared to all these reported cases CNOFs have several advantages. These can be synthesized easily and the one-pot reaction could be accomplished in water. The recently reported kenaf bio-cellulose based poly(hydroxamic acid) copper catalyst is highly active and works well at room temperature (Mandal 2016). However, preparation of the catalyst involves multiple steps and the click reactions are performed in methanol. In the case of CNOFs inert reaction conditions are not required, reaction times are less and product separation is very easy. These catalysts can also be reused several times.

3.4 Conclusions

In this chapter, we report the synthesis, characterization and catalytic applications of Cu nanoparticles covalently linked to an aromatic framework. Synthesis was accomplished in a one-pot reaction which involved $NaBH_4$ reduction of a bisdiazonium salt and $CuCl_2$. The structure and morphology of these materials were examined using XRD, XPS, SEM and HRTEM. These materials were found to catalyze the click reactions between azides and alkenes in water. We employed these materials as catalysts in the one-pot synthesis of 1,2,3-traizoles from azide precursors (halides or diazonium salts), sodium azide and alkynes and in all cases, the yields were very good.

The TON and TOF values were very high compared to previously reported catalysts. Most of the previously reported catalysts were prepared using harsh reaction conditions and required organic solvent as reaction medium or inert conditions to carry out the click reaction. On the other hand, the CNOFs are prepared in one step. The CNOF catalysts were highly stable and inert conditions were not required. We observed that the CNOF catalysts could be recovered and reused several times. They work well as catalyst for the click reaction both for the benzyl

azides generated from benzyl halides and for aromatic azides generated from the diazonium salts.

3.5 Experimental Section

3.5.1 Materials and methods

A reported procedure was used for the preparation of BPBDT (Schiemann 1943). Thermo-gravimetric analysis, as well as differential thermal analysis, were performed in atmospheric conditions at a heating rate of 10 °C/min from 35 to 900 °C by using a Shimadzu DTG-60 equipment. All the FTIR spectra were recorded on a Shimadzu IR Prestige 21 spectrometer. UV-Vis spectra were obtained using Shimadzu UV-2600 spectrophotometer. Bruker Avance DPX 500 MHz spectrometer was used to obtain the ^{1}H NMR data. X-ray diffractograms were obtained using Ni-filtered CuK$_\alpha$ radiation from a Phillips diffractometer. XPS data were obtained using Omicron Nanotechnology X-ray photoemission spectrometer which employed AlKα (1486.7 eV) as X-ray source. Fityk software was used for the spectral background (Shirely) deconvolution. A Zeiss-EVO 18cryo SEM was used to obtain the SEM images. CNOF suspensions in toluene were sonicated for 30 min prior to drop-casting on aluminum stud covered with aluminum foil and samples on the stud were sputtered with gold for 30 min before the measurements. HRTEM analyses were done by using the same stock solution after drop casting on a 400 mesh carbon-coated copper grid, using a FEI–TECNAI30 G2S-Twin 300 kV instrument. ICP-AES experiments were performed using Thermo Electron IRIS INTREPID II XSP DUO, Flexible axial and radial view instrument.

3.5.2 Experimental Details

3.5.2.1 Preparation of CNOFs

CNOF1: To a stirred mixed solvent system containing deionized and deaerated water (30 mL) and toluene (30 mL) was added BPBDT (381 mg, 1 mmol) and CuCl$_2$.2H$_2$O (682 mg, 4.0 mmol) followed by a methanolic solution of NaBH$_4$ (0.2 M, 50 mL). After 6 h stirring, the toluene layer was collected and washed with water (2 × 15 mL) and then diluted with methanol (50 mL). The mixture was filtered at pump and the solid was washed with methanol (2 × 15 mL). The material obtained was dried in a vacuum oven at 70 °C for 24 h. Yield was 290 mg.

CNOF2: For CNOF2 preparation the above procedure was used with 3.0 mmol (511 mg) of $CuCl_2.2H_2O$. Yield was 230 mg.

CNOF3: Same procedure repeated with 2.0 mmol (381 mg) of $CuCl_2.2H_2O$. Yield was 170 mg.

CNOF4: The above procedure repeated with 1.0 mmol (171 mg). Yield was 100 mg.

3.5.2.2 General procedure for the CNOF catalyzed click reactions

A mixture of azide precursor (halide or diazonium salt, 1.0 mmol), alkyne (1.0 mmol) sodium azide (72 mg, 1.0 mmol) and CNOF (5 mg) in water was stirred for the indicated time at the specified temperature. The product was then extracted into ethyl acetate (3×10 mL). The organic layer was dried and solvent removed to get the product. The yield was calculated by GC–MS using 1,2,3- trimethoxybenzene as an internal standard.

3.5.2.3 Recyclability of CNOF

The same amounts of materials as mentioned above were used for the catalyst recyclability study. At the end of the specified time, the mixture was cooled to room temperature. Ethyl acetate (20 mL) was added and stirring continued for 10 min. The mixture was taken in a separating funnel and allowed to settle. The catalyst settles to a thin layer between the aqueous and organic layers. The aqueous layer and the catalyst layer were carefully separated and reaction repeated with the same amount of reactants (except the catalyst). The product is present in the ethyl acetate layer. We have repeated the cycle 10 times and each time the ethyl acetate layer was analyzed to get the product yield. In a separate experiment, the catalyst was collected after the fifth cycle for HRTEM analysis.

3.5.2.4 ICP-AES analysis.

ICP–AES analyses were used to determine the leaching of Cu during the reaction as well as the Cu contamination of the product. Linear calibration curves were obtained using standard solutions containing 0, 1.0, 5.0 and 10.0 ppm copper in 2% nitric acid.

(a) Leaching of Cu during the reaction.

A reaction was carried out with a mixture of CNOF2 (5.0 mg), sodium azide (72 mg, 1.1 mmol), benzyl bromide (0.120 mL, 1mmol), and phenylacetylene (0.121 mL, 1.1 mmol) in water (5 mL) at 60 °C for half an hour. The hot aqueous layer was filtered and ICP- AES analysis was carried out. It was found that 2.05 ppm level (2.05 μg mL^{-1}) Cu was present in the aqueous layer. The catalyst used for this study was 1 mg mL^{-1}. That is equivalent to 810 μg mL^{-1} of Cu. Hence the result shows that only 0.25% leaching of the Cu was occurring during the catalytic reaction.

(b) Cu contamination of the product.

Click reaction was performed using a mixture of CNOF2 (15.0 mg), sodium azide (358 mg, 5.5 mmol), benzyl bromide (0.594 mL, 5 mmol), and phenylacetylene (0.550 mL, 5.5 mmol) in water (15 mL) at 60 °C for 2.5 hour. The product was extracted into ethyl acetate (3 × 25 mL) and filtered through celite column to remove suspended impurities. Removal of ethyl acetate gave the product (1.150 g, 98%). 0.5 g of the product was digested with a mixture of conc. HNO_3 (2 mL) and conc. $HClO_4$ (0.2 mL) for three days and heated at 150 °C for 2 h. A second sample was digested with the acids for five days and then heated at 150 °C for 2 h. Both the samples were then analyzed by ICP-AES.

3.5.2.5 Characterization of Click reaction products

The click reaction products were characterized using GC-MS, FT-IR and NMR techniques. The mass splitting pattern obtained from the GC-MS analysis were compared with the reported values. The FT-IR spectra of the starting materials (diazonium salts, azides, and alkenes) have characteristic IR bands at 2200 cm^{-1} of triple bond (C≡C and N≡N), which will be absent in the products. Hence FT-IR spectra are a powerful tool to follow the click reaction. The products obtained are characterized using HRMS and NMR analysis. Most of the products in Tables 3.10 and 3.11 are known molecules. The NMR and HRMS data of new molecules are given below.
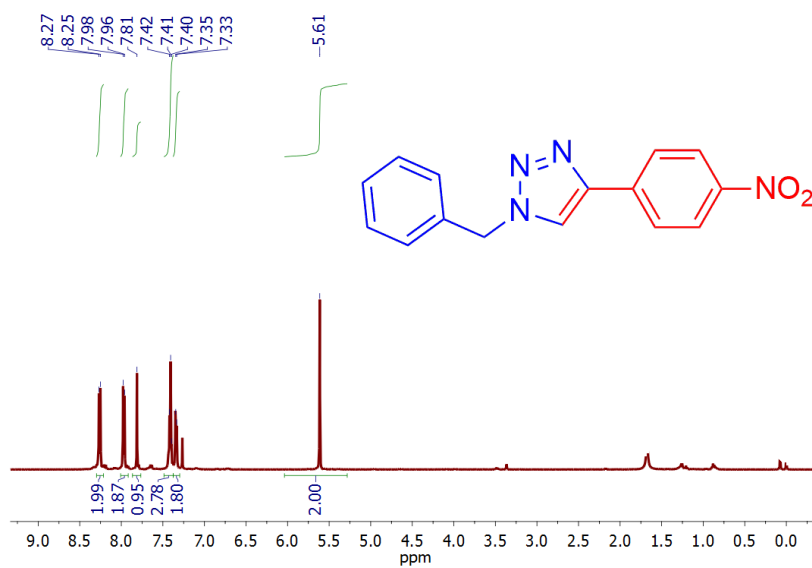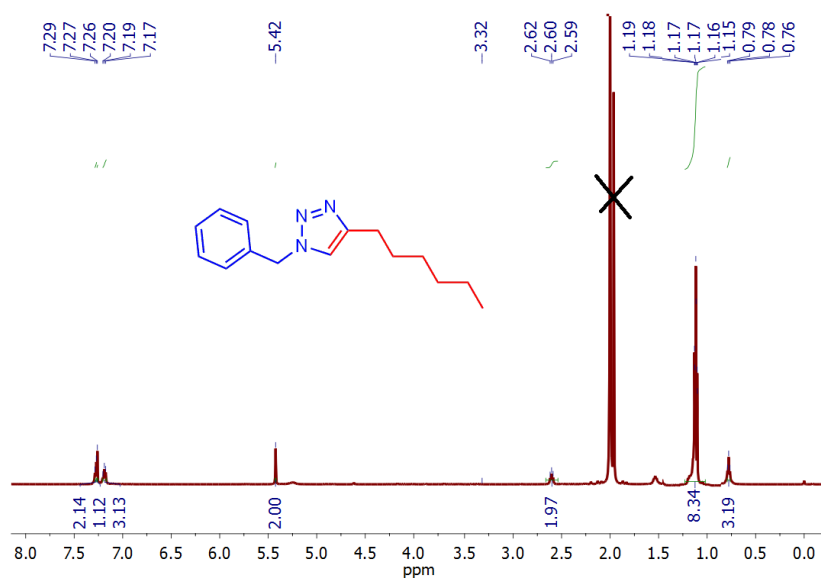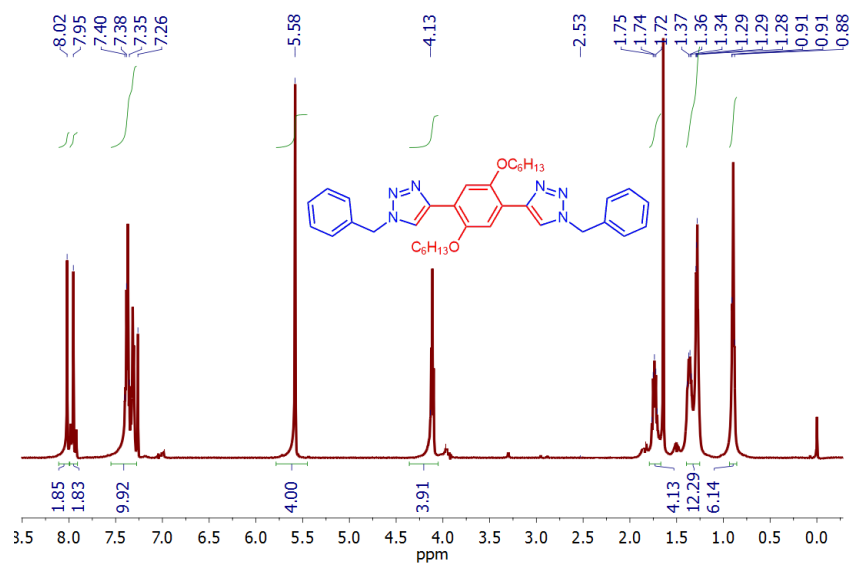
Data D:\Data\2016\SEPTEMBER 2016\TWO   ID: TWO   Time: 07/09/2016 16:04:12
Instrument: Thermo Exactive Orbitrap
TWO #79-93 RT: 1.18-1.38 AV: 15 SB: 122 0.14-1.95 NL: 6.66E6
T: FTMS {1,1} + p ESI Full lock ms [100.00-1500.00]
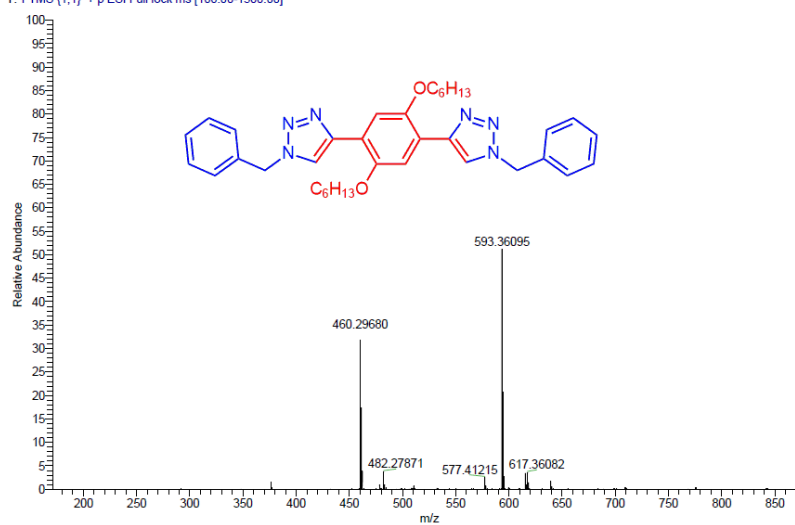
Data D:\Data\2016\SEPTEMBER 2016\SIX   ID: SIX   Time: 07/09/2016 16:25:02
Instrument: Thermo Exactive Orbitrap
SIX #69-78 RT: 1.03-1.15 AV: 10 SB: 122 0.14-1.95 NL: 5.38E7
T: FTMS {1,1} + p ESI Full ms [100.00-1500.00]
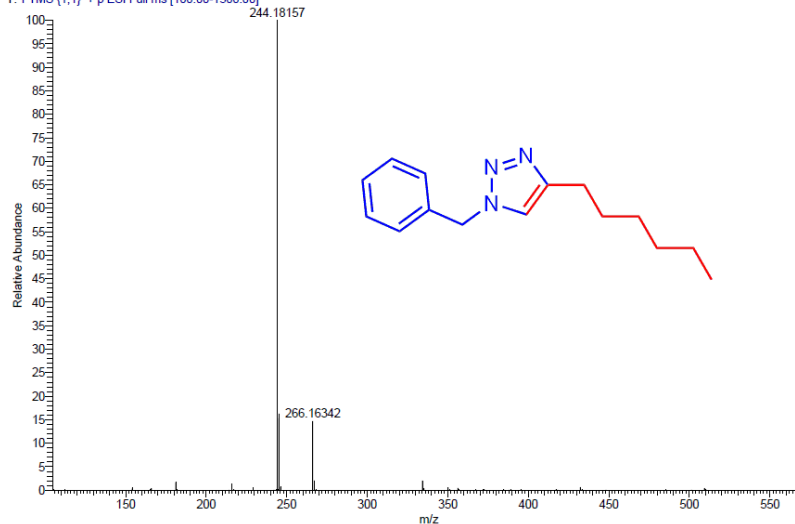
Data D:\Data\2016\SEPTEMBER 2016\ONE   ID: ONE   Time: 07/09/2016 15:57:16
Instrument: Thermo Exactive Orbitrap
ONE #68 RT: 1.01 AV: 1 SB: 121 0.14-1.95 NL: 1.26E6
T: FTMS {1,1} + p ESI Full lock ms [100.00-1500.00]

121
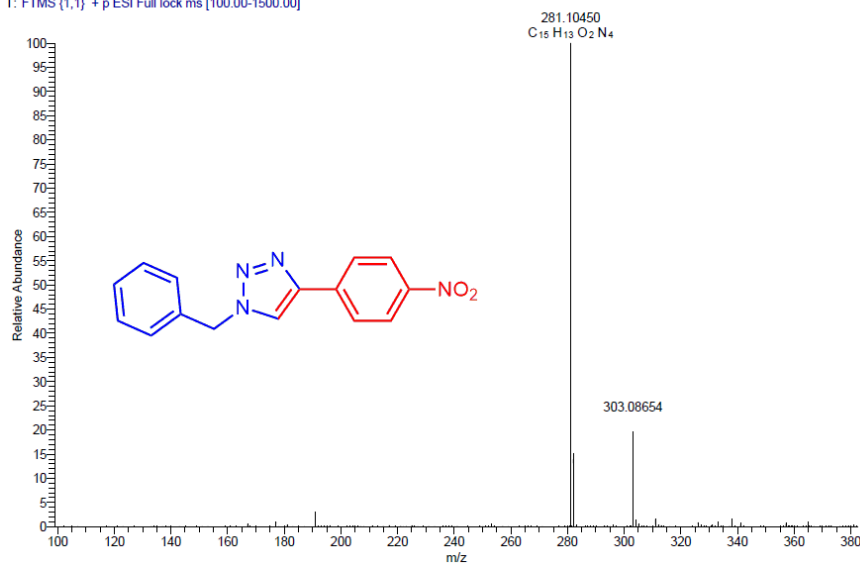
3.6 References

Abdulkin, P.; Moglie, Y.; Knappett, B. R.; Jefferson, D. A.; Yus, M.; Alonso, F.; Wheatley, A. E. H. *Nanoscale,* **2013***, 5*, 342-350.

Agalave, S. G.; Pharande, S. G.; Gade, S. M.; Pore, V. S. *Asian J. Org. Chem*. **2015**, *4*, 943-951.

Allen, S. E.; Walvoord, R. R.; Padilla-Salinas, R.; Kozlowski, M. C. *Chem. Rev.* **2013***, 113*, 6234-6458.

Alonso, F.; Moglie, Y.; Radivoy, G.; Yus, M. *Eur. J. Org. Chem*. **2010**, 1875-1884.

Alonso, F.; Moglie, Y.; Radivoy, G.; Yus, M. *Adv. Synth. Catal.* **2010***, 352*, 3208-3214.

Alonso, F.; Moglie, Y.; Radivoy, G.; Yus, M. *Org. Biomol. Chem*. **2011***, 9*, 6385-6395.

Alonso, F.; Moglie, Y.; Radivoy, G.; Yus, M. *J. Org. Chem*. **2011**, *76*, 8394-8405.

Alonso, F.; Moglie, Y.; Radivoy, G.; Yus, M. *Heterocycles*, **2012**, *84*, 1033-1044.

Alonso, F.; Moglie, Y.; Radivoy, G.; Yus, M. *J. Org. Chem*. **2013**, *78*, 5031-5037.

Alonso, F.; Moglie, Y.; Radivoy, G. *Acc. Chem. Res*. **2015**, *4*, 2516-2528.

Alvarez, R.; Velazquez, S.; San-Felix, A.; Aquaro, S.; De Clercq, E.; Perno, C.-F.; Karlsson, A.; Balzarini, J.; Camarasa, M. J. *J. Med. Chem*. **1994**, *37*, 4185-4194.

Aslan, E.; Patir, I. H.; Ersoz, M. *Chem. Eur. J.* **2015***, 21*, 4585-4589.

Araya, M.; Olivares, M.; Pizarro, F.; Llanos, A.; Figueroa, G.; Uauy, R. *Environ. Health Perspect.* **2004**, *112*, 1068-1073.

Bandari, R.; Höche, T.; Prager, A.; Dirnberger, K.; Buchmeiser, M. R. *Chem. Eur. J.* **2010**, *16*, 4650-4658.

Buckle, D. R.; Rockell, C. J. M.; Smith, H.; Spicer, B. A. *J. Med. Chem*. **1986**, *29*, 2262-2267.

Campelo, J. M.; Luna, D.; Luque, R.; Marinas, J. M.; Romero, A. A. *ChemSusChem* **2009***, 2*, 18-45.

Canning, P. S. J.; Maskill, H.; McCrudden, K. Sexton, B. *Bull. Chem. Soc. Jpn*. **2002**, *75*, 789-800.

Chahdoura, F.; Pradel, C.; Gómez, M. *ChemCatChem* **2014**, *6*, 2929-2936.

Chamoulaud, G.; Bélanger, D. *J. Phys. Chem. C* **2007***, 111,* 7501-7507.

Chanda, K.; Rej, S.; Huang, M. H. *Chem. Eur. J.* **2013***, 19*, 16036-16043.

Chassaing, S.; Sido, A. S. S.; Alix, A.; Kumarraja, M.; Pale, P.; Sommer, J. *Chem. Eur. J.* **2008**, *14*, 6713-6721.

Chaudhary, P. M. Chavan, S. R.; Shirazi, F.; Razdan, M.; Nimkar, P.; Maybhate, S. P.; Likhite, A. P.; Gonnade, R.; Hazara, B. G.; Deshpande, M. V.; Deshpande, S. R. *Bioorg. Med. Chem*. **2009**, *17*, 2433-2440.

Chen, S.; Sommers, J. M. *J. Phys. Chem. B* **2001,** *105,* 8816-8820.

Chen, B.; Li, F.; Huang, Z.; Xue, F.; Lu, T.; Yuan, Y.; Yuan, G. *ChemCatChem* **2012**, *4*, 1741-1745.

Chen, X.; Chockalingam, M.; Liu, G.; Luais, E.; Gui, A. L. Gooding, J. J. *Electroanalysis* **2011**, *23*, 2633-2642.

Choi, H. R.; Woo, H.; Jang, S.; Cheon, J. Y.; Kim, C.; Park, J.; Park, K. H.; Joo, S. H. *ChemCatChem* **2012**, *4*, 1587-1594.

Chtchigrovsky, M.; Primo, A.; Gonzalez, P.; Molvinger, K.; Robitzer, M.; Quignard, F.; Taran, F. Angew. *Chem. Int. Ed.* **2009**, *48*, 5916-5920.

Crisponi, G.; Nurchi, V. M.; Fanni, D.; Gerosa, C.; Nemolato, S.; Faa, G. *Coord. Chem. Rev.* **2010**, *254*, 876-889.

Das, D. *ChemistrySelect* **2016**, *1*, 1959-1980.

Dell'Amico, D. B.; Bertagnolli, H.; Calderazzo, F.; D'Arienzo, M.; Gross, S.; Labella, L.; Rancan, M.; Scotti, R.; Smarsly, B. M.; Supplit, R.; Tondello, E.; Wendel. E. *Chem. Eur. J.* **2009**, *15*, 4931-4943.

Deraedt, C.; Pinaud, N.; Astruc, D. *J. Am. Chem. Soc.* **2014**, *136*, 12092-12098.

Dubale, A. A.; Su, W.-N.; Tamirat, A. G.; Pan, C.-J.; Aragaw, B. A.; Chen, H.-M.; Chen, C.-H.; Hwang, B.-J. *J. Mater. Chem. A* **2014**, *2*, 18383-18397.

Fahrenbach, A. C.; Stoddart, J. F. *Chem. Asian J.* **2011**, *6*, 2660-2669.

Gawande, M. B.; Goswami, A.; Felpin, F.-X.; Asefa, T.; Huang, X.; Silva, R.; Zou, X.; Zboril, R.; Varma, R. S. *Chem. Rev.* **2016**, *116*, 3722-3811.

Ghosh, D.; Chen, S. *J. Mater. Chem*. **2008**, *18*, 755-762.

Guerrero, S.; Martínez-García, G.; Serafín, V.; Agüí, L.; Yáñez-Sedeño, P.; Pingarrón, J. M. *Analyst* **2015**, *140*, 7527-7533.

Guo, X.; Hao, C.; Jin, G.; Zhu, H.-Y.; Guo, X.-Y. *Angew. Chem. Int. Ed.* **2014**, *53*, 1973-1977.

Hein, C. D.; Liu, X.-M.; Wang, D. *Pharm Res.* **2008**, *25*, 2216-2230.

Hua, Y.; Flood, A. H. *Chem. Soc. Rev*. **2010**, *39*, 1262-1271.

Huisgen, R.; Szeimies, G.; Moebius, L. *Chem. Ber.* **1965**, *98*, 4014-4021.

Hurley, B. L.; McCreery, R. R. *J. Electrochem. Soc.* **2004**, *151*, B252-B259.

Iha, R. K.; Wooley, K. L.; Nystrom, M.; Burke, D. J.; Kade, M. J.; Hawker, C. J. *Chem. Rev*. **2009**, *109*, 5620-5686.

Jiang, D.; Sumpter, B. G.; Dai, S. *J. Am. Chem. Soc*. **2006**, *128*, 6030-6031.

Jin, T.; Yan, M.; Yamamoto, Y. *ChemCatChem*, **2012**, *4*, 1217-1229.

Jlalia, I.; Elamari, H.; Meganem, F.; Herscovici, J.; Girard, C. *Tetrahedron Lett*. **2008**, *49*, 6756-6758.

Johnson, J. A.; Finn, M. G.; Koberstein, J. T.; Turro, N. J. *Macromol. Rapid Commun*. **2008**, *29*, 1052-1072.

Kaur, R.; Giordano, C.; Gradzielski, M.; Mehta, S. K. *Chem. Asian J.* **2014**, 9, 189-198.

Kempe, K.; Krieg, A.; Becer, C. R.; Schubert, U. S. *Chem. Soc. Rev*. **2012**, *41*, 176-191.

Kolb, H. C.; Finn, M. G.; Sharpless, K. B. *Angew. Chem. Int. Ed*. **2001**, *40*, 2004-2021.

Kumar, V. K. R.; Gopidas, K. R. *Chem. Asian J.* **2010**, *5*, 887-896.

Kumar, V. K. R.; Gopidas, K. R. *Tetrahedron Lett.* **2011**, *52*, 3102-3105.

Kumar, V. K. R.; Krishnakumar, S.; Gopidas, K. R. *Eur. J. Org. Chem.* **2012**, 3447-3458.

Lamblin, M.; Nassar-Hardy, L.; Hierso, J.-C.; Fouquet, E.; Felpin, F.-X. *Adv. Synth. Catal.* **2010***, 352*, 33-79.

Lee, C.-T.; Huang, S.; Lipshutz, B. H. *Adv. Synth. Catal.* **2009**, *351*, 3139-3142.

Lewis, D. J. ; Day, T. M.; MacPherson, J. V.; Pikramenou, Z. *Chem. Commun.* **2006**, 1433-1435.

Li, P.; Wang, L.; Zhang, Y. *Tetrahedron* **2008***, 64*, 10825-10830.

Lin, J.-H.; Guliants, V. V. *ChemCatChem* **2012**, *4*, 1611-1621.

Liu, G.; Bçcking, T.; Gooding, J. J. *J. Electroanal. Chem.* **2007***, 600*, 335-344.

Lipshutz, B. H.; Taft, B. R. *Angew. Chem. Int. Ed.* **2006**, *45*, 8235-8238.

Luna, I. Z.; Chowdhury, S.; Gafur, M. A.; Khan, N.; Khan, R. A. *J. Chem. Eng. Chem. Res.* **2015**, *2*, 607-615.

Mandal, B. H.; Rahman, M. L.; Rahim, M. H. A.; Sarkar, S. M. *ChemistrySelect* **2016**, *1*, 2750-2756.

Meldal, M.; Tornøe, C. W. *Chem. Rev.* **2008,** *108,* 2952-3015.

Molnàr, À. *Chem. Rev.* **2011***, 111*, 2251-2320.

Moses, J. E. Moorhouse, A. D. *Chem. Soc. Rev.* **2007**, *36*, 1249-1262.

Mirkhalaf, F.; Paprotny, J.; Schiffrin, D. *J. Am. Chem. Soc.* **2006**, *128*, 7400-7401.

Nia, A. S.; Rana, S.; Döhler, D.; Jirsa, F.; Meister, A.; Guadagno, L.; Koslowski, E.; Bron, M.; Binder, W. H. *Chem. Eur. J.* **2015***, 21*, 10763-10770.

O'Neill, B. J.; Jackson, D. H. K.; Crisci, A. J.; Farberow, C. A.; Shi, F.; Alba-Rubio, A. C.; Lu, J.; Dietrich, P. J.; Gu, X.; Marshall, C. L.; Stair, P. C.; Elam, J. W.; Miller, J. T.; Ribeiro, F. H.; Voyles, P. M.; Greeley, J.; Mavrikakis, M.; Scott, S. L.; Kuech, T. F.; Dumesic, J. A. *Angew. Chem. Int. Ed.* **2013***, 52*, 13808-13812.

Pagliaro, M.; Pandarus, V.; Ciriminna, R.; Béland, F.; Carà, P. D. *ChemCatChem* **2012***, 4*, 432-445.

Pascanu, V.; Yao, Q.; GÓmez, A. B.; Gustafsson, M.; Yun, Y.; Wan, W.; Samain, L.; Zou, X.; Martín-Matute, B. *Chem. Eur. J.* **2013***, 19*, 17483-17493.

Pérez, J. M.; Crosbie, P.; Lal, S. Díez-González, S. *ChemCatChem* **2016**, *8*, 2222-2226.

Pinson, J.; Podvorica, F. *Chem. Soc. Rev.* **2005**, *34*, 429-439.

Popova, M.; Ristić, A.; Mazaj, M.; Maučec, D.; Dimitrov, M.; Tušar, N. N. *ChemCatChem* **2014**, *6*, 271-277.

Prakash, T. *Adv. Mat. Lett .***2011**, *2*,131-135.

Qiu, Z.; Yu, J.; Yan, P.; Wang, Z.; Wan, Q.; Yang, N. *ACS Appl. Mater. Interfaces* **2016***, 8*, 28291-28298.

Reck, F.; Zhou, F.; Girardot, M.; Kern, G.; Eyermann, C. J.; Hales, N. J.; Ramsay, R. R.; Gravestock, M. B. *J. Med. Chem.* **2005**, *48*, 499-506.

Rodionov, V. O.; Fokin, V. V.; Finn, M. G. *Angew. Chem .Int. Ed.* **2005**, *44*, 2210-2215.

Salisbury, C. M.; Cravatt, B. F. *QSAR Comb. Sci.* **2007**, *26*, 1229-1238.

Samim, M.; Kaushik, N. K.; Maitra, A. *Bull. Mater. Sci.* **2007**, *30,* 535-540.

Sanghamitra, N. J.; Phatak, P.; Das, S.; Samuelson, A. G.; Somasundaram, K. *J. Med. Chem.* **2005,** *48,* 977-985.

Schiemann, G.; Winkelmüller, W. *Organic Syntheses, Coll. Vol. 2* (Eds.: W. W. Hartman, J. R. Byers, J. B. Dickey), **1943**, pp. 188.

Sharghi, H.; Khalifeh R.; Doroodmand, M. M. *Adv. Synth. Catal.* **2009**, *351*, 207-218.

Shimura, T.; Aramaki, A. *Corros. Sci.* **2006***, 48*, 3784-3801.

Soltis, M. J.; Yeh, H. J.; Cole, K. A.; Whittaker, N.; Wersto, R. P.; Kohn, E. C. *Drug Metab. Dispos.* **1996**, *24*, 799-806.

Sreedhar, B.; Radhika, P.; Neelima, B.; Hebalkar, N. *Chem. Asian J.* **2008**, 3, 1163-1169.

Subramanian, T.; Pitchumani, K. *ChemCatChem* **2012**, *4*, 1917-1921.

Tamaekong, N.; Liewhiran, C.; Phanichphant, S. *J. Nanomater.* **2014**, *Article* ID 507978, 5 pages.

Upare, P. P.; Hwang, Y. K.; Lee, J.-M.; Hwang, D. W.; Chang, J.-S. *ChemSusChem* **2015***, 8*, 2345-2357.

Vukojević, S.; Trapp, O.; Grunwaldt, J.-D.; Kiener, C.; Schüth, F. *Angew. Chem. Int. Ed.* **2005**, *44*, 7978-7981.

Wang, S.; Huang, X.; He, Y.; Huang, H.; Wu, Y.; Hou, L.; Liu, X.; Yang, T.; Zou, J.; Huang, B. *Carbon* **2012**, *50*, 2119-2125.

Wang, C.; Huang, N.; Zhuang, H. Jiang, X. *ACS Appl. Mater. Interfaces* **2015**, *7*, 7605-7612.

Wang, C.; Wang, Do.; Yu, S.; Cornilleau, T.; Ruiz, J.; Salmon, L.; Astruc, D. *ACS Catal.* **2016**, *6*, 5424-5431.

Wang, C.; Ikhlef, D.; Kahlal, S.; Saillard, J.-Y.; Astruc, D. *Coord. Chem. Rev.* **2016**, *316*, 1-20.

Wojcieszak, R.; Gaigneaux, E. M.; Ruiz, P. *ChemCatChem* **2013***, 5*, 339-348.

Xia, Y. Fan, Z.; Yao, J.; Liao, Q.; Li, W.; Qu, F.; Peng, L. *Bioorg. Med. Chem. Lett.* **2006**, *16*, 2693-2698.

Yang, D.-Q.; Sacher, E. *Surf. Sci.* **2002**, 504, 125-137.

Yinghuai, Z.; Peng, S. C.; Emi, A.; Zhenshun, S.; Monalisa, Z.; Kempd, R. A. *Adv. Synth. Catal.* **2007***, 349*, 1917-1922.

Zhang, H.; Cao, J.-L.; Shao, G.-S.; Yuan, Z.-Y. *J. Mater. Chem.* **2009**, *19*, 6097-6099.

Synthesis, Functionalization, Characterization and Energy Applications of Nanographite Materials

4.1 Abstract

Reduction of 4,4'-Biphenylene-bisdiazonium tetrafluoroborate resulted in the formation of 4,4'-biphenylene biradicals which underwent rapid addition reactions to give a cross linked, planar aromatic framework. Scholl oxidation of the aromatic framework led to the formation of graphitic materials. The graphitic material was functionalized by sulfonation reaction. Primary characterizations as well as morphological studies of these materials were undertaken. Several experimental techniques were employed to probe the structures of these materials. These materials were evaluated for their performance as electrode materials in electric double layer capacitors. Capacitance value of 45.5 F g^{-1} was obtained for the sodium salt of sulfonated graphene in 3 electrode configuration.

4.2 Introduction

The field of graphene-related research has grown at a remarkable pace after publication of the paper titled "groundbreaking experiments regarding the two dimensional material, graphene" by Geim and Novoselov" in 2004 (Novoselov 2004). This exciting material for fundamental physics has now become the focus of efforts by scientists in various disciplines. Organic and material chemists are focusing on the production of high-quality single layer graphenes. Engineers are engaged in the development of devices to utilize its astonishing properties. One of the interesting aspects of graphene research is that depending upon the method of production the properties of these materials change drastically. Hence their potential for different applications will also change accordingly. The uncontrollable character of the various bottom-up and top-down approaches for graphene synthesis will restrict the quality of the resulting graphenes. The harsh reaction conditions reported for some graphene systems also is a drawback. Graphene nanoribbons produced by few organic synthetic protocols have recently received attention because they are

recognized as promising building blocks for nanoelectronic and spintronic devices in the carbon family.

The research towards bottom-up synthesis of graphene started long before the path breaking finding by Geim and Novoselov in 2004. In the early days molecules known as polycyclic aromatic hydrocarbons (PAH) were considered as two-dimensional graphite fragments (Clar 1953; Faust 1996). The research in PAH started along with their discovery in coal tar in the middle of the last century (Clar 1953). Even before the synthetic developments of PAH took place, theoreticians were fascinated by the different topologies of the simple and easily computable C6 rings in the PAH (Herndon 1990; Stein 1987; Dias 1987; 1991; 1993; Bredas 1985; Zander 1990). The graphene-like PAHs occupy an interesting place in between "molecular" and "macromolecular" structures and these are now attracting new interest as possible alternate routes towards graphene synthesis.

PAH are a class of compounds having at least three unsubstituted fused benzene rings (A Guide to IUPAC Nomenclature of Organic Compounds, 1997). PAH in the size range of 1-5 nm is defined by using the term 'graphene molecule' (Zhi 2008). PAH fragments having size between the range 1-100 nm are considered as 'nanographenes' (Zhi 2008). If the size of hexagonal sp^2 carbon network exceeds 100 nm they are regarded as graphene (Zhi 2008). Organic chemists have developed several methods for the synthesis of graphene molecules as well as nanographenes. Organic synthesis of graphene, however, still remain as a major challenge. In this chapter we tried to develop a new protocol for the synthesis of graphene sheets. Before discussing our results the present state of affairs in this area are summarized in the following section.

In first half of 20th century the direct synthesis of PAHs and their characterization were mainly due to the pioneering works of Scholl (Scholl 1910; 1912; 1922[a,b]) and Clar (Clar 1953; 1960; 1966; 1968; 1969; 1970; 1972 [a,b,c,d,]; 1974; 1979). In strongly oxidizing reaction melts and under drastic conditions these scientists prepared several PAHs. However, major breakthroughs occurred only in the last two decades (Müller 1995; 1996; 1997; 1998; Stabel 1995; Herwig 1996; Morgenroth 1997 [a,b,c,d]; 1998; Iyer 1997; van de Craats 1998). Although several groups contributed towards the organic synthesis of graphene type molecules, the

most outstanding contributions were made by Müllen and co-workers (Scott 2004; Tahara, 2006; Wu, 2007; Lambert 2005). Nanoribbon-like PAHs with size up to 12 nm in length having graphene-like behavior reported by Müllen and coworkers in 2008 is considered as a significant achievement in this area (Yang 2008). However, step-wise synthesis of graphene sheets still remains as a challenging task.

Several methods were available for the synthesis of well-defined PAHs (Müller 1998) and benzene-based macromolecules (Tyutyulkov 1998; Berresheim 1999; Dotz 2000; Watson 2001; Gutman 2004). Synthesis of large PAHs mainly involve two stages. The first stage involves the preparation of dendritic oligophenylene precursors with preferable sizes and shapes. The second stage involves intramolecular cyclodehydrogenation and planarization of the resulting precursors. Diels-Alder reaction (Dilthey 1934) or cyclotrimerization of suitable acetylene building blocks (Vollhardt 1970) are the mainly used reactions in the first stage. The most widely used reactions for the second cyclodehydrogenation stage are the Scholl (Balaban 1964) and Kovacic-type (Kovacic 1987) reactions. In these reactions Lewis acid-oxidant combinations are used as reagents. Wide application of this protocol for the preparation of PAHs started after the successful synthesis of hexa-*peri*-hexabenzocoronene (HBC) by Clar and co-workers (Clar 1958; 1959) (Scheme 4.1). Their strategy involved the bromination of 8H-benzo[fg]tetracene **1** followed by heating at 153 °C to prepare tetrabenzoperopyrene **2**. Cyclodehydrogenation of **2** by heating up to 481 °C gave the HBC **3**.
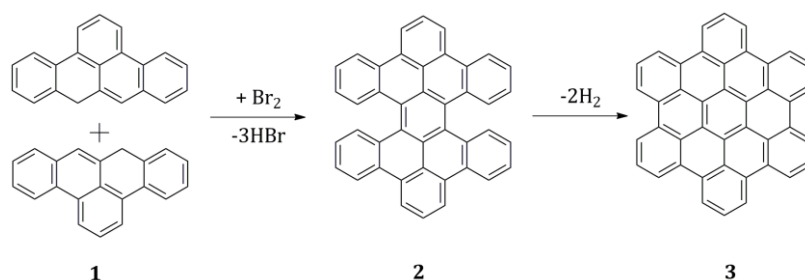
Scheme 4.1 Clar's route to HBC.

Later Halleux and co-workers achieved a major breakthrough by using molten AlCl₃/NaCl for cyclodehydrogenation of hexaphenylbenzene **4** (Halleux 1958) to **3** (Scheme 4.2). In 1986 a new method for the synthesis of **3** was reported

by Schmidt and co-workers (Hendel 1986). They have prepared HBC starting from quinone **5** as shown in Scheme 4.3. Initially AlCl₃/NaCl melt was used for cyclization of the diol **6** followed by the aromatization with Cu at 400 °C.

Scheme 4.2 Halleux's route to HBC.

Scheme 4.3 Schmidt's route to HBC.

      The harsh experimental procedures mentioned above and the poor yields obtained in these reactions were overcome by Müllen and co-workers who used Scholl type oxidative cyclodehydrogenation of hexaphenylbenzenes and branched oligophenylenes to prepare HBC and related PAH structures in high yields. They have used Cu(II) salts such as $CuCl_2$ and $Cu(OTf)_2$ catalyzed by $AlCl_3$ (Müller 1998) for the Scholl oxidation. The method used for the preparation of suitable hexaphenylbenzenes (Hyatt 1991) are the $Co_2(CO)_8$ catalyzed cyclotrimerization of diphenylacetylenes (Scheme 4.4). They have successfully prepared the six fold symmetric alkyl- (Herwig 1996), alkylphenyl- (Fechtenkötter 1999), and alkylester-substituted and parent HBCs (Kübel 2000) in high yields using this method. They observed that permethoxylated HBC (Wang 2005) behaves as a nonplanar graphene molecule due to the steric hinderence between the methoxy substituents. To

prepare substituents carrying lower symmetric HBCs Diels-Alder cycloadditions between tetraphenylcyclopentadienone and diphenylacetylene were used in the first stage to get the suitable precursor (Ito 2000; Fechtenkötter 2001). Flexible means for the production of functional HBCs were open up by using the insoluble iodine atom containing building blocks. Although the solubility is low for these derivatives, they exhibited high reactivity in Pd-catalyzed cross coupling reactions (Wu 2004; Wu 2003; 2004; 2006; Lee 2002). Recently large-scale preparation (>80% yield) of HBC was achieved through photocyclization of bisolefins by Xiao et al. (Xiao 2005).
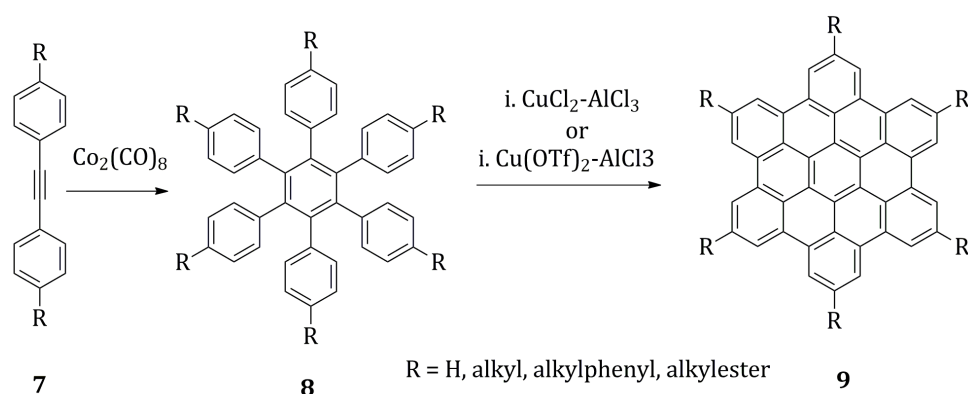
Scheme 4.4 Müller's route for six fold symmetric HBCs.

Synthesis of giant graphene molecules were attempted by extending the methodologies developed for HBC synthesis (Debije 2004). Müllen and co-workers employed Diels- Alder reactions to synthesize alkyl chain substituted as well as non-substituted oligophenylenes followed by oxidative cyclodehydrogenation to prepare PAHs larger than HBC. They synthesized PAHs containing 90 (**10**) (Wu 2004), 96 (**11**) (Tomović 2004), 132 (**12**) (Simpson 2003), 150 (**13**) (Wu 2004) and 222 (**14**) (Simpson 2002) carbon atoms in the cores and with various substituents (Figure 4.1). Among these the giant graphite disc **14** is the largest molecule characterized till to date (Simpson 2002).

By connecting HBC oligomers or their corresponding polymers it was possible to produce a series of well-defined graphene ribbon structures through multistep procedures by extending the length in one dimension (Kübel 2000; Iyer 1997; 1998; Müller 1997; Wasserfallen 2006; Wu 2004; Dötz 2000; Wang 2004;
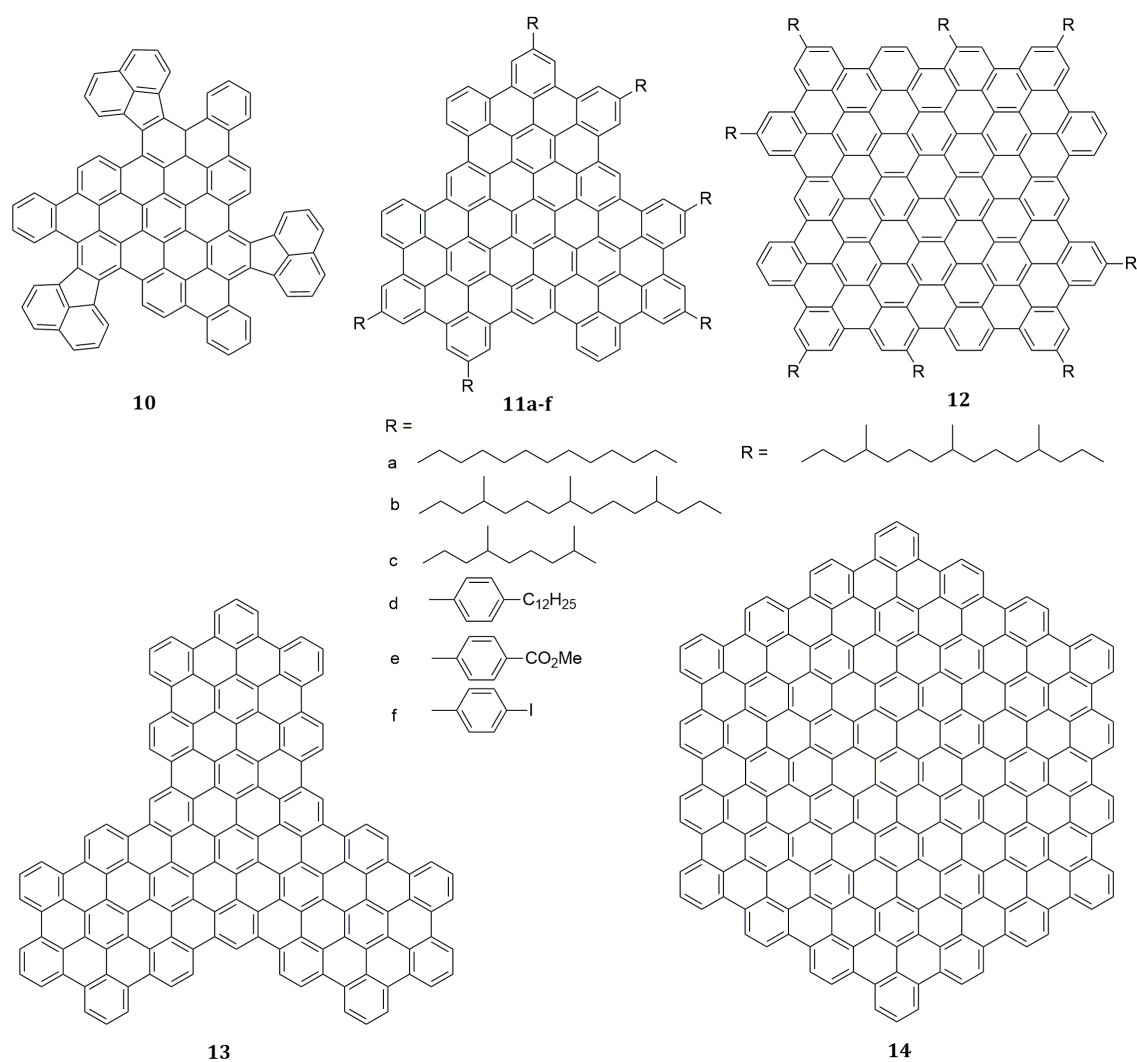
Figure 4.1 Large graphene molecules.

Kastler 2006)**.** The two dimensional extension of graphene molecules into large sheets is still remaining as a great challenge as evident from the studies on planarization of a C474 oligophenylene dendrimer, which resulted in partially closed three-dimensional (3D) graphite propeller (Scheme 4.5). This study showed that, after reaching a certain limit oxidative cyclodehydrogenation takes place only partially (Simpson 2004).

A major factor that controls the size and quality of the graphene material is the way in which the parent oligophenylenes are prepared. With increase in size synthesis of the required oligophenylene precursor becomes difficult due to lack of solubility. Secondly, as the number of linkages between the adjacent phenyl rings decrease, planarity of the precursor will also decrease. Hence geometry will became

unfavorable so that final cyclodehydrogenation reactions will only lead to partially fused compounds (Wu 2003; 2004; Feng 2006).
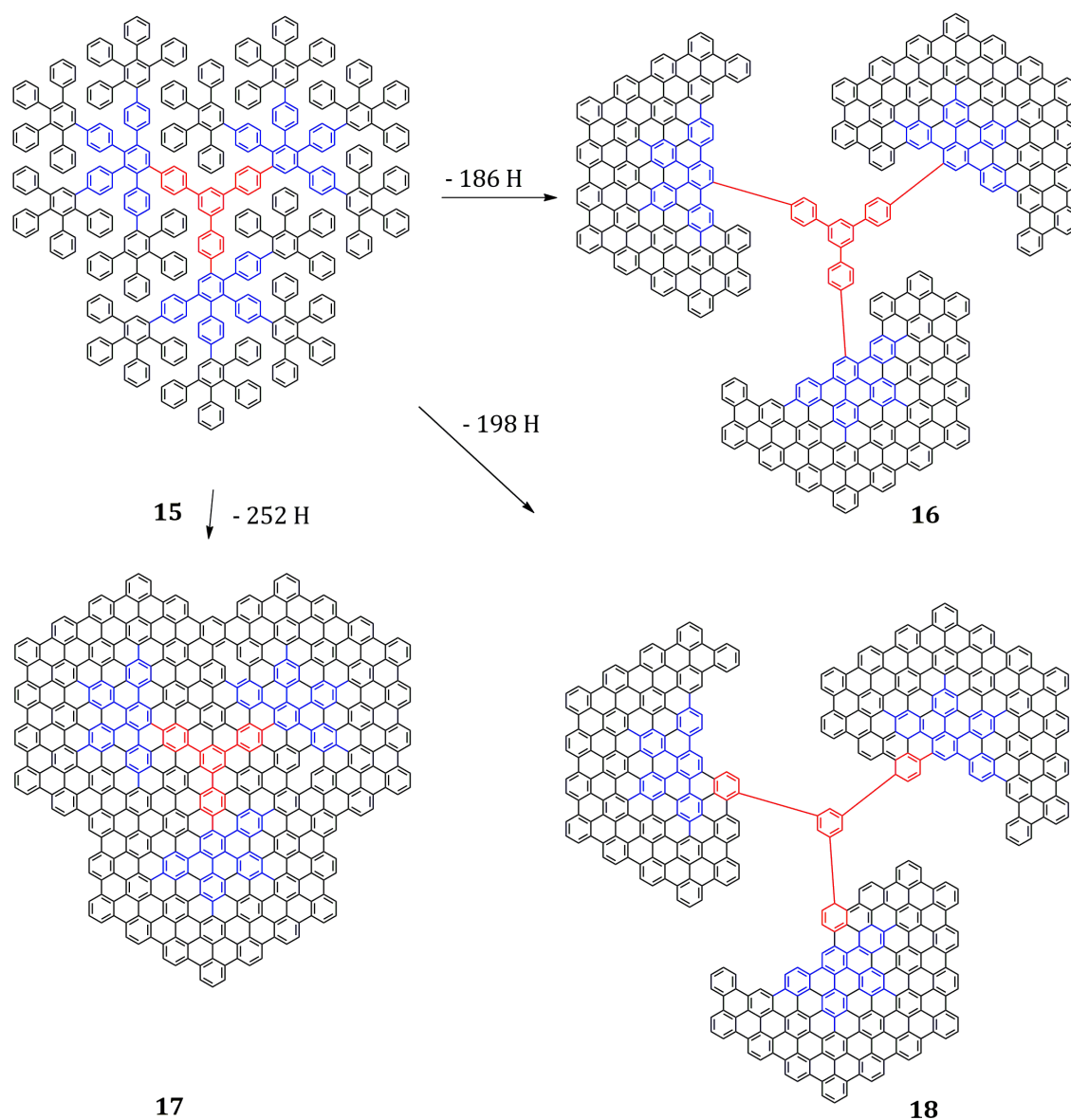
Scheme 4.5 Results of Simpson's route for the planarization of a C474 oligophenylene dendrimer.

The cyclodehydrogenation step is also affected by various factors. Theoretical studies have been performed to understand the mechanism of intramolecular Scholl reactions (Rempala 2004; Stefano 2005). But still very little is known about it. Isolation of partially ring-closed intermediates in the cyclodehydrogenation of hexaphenylbenzene suggested a step-wise cyclization

mechanism (Kübel 2000). Rempala et al. suggested a stepwise arenium cation mechanism (Rempala 2004) instead of a radical cation mechanism predicted by Stefano et al. (Stefano 2005). The stability and reactivity of the radical cations formed will determine the selectivity of the reaction. Complete cyclodehydrogenation of large oligophenylene precursors need careful control of the experimental conditions such as time, oxidants, and the amount of reagents.

Herein, we report a new protocol for the step-wise bottom-up chemical synthesis of two dimensional graphene materials wherein we have exploited the covalent bond forming capability of aryl radicals generated from diazonium salts. Our strategy involved the reduction of a bisdiazonium salt by $NaBH_4$ (Scheme 4.6). The bisdiazonium salt upon reduction eliminates two nitrogen molecules and forms a highly reactive biradical that undergo random coupling or radical radical addition
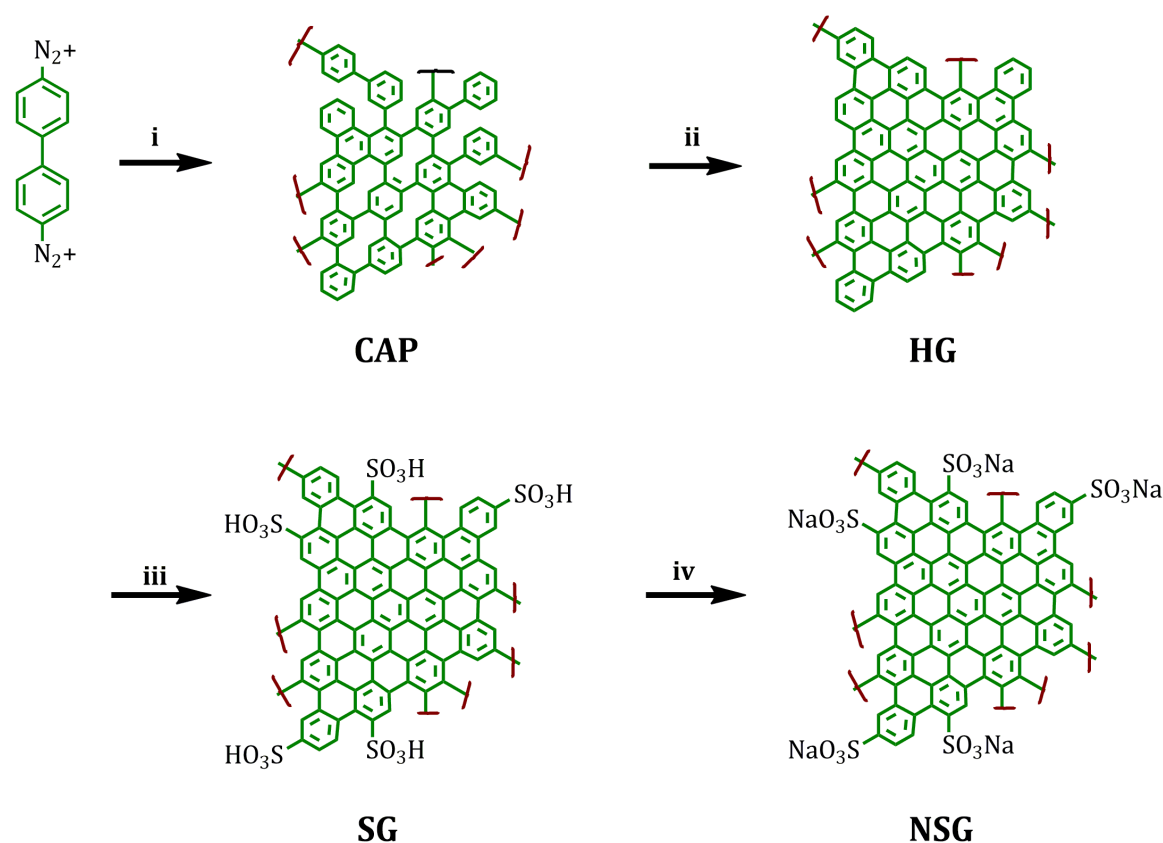
i. (Reduction) H_2O, $NaBH_4$, RT, 24 h.; ii. (Scholl Oxidation) $AlCl_3$, NaCl, 160 °C, 4 h.; iii. (Sulfonation) Oleum, 180 °C, 24 h.; iv. (Neutralisation) H_2O, $NaHCO_3$, RT, 6 h.

Scheme 4.6 Synthesis of CAP, HG, SG and NSG.

reactions leading to the formation of a cross-linked aromatic polymeric (CAP) material. Since radical coupling and radical-radical additions can occur only in the plane of the aromatic rings, the CAP formed will have a planar structure similar to that shown in Scheme 4.5. The CAP was then subjected to Scholl reaction to give giant graphene (HG) molecules. Functionalizations of HG was achieved through sulfonation reaction to give sulfonated graphene (SG), which was converted to the water soluble sodium salt (NSG) (Scheme 4.6). All the materilas (CAP, HG, SG and NSG) were analyzed using different spectroscopic and microscopic techniques. A commercially available multi-layer graphene (CG) was also employed for comparison purpose. The 2D and 3D graphite structures prepared by bottom-up organic synthetic methods showed pronounced "charge storage" applications (Megahead 1994). Hence we have also evaluated the potential of these materials for electrochemical energy storage systems.

4.3 Results and Discussion

4.3.1 Synthesis

Synthesis of the materials were achieved as per Scheme 4.6. CAP was synthesized by the reduction of 1,4-biphenylene-bis-diazonium fluoroborate (BPBDT) (Schiemann 1943) in water by $NaBH_4$. The material was separated by centrifugation and purified by repeated washing with water and 20% HCl followed by drying in vacuum. The CAP was then subjected to Scholl oxidation in 2:1 $AlCl_3$:NaCl melt at 165 °C for 6 h to get HG. The reaction mixture was quenched with water and centrifuged to separate the solid material. Further purification was done by sonicating in 40% HCl, water, acetone and ether, respectively. The material was then dried in a vacuum oven. SG was synthesized from HG by stirring with oleum at 180 °C for 24 h, followed by washing with large amounts of water and separation by centrifugation. The material was then washed with acetone and ether and finally dried at 80 °C under vacuum for 12 h. NSG, the sodium salt of SG, was prepared by treating a suspension of SG in water with $NaHCO_3$ followed by addition of ethanol. The material was collected by centrifugation followed by washing with ethanol, acetone and ether and finally dried under vacuum at 80 °C.

4.3.2 Characterizations

4.3.2.1 TGA Analysis

Thermogravimetric analyses (TGA) and differential thermal analysis (DTA) of CAP, HG, SG, NSG and commercially available graphene (CG) were carried out at a heating rate of 10 °C/min. and the results obtained are presented in Figure 4.2. All the materials were found to exhibit high thermal stability. For CG, decomposition started above 500 °C (Figure 4.2a). DTA of CG showed a peak around 600 °C. Data similar to this were obtained for all the samples except for NSG. The results show that the thermal stabilities of the synthesized materials are similar to that of commercially available graphene. In the case of CAP 100% decomposition occurred around 590 °C. The Scholl reaction product HG exhibited slightly higher stability and decomposed only at 625 °C. This value is closer to the decomposition temperature 640 °C of CG. In the case of CAP the first decomposition (< 5%) was observed around 200 °C. The corresponding peak was observed at 310 °C for CG and HG. The weight reduction observed around 200 °C for CAP is similar to the weight loss observed in standard PAH mixtures and this corresponds to low molecular weight (2-7 ring) PAHs (Guillén 1992, 1995). For HG first decomposition occurred above 300 °C and
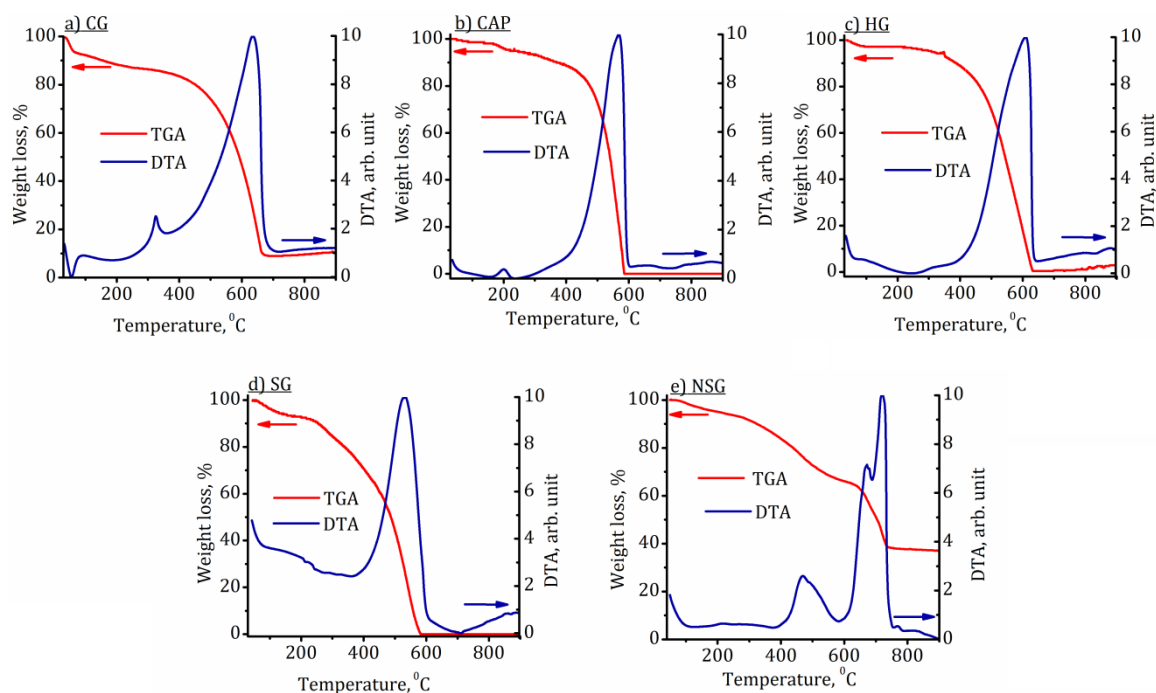
Figure 4.2 TGA (red) and DTA (blue) analysis of the materials.

this most probably would correspond to the loss of relatively heavier species (Gargiulo 2015). In SG about 13% of the material decomposed in the 100 - 250 °C range. This can be attributed to the elimination of SO_3H groups present in the molecule. Further decomposition of the carbon network was observed at 580 °C. Similar results were obtained for NSG also, but in this case nearly 40% material remained even after heating above 800 °C. The residue remaining above 800 °C most probably are compounds of sodium such as Na_2SO_4 or Na_2O, for which decomposition temperatures are above 850 °C.

4.3.2.2 FTIR studies

FTIR spectra of CG, CAP, HG, SG and NSG are shown in Figure 4.3. CG did not exhibit any characteristic feature in its IR spectrum. All other materials exhibited few IR absorptions, but none of them showed the band at 2274 cm^{-1} which is characteristic of the diazo group (Chapter 1), confirming the complete removal of the diazonium group during the reduction reaction. IR absorptions corresponding to C-H (3033 cm^{-1}) and C-C (peaks between 1600 and 1400 cm^{-1}) vibrations were present in CAP. The intensities of these bands were observed to decrease in HG
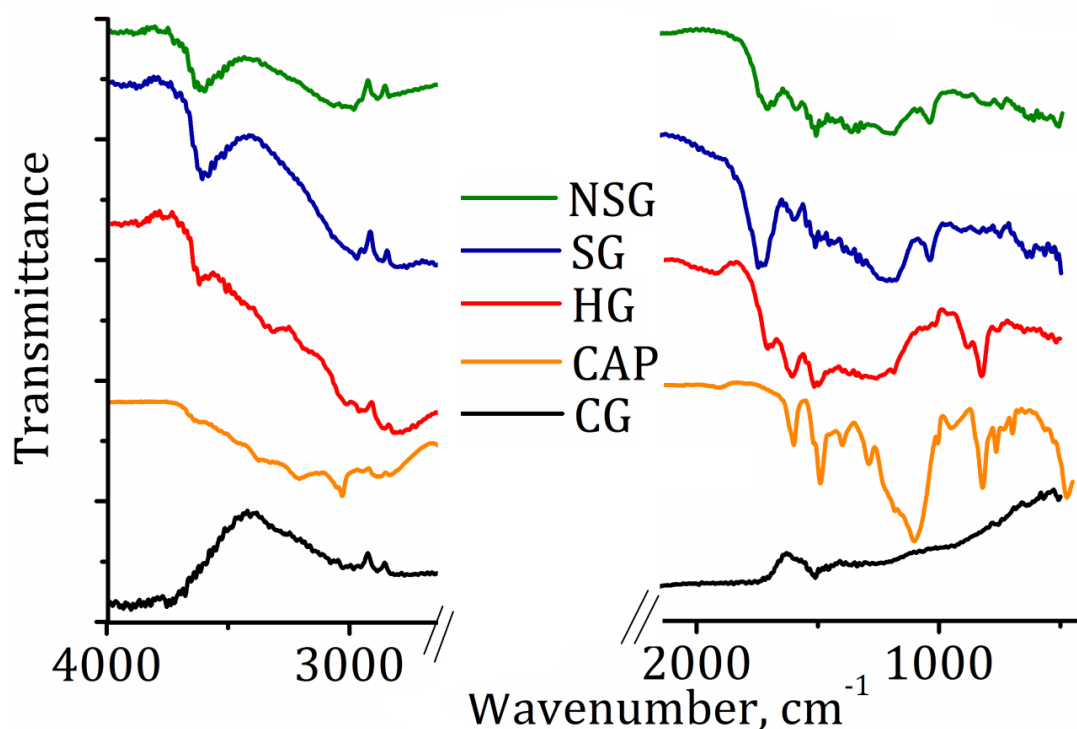
Figure 4.3 IR spectra of CG, CAP, HG, SG and NSG.

suggesting the removal of some of the hydrogen atoms during the Scholl reaction. In the case of SG and NSG the peaks at 1175, 1126, and 1040 cm^{-1} (two νS-O and one νS-phenyl) confirm the presence of a sulfonic acid group (Eigler 2013; Zhou 2014). It may be noted that the peaks observed for CAP at 698, 750, and $\sim$ 3060 cm^{-1} which are characteristic of monosubstituted benzene rings are considerably less intense in HG and almost absent in SG and NSG. This suggested that the number of free phenyl rings have decreased considerblay due to the Scholl reaction.

4.3.2.3 NMR studies

Due to the lack of solubility in organic solvents we employed sonicated suspensions of the materials for obtaining ^{1}H NMR pectra. DMSO-d$_6$ was used as the solvent for CAP, HG and SG and D$_2$O was used for NSG. The results obtained are shown in Figure 4.4. The CAP sample exhibited a very complex NMR pattern in the δ 7–8 ppm range suggesting the presence of aromatic protons. HG, which is the Scholl reaction product of CAP, showed only three weak bands in the aromatic region suggesting the removal of most of the protons in the Scholl reaction. Broadening of the signals suggested that free rotation of the aryl rings responsible for the signals are restricted. This may be attributed to the formation of large extended networks. For SG and NSG no signals could be seen in the ^{1}H NMR spectra. Most probably there are some proton signals which are highly broadened due to lack of free rotation and hence not distinguishable from the baseline.
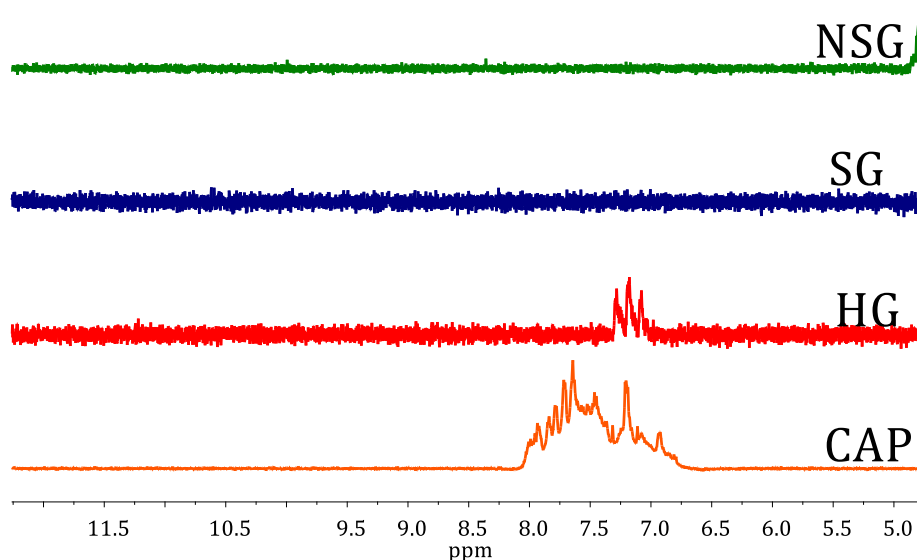
Figure 4.4 NMR spectra of CAP, HG, SG and NSG.

4.3.2.4 Absorption studies

Dispersions of the materials in DMF were sonicated for five minutes, filtered and the resulting clear solutions were subjected to UV-Visible spectroscopy. NSG exhibited some water solubility and hence an aqueous solution was used for UV-visible studies. Absorption specta obtained for these molecules are shown in Figure 4.5. The materials showed progressively increasing absorbance at higher energy. Except for CAP all the materials exhibited absorption above 800 nm. CAP exhibited absorption up to 600 nm with weak shoulders around 350 and 475 nm. Since the absorption onset is only 600 nm we can also conclude that CAP most probably is a polyphenyl substituted PAH. For the HG and CG large residual absorptions could be seen above 800 nm and most probably these have significant contributions from scattering due to the very small particles present in the solution. The sulfonated derivatives SG and NSG exhibited very little absorption above 800 nm. For all these materials absorptions above 800 nm may be due to the presence of fused benzene ring networks.
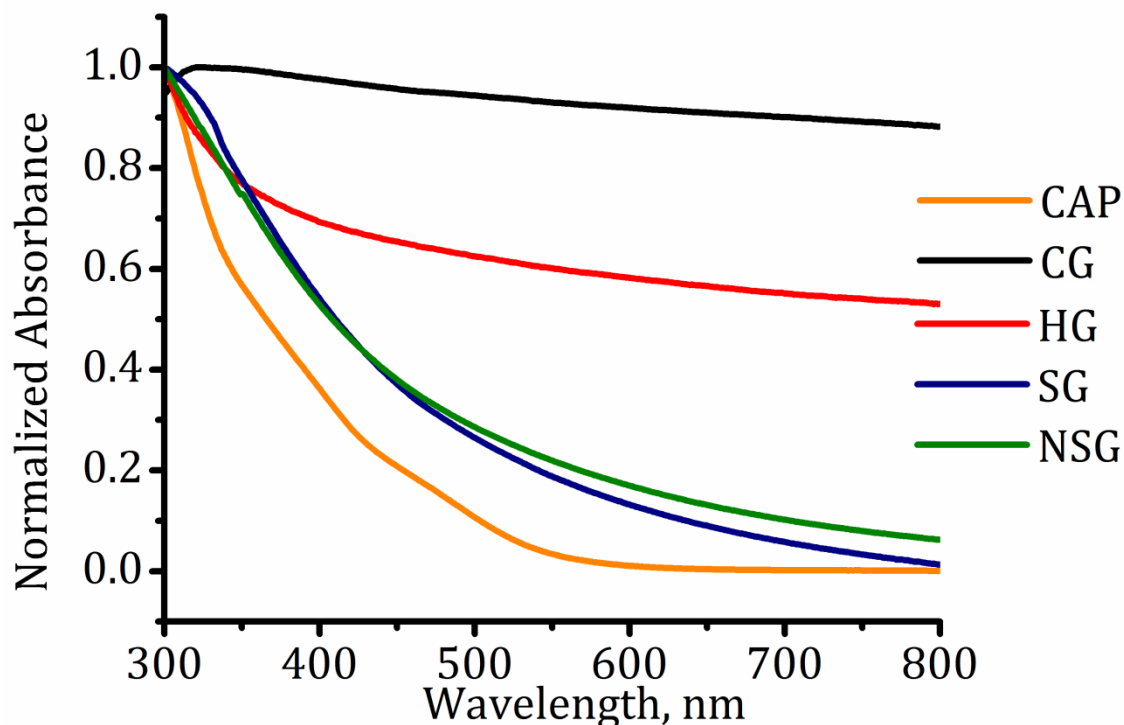
Figure 4.5 Absorption spectra of the graphene materials.

4.3.2.5 XRD analysis

       Powder X-ray diffraction data for the graphene materials are presented in Figure 4.6. The XRD pattern of CG showed a sharp peak at 26.2° corresponding to the reflection from the (002) plane with a 'd' value of 0.34 nm, which is typically observed in graphene based materials. The CAP molecule synthesized exhibited several peaks in the 10 to 50° range which is similar to the XRD pattern exhibited by organic polymers. Most of these peaks disappeared after the Scholl reaction and only the peak corresponding to (002) plane was observed in HG, SG and NSG, suggesting that all these materials contain a graphene network. In the case of HG a broad peak centered at 22.6° was observed with a 'd' value of 0.39 nm. The braod nature of the peak indicates that materials with amorphous nature are also formed during the Scholl reaction. In the case of SG the peak was observed at 24.9° with 'd' value 0.36 nm. In the case of NSG the peak was observed at 26.2° with 'd' value of 0.34 nm. On going from HG to SG to NSG, the peak became sharper along with a decrease in 'd' value suggesting an increase in crystallanity at each stage. This suggested that some of the amorphous and impure non-graphitic carbonacious materials were separated and removed during each reaction step.
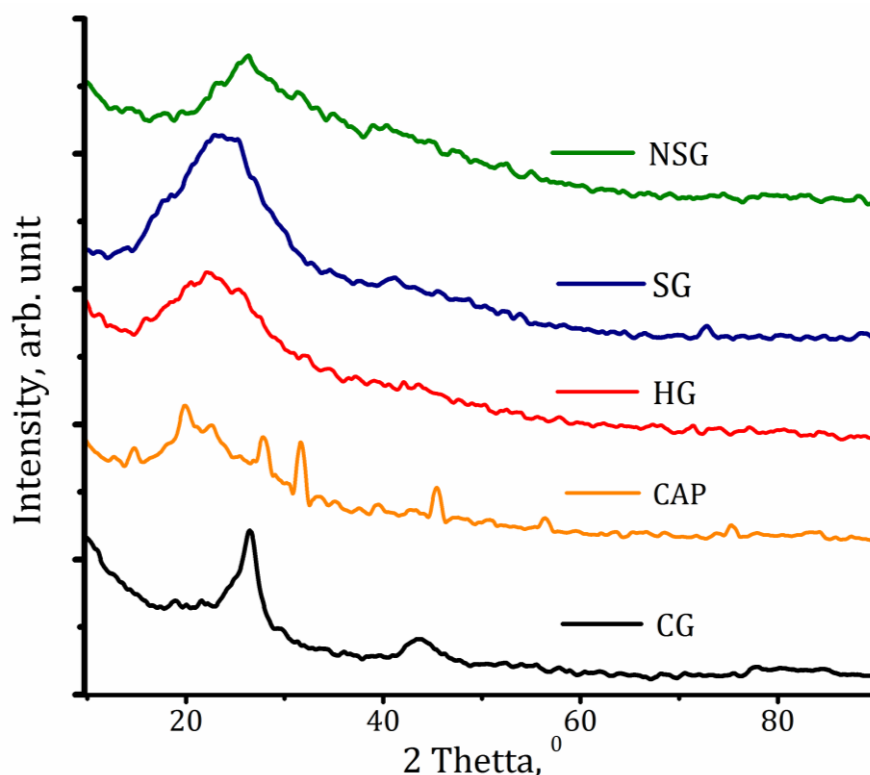
Figure 4.6 XRD patterns for the graphene materials.

4.3.2.7 Raman analysis

Raman spectroscopy is widely used for the identification of ordered and disordered crystal structures of carbon. Carbon materials made up of sp^2 carbon atoms will give two first order bands namely, G band (graphite band) and D band (disorder band). We have carried out Raman analysis of the HG, SG and NSG materials and the spectra obtained are shown in Figure 4.7. All the materilas displayed strong G band at 1580 cm^{-1} and D band at 1350 cm^{-1}. These values are consistant with the reported literature values (Cao 2012). The D band is relatively intense for all three materials. This could be due to the contribution of the edges as defects (Liu 2012). The presence of atoms/groups like H and SO_3 will also contribute to the defects and hence an intense D band is expected in these cases. The presence of defects within the graphene materials can be measured using the ratio between the intensities of the D and G bands (I_D/I_G) (Vinayan 2011). This ratio is foung to be 1.11 for HG, 0.93 for SG and 0.77 for NSG. This corresponds to the crystallite sizes (*La*) of 34.2 nm for HG, 40.8 nm for SG and 49.3 nm for NSG respectively (Cançado 2006). This decrease in the I_D/I_G ratio and increase in *La* value after sulfonation suggests the decrease of surface defects.
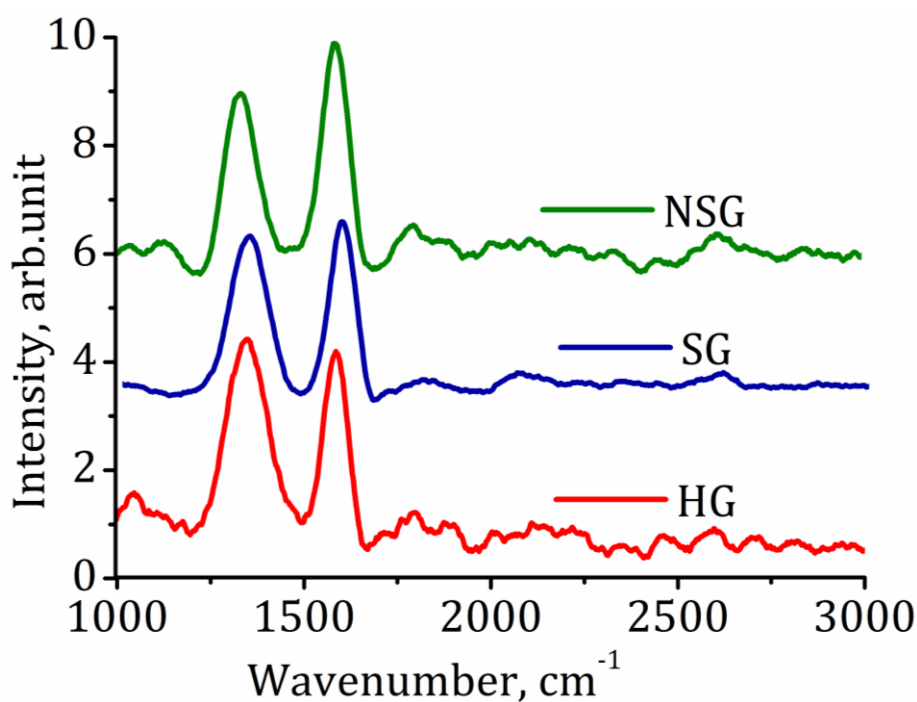
Figure 4.7 Raman spectra of the materials.

For good quality graphene a 2D band appears around 2700 cm^{-1}. In the Raman spectra of HG, SG and NSG this band is very weak or absent. The absence or low intensity of the 2D band can be due to several reasons. Reasonably large graphitic sp^2 crystalline domain is required for the observation of the 2D band. Although we observe plnar sheets of ~2 μm size for some of these materials (in AFM and TEM, vide infra), the actual size of the crystalline graphitic domain may be much less. In fact very weak 2D bands were observed for solar exfoliated graphenes and poly-(diallyldimethylammonium chloride) functionalized graphenes (Vinayan 2012). Most probably some of the phenyl groups present in CAP were not transformed into graphene network and these may be existing as functional groups attached to the graphene core. The low intensity of 2D band can also be due to the low energy of the 633 nm laser source used for the Raman experiment (Zhao 2011; Costa 2012).

4.3.2.8 HRTEM analysis

TEM images of HG material taken at different magnifications are given in Figure 4.8a-i. The HG sheets are transparent and very stable to electron beam exposure. Most of the HG sheets have sizes in the 100 - 500 nm range. We could also observe few large sheets of 2 μm size (Figure 4.8a). The selected area electron diffraction (SAED) of the 2 μm sized graphitic structure is shown in Figure 4.8c. The well-defined diffraction spots confirm the crystalline structure of the HG sheets. Most of the sheets have resemblance to crumpled silk veil waves and these types of corrugated and scrolled nature are intrinsic properties of graphene nanosheets (Meyer 2007). In most cases the edges of the suspended film fold back as seen in Figures 4.8d and 4.8e. Smaller sized graphene sheets exhibited a tendency to form aggragates (Figure 4.8g). Even then lattice planes can be clearly seen in the TEM (Figure 4.8h). On the other hand most of the larger sheets (Figure 4.8d and 4.8e) are poly crystalline (Figure 4.8f). Few mono crystalline large sheets were also observed suggesting loss of crystallinity with increase in size of the sheets.

TEM images of SG are given in Figures 4.9a-d and that of NSG are given in Figures 4.10a-d. These TEM images are similar to images of graphene sheets (Si 2008; Liu 2012). The sheets appeared transparent and folded over at the edges. Few isolated small fragments can also be seen on their surfaces as in Figure 4.9b. These
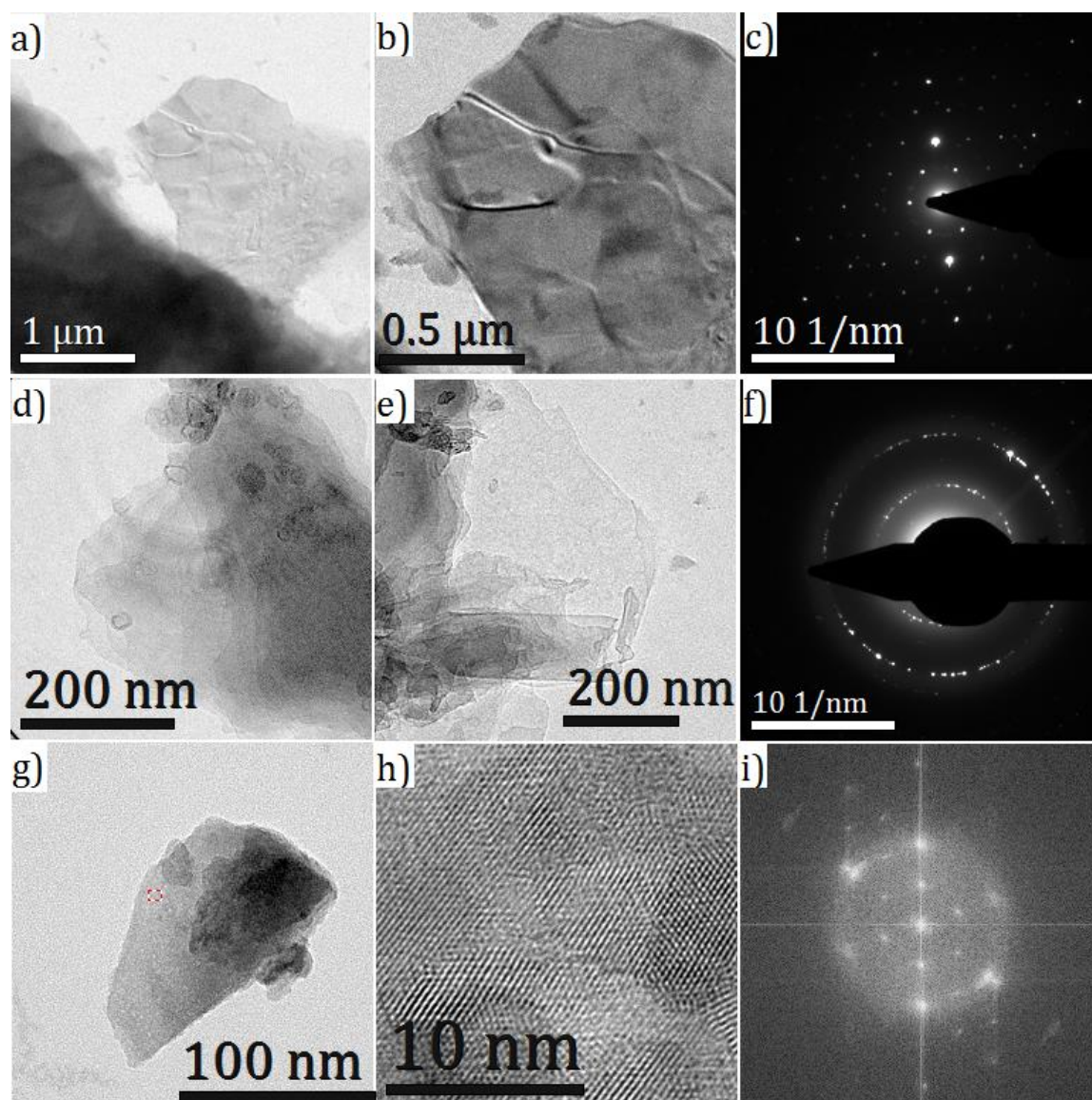
Figure 4.8 (a, b) HRTEM images monocrystalline single layer HG; (c) corresponding SAED pattern; (d, e) HRTEM images of polycrystalline layers of HG; (f) corresponding SAED pattern; (g) HRTEM images of few layer HG; (h) enlarged image of the marked area in g; and (i) reduced FFT image of the few layer HG in h.
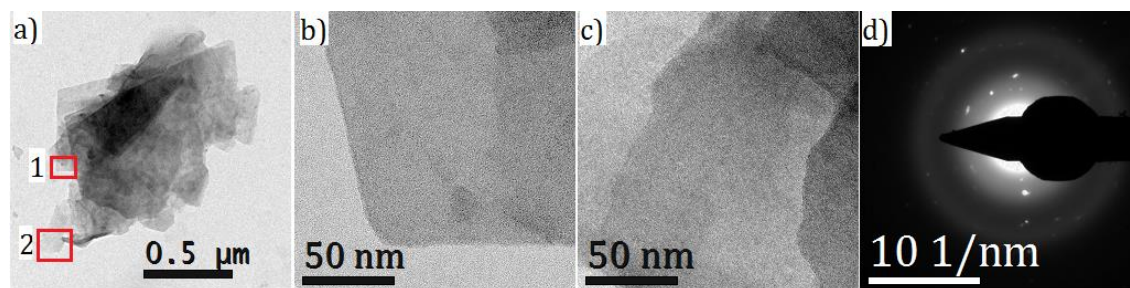
Figure 4.9 (a) HRTEM image of SG; (b) and (c) are enlarged images of marked areas 1 and 2, respectively, in a; (d) SAED pattern.
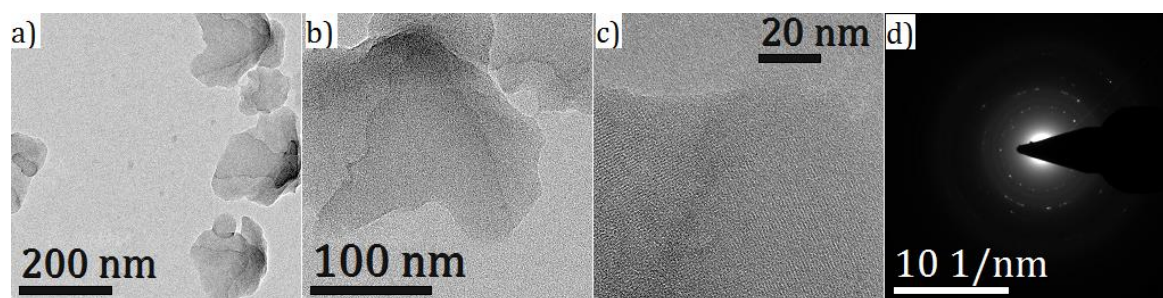
Figure 4.10 (a, b) HRTEM images of NSG, (c) enlarged images showing the lattice planes and (d) corresponding SAED pattern.

observations indicate that the sulfonated graphene materials SG and NSG are similar to graphene sheets obtained by peeling of HOPG (Qian 2010). SAED patterns (Figure 4.9d and figure 4.10d) indicate that both SG and NSG sheets are poly crystalline as no ordered patterns are seen. This crystalline pattern suggests that the sulfonated groups are attached without affecting the microstructure of the graphene sheets (Yuan 2012).

4.3.2.9 AFM analysis

The AFM images obtained for HG are shown in the Figure 4.11. Most of the particles have size below 100 nm, but few large particles (400-600 nm) were also
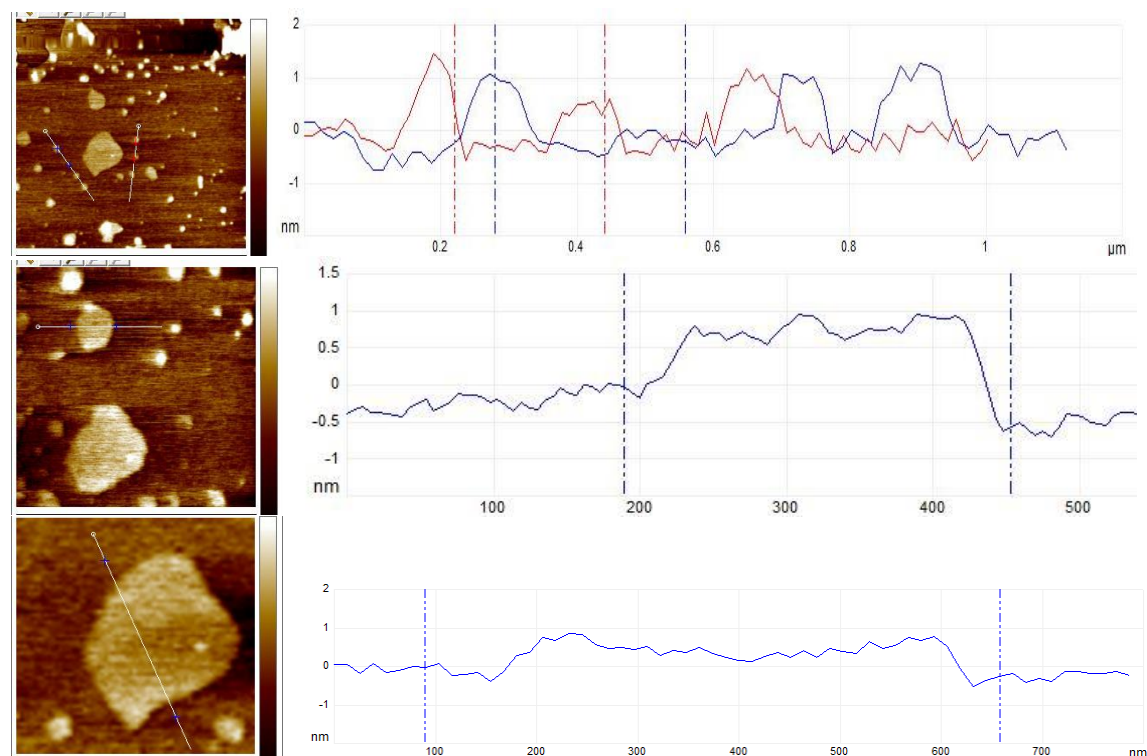
Figure 4.11 AFM images of HG

seen in the AFM. For all these particles the heights were found to be slightly below 1 nm, suggesting that these are single layer sheets.

AFM images of SG revealed that these materials have a high tendency for aggragation. The AFM images (Figure 4.12) showed that the sheets are stacked in an irregular manner. The height profile showed the presence of single layer as well as few layer thick sheets.
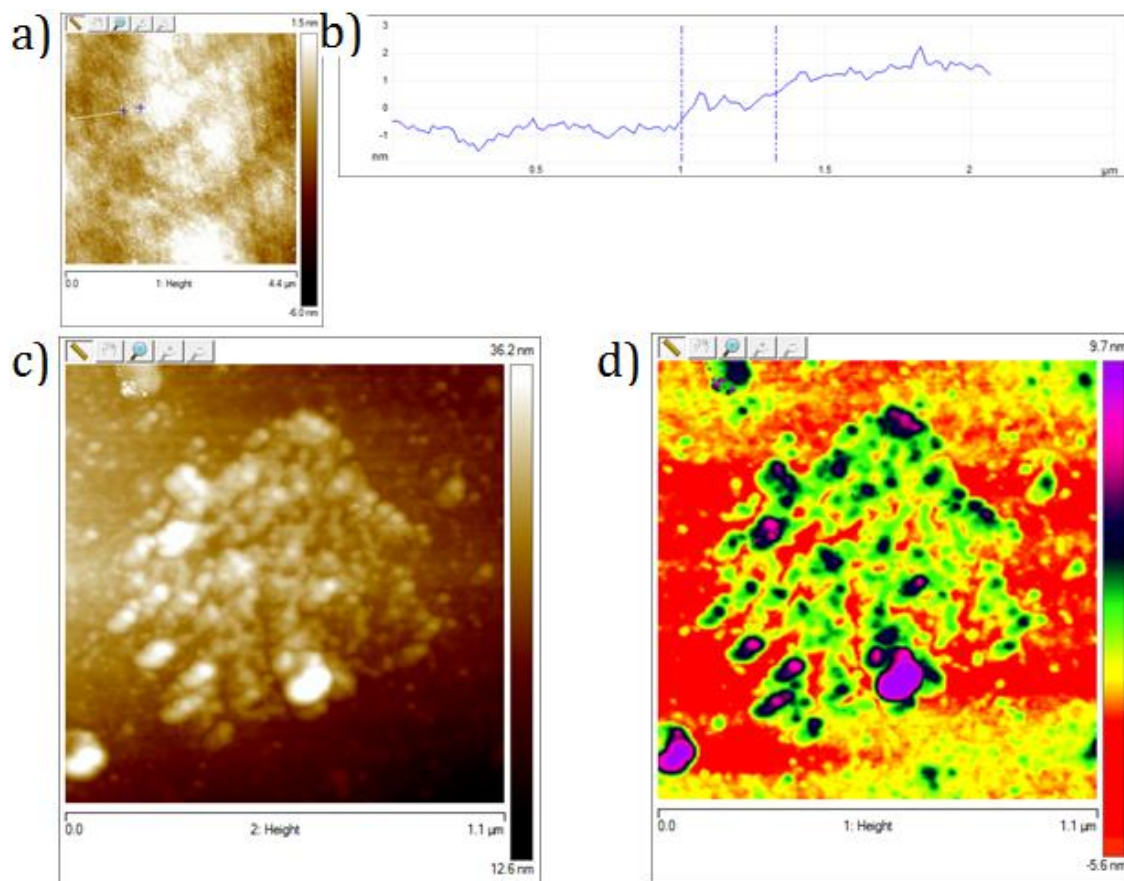
Figure 4.12 (a) AFM image of SG showing single layer structure; (b) corresponding hight profile; (c) AFM image of SG aggragtes and (d) corresponding colored hight profile.

The AFM images of NSG are shown in Figure 4.13. The particles appeared like perforated sheets of irregular shape. The height images showed that the thickness of the materials are well below 1 nm confirming that these are single layer structures. Most probably the presence of negatively charged sulfonate groups at the periphery

of the particles led to repulsive interaction between the particles and prevented aggregation of particles.
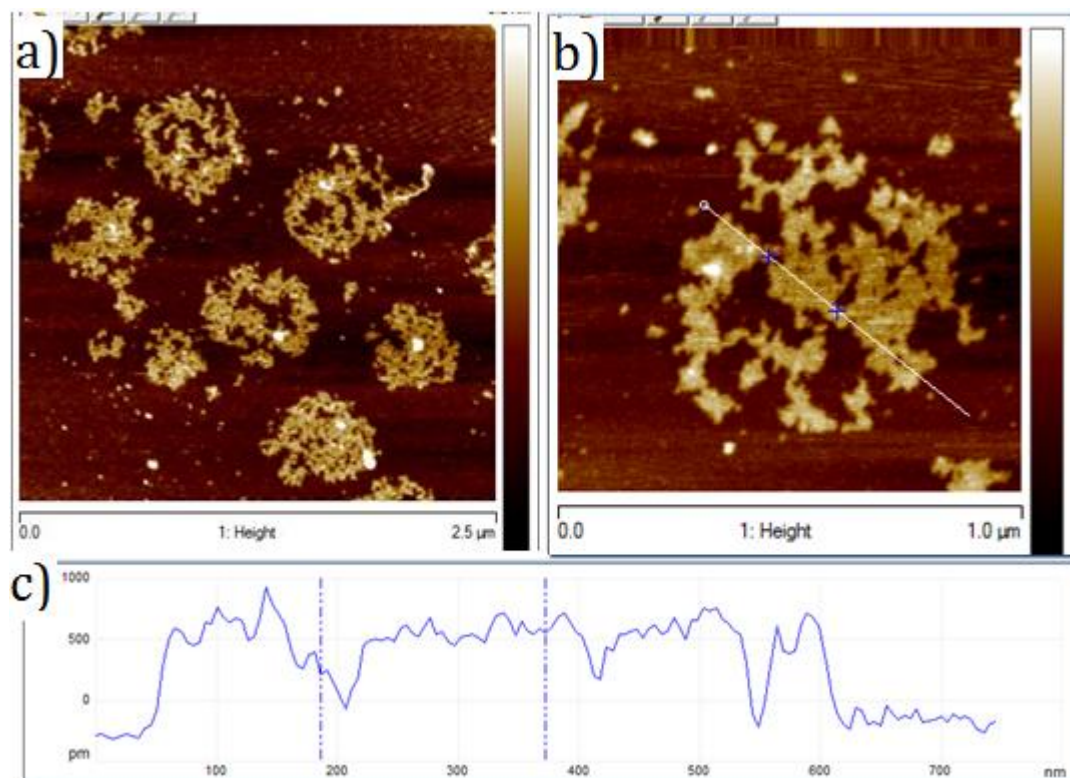
Figure 4.13 AFM images of (a) & (b) NSG and corresponding (c) hight profile

Synthesis of small "graphene molecules" is interesting as these preparations are expected to generate graphenes with well-defined structures. Most of these procedures use PAH as starting materials for graphene synthesis. Large PAH molecules are insoluble in most solvents and this remains as a major drawback of the method which restricts the maximum size of the synthesized graphene molecules to a few nanometers. For example, the pioneering work of Müllen and co-workers only gave graphene molecules with a maximum size of 3.2 nm (Yang 2008) and graphene nano ribbons of 30 nm length (Cai 2010). These reactions required several steps and the overall yields were very low. For example synthesis of 3.2 nm sized graphene molecules involves five steps that include extreme dry reaction like Grignard reaction and anaerobic Suzuki coupling reaction which provides overall yield of around 25%. Synthesis of the molecular precursors of nano ribbons involve three to five reaction steps followed by the thermal sublimation of these monomers onto a gold surface. In this context the strategy we developed appears to have

several advantages. First of all our starting material is a low molecular weight bis-diazonium salt that can be easily prepared from the commercially available 4,4'-diaminobiphenyl in a one-step reaction. In our approach the diazonium salt was converted in two steps to a large graphene-like network HG in very high yield. The CAP molecule, which is the precursor of HG, is insoluble in most solvents, but this is not a drawback because the aryl radical produced by the decomposition of the diazonium salt can add to solid substrates. Majority of the HG nanostructures have sizes above 100 nm and few of them infact exhibited sizes as high as 2 μm. A major disadvantage of our method is the non uniformity of sizes and presence of defects in the structure.

Earlier attempts to extend the size of graphene molecules ended up in propeller-shaped objects as observed in the case of C474 (Simpson 2004). Attempts to visualize the objects through TEM also failed. The authors pointed out the difficulty in getting separated single molecules on the grid from the insoluble mass. It was only possible to observe large clusters of particles of about 100 nm with very low degree of order (Simpson 2014). In our studies we were able to observe isolated single layer and few layer sheets, although aggregation remained as a major challenge. In the case of the sulfonated material, particularly the sodium salt, we could actually observe single layer sheets with height ~0.5 nm.

4.3.4 Energy storage Applications

The development of renewable, sustainable and alternative energy sources is a major concern all over the world (Li, 2013). Sustainability of energy is closely linked to its storage. Hence development of energy storage systems (ES) are also of great importance. Minimizing the stored energy losses in commercial, domestic, and industrial processes can have a positive impact on the world's energy sustainability (Amin 2008). In developing countries like India, where the means of energy generation are less sophisticated, advanced storage technologies are highly essential to acquire energy sustainability (Divya 2009). Electrochemical capacitor (EC) is one of the ES system that have been widely used in electronics, electric vehicles, aircrafts etc. (Chen 2013).

Depending on the charge storage mechanism as well as the active materials used, several types of ECs can be distinguished. Electric double layer capacitors

(EDLC), the most common devices at present, use carbon-based active materials with high surface area. Electric energy storage occurs by the formation of electric double layers on the surfaces of both negative and positive electrodes in EDLCs. In general, carbon based materials are used as electrodes for EDLCs (Gu 2014; Mombeshora 2015). Activated carbon is the main material exploited for commercial applications of electrochemical capacitors. More recently, carbon nanotubes and graphene are evaluated for their performance in EDLC (Simon 2008; Zhao 2011) as these materials are electrochemically stable, porous, highly conductive and exhibit good processability (Njomo 2014; Sharma 2009).

We have carried out CV studies of HG, SG and NSG to evaluate their electrochemical capacitor characteristics and stable electrochemical activity. The results obtained are given in Figure. 4.14. CV curves were recorded at different scan rates in the potential range between -0.7 V and 0.3 V, respectively. The CV loops of
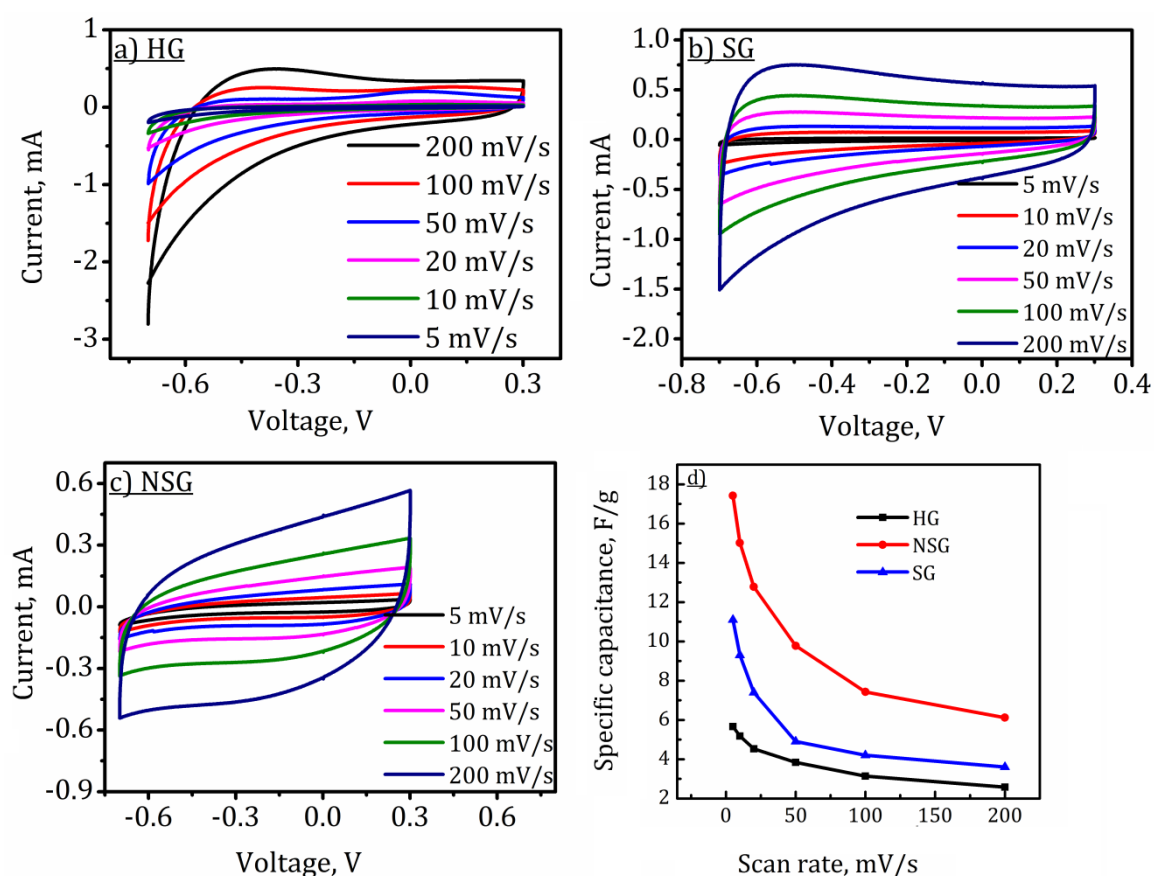
Figure 4.14 Cyclic voltammograms of (a) HG, (b) SG and (c) NSG at different scan rates and (d) the C_{sp} change as a function of scan rate.

NSG based capacitor exhibited nearly rectangular shape. This designates good charge propagation at the interface of electrodes made from this material (Chen 2011). Occurrence of EDLC is evident since with increasing sweep rates the area of CV curves gradually increased with all CV loops (Chen 2011). The method of calculation of specific capacitance (C_{sp}) is given in the material and methods section. The calculated C_{sp} values are summarized in Table. 4.1. The plot of C_{sp} at different sweep rates is shown in Figure 4.14d.

Table 4.1 The C_{sp} change as a function of scan rate in symmetric 2 electrode configuration.

Scan rate (mV/s)	C_{sp} (F/g) of the Sample		
	HG	SG	NSG
5	5.66	11.12	17.42
10	5.18	9.31	15.02
20	4.53	7.42	12.78
50	3.84	4.91	9.78
100	3.14	4.22	7.43
200	2.58	3.60	6.12

The galvanostatic charge–discharge curves of supercapacitors with electrodes made by HG, SG and NSG at different current densities were measured and results obtained are shown in Figure 4.15. Also the corresponding plot of variation of C_{sp} with current density is shown in Figure 4.15d.

Higher C_{sp} values were obtained for the electrode made with NSG. In order to identify the reason for the improved capacitance of NSG based capacitor, electrochemical performance of NSG sample was analyzed in 3 electrode configuration using CV measurements. Results obtained from the measurements are shown in Figure 4.16 and C_{sp} values obtained at different scan rates are given in Table 4.2.

It is found that sweep rate and C_{sp} are inversely proportional to each other. This is due to the fact that at lower sweep rates transport of large number of ions are possible. While at higher sweep rates ion diffusion into the electro-active graphene
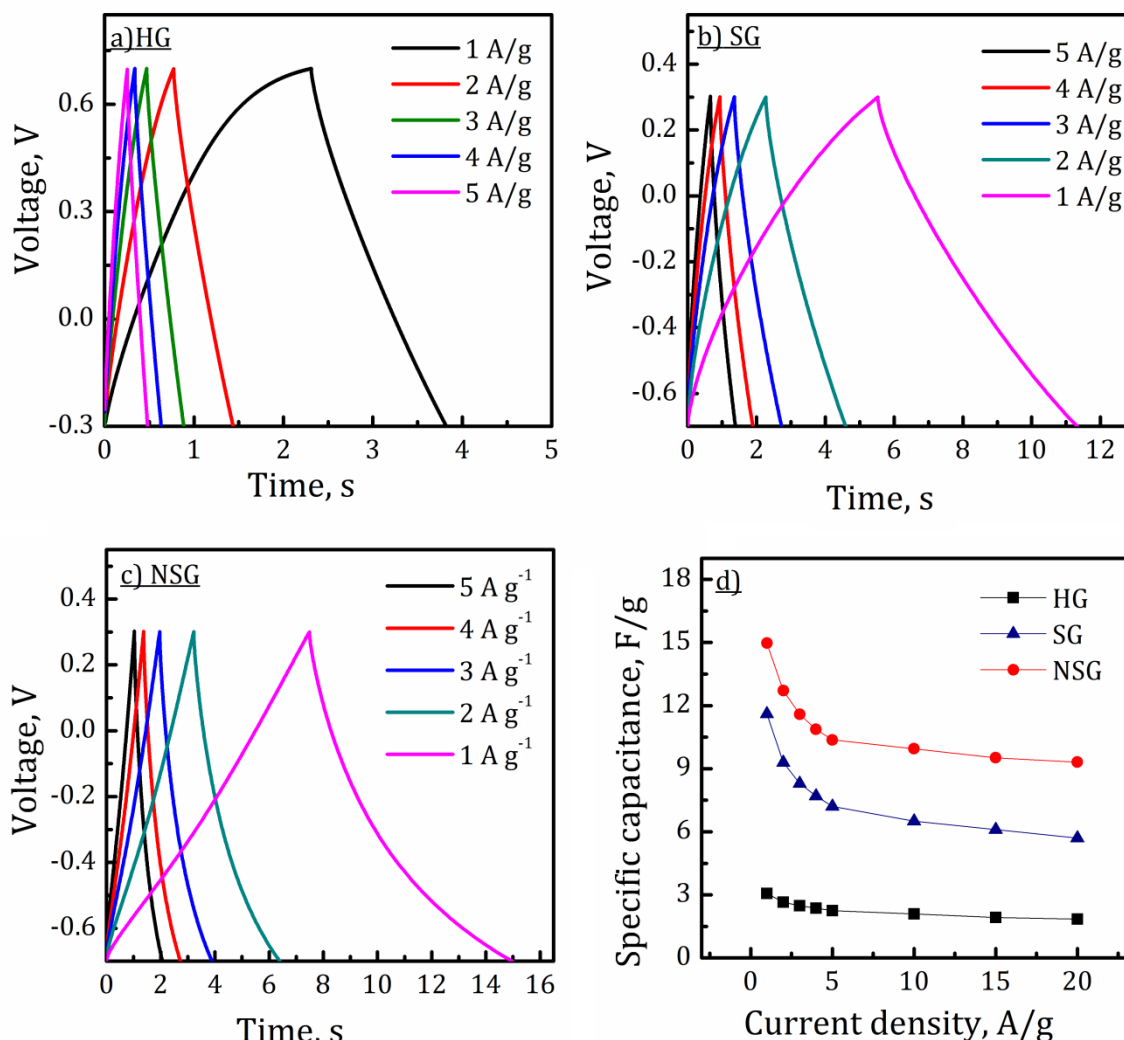
Figure 4.15 Galvanostatic charge–discharge curves of (a) HG, (b) SG and (c) NSG based supercapacitors at different current densities and (d) the C_{sp} change as a function current density.

materials occurs only slowly. NGS prepared through this simple preparative method exhibited a specific capacitance of 45.5 F/g in 30 wt% aqueous KOH electrolyte. This value is comparatively higher than the specific capacitance reported in earlier studies of pure graphene film (Zhang 2009) and graphene nanosheets prepared by tri-solvent mediated ultrasonic exfloation of graphene powder (Balasubramaniam

2016). The comparatively higher value may be due to the prevention of aggregation due to the charged functional group ($SO_3^{\ominus}$) present in NSG. This functionality prevents the restacking of individual nanosheets thereby the active sites of graphene can be fully accessed by the ions in the electrolyte.
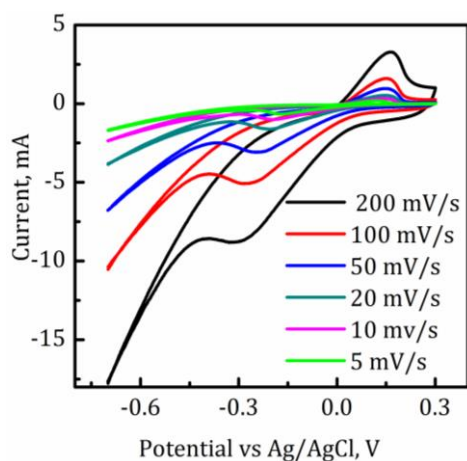
Figure 4.16 Cyclic voltammograms of NSG analyzed in 3 electrode configuration.

Table 4.2 The C_{sp} change as a function of scan rate for NSG from 3 electrode measurements.

Scan rate (mV/s)	C_{sp} (F/g)
5	45.5
10	33.2
20	27.4
50	20.1
100	16.2
200	14.1

4.4 Conclusions

In this chapter we report a new method for the organic synthesis of graphene and sulfonated graphene materials. Their characterization and energy storage applications are also provided. Synthesis was accomplished in a two step reaction which involved $NaBH_4$ reduction of a bisdiazonium salt followed by Scholl oxidation of the resultant product. The structure and morphology of these materials were examined using XRD, Raman and HRTEM. These sulfonated graphene materials were found to have potential as elctode material for energy storage applications.

4.5 Experimental Section

4.5.1 Materials and methods

A reported procedure was used for the preparation of BPBDT (Schiemann 1943). Commercial graphene (CG) was obtained from the Nanoshel (a Nanotechnology Company in India). Thermo-gravimetric analysis as well as differential thermal analysis were performed in atmospheric conditions at a heating

rate of 10 $^{\circ}$C/min from 35 to 900 $^{\circ}$C using a Shimadzu DTG-60 equipment. All the FTIR spectra were recorded on a Shimadzu IR Prestige 21 spectrometer. UV-Vis spectra were obtained using Shimadzu UV-2600 spectrophotometer. Bruker Avance DPX 500 MHz spectrometer was used to obtain the ^{1}H NMR data. X-ray diffractograms were obtained using Ni-filtered CuK$_{\alpha}$ radiation from a Phillips diffractometer. For the AFM analysis stock solution having concentration 0.1 mg mL^{-1} were prepared in DMF for HG and SG. For NSG the solution were prepared in water. The solutions were drop-cast on freshly cleaved mica, evaporated and AFM images were recorded on Multimode SPM (Bruker Nanoscope V) operating with a tapping mode regime. Antimony doped silicon cantilever with a resonant frequency of 300 kHz and spring constant of 40 Nm^{-1} were used. HRTEM analyses were done by using the same stock solution after drop casting on a 400 mesh carbon-coated copper grid, using a FEI–TECNAI30 G2S-Twin 300 kV instrument. Raman confocal microscopy analyses were done using WITec alpha 300R at room temperature by using a 633 nm Ar^{+} laser source for excitation. The number of accumulation was 5, and integration time was 1 s.

4.5.2 Experimental Details

4.5.2.1 Preparation of CAP

To a stirred solution of BPBDT (760 mg, 1 mmol) in deionized and deaerated water (30 mL) was added a methanolic solution (50 mL) of NaBH$_4$ (760 mg, 20 mmol). After 12 h stirring the precipitate was filtered and washed with HCl (20%, 2 × 15 mL) and water (2 × 15 mL). The precipitate was dried first in air and then in a vacuum oven at 80 °C for over night. Yield was 280 mg.

4.5.2.2 Preparation of HG

To CAP (500 mg), AlCl$_3$ (6.0 g) and NaCl (3.0 g) were added and mixed well by grinding. The mixture obtained was heated at 165 °C in a sealed tube for 4 h with stirring. The mixture obtained after cooling was sonicated with distilled water and the suspension obtained was centrifuged to separate the solid. The solid was washed with HCl (25%, 2 × 50 mL), acetic acid (2 × 50 mL), water (2 × 50 mL), acetone (2 × 50 mL) and ether (2 × 50 mL). The final product obtained was dreid at 80 °C in a

vacuum oven for over night. The dried material was used for further studies. The yiled was 420 mg.

4.5.2.3 Preparation of SG

Powdered HG (400 mg) was mixed with oleum (25 mL) in a sealed tube and heated at 180 °C for 24 h with stirring. After cooling the mixture was added to crushed ice and allowed to warm to room temperature. The precipitate was separated by centrifugation, followed by washing with water (2 × 40 mL), acetone (2 × 40 mL) and ether (2 × 40 mL). The product obtained was dried at 80 °C in a vacuum oven for over night. Yield was 430 mg.

4.5.2.4 Preparation of NSG

SG (100 mg) was suspended in water (15 mL) and aqueous $NaHCO_3$ (0.5 M) solution was added dropwise with stirring till the solution turns alkaline. Ethanol (20 mL) was added to the solution and centrifuged. The precipitate obtained was washed with 1:1 water-ethanol mixture (2 × 20 mL) and then with ethanol (2 × 20 mL). The final product obtained was dried at 80 °C in a vacuum oven for over night. Yield was 110 mg.

4.5.2.5 General procedure for the electrode preparation for capacitance studies

Supercapacitor electrodes with an area of 1 cm^2 were prepared using the materials (HG, SG and NSG) by the following procedure. The material was mixed with a polytetrafluoroethylene (PTFE) binder in a mass ratio of 95: 5 and dispersed in ethanol. The resulting mixture was homogenized by ultrasonication and coated onto the conductive carbon cloth (ELAT, NuVant Systems Inc.) substrate, which was followed by drying at 100 °C for 6 h in a vacuum oven. For HG sample, the mass of active material per electrode was 2 mg and for SG and NSG samples, each electrode contained 1 mg of electroactive material. Two symmetric electrodes, separated by a thin polymer separator (Celgard 3501) in a 30 wt. % KOH aqueous electrolyte, were sandwiched in a supercapacitor test cell (ECC-std, EL-Cell GmbH). The electrochemical properties of the supercapacitor electrodes were studied by symmetric assemblies of each material in a two-electrode configuration by cyclic voltammetry (CV), galvanostatic charge–discharge and electrochemical impedance

spectroscopy (EIS) using a VMP3 Biologic electrochemical workstation. Since the measurements are made on symmetric assemblies of materials by the basic circuit relationship for series capacitors, what is actually measured is 1/2 of the capacitance of the freestanding electrode. The cell capacitance (C) was then calculated from the cyclic voltammograms (CVs) according to eqn (4.1) or from the charge–discharge curves according to eqn (4.2)

$$C = \frac{A}{2fV} \tag{4.1}$$

where 'A' is the area of CV loop and V is the voltage and 'f' is the scan rate,

$$C = \frac{I}{\left(\frac{\Delta V}{\Delta t}\right)} \tag{4.2}$$

where 'I' is the constant current for charge- discharge, $\frac{\Delta V}{\Delta t}$ is slope of the discharge curve. The specific capacitance (C_{sp}) was then calculated as

$$C_{sp} = \frac{2C}{m} \tag{4.3}$$

where 'm' is the mass of active material in each electrode.

The specific capacitance from the three electrode measurements can be calculated as

$$C_{sp} = \frac{A}{2fVm} \qquad \text{or} \qquad C_{sp} = \frac{I}{m\left(\frac{\Delta V}{\Delta t}\right)} \tag{4.4}$$

4.6 References

A Guide to IUPAC Nomenclature of Organic Compounds, Blackwell Scientific Publications, London, **1997**.

Alwarappan, S.; Erdem, A.; Liu, C.; Li, C. Z. *J. Phys. Chem. C* **2009**, *113*, 8853-8857.

Amin, M.; Stringer, J. *MRS Bull.* **2008**, *33*, 399-407.

Balaban, A. T.; Nenitzescu C. D. *Friedel-Crafts and Related Reactions*, *Part 2* (Ed.: Olah G. A.) **1964**, pp. 979.

Balasubramaniam, M.; Balakumar, S. *Mater. Lett.* **2016**, *182,* 63-67.

Berresheim, A. J.; Müller, M.; Müllen, K. *Chem. Rev.* **1999**, *99,* 1747-1786.

Bredas, J. L.; Baughman, R. H. *J. Chem. Phys.* **1985**, *83*, 1316-1322.

Cai, J.; Ruffieux, P.; Jaafar, R.; Bieri, M.; Braun, T.; Blankenburg, S.; Muoth, M.; Seitsonen, A. P.; Saleh, M.; Feng, X.; Müllen, K.; Fasel, R. *Nature* **2010**, *466*, 470-473.

Cançado, L. G.; Takai, K.; Enoki, T.; Endo, M.; Kim, Y. A.; Mizusaki, H.; Jorio, A.; Coelho, L. N.; Magalhães-Paniago, R.; Pimenta, M. A. *Appl. Phys. Lett.* **2006**, *88*, 163106.

Cao, H. Q.; Wu, X. M.; Yin, G.; Warner, J. H. *Inorg. Chem.* **2012**, *51*, 2954-2960.

Chen, Y. L.; Hu, Z. A.; Chang, Y. Q.; Wang, H. W.; Zhang, Z. Y.; Yang, Y. Y.; Wu, H. Y. *J. Phys. Chem. C* **2011**, *115*, 2563-2571.

Chen, J.; Li, C.; Shi, G. *J. Phys. Chem. Lett.* **2013**, *4*, 1244-1253.

Clar, E.; Stewart, D. G. *J. Am. Chem. Soc.* **1953**, *75*, 2667-2672.

Clar, E.; Ironside, C. T. *Proc. Chem. Soc.* **1958**, 150.

Clar, E.; Ironside, C. T.; Zander, M. *J. Chem. Soc.* **1959**, 142-147.

Clar, E.; Fell, G. S.; Ironside, C. T.; Balsillie, A. *Tetrahedron* **1960**, *10*, 26-36.

Clar, E.; Ironside, C. T.; Zander, M. *Tetrahedron* **1966**, *22*, 3527-3533.

Clar, E.; Müllen, A. *Tetrahedron* **1968**, *24*, 6719-6724.

Clar, E.; Müllen, A.; Sanigök, Ü. *Tetrahedron* **1969**, *25*, 5639-5648.

Clar, E.; McAndrew, B. A. Stephen, J. F. *Tetrahedron* **1970**, *26*, 5465-5478.

Clar, E.; McAndrew, B. A. *Tetrahedron* **1972**, *28*, 1137-1142.

Clar, E.; McAndrew, B. A. *Tetrahedron* **1972**, *28*, 1237-1240.

Clar, E.; Mackay, C. C. *Tetrahedron* **1972**, *28*, 5049-5054.

Clar, E.; Mackay, C. C. *Tetrahedron* **1972**, *28*, 6041-6047.

Clar, E.; Lovat, M. M.; Simpson, W. *Tetrahedron* **1974**, *30*, 3293-3298.

Clar, E.; Schmidt, W. *Tetrahedron* **1979**, *35*, 2673-2680.

Costa, S. D.; Righi A.; Fantini, C.; Hao. Y.; Magnuson, C.; Colombo, L.; Ruoff, R. S.; Pimenta, M. A. *Solid State Commun.* **2012**, *152*, 1317-1320.

Debije, M. G.; Piris, J.; de Haas, M. P.; Warman, J. M.; Tomović, Ž.; Simpson, C. D.; Watson, M. D.; Müllen, K. *J. Am. Chem. Soc.* **2004**, *126*, 4641- 4645.

Dias, J. R. *Thermochim. Acta* **1987**, *122*, 313-337.

Dias, J. R. *J. Chem. Inf. Comput. Sci.* **1991**, *31*, 89-96.

Dias, J. R. *J. Chem. Inf. Comput. Sci.* **1993**, *33*, 117-127.

Dilthey, W.; Hurtig, G. *Chem. Ber.* **1934**, *67*, 495-496.

Divya, K. C.; Østergaard, J. *Electric Power Systems Research* **2009**, *79*, 511-520.

Dötz, F.; Brand, J. D.; Ito, S.; Gherghel, L.; Müllen, K. *J. Am. Chem. Soc.* **2000**, *122*, 7707-7717.

Eigler, S.; Dotzer, C.; Hof, F.; Bauer, W.; Hirsch, A. *Chem. Eur. J.* **2013**, *19*, 9490-9496.

Faust, R. *Angew. Chem.* **1996**, *108*, 2411.

Fechtenkötter, A.; Saalwächter, K.; Harbison, M. A.; Müllen, K.; Spiess, H. W. *Angew. Chem. Int. Ed.* **1999**, *38*, 3039-3042.

Fechtenkötter, A.; Tchebotareva, N.; Watson, M.; Müllen, K. *Tetrahedron* **2001**, *57*, 3769-3783.

Feng, X.; Wu, J.; Enkelmann, V.; Müllen, K. *Org. Lett.* **2006**, *8*, 1145-1148.

Gargiulo, V.; Apicella, B.; Alfe, M.; Russo, C.; Stanzione, F.; Tregrossi, A.; Amoresano, A.; Millan, M.; Ciajolo, A. *Energy Fuels* **2015**, *29*, 5714-5722.

Gu, W.; Yushin, G. *WIREs Energy Environ.* **2014**, *3*, 424-473.

Guillén, M. D.; Iglesias, M. J.; Dominguez, A.; Blanco, C. G. *Energy Fuels* **1992**, *6*, 518-525.

Guillén, M. D.; Domínguez, A.; Iglesias, M. J.; Blanco, C. G. *Fuel* **1995**, *74*, 233-240.

Gutman, I.; Tomović, Ž.; Mullen, K.; Rabe, E. P. *Chem. Phys. Lett.* **2004**, *397*, 412-416.

Halleux, A.; Martin, R. H.; King, G. S. D. *Helv. Chim. Acta* **1958**, *129*, 1177-1183.

Hendel, W.; Khan, Z. H.; Schmidt, W. *Tetrahedron* **1986**, *42*, 1127-1134.

Herndon, W. C. *J. Am. Chem. Soc.* **1990**, *112*, 4546-4547.

Herwig, P.; Kayser, C. W.; Müllen, K.; Spiess, H. W. *Adv. Mater.* **1996**, *8*, 510-513.

Hyatt, J. A. *Org. Prep. Proced. Int.* **1991**, *23*, 460-463.

Ito, S.; Wehmeier, M.; Brand, J. D.; Kübel, C.; Epsch, R.; Rabe, J. P.; Müllen, K. *Chem. Eur. J.* **2000**, *6*, 4327-4342.

Iyer, V. S.; Wehmeier, M.; Brand, J. D.; Keegstra, M. A.; Müllen, K. *Angew. Chem. Int. Ed.* **1997**, *36*, 1604-1607.

Iyer, V. S.; Yoshimura, K.; Enkelmann, V.; Epsch, R.; Rabe, J. P.; Müllen, K. *Angew. Chem. Int. Ed.* **1998**, *37*, 2696-2699.

Kastler, M.; Schmidt, J.; Pisula, W.; Müllen, K. *J. Am. Chem. Soc.* **2006**, *128*, 9526-9534.

Kovacic, P.; Jones, M. B. *Chem. Rev.* **1987**, *87*, 357-379.

Kübel, C.; Eckhardt, K.; Enkelmann, V.; Wegner, G.; Müllen, K. *J. Mater. Chem.* **2000**, *10*, 879-886.

Lambert, C. *Angew. Chem. Int. Ed.* **2005**, *44*, 7337-7339.

Lee, M.; Kim, J.; Peleshanko, S.; Larson, K.; Yoo, Y.; Vaknin, D.; Markutsya, S.; Tsukruk, V. V. *J. Am. Chem. Soc.* **2002**, *124*, 9121-9128.

Li, S-M.; Wang, Y-S.; Yang, S-Y.; Liu, C-H.; Chang, K-H.; Tien, H-W.; Wen, N-T.; Ma, C-C. M.; Hu, C-C. *J. Power Sources* **2013**, *225*, 347-355.

Liu, F. J.; Sun, J.; Zhu, L. F.; Meng, X. J.; Qi, C. Z.; Xiao, F. S. *J. Mater. Chem.* **2012**, *22*, 5495-5502.

Megahead, S.; Scosati, B. *J. Power Sources* **1994**, *51*, 79-104.

Meyer, J. C.; Geim, A. K.; Katsnelson, M. I.; Novoselov, K. S.; Booth, T. J. *Nature* **2007**, *446*, 60-63.

Morgenroth, F.; Reuther, E. Müllen, K. *Angew. Chem. Int. Ed.* **1997**, *36*, 631-634.

Morgenroth, F.; Müllen, K. *Tetrahedron* **1997**, *53*, 15349-15366.

Morgenroth, F.; Kübel, C. Müllen, K. *J. Mater. Chem*. **1997**, *7*, 1207-1211.

Morgenroth, F.; Kübel, C. Müller, M. Wiesler, U.-M. Berresheim, A. J. Wagner, M. Müllen, K. *Carbon* **1998**, *36*, 833-837.

Müller, M.; Iyer, V. S.; Kübel, C.; Enkelmann, V.; Müllen, K. *Angew. Chem. Int. Ed.* **1997**, *36*, 1604-1607.

Müller, M.; Kübel, C.; Müllen, K. *Chem. Eur. J.* **1998**, *4*, 2099-2109.

Müller, M.; Mauermann-Düll, H.; Wagner, M.; Enkelmann, V.; Müllen, K. *Angew. Chem. Int. Ed*. **1995**, *34*, 1583-1586.

Müller, M.; Petersen, J.; Strohmaier, R.; Günther, C.; Karl, N.; Müllen, K. *Angew. Chem. Int. Ed*. **1996**, *35*, 886-888.

Müller, M.; Iyer, V. S.; Kübel, C.; Enkelmann, V.; Müllen, K.; *Angew. Chem. Int. Ed*. **1997**, *36*, 1607-1610.

Müller, M.; Kübel, C.; Morgenroth, F.; Iyer, V. S.; Müllen, K. *Carbon* **1998**, *36*, 827-831.

Njomo, N.; Waryo, T.; Masikini, M.; Ikpo, C. O.; Mailu, S. Tovide, O.; Ross, N.; Williams, A.; Matinise, N.; Sunday, C. E. Mayedwa, N. Bakera, P. G. L.; Ozoemena, K. L.; Iwuoh, E. I. *Electrochim. Acta* **2014**, *128*, 226-237.

Novoselov, K. S.; Geim, A. K.; Morozov, S. V.; Jiang, D.; Zhang, Y.; Dubonos, S. V.; Grigorieva, I. V.; Firsov, A. A. *Science* **2004***, 306*, 666-669.

Qian, M.; Zhou, Y. S.; Gao, Y.; Park, J. B.; Feng, T.; Huang, S. M.; Sun, Z.; Jiang, L.; Lu, Y. F. *Appl. Phys. Lett*. **2011**, *98*, 173108.

Reina, A.; Jia, X. T.; Ho, J.; Nezich, D.; Son, H.; Bulovic, V.; Dresselhaus, M. S.; Kong, J. *Nano Lett*. **2009**, *9*, 30-35.

Rempala, P.; Kroulik, J.; King, B. T. *J. Am. Chem. Soc.* **2004**, *126*, 15002-15003.

Schiemann, G.; Winkelmüller, W. *Organic Syntheses, Coll. Vol. 2* (Eds.: Hartman, W. W.; Byers, J. R.; Dickey J. B.) **1943**, pp. 188.

Scholl, R.; Seer, C.; Weitzenböck, R. *Chem. Ber*. **1910**, *43*, 2202-2209.

Scholl, R.; Seer, C. *Liebigs Ann. Chem*. **1912**, *394*, 111-123.

Scholl, R.; Neumann, H. *Chem. Ber*. **1922**, *55*, 118-126.

Scholl, R.; Seer, C. *Chem. Ber*. **1922**, *55*, 330-341.

Scott, L. T. *Angew. Chem. Int. Ed.* **2004**, *43*, 4994-5007.

Sharma, R. K. Zhai, L. *Electrochim. Acta* **2009**, *54*, 7148-7155.

Si, Y.; Samulski, E.T. *Nano Lett.* **2008**, *8*, 1679-1682.

Simon, P.; Gogotsi, Y. Nat. Mater. **2008**, *7*, 845-854.

Simpson, C. D.; Brand, J. D.; Berresheim, A. J.; Przybilla, L.; Räder, H. J.; Müllen, K. *Chem. Eur. J.* **2000**, *8*, 1424-1429.

Simpson, C. D. Ph.D. Thesis, University of Mainz, **2003**.

Simpson, C. D.; Mattersteig, G.; Martin, K.; Gherghel, L.; Bauer, R. E.; Ra¨der, H. J.; Müllen, K. *J. Am. Chem. Soc.* **2004**, *126*, 3139-3147.

Stabel, A.; Herwig, P. Müllen, K. Rabe, J. P. *Angew. Chem. Int. Ed.* **1995**, *34*, 1609-1611.

Stefano, M. D.; Negri, F.; Carbone, P.; Müllen, K. *Chem. Phys.* **2005**, *314*, 85-89.

Stein, S. E.; Brown, R. L. *J. Am. Chem. Soc.* **1987**, *109*, 3721-3729.

Tahara, K.; Tobe, Y. *Chem. Rev.* **2006**, *106*, 5274-5290.

Tomović, Ž.; Watson, M. D.; Müllen, K. *Angew. Chem. Int. Ed.* **2004**, *43*, 755-758.

Tyutyulkov, N.; Madjarova, G.; Dietz, F.; Müllen, K. *J. Phys. Chem. B* **1998**, *102*, 10183-10189.

van de Craats, A. M.; Warman, J. M.; Müllen, K.; Geerts, Y.; Brand, J. D. *Adv. Mater.* **1998**, *10*, 36-38.

Vinayan, B. P.; Nagar, R.; Raman, V.; Rajalakshmi, N.; Dhathathreyan K. S.; Ramaprabhu S. *J. Mater. Chem.* **2012**, *22*, 9949-9956.

Vinayan, B. P.; Nagar, R.; Sethupathi, K.; Ramaprabhu, S. *J Phys. Chem. C* **2011**, *115*, 15679- 15685.

Vollhardt, K. P. C. *Acc. Chem. Res.* **1977**, *10*, 1-8.

Wang, G. X.; Yang, J.; Park, J.; Gou, X. L.; Wang, B.; Liu, H.; Yao, J. *J. Phys. Chem. C* **2008**, *112*, 8192-8195.

Wang, Z.; Dötz, F.; Enkelmann, V.; Müllen, K. *Angew. Chem. Int. Ed.* **2005**, *44*, 1247-1250.

Wang, Z.; Tomović, Ž.; Kastler, M.; Pretsch, R.; Negri, F.; Enkelmann, V.; Müllen, K. *J. Am. Chem. Soc.* **2004**, *126*, 7794-7795.

Wasserfallen, D.; Kastler, M.; Pisula, W.; Hofer, W. A.; Fogel, Y.; Wang, Z.; Müllen, K. *J. Am. Chem. Soc.* **2006**, *128*,1334-1339.

Watson, M. D.; Fechtenkotter, A.; Müllen, K. *Chem. Rev.* **2001**, *101*, 1267-1300.

Wu, J.; Pisula, W.; Müllen, K. *Chem. Rev.* **2007**, *107*, 718-747.

Wu, J.; Gherghel, L.; Watson, M. D.; Li, J.; Wang, Z.; Simpson, C. D.; Kolb, U.; Müllen, K. *Macromolecules* **2003**, *36*, 7082-7089.

Wu, J.; Baumgarten, M.; Debije, M. G.; Warman, J. M.; Müllen, K. *Angew. Chem. Int. Ed.* **2004**, *43*, 5331-5335.

Wu, J.; Watson, M. D.; Müllen, K. *Angew. Chem. Int. Ed.* **2003**, *42*, 5329-5333.

Wu, J.; Watson, M. D.; Zhang, L.; Wang, Z.; Müllen, K. *J. Am. Chem. Soc.* **2004**, *126*, 177-186.

Wu, J.; Li, J.; Kolb, U.; Müllen, K. *Chem. Commun.* **2006**, 48-50.

Wu, J.; Tomović, Ž.; Enkelmann, V.; Müllen, K. *J. Org. Chem.* **2004**, *69*, 5179-5186.

Wu, J.; Watson, M. D.; Tchebotareva, N.; Wang, Z.; Müllen, K. *J.Org. Chem.* **2004**, *69*, 8194-8204.

Wu, M-S.; Chan, D-S.; Lin, K-H.; Jow, J-J. *Mater. Chem. Phys.* **2011**, *130*, 1239-1245.

Xiao, S.; Myers, M.; Miao, Q.; Sanaur, S.; Pang, K.; Steigerwald, M. L.; Nuckolls, C. *Angew. Chem. Int. Ed.* **2005**, *44*, 7390-7394.

Yang, X.; Dou, X.; Rouhanipour, A.; Zhi, L.; Räder, H. J.; Müllen, K. *J. Am. Chem. Soc.* **2008**, *130*, 4216-4217.

Yuan, C.; Chen, W.; Yan, L. *J. Mater. Chem.* **2012**, *22*, 7456-7460.

Zander, M. *Top. Curr. Chem.* **1990**, *153*, 101-122.

Zhang, Y.; Li, H.; Pan, L.; Lu, T.; Sun, Z. *J. Electroanal. Chem.* **2009**, *634*, 68-71.

Zhao, W.; Tan, P. H.; Liu, J.; Ferrari, A. C. *J. Am. Chem. Soc.* **2011**, *133*, 5941-5946.

Zhao, X.; Mendoza-Sa´nchez, B.; Dobson, P. J.; Grant, P. S. *Nanoscale* **2011**, *3*, 839-855.

Zhi, L.; Müllen, K. *J. Mater. Chem.* **2008**, *18*, 1472-1484.

Zhou, L.; Lin, X.; Huang, T.; Yu, A. *J. Mater. Chem. A* **2014**, *2*, 5117-5123.

List of publications

1. Palladium-Nanoparticle-Linked Organic Frameworks: Heterogeneous Recyclable Catalysts in Aqueous Medium.
   S. P. Prakash and Karical R. Gopidas* *ChemCatChem* **2014**, *6,* 1641-1651.

2. Highly Stable Copper Nanoparticles Linked to Organic Frameworks as Recyclable Catalyst for Three- Component Click Cycloaddition in Water.
   S. P. Prakash and Karical R. Gopidas* *ChemistrySelect* ***ChemistrySelect*** 2016, *1,* 4803-4813.

3. Diazonium Salts to Graphene: A New Method for the Synthesis of Graphitic Materials, Modifications and Energy Storage Applications.
   S. P. Prakash and Karical R. Gopidas* (manuscript to be submitted)

Oral Presentations

1. "Palladium Nanoparticle-Linked Organic Frameworks: Synthesis, Characterization and Application as Heterogeneous Recyclable Catalyst in Aqueous Medium" **S. P. Prakash** and K. R. Gopidas, *9th JNC Research Conference, 15th October, 2013, Trivandrum.*

Poster presentations

1. "Palladium-Nanoparticle-Linked Organic Frameworks: Heterogeneous Recyclable Catalysts in Aqueous Medium" **S. P. Prakash** and K. R. Gopidas, *8th Mid-CRSI National Symposium in Chemistry, July 10-12, 2014, Jorhat.*